

---

# **We Are What We Eat: Identifying a Regulatory Crosstalk between Central Carbon Metabolism and Cell Division in Bacteria**

---

Riti Mann

A thesis submitted in fulfilment of the requirements for the degree of  
Doctor of Philosophy

The ithree institute

University of Technology Sydney

June 2019

---

---

# Certificate of Authorship/ Originality

I, Riti Mann, certify that the work in this thesis has not previously been submitted for a degree nor has it been submitted as part of requirements for a degree except as fully acknowledged within the text.

I also certify that the thesis has been written by me. Any help that I have received in my research work and the preparation of the thesis itself has been acknowledged. In addition, I certify that all information sources and literature used are indicated in the thesis.

This research is supported by an Australian Government Research Training Program.

Production Note:  
Signature removed prior to publication.

---

Riti Mann, June 2019

---

# Acknowledgements

My PhD journey has been exciting, challenging, sometimes frustrating, but immensely rewarding! I knew from the beginning that pursuing doctoral study is a difficult and challenging task. I would have never been able to successfully complete this long journey without the support and guidance of numerous people, whom I am extremely thankful to.

First of all, I thank the Almighty for keeping me healthy, and giving me the strength and patience to work through all these years so that today I can stand proudly. I wish to express my immense gratitude to my supervisor Professor Liz Harry; without whom none of this would have been possible. Thank you for everything Liz! I will always remember the first Skype conversation I had with Liz, when she introduced me to this interesting and exciting PhD project. Liz has been a very encouraging and understanding supervisor, who cares for everyone around her. Liz has not only taught me how to do good science but also how to live a balanced life. I will always remember her statement – “Take care of yourself as well”. Finally, I would like to thank her for the precious time that she spent on reading and commenting through this thesis, and shaping it in the form it is now!

I particularly wish to thank my co-supervisors Dr. Amy Bottomley and Dr. Leigh Monahan for their continuous encouragement and motivation throughout my PhD candidature. I thank them for mentoring me and being my pillars of support every now and then. I am also grateful to them for their valuable discussions related to my project and for their insightful comments on almost every piece of writing that I wrote during these years. Thank you! I would like to thank Dr. Christopher Rodrigues for bringing his expertise to this project and for all the

---

helpful discussions related to my project. I also wish to extend my appreciation to Dr. Cindy Gunawan for her precious time on mentoring me during my PhD years.

Thank you to all past and present members of the Harry lab, who over the years have made it a friendly place to work: Isa, Ken, Nural, Daniel, Beth and Shirin. I thank them for encouraging me at every step along the way and for many helpful advices.

I owe thanks to a very special person, the love of my life - my husband, Vikas (Vicky) who has supported me throughout this process and has constantly encouraged me when the tasks seemed impossible. Thank you for cheering me up when my experiments did not work! I thank him for his continued and unfailing love, support and understanding during my pursuit of PhD degree that made the completion of this thesis possible. Apart from this, I don't really have words to explain all that you have done for me!! I also wish to extend a special thanks to my parents for letting me pursuit my dreams and supporting me to become what I am today.

Lastly, I would like to acknowledge the financial assistance provided by the Australian Government Research Training Program Scholarship.

---

# Abstract

Cell division is crucial to the survival and propagation of all living organisms. In bacteria, the process of cell division is initiated by the formation of the cytokinetic Z ring, made up of the tubulin-like protein FtsZ, at the cell centre (midcell). Research into the control of Z ring positioning in the well-studied rod-shaped bacteria has focused on two main regulatory systems, the Min system and nucleoid occlusion. However, an aspect of cell division control that remains often overlooked is the need to coordinate cell cycle events with the nutrient availability.

Central Carbon Metabolism (CCM), being the entry point for almost all the raw materials required for cellular growth and proliferation, forms the hub for coordinating nutrient availability to cell growth, size and the division process. Our lab recently identified a novel link between the central carbon metabolic pathway of glycolysis and cell division, wherein disrupting glycolysis by deleting the pyruvate kinase (*pyk*) enzyme was shown to affect the correct positioning of the Z ring at the cell centre, such that 1/3<sup>rd</sup> of the Z rings formed at acentral positions. Interestingly, the addition of pyruvate (the end product of the pyruvate kinase reaction), alleviated this Z ring positioning defect of  $\Delta pyk$  cells.

Pyruvate is a metabolite that lies at the intersection of many metabolic pathways, raising the possibility of any of the potential metabolic fates of pyruvate being actually responsible for the Z ring positioning rescue of  $\Delta pyk$  cells. The experimental results presented in this thesis confirm that pyruvate, and not any of its potential metabolic fates, is the key metabolite coordinating CCM to cell division in *Bacillus subtilis*. Furthermore, this thesis also provide evidence for the role of DNA replication and nucleotide synthesis in the Z ring positioning defect of  $\Delta pyk$  cells. Collectively, the work presented here demonstrates the importance of one specific metabolite - pyruvate, in maintaining the coordination between the cellular events of

division, metabolism and DNA replication in *B. subtilis*; which leads to the hypothesis that pyruvate might be acting as a signaling molecule to synchronize cell cycle events with the nutrient availability.

---

# Table of Contents

<b>Certificate of Authorship/Originality .....</b>	<b>i</b>
<b>Acknowledgements .....</b>	<b>ii</b>
<b>Abstract .....</b>	<b>iv</b>
<b>Table of Contents.....</b>	<b>vi</b>
<b>List of Figures and Tables .....</b>	<b>xii</b>
<b>Publications and Awards .....</b>	<b>xvii</b>
<b>Abbreviations.....</b>	<b>xxi</b>
<b>Chapter 1. Introduction .....</b>	<b>1</b>
1.1 Preface .....	2
1.2 The Bacterial cell cycle .....	3
1.3 Bacterial cell division .....	5
1.3.1 The divisome .....	6
1.3.2 FtsZ protein and the assembly of the Z ring .....	8
1.4 Spatio-temporal regulation of bacterial cell division .....	10
1.4.1 Negative and positive regulators of Z ring placement.....	10
1.5 Bacterial cellular processes are interconnected .....	16
1.5.1 The early stages of DNA replication are connected to division site selection .....	16
1.5.2 Metabolism is not simply an energy engine .....	17
1.6 Nutrient-dependent control of bacterial cell size.....	18
1.7 Metabolic control of bacterial cell division.....	26
1.7.1 Connection of central carbon metabolism (CCM) to cell division.....	30

---

1.8 Thesis aims .....	36
<b>Chapter 2. Materials and Methods .....</b>	<b>39</b>
2.1 Chemicals, reagents and solutions.....	40
2.2 <i>B. subtilis</i> strains and growth media.....	41
2.2.1 Testing for the disruption of the <i>amyE</i> locus.....	43
2.3 Preparation and transformation of competent <i>B. subtilis</i> cells .....	43
2.3.1 Preparation of competent <i>B. subtilis</i> cells .....	43
2.3.2 Transformation of competent <i>B. subtilis</i> cells .....	44
2.4 General DNA methods .....	44
2.4.1 <i>Bacillus subtilis</i> chromosomal DNA extraction .....	44
2.4.2 Measurement of DNA concentration.....	45
2.4.3 Agarose gel electrophoresis.....	45
2.4.4 Polymerase Chain Reaction (PCR) and oligonucleotides .....	46
2.4.5 Colony PCR.....	47
2.4.6 DNA sequencing .....	48
2.5 Gibson assembly.....	48
2.6 Microscopy methods .....	51
2.6.1 Immunofluorescence microscopy (IFM).....	51
2.6.2 Preparation of cells for live cell fluorescence microscopy.....	52
2.6.3 Phase-contrast and fluorescence microscopy .....	53
2.6.4 Cell scoring and statistics .....	53
2.7 Growth curve .....	54
2.8 Measurement of pyruvate in <i>Bacillus subtilis</i> cells .....	54
2.9 Metabolite-FtsZ interaction using Triple Ligand Detect method.....	55



---

2.10 Marker Frequency Analysis .....	56
2.10.1 Isolation of spore DNA .....	56
2.11 RNA-Sequencing.....	57
2.11.1 RNA extraction.....	57
2.11.2 Sequencing and read mapping.....	58
2.12 Validation of RNA-Sequencing results .....	59
2.12.1 cDNA preparation .....	59
2.12.2 qPCR reaction set up .....	60
2.12.3 qPCR efficiency evaluation.....	60
2.12.4 Quantification of mRNA expression using the Comparative C <sub>T</sub> methods.....	61
<b>Chapter 3. Identification of a key metabolite in the coordination of central carbon metabolism and Z ring positioning in <i>B. subtilis</i> .....</b>	<b>62</b>
3.1 Introduction .....	63
3.1.1 The link between central carbon metabolism and cell division in <i>B. subtilis</i> .....	63
3.1.2 Potential fates of pyruvate in a bacterial cell.....	64
3.2 Chapter aims.....	65
3.3 Results .....	66
3.3.1 Confirming the results published by Monahan <i>et al.</i> .....	66
3.3.2 L-alanine, a product of pyruvate metabolism, rescues the Z ring positioning defect of $\Delta pyk$ cells in a growth-rate independent manner .....	69
3.3.3 Testing fatty acids for their role in Z ring positioning via the construction of a fatty acid synthesis mutant.....	73
3.3.4 Investigating the correlation between nucleoid morphology and Z ring positioning in $\Delta pyk$ cells.....	76

---

3.3.5 L-alanine conversion to pyruvate causes the Z ring positioning rescue.....	79
3.3.6 Pyruvate does not interact directly with FtsZ.....	84
3.4 Discussion.....	88
<b>Chapter 4. Investigating the possible role for known Z ring regulatory mechanisms and DNA replication in acentral Z ring positioning in <math>\Delta pyk</math> cells .....</b>	<b>94</b>
4.1 Introduction .....	95
4.2 Chapter aims.....	97
4.3 Results .....	98
4.3.1 Acentral Z rings of the <i>pyk</i> mutant are not due to inactivation of the Min system	98
4.3.2 Nucleoid occlusion is involved in the acentral Z ring positioning in $\Delta pyk$ cells .	104
4.3.3 Quantification of the spread nucleoid morphology of $\Delta pyk$ cells .....	107
4.3.4 $\Delta pyk$ cells have a DNA replication defect, which is rescued after pyruvate addition .....	109
4.3.5 The interplay between Noc and DNA replication initiation frequency in $\Delta pyk$ cells .....	112
4.4 Discussion.....	115
<b>Chapter 5. Investigating the link between central carbon metabolism and cell division using a global transcriptomic approach .....</b>	<b>121</b>
5.1 Introduction and chapter aims .....	122
5.2 Results .....	124
5.2.1 Assessing the sample-to-sample variation using PCA and heat map analysis.....	124
5.2.2 Comparison of the quantity of differentially expressed genes under different experimental conditions.....	128

---

5.2.3 Functional annotation of differentially expressed genes in the pyruvate kinase mutant.....	130
5.2.4 Major pathways whose genes are altered in $\Delta pyk$ cells.....	149
5.2.5 qPCR validation of the downregulation of <i>pyr</i> genes .....	156
5.2.5.1 Selection of target genes.....	156
5.2.5.2 PCR efficiency evaluation and confirmation of RNA-seq results .....	157
5.2.6 Testing the role of pyrimidine synthesis in Z ring positioning by constructing pyrimidine synthesis mutants .....	158
5.3 Discussion.....	165
<b>Chapter 6. General Discussion .....</b>	<b>171</b>
6.1 Introduction .....	172
6.2 Pyruvate is the key metabolite in the CCM-division link .....	173
6.3 A role for nucleoid occlusion in acentral Z ring positioning of $\Delta pyk$ cells.....	175
6.4 Insights into other factors contributing to the formation of acentral Z rings in $\Delta pyk$ cells .....	177
6.4.1 Does the DNA replication defect of $\Delta pyk$ cells contribute to their Z ring positioning defect?.....	177
6.4.2 Does the dispersed nucleoid morphology of $\Delta pyk$ cells contribute to their Z ring positioning defect?.....	179
6.4.3 Does the downregulation of pyrimidine synthesis in $\Delta pyk$ cells contribute to their Z ring positioning defect? .....	179
6.5 Concluding remarks and future directions .....	181
<b>Appendices .....</b>	<b>184</b>

---

Appendix I .....	185
Appendix II.....	195
<b>References .....</b>	<b>200</b>

# List of Figures and Tables

## List of Figures

<b>Figure 1.1.</b> The life cycle of <i>B. subtilis</i> .....	4
<b>Figure 1.2.</b> Cell division in rod-shaped bacteria- <i>E. coli</i> and <i>B. subtilis</i> .....	6
<b>Figure 1.3.</b> Schematic representation of the <i>B. subtilis</i> divisome.....	7
<b>Figure 1.4.</b> Formation and disassembly of the Z ring in <i>E. coli</i> .....	9
<b>Figure 1.5.</b> The combined action of FtsZ and peptidoglycan metabolism in driving cell division .....	9
<b>Figure 1.6.</b> Positioning of Z ring in <i>B. subtilis</i> and <i>E. coli</i> by the combined action of nucleoid occlusion and the Min system .....	11
<b>Figure 1.7.</b> Schematic model for Z ring positioning in <i>E. coli</i> by the nucleoid occlusion and Min systems.....	12
<b>Figure 1.8.</b> Negative and positive regulators of Z ring placement .....	15
<b>Figure 1.9.</b> Equilibrium between the two interaction states of UgtP (UgtP-UgtP and UgtP- FtsZ) influenced by UDP-glucose levels.....	20
<b>Figure 1.10.</b> Metabolic signals controlling the cell division process in various bacterial genera .....	27
<b>Figure 1.11.</b> The coordination between central carbon metabolism and cell division in <i>B.</i> <i>subtilis</i> .....	31
<b>Figure 1.12.</b> Localization pattern of pyruvate dehydrogenase E1 $\alpha$ restored by the addition of pyruvate to $\Delta$ <i>pyk</i> cells.....	33
<b>Figure 1.13.</b> Role of PDHE1 $\alpha$ in Z ring formation.....	34
<b>Figure 2.1.</b> Schematic diagram of the steps involved in constructing an alanine dehydrogenase ( <i>ald</i> ) mutant .....	50

---

<b>Figure 3.1.</b> Potential fates of pyruvate in <i>B. subtilis</i> .....	65
<b>Figure 3.2.</b> The effect of pyruvate on the Z ring positioning of $\Delta pyk$ cells.....	67
<b>Figure 3.3.</b> The effect of L-alanine on the Z ring positioning of $\Delta pyk$ cells .....	71
<b>Figure 3.4.</b> Role of fatty acids in Z ring positioning and cell length in <i>B. subtilis</i> .....	75
<b>Figure 3.5.</b> Z ring positioning, growth rate and cell length of the alanine dehydrogenase mutant .....	81
<b>Figure 3.6.</b> Measurement of pyruvate levels in wild type (SU5), $\Delta pyk$ (SU6664), $\Delta pyk$ +1% pyruvate, $\Delta pyk$ +1% L-alanine and $\Delta ald$ (SU826) <i>B. subtilis</i> cells.....	83
<b>Figure 3.7.</b> Investigation of the interaction between pyruvate and FtsZ using triple-ligand detect (TLD) NMR.....	87
<b>Figure 4.1.</b> The effect of <i>minCD</i> deletion on Z ring positioning of $\Delta pyk$ cells .....	100
<b>Figure 4.2.</b> The effect of <i>noc</i> deletion on the Z ring positioning of $\Delta pyk$ cells .....	106
<b>Figure 4.3.</b> Quantitative analysis of the nucleoid morphology of wild-type and $\Delta pyk$ .....	108
<b>Figure 4.4.</b> Analysis of the frequency of DNA replication initiation in wild-type (SU492), $\Delta pyk$ (SU679) and $\Delta pyk$ + 1% pyruvate using marker frequency analysis .....	111
<b>Figure 4.5.</b> Analysis of the frequency of DNA replication initiation in wild-type (SU492), $\Delta noc$ (SU657) and $\Delta noc \Delta pyk$ (SU877) using marker frequency analysis.....	114
<b>Figure 5.1.</b> PCA analysis of different experimental groups .....	125
<b>Figure 5.2.</b> Heat maps combined with hierarchical clustering using a dendrogram.....	127
<b>Figure 5.3.</b> Pie chart demonstrating the percentage share of different biological processes differentially expressed in $\Delta pyk$ cells .....	131
<b>Figure 5.4.</b> A Venn diagram representing the number of differentially expressed genes overlapping under different experimental conditions.....	151
<b>Figure 5.5.</b> The siderophore and pyrimidine synthesis gene clusters differentially expressed in the <i>pyk</i> mutant.....	154

---

<b>Figure 5.6.</b> The effect of <i>pyrE</i> deletion on Z ring positioning.....	160
<b>Figure 5.7.</b> The effect of <i>pyrR</i> deletion on Z ring positioning.....	163

---

## **List of Tables**

<b>Table 1.1.</b> Proteins involved in positive and negative regulation of Z ring positioning in diverse bacterial genera.....	14
<b>Table 2.1.</b> Commonly used buffers and solutions .....	40
<b>Table 2.2.</b> <i>B. subtilis</i> strains .....	41
<b>Table 2.3.</b> <i>B. subtilis</i> growth media .....	42
<b>Table 2.4.</b> Antibiotics used for selection in <i>B. subtilis</i> .....	42
<b>Table 2.5.</b> Primers used for PCR reaction, Gibson assembly and Marker frequency analysis .....	47
<b>Table 3.1.</b> The effect of different metabolites on the doubling time and Z ring positioning in $\Delta pyk$ cells.....	68
<b>Table 3.2.</b> Types of nucleoid morphologies observed under different experimental conditions and their correlation with Z ring positioning.....	77
<b>Table 4.1.</b> Frequencies of polar and non-polar acentral Z rings in different strains.....	103
<b>Table 5.1.</b> The number of differentially expressed genes under each experimental condition .....	129
<b>Table 5.2.</b> Functional groups differentially expressed in the <i>pyk</i> mutant in comparison to the wild type cells.....	133
<b>Table 5.3.</b> Differential expression of selected pathways in the <i>pyk</i> mutant.....	150
<b>Table 5.4.</b> Relative abundance of pyrimidine synthesis gene transcripts in $\Delta pyk$ as compared to wild type <i>B. subtilis</i> cells.....	158



---

## **List of appendices**

### **Appendix I**

<b>Figure 1.</b> The effect of L-valine on the Z ring positioning of $\Delta pyk$ cells .....	186
<b>Figure 2.</b> The effect of L-leucine on the Z ring positioning of $\Delta pyk$ cells .....	187
<b>Figure 3.</b> The effect of acetate on the Z ring positioning of $\Delta pyk$ cells.....	189
<b>Figure 4.</b> The effect of acetoin on the Z ring positioning of $\Delta pyk$ cells .....	190
<b>Figure 5.</b> The effect of L-lactate on the Z ring positioning of $\Delta pyk$ cells.....	192
<b>Figure 6.</b> The effect of D-alanine on the Z ring positioning of $\Delta pyk$ cells .....	193
<b>Table 1.</b> The effect of different metabolites on the doubling time of wild type cells.....	194

### **Appendix II**

<b>Table 1.</b> Comparing the RNA-Seq transcriptomes of pyruvate kinase mutant with the addition of pyruvate (1%) (pykP) and wild type <i>B. subtilis</i> cells.....	195
--	-----

---

# Publications and Awards

## Awards

New Horizons Young Investigator **Popular Choice award** 2018

New South Wales semi-finalist for **Fame Lab** 2018

Australian Society of Microbiology **Becton Dickinson award** 2017

## Journal articles

**Mann R**, Mediati DG, Duggin IG, Harry EJ and Bottomley AL (2017) Metabolic Adaptations of Uropathogenic *E. coli* in the Urinary Tract. *Front. Cell. Infect. Microbiol.* 7:241

**Mann R**, Monahan L, Harry E and Bottomley A (2017) We Are What We Eat: True for Bacteria Too. *Front Young Minds.* 5:54

Kusrini E, Hashim F, Gunawan C, **Mann R**, Noor Azmi WNNW, Amin NM (2018) Anti-amoebic activity of acyclic and cyclic-samarium complexes on *Acanthamoeba*. *Parasitol. Res.*, 117(5):1409-1417

**Mann R** (2017) We are what we eat: Metabolic control of the division process in bacteria. *ASM Syntrophy.* 18:4

---

## **Conference proceedings\***

Mann R, Bottomley A, Monahan L and Harry E - *New Horizons 2018 (November 19-20), Sydney, Australia* - **Oral presentation** - “We are what we eat: Identifying a regulatory crosstalk between central carbon metabolism and cell division in bacteria”

Mann R, Bottomley A, Monahan L, Sonenshein A and Harry E - *ComBio 2018 (September 23-26), Sydney, Australia* – **Poster teaser oral and poster presentation** - “We are what we eat: Connecting central carbon metabolism to cell division in *Bacillus subtilis*”

Mann R, Bottomley A, Monahan L, Sonenshein A and Harry E - *Gordon Research Conference on Microbial stress response 2018 (July 15-20), Massachusetts, United States* – **Poster presentation** - “We are what we eat: Identifying a regulatory crosstalk between central carbon metabolism and cell division in bacteria”

Mann R, Bottomley A, Monahan L, Sonenshein A and Harry E - *Gordon Research Seminar on Microbial stress response 2018 (July 14-15), Massachusetts, United States* – **Oral and poster presentation** - “We are what we eat: Identifying a regulatory crosstalk between central carbon metabolism and cell division in bacteria”

Mann R, Bottomley A, Monahan L, Sonenshein A and Harry E - *Gordon Research Conference on Bacterial Cell Surfaces 2018 (June 24-29), Mount Snow, West Dover, United States* – **Oral and poster presentation** - “We are what we eat: Identifying a regulatory crosstalk between central carbon metabolism and cell division in bacteria”

---

Mann R, Bottomley A, Monahan L, Sonenshein A and Harry E - *Gordon Research Seminar on Bacterial Cell Surfaces 2018 (June 23-24), Mount Snow, West Dover, United States* – **Oral and poster presentation** - “We are what we eat: Identifying a regulatory crosstalk between central carbon metabolism and cell division in bacteria”

Bottomley A, Mann R, Sonenshein A, Monahan L and Harry E - *ComBio 2017 (October 2-5), Adelaide, Australia* – **Poster presentation** - “We are what we eat: Identifying a regulatory crosstalk between central carbon metabolism and cell division in bacteria”

Mann R, Bottomley A, Monahan L and Harry E - *Australian Society of Microbiology Annual Scientific Meeting 2017 (July 2-5), Hobart, Australia* – **Oral presentation** - “We are what we eat: Identifying a regulatory crosstalk between central carbon metabolism and cell division in bacteria”

Bottomley A, Mann R, Sonenshein A, Monahan L and Harry E – *19<sup>th</sup> International Conference on Bacilli & Gram-Positive Bacteria 2017 (June 11-15), Berlin, Germany* – **Oral presentation** - “We are what we eat: Identifying a regulatory crosstalk between central carbon metabolism and cell division in bacteria”

Mann R, Bottomley A, Monahan L and Harry E – *6<sup>th</sup> Annual JAMS (Joint Academic Microbiology Seminars) Symposium 2017 (March 22), Australian Museum, Sydney, Australia* – **Poster presentation** - “We are what we eat: Identifying a regulatory crosstalk between central carbon metabolism and cell division in bacteria”

Mann R, Bottomley A, Monahan L and Harry E - *Third Annual Sydney Micro meeting 2017 (February 3), Sydney, Australia* – **Oral presentation** - “We are what we eat: Identifying a regulatory crosstalk between central carbon metabolism and cell division in bacteria”

Monahan L, Mann R, Bottomley A, Hajduk I, Harry E - *New Horizons 2015 (November 23-25), Sydney, Australia* – **Poster presentation** - “Coordinating bacterial cell division with nutrient availability: a role for glycolysis”

\*The presenting author is underlined

---

## Abbreviations

---

AGRF	Australian Genome Research Facility
Ab	Antibody
<i>B.</i>	<i>Bacillus</i>
bp	Base pair (s)
BP	Band pass
BSA	Bovine serum albumin
CAA	Casamino acids
<i>cat</i>	Chloramphenicol
cm	Centimetres
CCD	Charged coupled device
DAPI	4'6-diamidino-2-phenylindole
DNA	Deoxyribonucleic acid
<i>E.</i>	<i>Escherichia</i>
EDTA	ethylenediaminetetraacetic acid
<i>erm</i>	Erythromycin
<i>et al.</i>	and others
<i>fts</i>	Filamentation temperature sensitive
<i>g</i>	Centrifugal force
g	Gram (s)
GFP	Green fluorescent protein
GTP	guanosine 5'-triphosphate
h	Hour (s)
IFM	Immunofluorescence microscopy
IgG	Immunoglobulin G
IPTG	Isopropyl-1-thio- $\beta$ -D-galactopyranoside
<i>kan</i>	Kanamycin
kb	Kilobase pair (s)
L	Litre (s)
LP	Long pass
M	Moles per litre
min	Minute (s)

---

---

MQW	Milli-Q purified water
MSA	Mineral salts A
NA	Numerical aperture
N/A	Not applicable
OD <sub>x</sub>	Optical density at (x refers to the wavelength in nm)
P <sub>xyI</sub>	Xylose-inducible promoter
PBS	Phosphate buffered saline
PCR	Polymerase chain reaction
pH	Power of hydrogen
RNA	Ribonucleic acid
RNase	Ribonuclease A
ROW	Reverse osmosis purified water
rpm	Revolutions per minute
RT	Room temperature
SDS	Sodium dodecyl sulfate
SEM	Standard error of the mean
spp.	Species
<i>spec</i>	Spectinomycin
TBAB	Tryptose blood agar base
TE	Tris-EDTA buffer
TES	Tris-EDTA-salt buffer
<i>tet</i>	Tetracycline
Tris	Tris(hydroxymethyl)methylamine
ts	Temperature sensitive
UV	Ultraviolet
V	Volt (s)
v/v	Volume per volume
w/v	Weight per volume
YFP	Yellow fluorescent protein
μ	Micro (10 <sup>-6</sup> )

---



# Chapter 1

---

## Introduction



---

## 1.1 Preface

In contrast to pure cultures studied in the laboratory, bacteria in the ‘real world’ inhabit a huge range of environmental niches and are subjected to constantly changing environments of varying nutrient availability (Lok 2015). These titanic and sudden changes necessitate a bacterial cell to rapidly adapt to the changing situation by accurately coordinating its cell-cycle processes like metabolism, DNA replication, cell growth, size and division (Fantes and Nurse 1977; Boye and Nordström 2003; Jonas 2014; Song et al. 2017). This is essential for bacteria to survive, competitively persist and produce viable daughter cells with the correct genetic complement. How bacteria adapt to these changes of differing nutritional conditions via adjusting their cellular processes is a fundamentally important but thus far unsolved question. Bacterial metabolism, including central carbon metabolism and accessory pathways, has emerged as the key player in transmitting nutritional information in the form of metabolic signals to the cell division machinery (Haeusser and Levin 2008; Wang and Levin 2009). Recent studies have revealed the moonlighting roles of several metabolic enzymes, which in addition to their primary enzymatic functions play a second role of interacting with and thereby regulating other bacterial cell-cycle processes (Jeffery 2009; Heinemann and Sauer 2010). Considering the intertwined functionality of biochemical pathways, systematic protein-protein interaction studies are expected to identify more metabolic enzymes with this kind of dual role within the bacterial cell (Commichau et al. 2009).

The link between individual bacterial processes of cell growth, cell size, DNA replication, cell division and metabolism has long been investigated (Jannièrè et al. 2007; Weart et al. 2007; Chien et al. 2012a, b; Murray and Koh 2014), but the broader picture of how bacterial cell-cycle events are controlled as a whole is still unclear. This work, via studying the mechanisms that coordinate cell division with central carbon metabolism in a soil bacterium

*Bacillus subtilis*, aims to move one step closer in answering this outstanding question. *B. subtilis* is a well-studied Gram-positive bacterium, which serves as a model organism for lab research. This would help us understand the mechanisms that enable bacteria to rapidly adjust to fluctuating environmental conditions. The outcomes of this work could eventually provide us with new targets for drug discovery, an urgent need in view of emerging antibiotic resistance in today's scenario. This research finds potential to be extrapolated to bacterial pathogens and would further find implications in understanding the metabolic mechanisms that these pathogens embark on for their persistence within the human body.

## **1.2 The Bacterial Cell Cycle**

The bacterial cell cycle, unlike eukaryotes, is not divided into distinct stages and the cellular processes such as growth, DNA replication, chromosome segregation and the assembly of division machinery overlap each other in time (Chien et al. 2012a). In *B. subtilis* the amount of available nutrients governs the choice of two types of life cycles: the vegetative cell cycle and sporulation (Figure 1.1).

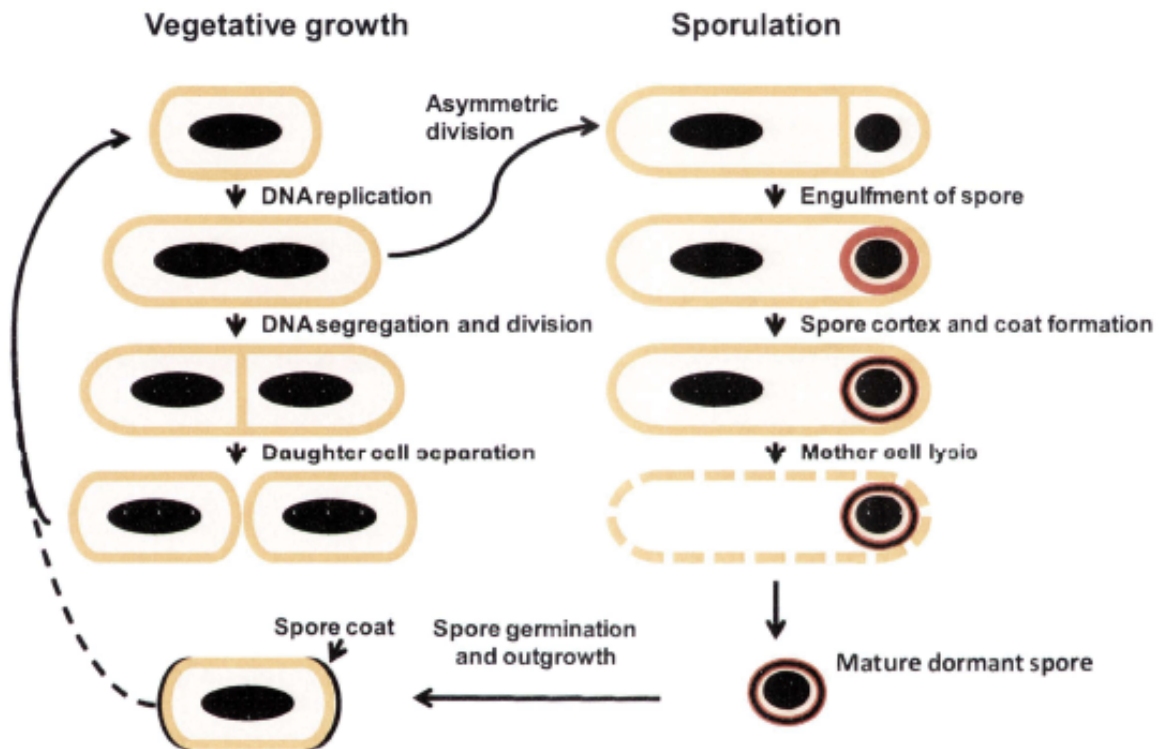


**Figure 1.1. The life cycle of *B. subtilis*.** Vegetative growth occurs when nutrients are readily available, producing two identical daughter cells (left). Under nutrient starvation conditions *B. subtilis* cells enter an alternative cycle called sporulation, which results in the formation of dormant structures known as spores (right). During the latter type of cell cycle, asymmetric division close to one of the cell poles produces a smaller compartment called the forespore that matures and forms a spore. The dormant spore is eventually released by the mother cell, germinates in the presence of nutrients and enters the vegetative growth cycle [Reproduced from (Rodrigues 2011)]

When nutrients are freely available, *B. subtilis* undergoes normal vegetative growth. During this type of growth, rod-shaped cells elongate along the longitudinal axis of the cell until it has doubled in length, followed by formation of a centrally-located septum which eventually produces two genetically and morphologically identical daughter cells (Errington and Daniel 2002; Eichenberger 2012; Leggett et al. 2012).

---

*B. subtilis* cells show a complex adaptive response to nutrient starvation and undergo a major developmental change, giving rise to a dormant spore (Figure 1.1) (Eichenberger 2012; Higgins and Dworkin 2012). Under the conditions of nutrient scarcity, the vegetative cell undergoes asymmetric septum formation near one cell pole, producing two compartments- the forespore and the mother cell (Errington 2003; Thompson et al. 2006). The mother cell lyses to release the dormant spore, which germinates under nutrient-favourable environment, outgrow and re-enters the vegetative lifecycle (Smith and Foster 1995; Errington and Daniel 2002). Although the mechanisms of response to nutrient levels vary between bacterial species, certainly all bacteria are capable of adjusting their cell cycle to accommodate the fluctuating nutrient levels.

### 1.3 Bacterial Cell Division

Bacterial cell division is a crucial process to ensure survival, development and continual existence of these living organisms. It initiates with the selection of division site, followed by invagination of the cell envelope layers between two chromosomes and ends with the separation into two daughter cells (Figure 1.2) (Errington et al. 2003; Lock and Harry 2008; Monahan et al. 2014b, a). There are two modes of division in rod-shaped bacteria based on the process of cellular constriction and the timings at which different events occur. In *E. coli*, the hydrolysis of cell wall and the separation of cell into two daughter cells occur simultaneously with the synthesis of division septum, this process is called ‘constriction’. As a different mechanism in *B. subtilis* a new peptidoglycan cross wall called the septum first divides the cell into two equal parts, which is followed by the sequential hydrolysis of cell wall that separates the cell into two daughter cells. This process of division in *B. subtilis* is known as ‘septation’. The division septum in *B. subtilis* gets degraded and remodelled to form the hemi-spherical

cell poles of the newly formed daughter cells. (Errington et al. 2003; Goehring and Beckwith 2005; Adams and Errington 2009).

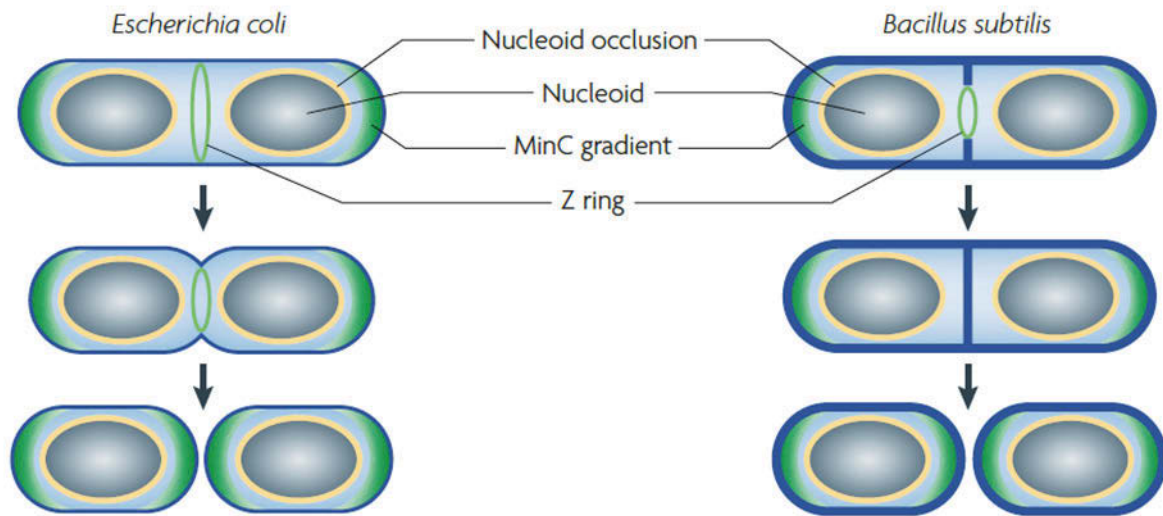


**Figure 1.2. Cell division in rod-shaped bacteria- *E. coli* and *B. subtilis*.** Two different modes of division occur in *E. coli* and *B. subtilis*. In *E. coli*, the formation of division septum and cell wall constriction occur simultaneously; whereas in *B. subtilis*, the division septum first divides the cell into two equal parts. This is followed by the hydrolysis of cell wall, which separates the cell into two daughter cells. [Adapted from (Adams and Errington 2009)]

### 1.3.1 The divisome

Cell division is mediated by a multi-protein apparatus known as the divisome (Rowlett and Margolin 2015b). In *E. coli* and *B. subtilis*, the first protein to localize at the division site is FtsZ, which then recruits other constituent proteins of the division apparatus to form the divisome (Adams and Errington 2009) (Figure 1.3). Detailed descriptions of each protein will not be discussed here; however, some crucial functions of these proteins include the formation and stabilisation of the Z ring, recruitment and stabilisation of downstream divisome proteins, maintenance of the Z ring dynamics and involvement in septum formation. For further details on the functions of divisome proteins, refer to the review articles by Haeusser and Margolin

2016, and Adams and Errington 2009 (Goehring and Beckwith 2005; Lock and Harry 2008; Robichon et al. 2008; Adams and Errington 2009; de Boer 2010).

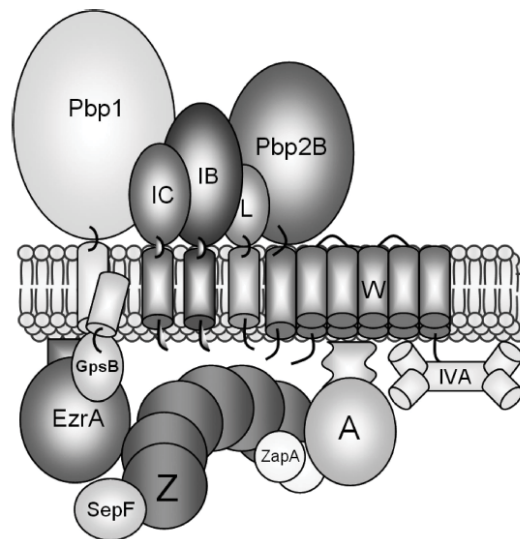


**Figure 1.3. Schematic representation of the *B. subtilis* divisome.** For simplification, protein names have been abbreviated by removing Fts and Div. Following FtsZ recruitment and the initiation of Z ring assembly at midcell division site, the newly-formed Z ring serves as a scaffold for the assembly of at least 12 other proteins required for division, together forming a complex called the divisome. This is followed by the constriction of Z ring, and sequential synthesis of cell wall and membrane to form a septum. Eventually the cell gets separated into two identical daughter cells. [Reproduced from (Gamba et al. 2009)]

The divisome assembles before the formation of septum and it disassembles in a coordinated fashion when the septation process is complete (Errington et al. 2003; Aarsman et al. 2005; Daniel et al. 2006; Goehring et al. 2006; Lock and Harry 2008; Gamba et al. 2009; Söderstrom et al. 2016). Divisome disassembly occurs simultaneously with the cell wall and membrane synthesis, eventually leading to the production of two identical daughter cells.

### 1.3.2 FtsZ protein and the assembly of the Z ring

FtsZ is the most widely conserved division protein, found in almost all eubacteria, most archaea and eukaryotic organelles - mitochondria and chloroplasts (Beech et al. 2000; Vitha et al. 2001; Vaughan et al. 2004; Weiss 2004; Adams and Errington 2009). It is a tubulin-like cytoplasmic protein that exhibits GTPase and GTP-dependent polymerization activity (Erickson et al. 1996; Löwe and Amos 1998, 1999; Romberg et al. 2001; Erickson 2007). Polymerization of FtsZ as a contractile Z ring (Figure 1.4) at the inner cytoplasmic membrane surface is the earliest event in bacterial cell division. Individual subunits of FtsZ polymerizes cooperatively and reversibly in a GTP-dependent manner in head-to-tail fashion to form protofilaments (Mukherjee and Lutkenhaus 1994; Erickson et al. 1996; Löwe and Amos 1999; Lu et al. 2000; Harry et al. 2006; Adams and Errington 2009). Several of these FtsZ protofilaments associate laterally to form the Z ring (Lu et al. 1998). The Z ring plays a key role in coordinating the entire process of division by marking the position of future division site and by contracting to provide signal for division at later stages of the cell cycle (Ma et al. 1996; Errington et al. 2003; Goehring et al. 2006; Adams and Errington 2009; Gamba et al. 2009; de Boer 2010; Erickson et al. 2010; Xiao and Goley 2016) (Figure 1.5).

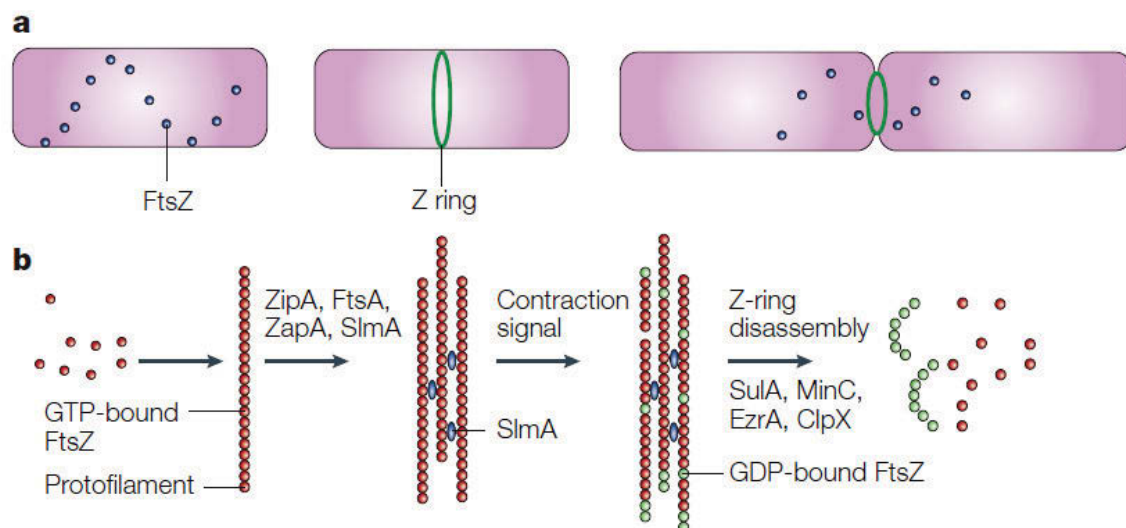


**Figure 1.4. Formation and disassembly of the Z ring in *E. coli*.** a) FtsZ is present in spiral patterns in a newly born cell. As the cell grows, these FtsZ subunits start forming protofilaments and polymerizes as a Z ring. This ring contracts when the cell needs to divide into two daughter cells. b) GTP-bound FtsZ dimers indicated as red dots assemble into protofilaments. Proteins like ZapA, ZipA, SlmA (nucleoid occlusion protein in *E. coli*-discussed in the next section of this review) and FtsA bundle the protofilaments together and anchor the Z ring to the cytoplasmic membrane. The exact signal for ring contraction is unknown but GTP hydrolysis might be a contributing factor to it [Reproduced from (Margolin 2005)]

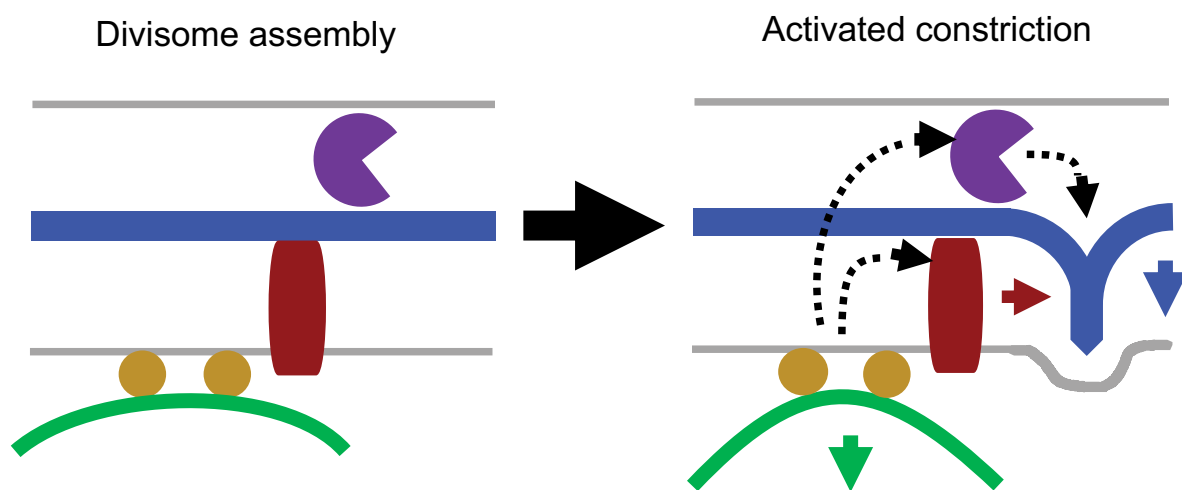


**Figure 1.5. The combined action of FtsZ and peptidoglycan metabolism in driving cell division.** Left: Z ring (green line) assembles close to the cell membrane through interactions with membrane tethering proteins (yellow). This is the initiation of divisome assembly as well the activation of peptidoglycan synthesis machinery (red) and its hydrolysis (purple Pac man). Right: Z ring generates a moderate force (green arrow), which is sent as a signal (black dashed arrows) to the peptidoglycan synthesis and hydrolysis factors. These factors provide directionality to the synthesis of invaginating septum (blue line), drives the inner membrane and provides the force for constriction (blue arrow) [Adapted from(Xiao and Goley 2016)]



---

While regulating the cell division process, the formation of Z ring is itself under the control of many cellular signals. These signals include regulatory proteins involved in spatio-temporal control of the Z ring formation. Moreover, a comparatively less attended area remains the role of other bacterial processes like DNA replication and metabolism in controlling the division process. The likelihood of this type of regulation is supported by the integrated nature of biochemical pathways. There are evidences for the connection between DNA replication and central carbon metabolism (Janni re et al. 2007; Maciag et al. 2012) as well as between DNA replication, chromosome segregation, nucleoid position and cell division (Maciag-Dorszyńska et al. 2012; Hajduk et al. 2016). These other bacterial processes can have novel roles in controlling the formation of the Z ring directly or indirectly by guiding the function of regulatory proteins via some signals.

## **1.4 Spatio-temporal regulation of bacterial cell division**

The division process is governed by numerous spatial and temporal regulators (Margolin 2005) involved in the tight control of Z ring positioning (Ryan and Shapiro 2003; Weart and Levin 2003). There are both ‘negative’ and ‘positive’ regulators. Negative regulators inhibit the assembly of Z ring at inappropriate sites while the positive regulators support this assembly at the appropriate midcell site.

### **1.4.1 Negative and positive regulators of the Z ring placement**

The two well-studied negative regulatory systems in *E. coli* and *B. subtilis* are the Min system and the nucleoid occlusion. The combined effect of these two systems prevents the Z ring formation at inappropriate sites within the cell, thereby allowing assembly only at midcell (Reeve et al. 1973; Teather et al. 1974; de Boer et al. 1989; Harry 2001; Harry et al. 2006;

Rowlett and Margolin 2015a; Hajduk et al. 2016; Monahan and Harry 2016) (Figure 1.6). Nucleoid occlusion prevents the Z ring assembly over the nucleoid and the Min system blocks unwanted potential division sites at the cell poles (Levin et al. 1998; Pichoff and Lutkenhaus 2001; Wu and Errington 2004; Bernhardt and De Boer 2005). The net effect of these two systems is that the Z ring forms only at midcell once the replicated chromosomes move away from this site (Weiss 2004; Monahan et al. 2014b). However, the Min system and nucleoid occlusion are themselves not responsible for identifying the division site, they only ensure the efficient utilization of midcell site. This suggests towards the existence of additional mechanisms for identification of the division site (Rodrigues and Harry 2012).

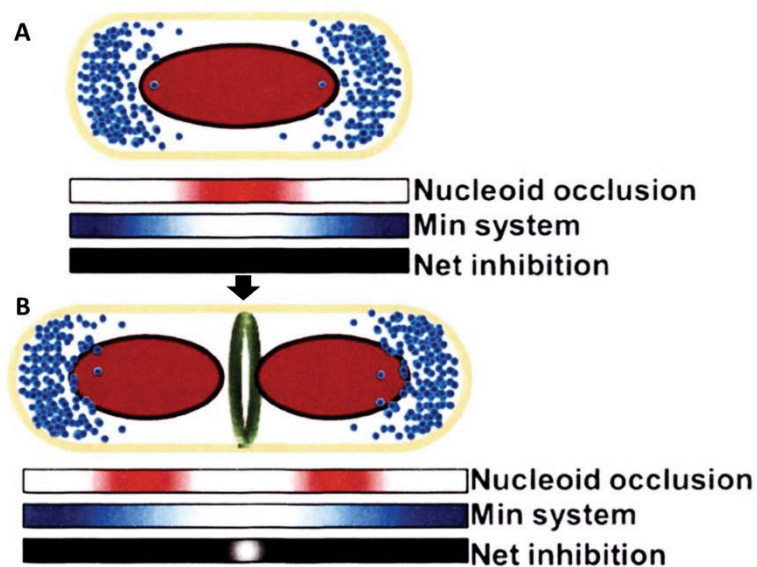


**Figure 1.6. Positioning of Z ring in *B. subtilis* and *E. coli* by the combined action of nucleoid occlusion and the Min system.** A) In the early stages of the cell cycle, the Min system (at the cell poles) and the nucleoid occlusion (at the cell centre) proteins together prevent the Z ring formation along the entire length of the cell. B) At the later stages during cell cycle progression, the chromosomes get segregated which creates a DNA-free region at midcell for the Z ring (in green) to be formed [Adapted from (Rodrigues 2011)]

In *E. coli*, the Min system comprises of three proteins: MinC, MinD and MinE; whereas in *B. subtilis*, four proteins named MinC, MinD, MinJ and DivIVA form the Min system. In both these organism, MinC, together with the membrane bound ATPase MinD, forms the MinCD complex that associates with the cytoplasmic membrane as a polymerized structure (Figure 1.7) (Errington et al. 2003; de Boer 2010) and acts as the negative regulator of the Z ring assembly (Bramkamp and Baarle 2009). In both *E. coli* and *B. subtilis*, MinC is the actual inhibitor of the Z ring assembly by interacting directly and destabilising FtsZ polymers; however, the mechanisms by which MinC is directed to the cell poles in these two bacteria are fundamentally different.

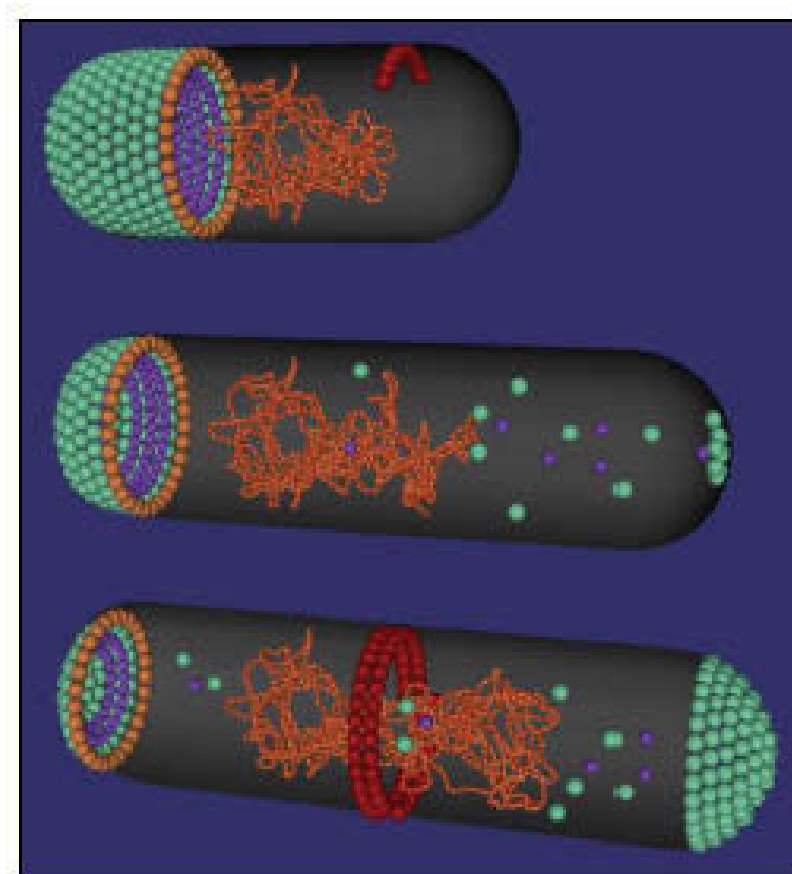


**Figure 1.7. Schematic model for the Z ring positioning in *E. coli* by the nucleoid occlusion and Min systems.** Upper illustration: inhibition of polar Z ring formation by the Min system and nucleoid occlusion. MinC (green) bound to MinD (purple) assembles on the cytoplasmic membrane and prevents the Z ring formation here. Middle illustration: During the course of cell cycle progression, MinE

---

(orange) displaces MinCD complex from the membrane. MinC and MinD subunits then reassemble at the other cell pole. Lower illustration: After the two daughter nucleoids have moved apart, the combined action of Min system and the nucleoid occlusion system targets the Z ring to the cell centre [Reproduced from (Vendeville et al. 2011)]

Nucleoid occlusion is mediated by proteins called Noc in *B. subtilis* and SlmA in *E. coli* (Wu and Errington 2004; Bernhardt and De Boer 2005; Harry et al. 2006; Adams et al. 2014; Monahan et al. 2014b). Both these proteins bind to specific DNA sequences and inhibit the Z ring assembly. These binding sequences are absent in the terminus region of chromosome (Wu et al. 2009). When the chromosome replication is near completion, these terminus regions of the chromosomes occupy midcell site. This prevents the binding of Noc and SlmA at this site and hence, the midcell site gets a relief from nucleoid occlusion for the Z ring formation after chromosome segregation (Wu and Errington 2004). SlmA interferes with FtsZ polymerization directly (Bernhardt and De Boer 2005), while the mechanism of action of Noc is not known (Monahan et al. 2014b). In a recent model suggested by Adams *et al.* (Adams et al. 2015), Noc in *B. subtilis* prevents the Z ring formation at the space in between DNA and the cell membrane by being physically present there. This model is, however, not conclusive and raises few questions. Is there a high enough abundance of Noc inside the cell to mediate this type of crowding effect? And, are there other additional proteins involved in mediating this Noc's crowding effect in between DNA and the cell membrane? (Hajduk et al. 2016).

As some bacteria can divide accurately in the absence of either Min or Noc system, this challenges their solitary role in regulating the correct placement of the Z ring (Hajduk et al. 2016). One example is of the  $\alpha$ -proteobacterium *Caulobacter crescentus*, which has a protein named MipZ playing a role similar to the Min system but has no homology with Min proteins (Thanbichler and Shapiro 2006). Additionally, there are regulatory proteins that are not well

conserved among bacterial genera but demonstrate roles in Z ring regulation under particular environmental cues. For instance the SOS response protein Sula that is active under DNA damage in *E. coli*, brings the division process to a stall by inhibiting the Z ring formation so as to give the cells sufficient time to repair the damage caused to DNA (Adams and Errington 2009). In addition to the negative regulation of the Z ring formation, regulators that promote the Z ring assembly at appropriate sites have also been identified. All the negative and positive regulatory systems operational in different bacterial genera are summarized in Table 1.1 and illustrated in Figure 1.8.

**Table 1.1. Proteins involved in positive and negative regulation of the Z ring positioning in diverse bacterial genera**

<b>Organism</b>	<b>Positive regulators</b>	<b>Negative regulators</b>
<i>E. coli</i>	Not known	Min system, nucleoid occlusion
<i>B. subtilis</i>	Not known	Min system, nucleoid occlusion
<i>Caulobacter crescentus</i>	MipZ (Thanbichler and Shapiro 2006)	Absence of Min and nucleoid occlusion (Pinho et al. 2013)
<i>Streptococcus pneumoniae</i>	MapZ or LocZ (Fleurie et al. 2014; Grangeasse and Lesterlin 2015; Holečková et al. 2015)	Absence of Min and nucleoid occlusion (Pinho et al. 2013)
<i>Myxococcus xanthus</i>	PomZ (Treuner-Lange et al. 2013)	Absence of Min, MipZ and SsgAB (Treuner-Lange et al. 2013)
<i>Streptomyces</i>	SsgA + SsgB (Traag and van Wezel 2008; Willemse et al. 2011)	Absence of Min and nucleoid occlusion (Willemse et al. 2011)

Positive regulators function by localizing to division site before FtsZ, thereby defining the site for the Z ring subunits to assemble (Hajduk et al. 2016). In *Streptococcus pneumoniae*, MapZ (Midcell Anchored Protein Z) or LocZ (Localising at midcell of FtsZ) is a positive regulator of FtsZ assembly. It localises before FtsZ at the future division sites, guides FtsZ positioning to this site and hence marks the division site (Fleurie et al. 2014; Grangeasse and Lesterlin 2015; Holečková et al. 2015). PomZ (Positioning at Midcell of FtsZ), a ParA-like protein, is a positive regulator of the Z ring positioning identified in *Myxococcus xanthus*. It localizes to midcell after chromosome segregation but prior to, and independently of, FtsZ (Treuner-Lange et al. 2013). In *Streptomyces*, SsgB is a membrane-associated divisome protein that directly recruits FtsZ to the division site and promotes FtsZ polymerization. After the recruitment of FtsZ at division site, SsgB remains associated with the divisome. The localization of SsgB in turn is mediated by the ortholog SsgA (Traag and van Wezel 2008; Willemse et al. 2011).

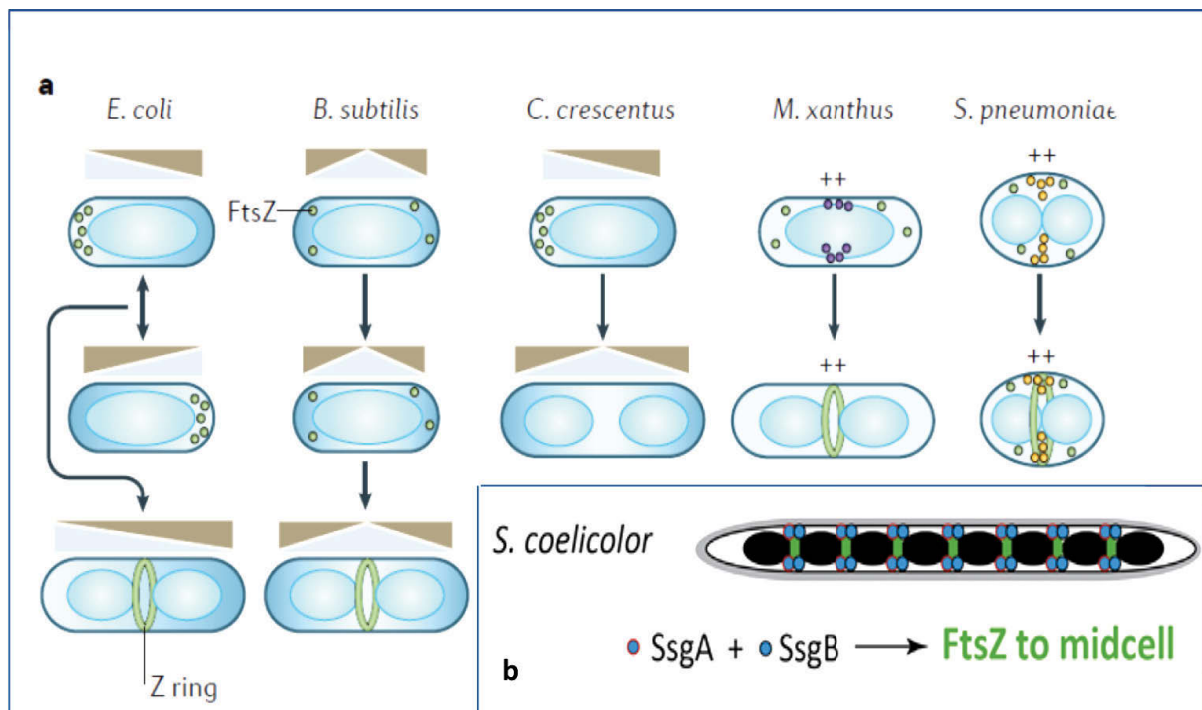


**Figure 1.8. Negative and positive regulators of the Z ring placement.** Distinct mechanisms for the correct positioning of the Z ring. (a) In *E. coli* and *B. subtilis*, the Min system and nucleoid occlusion

---

targets the Z ring to midcell. In the marine bacterium, *Caulobacter crescentus*, a protein called MipZ regulates the Z ring positioning via formation of a bipolar gradient. The positive regulators of the Z ring assembly in *Myxococcus xanthus* and *Streptococcus pneumoniae* guide the assembly of FtsZ subunits by localizing to midcell site before FtsZ [Adapted from (Haeusser and Margolin 2016)]. (b) In *Streptomyces coelicolor*, SsgA and SsgB directly recruits FtsZ to the division site [Adapted from (Hajduk et al. 2016)]

The enormous number of mechanisms guiding the Z ring assembly indicates the diversity of mechanisms controlling this process and signifies the importance of correct Z ring positioning in bacteria. Use of genetic and biochemical approaches as well as the recent advancements in super-resolution imaging, has improved our understanding of division regulation. However, the alterations in division process under different types of growth conditions still needs to be explored (Rowlett and Margolin 2015b). Another point to note is that the available knowledge about cell division regulation has come from studies performed under growth conditions where there are no fluctuations in nutrient availability. Hence, the mechanisms functional under nutrient fluctuating conditions need attention.

## **1.5 Bacterial cellular processes are interconnected**

Bacterial cell division is not only internally regulated but is also under the control of other cellular processes. This is necessary because the cell cycle events must remain coordinated under all situations for continued survival and persistence of bacterial population.

### **1.5.1 The early stages of DNA replication are connected to division site selection**

DNA replication is an ordered and tightly regulated process that occurs in three stages: initiation, elongation (DNA synthesis) and termination (Hajduk et al. 2016). Septum formation

must be tightly coordinated with replication and chromosome segregation to avoid damaging the genetic material and to ensure that each newborn cell receives a complete complement of the genetic material (Adams et al. 2014). For this to happen, there must be multiple regulatory pathways active within a bacterial cell for connecting DNA replication to other essential cellular activities (Murray and Koh 2014). In *E. coli*, the presence of an incompletely replicated DNA or unsegregated chromosome at midcell division site inhibits the assembly of Z ring independently of the nucleoid occlusion protein SlmA, indicating the connection between DNA replication and cell division (Cambridge et al. 2014). These two cellular processes are connected such that the division site gets increasingly potentiated for the Z ring formation with progression in initial stages of DNA replication and gets completely potentiated after completion of initiation of replication (Moriya et al. 2010). This indicates that the initial stages of DNA replication are linked to the selection of division site. However, the exact relationship between the early stages of DNA replication and division site selection needs to be explored. This involves the analysis of proteins present at the origin of replication for their role in division site selection.

### **1.5.2 Metabolism is not simply an energy engine**

Metabolism is not merely an engine for producing energy but is also steering many other processes. Feedback signals are fed from metabolism into other regulatory networks that govern important cellular decisions like cell growth and death (Gerosa and Sauer 2011). Metabolism is indeed believed to be more complex than all other cellular processes, influenced by regulatory actions at several cellular levels, controlling itself and feeding almost all other cellular systems (Heinemann and Sauer 2010). Glycolytic enzymes in particular are crucial for linking metabolism to other cellular events (Buchakjian and Kornbluth 2010). Moreover, recent breakthroughs in the area of moonlighting proteins functional in a bacterial cell demonstrate



---

that the metabolic information in the form of nutritional signals can be transmitted to the cell cycle machinery (Jeffery 2009).

## 1.6 Nutrient-dependent control of bacterial cell size

Nutritional reduction of bacterial growth rate by supplying poor growth medium has been shown to decrease the cell size in the fission yeast *Schizosaccharomyces pombe* (Fantes and Nurse 1977) and that the cell size of *Salmonella typhimurium* has been shown to be dependent on the composition of the growth medium (Schaechter et al. 1958). These observations elucidate the importance of nutritional status of a cell in deciding its size. Bacterial cells also respond to changing environment by adjusting their shape, which is outside the focus of this review [for more information, refer to the review by Sperber and Herman, 2017 (Sperber and Herman 2017)]

Bacterial cells under steady state conditions exhibit little variation in their average cell size (Weart et al. 2007). This suggests the existence of mechanisms precisely controlling cell division in a spatio-temporal manner, so that the cells by altering the length of their cell cycle can undergo transient increase or decrease in cell size to compensate for differing nutrient status. However, recent studies using single-cell microscopy have demonstrated that the bacterial cell size homeostasis is achieved by the cellular growth occurring to the same extent in between the division processes, irrespective of the cell length at birth (Campos et al. 2014; Taheri-Araghi et al. 2014). Hence, it becomes vital that the cell division is precisely coordinated with the growth rate, so that smaller cells are not produced because of division happening before the doubling of cellular mass. Division process should also not be delayed, as it can produce longer cells in rod-shaped bacteria (Chien et al. 2012a). These long cells would not be able to undergo division accurately and produce daughter cells lacking complete

---

genetic complement of the parent cell. Overall, small fluctuations in cell size are allowed but major variations are prevented by the action of strict cell size controlling mechanisms operational in a bacterial cell.

A study by Weart and colleagues from Petra Levin's lab in 2007 identified the first link between metabolism, cell size and division in bacteria (Weart et al. 2007). They showed that the nutrient-dependent changes in cell size are mediated in part by the direct interaction between an enzyme in the glucolipid biosynthesis pathway-UgtP and FtsZ in *B. subtilis* under conditions that promote rapid growth. UgtP is a glucosyltransferase enzyme that in addition to its role in glucolipid biosynthesis localizes to the cell division site under high nutrient conditions and inhibits the assembly of FtsZ. This mechanism is proposed to let sufficient time for replication and chromosome segregation under nutrient-rich conditions, such that a critical cell mass is reached before cytokinesis can occur. The role of UgtP in cell division depends on its interaction state: UgtP-UgtP or UgtP-FtsZ. The equilibrium between these two states is governed partly by the levels of UDP-glucose, the substrate of UgtP (Figure 1.9-left panel). While interacting with FtsZ (UgtP-FtsZ) under nutrient-rich conditions (high levels of UDP-glucose) it causes division inhibition leading to an increase in cell size, whereas under nutrient-poor conditions (low levels of UDP-glucose) it interacts with itself (UgtP-UgtP) and allows plenty of FtsZ to be available for assembly into the Z ring (Weart et al. 2007; Chien et al. 2012b). The resulting balance in equilibrium ensures that cell size remains coordinated with nutrient availability and growth rate in *B. subtilis* (Figure 1.9-right panel) (Chien et al. 2012b). The glucolipid biosynthesis pathway therefore, acts as a link between metabolism and cell division in *B. subtilis* (Weart et al. 2007; Chien et al. 2012b). This mechanism also helps to maintain a constant ratio of length per FtsZ ring regardless of the growth rate (Weart et al. 2007).

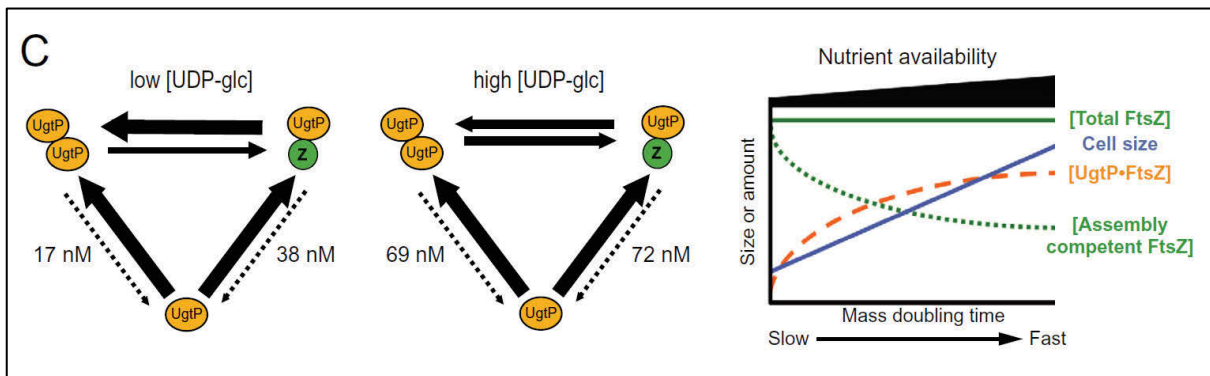


**Figure 1.9. Equilibrium between the two interaction states of UgtP (UgtP-UgtP and UgtP-FtsZ) influenced by UDP-glucose levels, functions as an intracellular signal to coordinate cell size with nutrient availability in *B. subtilis*.** Left panel: Under nutrient-poor conditions, low UDP-glucose levels favour UgtP-UgtP interaction. This increases the availability of FtsZ for assembly into the Z ring, allowing division to occur without hindrance and reducing the cell size. Under nutrient-rich conditions, increased levels of UDP-glucose shifts the equilibrium to the UgtP-FtsZ form, decreasing the amount of FtsZ available for the Z ring assembly, thereby increasing the cell size. Right panel: Graphical representation of the growth rate and nutrient-dependent regulation of cell size in *B. subtilis*. Green line depicts the constant cytoplasmic concentration of FtsZ regardless of the growth rate and the cell size, orange line shows that the increased intracellular UDP-glucose concentration increases the levels of UgtP available to interact with FtsZ [Adapted from (Chien et al. 2012b)]

Subsequent study published recently from the Levin's lab elucidated that the UgtP-dependent cell size control in *B. subtilis* is regulated by a post-translational mechanism involving the conditional proteolysis activity of ClpP protease (Hill et al. 2018). UgtP levels were observed to increase linearly with nutrient availability and growth rate when *B. subtilis* cells were grown in media of different nutritional standings. Further investigation revealed that a strain defective for ClpP protease did not show this decrease in UgtP levels when grown under nutrient-poor conditions, indicating that ClpP protease is somehow responsible for the decreased levels of UgtP observed in cells cultured in minimal medium (Hill et al. 2018). ClpP

---

is a serine protease that works in association with AAA+ ATPase Clp chaperones. These chaperones recognize the target protein, unfold it using the energy of ATP hydrolysis and translocate the unfolded polypeptide into the proteolytic chamber of ClpP (Baker and Sauer 2012). There are three known Clp chaperones (ClpC, ClpX and ClpE) in *B. subtilis*. Interestingly, all these three chaperones function redundantly in controlling the accumulation of UgtP in a growth-dependent manner in *B. subtilis*. In addition, the study showed that under nutrient-poor conditions, UgtP gets degraded by ClpXP complex via a direct interaction between this complex and UgtP, causing decreased UgtP levels. Due to the unavailability of UgtP, there is now plenty of freely available FtsZ to assemble as the Z ring, thereby resulting in decreased cell size (Hill et al. 2018). This additional level of regulation on UgtP apart from nutrient-mediated (dependent on UDP-Glucose) affinity towards itself, is to ensure that UgtP only accumulates under nutrient-rich conditions when its activity against cell division process is required and not under nutrient-poor conditions when its activity is not required (Hill et al. 2018).

UDP-glucose appears to be a well-conserved component of the nutrient-dependent cell-size control mechanisms in bacteria, as its role in coupling cell size to metabolism is also demonstrated in *E. coli*. This is consistent with the fact that synthesis of UDP-glucose (glycolipid synthesis pathway) requires precursors from the central carbon metabolic pathway, which is conserved in all bacteria, and it is likely to accumulate under nutrient-rich conditions. However, UDP-glucose is not a direct part of bacterial central carbon metabolic pathway. The integral inner-membrane protein OpgH, a glucosyltransferase, is identified as a nutrient-dependent regulator of cell-size in *E. coli*. In addition to its role in synthesizing osmoregulated periplasmic glucans (OPGs), it is also a UDP-glucose-activated inhibitor of the FtsZ ring formation that demonstrates no homology with UgtP from *B. subtilis*; instead they have distinct

---

enzymatic activities and inhibit FtsZ through a different biochemical mechanism. During rapid growth under nutrient-rich conditions or the abundance of UDP-glucose, UDP-glucose binds to OpgH causing a conformational change that reveals an FtsZ interaction site. OpgH then via its N-terminal domain interacts directly with FtsZ obstructing its assembly at the division site, delaying cell division, leading to an increase in cell size. This phenomenon reduces the availability of FtsZ for assembly into the cytokinetic ring. Cells increase in size until FtsZ accumulates to a sufficient FtsZ level to support the assembly of the Z ring. Nutrient-dependent changes in OpgH levels are proposed to be inversely proportional to the levels of available FtsZ subunits. On the contrary, under nutrient-poor conditions, OpgH assumes a conformation unfavourable for OpgH-FtsZ interaction causing FtsZ assembly to continue unimpeded, leading to reduced cell size (Hill et al. 2013).

It is critical to point out that under steady-state conditions neither *ugtP* nor *opgH* mutants exhibit any apparent defect in cellular growth pattern or the timing of Z ring assembly (Weart et al. 2007; Hill et al. 2013). Contrary to the role of OpgH and UgtP in coupling cell size to metabolism in *E. coli* and *B. subtilis* respectively, the UgtP homolog (*yfpP*) does not contribute to the cell size maintenance in *Staphylococcus aureus* and does not show the same localization dynamics as observed in *B. subtilis* (Reichmann et al. 2014). In fact, the YfpP protein is uniformly present throughout the cell membrane, instead of localizing at the cell division site as observed in *B. subtilis* (Weart et al. 2007; Reichmann et al. 2014). All these observations, along with the fact that the *ugtP* (*B. subtilis*) and *opgH* (*E. coli*) mutants still increase in size in response to an increase in nutrient availability, suggest that there must be other mechanisms active in these bacteria for coupling division to cellular growth so as to maintain a proper cell size (Monahan and Harry 2016).

---

A recent study by Vadia *et al.* demonstrated a positive relationship between fatty acid synthesis and cell size in bacteria (*Bacillus subtilis*, *E. coli*) and the yeast *Saccharomyces cerevisiae* (Vadia et al. 2017). Fatty acid availability via its effect on plasma membrane plasticity was identified to be the primary and conserved determinant of cell size in these organisms. An increase in fatty acid synthesis increased the cell size, whereas scarcity of fatty acids caused by using inhibitors of fatty acid synthesis decreased the cell size of these organisms in a dose-dependent manner. This decrease in cell size was rescued when exogenous fatty acids were added to the growth medium. Also, the cell size increase was observed to be directly linked to an increase in phospholipid content (plasma membrane plasticity) of the cells and a diversion of fatty acids from phospholipid synthesis counteracted this increase in cell size, thereby indicating towards a direct positive connection between cell size and fatty acid availability (Vadia et al. 2017).

Based on the above findings, the authors proposed a model wherein larger cell size observed under high-nutrient conditions is a result of altered balance between cell cycle progression and biosynthetic capacity of a cell (Vadia et al. 2017). The authors propose that during balanced growth, fatty acid synthesis is coupled to the cell cycle clocks such that there is regular addition of a constant volume to the cell in each generation. However, when the cells are shifted to a carbon-rich medium, there is an increase in the rate of fatty acid synthesis that is almost completely directed towards plasma and outer membrane synthesis, thereby altering the equilibrium between cell cycle progression and biosynthetic processes until a cell increases in size and a new equilibrium is attained between these two processes (Vadia et al. 2017).

Interestingly, the relation between cell size and nutrient availability was also observed to be retained in the cells defective for ppGpp synthesis (Vadia et al. 2017). ppGpp is a

---

guanosine tetraphosphate known to be a pleiotropic inhibitor of biosynthetic pathways and has been shown to correlate negatively with the bacterial cell size. Direct overexpression of the ppGpp synthase enzyme RelA has been shown to reduce the cell size as well as the growth of *E. coli* cells (Schreiber et al. 1995). As well, the accumulation of ppGpp by starving the cells of amino acids or by limiting their fatty acid synthesis process has also been shown to reduce the cell size and growth rate (Tehranchi et al. 2010; Yao et al. 2012; Pulschen et al. 2017). However, the observation of cell size-nutrient availability relation being maintained in the cells defective for ppGpp synthesis highlight the idea that fatty acid/lipid synthesis is the primary determinant of cell size maintenance rather than the alarmone ppGpp (Vadia et al. 2017). Instead, the authors suggest the role of ppGpp in coupling the fatty acid synthesis process to other biosynthetic processes within a bacterial cell (Vadia et al. 2017). Interestingly, the study by Yao *et al.* in 2012 also demonstrated the role of fatty acid biosynthesis in regulating the cell size of *E. coli* cells and found that an enzyme involved in fatty acid synthesis *fabH*, which is otherwise not essential in wild type cells, become essential in the cells defective for ppGpp synthesis (Yao et al. 2012).

Another study published very recently by the Levin lab undertook a high-throughput analysis approach to identify additional connections between central carbon metabolism and cell size in *E. coli* (Westfall and Levin 2018). Cells defective in 44 non-essential genes of the central carbon metabolic pathways were phenotypically analysed using the ImageJ software and their growth rate was monitored in order to identify the key steps of CCM that could have an impact on the growth and size of *E. coli*. The study revealed that rather than one primary factor dictating the cell size and morphology, indeed there are important roles of multiple metabolic nodes in determining the cell size and thereby shaping the morphology of *E. coli*

---

cells. These multiple metabolic nodes include the first branch point of glycolysis, acetyl-CoA metabolism and the pentose phosphate pathway.

In the above study, mutants of *crr*, encoding for the phosphotransferase system subunit EIIA involved in the glycolysis pathway, showed significant reduction in cell size and growth rate as compared to the wild type cells (Westfall and Levin 2018). Subsequent experiments demonstrated that these phenotypes shown by *crr* mutants are a result of cAMP synthesis defects, as the mutants of genes (*cyoA*, *crp*) involved in cAMP synthesis showed defects identical to the *crr* mutants. One of the other metabolic nodes identified in this study was the acetyl-CoA metabolism. Similar to *crr* mutants, cells perturbed in acetyl-CoA metabolism (*aceE*, *pta*, *ackA*) also showed reduced cell size and slower growth rates, which based on subsequent experiments was linked to the changes in fatty acid synthesis in these mutants. In addition, *aceE* or *ackA* deletions were also able to increase the viability of a temperature sensitive (*ftsZ84*) mutant of *ftsZ* by 10,000-fold (Westfall and Levin 2018). This mutant under non-permissive conditions is defective in FtsZ assembly and division, thereby causing filamentation and eventually cell death (Arjes et al. 2015). Also, loss of function mutations in *pta*, *tktA* and *crr* were also observed to mildly (100-fold) increase the viability of *ftsZ84*. *tktA* encodes for an enzyme transketolase belonging to the pentose phosphate pathway and cells defective in *tktA* also showed a significantly reduced cell size and slower growth rate, similar to *crr* (glycolysis) and acetyl-CoA metabolism mutants (Westfall and Levin 2018).

Overall, the study by Westfall and Levin in addition to demonstrating the roles of multiple nodes in coordinating metabolism to cell size in *E. coli*, also identified the key player – cAMP in maintaining the correct cell size in *E. coli*. Furthermore, the study also demonstrated that cAMP reduces the cell width under nutrient-poor conditions by impacting the morphogenic



---

factor BolA and cell length by having an impact on FtsZ assembly (Westfall and Levin 2018). *bolA* encodes for a transcription factor that inhibits *mreB* transcription (Yamamoto et al. 2000). *mreB* encodes for an important component of the cellular elongation machinery and therefore, any reductions in MreB activity leads to a block in lateral cell wall synthesis, leading to the production of wide and rounded cells (Divakaruni et al. 2007).

## 1.7 Metabolic control of bacterial cell division

FtsZ is an essential protein for bacterial cell division and therefore, construction of a null mutant of FtsZ is not possible. However, *ftsZ* null mutants in *E. coli* are shown to grow when complemented with foreign FtsZ upon acquisition of a suppressor mutation in some metabolic pathways, thereby suggesting a connection between the cell division and metabolism (Arkus Gardner et al. 2017). Furthermore, some metabolic enzymes are essential even under conditions when their enzymatic activity would not normally be required (Noirot-Gros et al. 2002), elucidating the ways by which proteins primarily devoted to metabolism link cell cycle advancement with nutrient availability. The other functions performed by these metabolic proteins involve their regulatory crosstalk with other fundamental non-metabolic pathways in the cell (Jeffery 2009), thereby assisting the coordination of bacterial cell cycle as a whole. Several metabolic enzymes with moonlighting roles have been identified in different bacterial genera (Figure 1.10), as explained below.

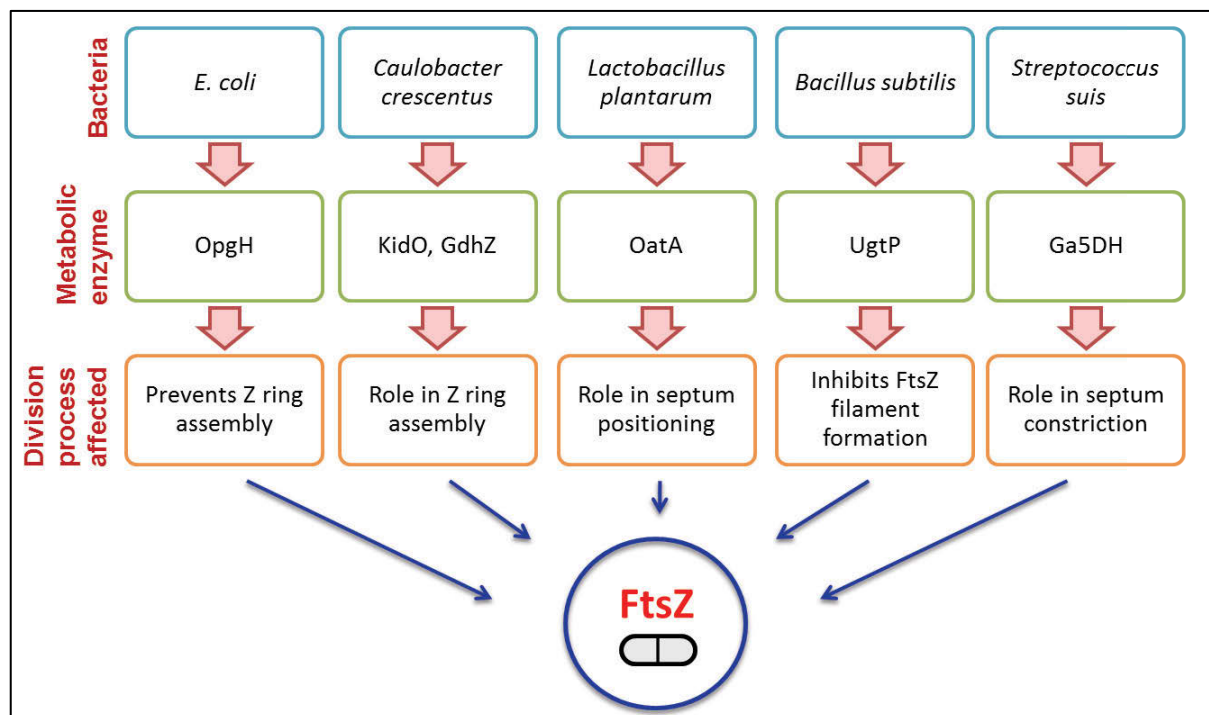


**Figure 1.10. Metabolic signals controlling the cell division process in various bacterial genera.**

Moonlighting functions of some metabolic enzymes identified in different bacterial genera (OpgH- glucosyltransferase, KidO- Kinase and division-regulating oxidoreductase homolog, GdhZ- glutamate dehydrogenase interacting with FtsZ, OatA-O-acetyltransferase, UgtP- UDP-glucose diacylglycerol glucosyltransferase, Ga5DH- Gluconate-5-dehydrogenase)

In the  $\alpha$ -proteobacterium *C. crescentus*, two proteins- GdhZ (glutamate dehydrogenase interacting with FtsZ) (Beaufay et al. 2015) and KidO (Kinase and division-regulating oxidoreductase homolog) (Radhakrishnan et al. 2010), are proposed to coordinate cell division with the cellular metabolic status. GdhZ is the FtsZ associated form of the metabolic enzyme- glutamate dehydrogenase (GDH) and *gdhZ* loss-of-function mutants had a strong growth defect and the cells were elongated and branched, a typical cell division defect observed in bacteria growing from one pole. The anti-FtsZ activity of GdhZ and KidO depends on their substrate binding, which suggests that this regulatory pathway is controlled by the nutritional status of the cell (Monahan and Harry 2016). Both these proteins function in synergy to prevent the

---

premature assembly of the Z ring in early cell cycle stages and stimulate the disassembly of the Z ring at later stages of the cell cycle when the divisome needs to constrict for cytokinesis. However, the underlying molecular mechanisms to accomplish this task are distinctly different. GdhZ causes Z ring disassembly by stimulating the GTPase activity of FtsZ and KidO causes the Z ring disassembly in a NAD (H)-dependent manner by disrupting the higher order lateral interactions that hold FtsZ polymers together (Beaufay et al. 2015).

The metabolic role of GDH (glutamate dehydrogenase) is to catalyze the interconversion of glutamate to  $\alpha$ -ketoglutarate, thereby bridging the nitrogen cycle and TCA cycle. It is suggested that high GDH activity, and therefore, ample nutrients, could be sensed as a signal by the cell division apparatus to allow the generation of daughter cells (Beaufay et al. 2015). Considering the observation that cell division defects in *gdhZ* mutants can be suppressed by adding other carbon sources like xylose and glucose, which do not require the enzymatic activity of GdhZ, suggests the existence of other metabolic components controlling cell division in *C. crescentus* (Monahan and Harry 2016). Furthermore, the cell division controlling function of GdhZ has also been shown to be conserved in the facultative intracellular pathogen *Brucella abortus* (Beaufay et al. 2016). Similar to the observation in *C. crescentus*, *B. abortus*  $\Delta$ *gdhZ* mutant displayed growth defects in complex growth medium with cells being slightly longer and branched. These growth and division defects were however rescued when glucose or xylose was supplemented to the growth medium. Altogether, these results suggest that the cell division controlling role of GdhZ is conserved in *B. abortus* and more likely in other  $\alpha$ -proteobacteria as well (Beaufay et al. 2016).

The metabolic enzyme Gluconate-5-dehydrogenase (Ga5DH) is important in maintaining the correct cell shape in the emerging zoonotic pathogen *Streptococcus suis* (Shi

---

et al. 2014). Ga5DH catalyzes the inter-conversion of D-gluconate and 5-ketogluconate with simultaneous generation of a hydrogen donor (NADPH) for many biosynthetic processes. Ga5DH deprivation leads to aberrant Z ring formation, increased cell length, presence of non-constricted septa and reduced growth rate. Complementation of the *ga5dh* gene restores normal Z ring localization pattern, normal cell length and partially restores the growth defect. Further, Ga5DH is shown to localize to the division site and is capable of interacting with FtsZ *in vitro*. These observations suggest the involvement of Ga5DH in coordinating cell division with metabolism in this pathogen and indicate the role of Ga5DH in septum constriction. However, whether Ga5DH has a direct impact on FtsZ localization and subsequent division process or this is accomplished by an indirect effect on the Z ring formation, still remains to be investigated (Shi et al. 2014). Since Ga5DH influences cellular morphology, it might be due to its effect on cell wall (peptidoglycan) synthesis, which produces non-constricting septa in *ga5dh* mutant cells.

A link between peptidoglycan synthesis and septum positioning has been shown in *Lactobacillus plantarum*. This involves the membrane-bound O-acetyltransferase OatA, which catalyzes the acetylation reaction in peptidoglycan, and also demonstrates the capacity to act as an important roleplayer in the division process (Bernard et al. 2012). In *L. plantarum*, OatA protein is needed for uncoupling the elongation and septation phases of the cell cycle, by localizing to the septum site, where it interferes with the septum positioning. This occurs via an appropriate inhibition of the division process by the Min system. Overall, OatA is involved in the spatio-temporal recruitment of the divisome complex at midcell by localizing to the midcell site during the early stages of the division process and interfering with the septum positioning, leading to the formation of aberrant septa. Hence, OatA appears to act as an important player in deciding the readiness to divide in *L. plantarum*.

---

### 1.7.1 Connection of central carbon metabolism (CCM) to cell division

Cell division must remain coordinated with other cellular processes for the viability of newborn daughter cells. Central carbon metabolism, being the entry point for almost all the raw materials required for cellular growth and proliferation, forms the hub for coordinating nutrient availability to cell growth, size and the division process (Westfall and Levin 2018). The first study to identify the link between bacterial cell division and the central carbon metabolic pathway of glycolysis was conducted by Monahan *et al.* in 2014 (Monahan et al. 2014a). This study showed that a key metabolic enzyme- pyruvate dehydrogenase - positively regulates the process of Z ring assembly in *B. subtilis* in a nutrient-dependent manner.

Central carbon metabolism is essential for a cell to produce precursors for the synthesis of cellular building blocks and to generate energy for cellular processes. Changes in flux through CCM are known to impact cell cycle progression as well as cell growth such that the cell size of daughter cell produced after division remain sensitive to changes in nutrient availability (Westfall and Levin 2017). Interestingly, the study by Monahan and colleagues showed that pyruvate, produced in the final step of the central carbon metabolic pathway of glycolysis by an enzyme-pyruvate kinase (*pyk*), regulates midcell Z ring formation and is therefore, a key metabolite in coordinating cellular metabolic levels to bacterial division machinery [Figure 1.11 (I)]. Cells lacking the enzyme *pyk* formed 1/3 of the Z rings at cell poles, in contrast to wild type cells where Z rings form at midcell [Figure 1.11 (II)]. These cells occasionally showed the formation of multiple Z rings with a Z ring forming at midcell and one at each cell pole [Figure 1.11 (II)]. The acentral Z ring positioning defect of the *pyk* mutant was alleviated when pyruvate was added to the growth medium [Figure 1.11 (III)]. These results pointed out that the enzyme pyruvate kinase is not itself involved in mediating the

assembly of the Z ring, rather pyruvate (or a downstream metabolite) is involved in this process (Monahan et al. 2014a).

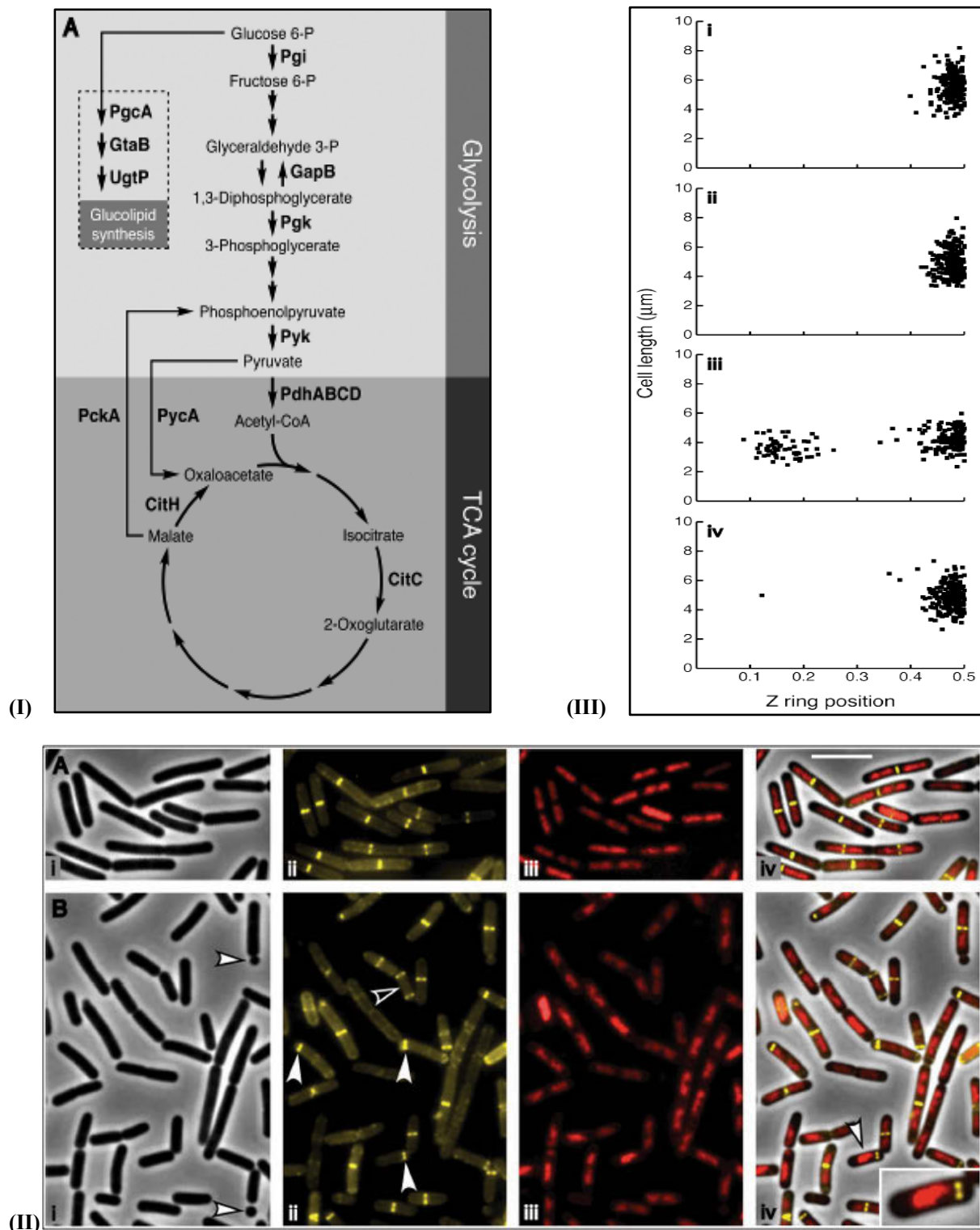


**Figure 1.11. The coordination between central carbon metabolism and cell division in *B. subtilis*.**

**(I)** Schematic representation of the main central carbon metabolism in bacteria: glycolysis, the

---

**TCA cycle and the phospholipid synthesis pathway diverging from Glucose-6-phosphate.**

Phosphoglucose isomerase (Pgi), glyceraldehyde-3-phosphate dehydrogenase (GapB), phosphoglycerate kinase (Pgc), pyruvate kinase (Pyk), pyruvate dehydrogenase complex (PdhABCD), isocitrate dehydrogenase (CitC), malate dehydrogenase (CitH), phosphoenolpyruvate carboxykinase (PckA), pyruvate carboxylase (PycA), phosphoglucomutase (PgcA), uridine-diphosphoglucose pyrophosphorylase (GtaB), uridinediphosphate glucosyltransferase (UgtP). **(II) Cells lacking *pyk* show defects in the Z ring formation.** Upper panel: wild type cells with the Z rings formed at midcell. Lower panel:  $\Delta pyk$  cells with 1/3<sup>rd</sup> of the Z rings formed at the cell poles. [(i) Phase contrast images, (ii) FtsZ-YFP false coloured in yellow, (iii) DAPI staining of DNA falsely coloured in red, (iv) merged images]. **(III) Scatter plots for Z ring positioning.** Addition of pyruvate to  $\Delta pyk$  rescues its Z ring defect. (i) wild type cells without pyruvate, (ii) wild type cells with pyruvate, (iii)  $\Delta pyk$  cells without pyruvate, (iv)  $\Delta pyk$  cells with pyruvate [Adapted from (Monahan et al. 2014a)]

Subsequent work in the same study showed that pyruvate levels may be coupled to the Z ring assembly via an enzyme that metabolises pyruvate: E1 $\alpha$  subunit of pyruvate dehydrogenase (*pdhA*) [Figure 1.11(I)]. In wild type *B. subtilis* cells, PDH E1 $\alpha$  was observed to co-localize with the nucleoid using a strain having an ectopic copy of PDH E1 $\alpha$  fused with YFP, while this co-localisation was completely abolished in *pyk*-deleted cells. Instead PDH E1 $\alpha$  localized to the DNA-free cell poles (Figure 1.12). This coincides with the increased polar Z ring phenotype of *pyk*-deleted cells. The addition of pyruvate returned the localization pattern of PDH E1 $\alpha$  to the nucleoid in these cells (Monahan et al. 2014a).

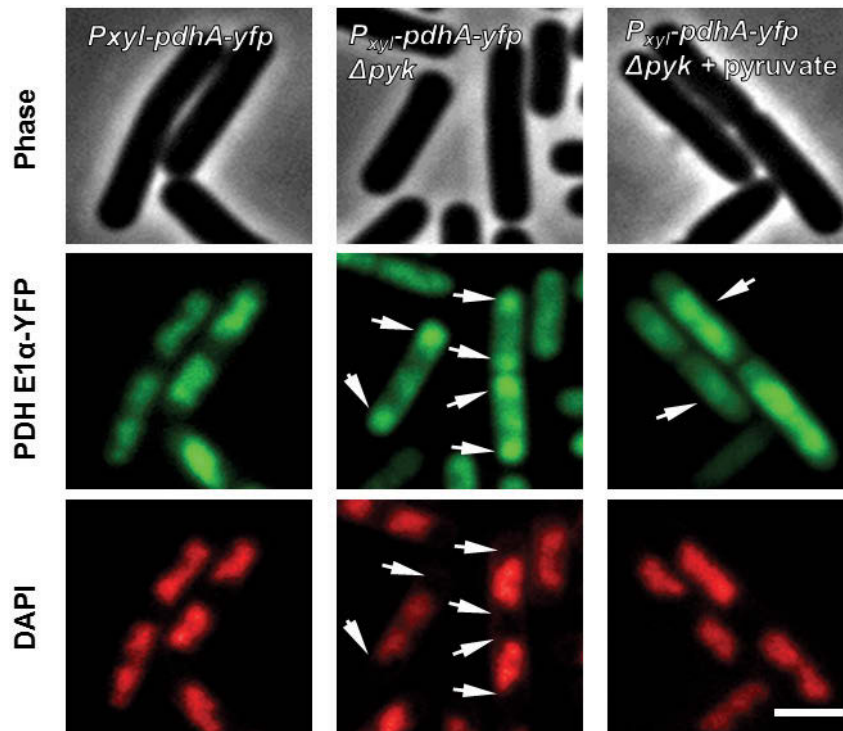


**Figure 1.12. Localization pattern of pyruvate dehydrogenase E1 $\alpha$  restored by the addition of pyruvate to  $\Delta pyk$  cells.** Left panel: Wild type cells in L broth without pyruvate, middle panel:  $\Delta pyk$  cells in L broth without pyruvate, right panel:  $\Delta pyk$  cells in L broth with 1% pyruvate. For all panels, top row: phase-contrast image, middle row: PDH E1 $\alpha$ -YFP localization, bottom row: DAPI staining of DNA, scale bar 1 $\mu$ m. Arrows point towards the localization of PDHE1 $\alpha$  for comparison with the nucleoid localization pattern [Adapted from (Monahan et al. 2014a)]

Based on these above observations, Monahan *et al.* proposed a model for the metabolic regulation of Z ring assembly in *B. subtilis* (Figure 1.13). As per this model, PDH E1 $\alpha$  exists within a cell in two forms: nucleoid-associated and non-associated, and the equilibrium between these two forms is regulated by pyruvate levels. Under nutrient-rich conditions when the pyruvate levels are high, and cells need to divide fast, PDH E1 $\alpha$  localizes over the nucleoid and stimulates more efficient Z ring formation at midcell. While under nutrient-poor conditions when the pyruvate levels are low, PDH E1 $\alpha$  still preferentially co-localizes with the nucleoid but not as strongly as in rich medium and allows less frequent division under these conditions.



In *pyk*-deleted cells, wherein the synthesis of pyruvate is artificially blocked, the PDH E1 $\alpha$  equilibrium is shifted almost entirely to the non-associated form and it accumulates at the cell poles. Here, PDH E1 $\alpha$  overcomes the normal Z ring inhibition activity of the polar Min complex and promotes the Z ring formation in this region of the cell (Monahan et al. 2014a).

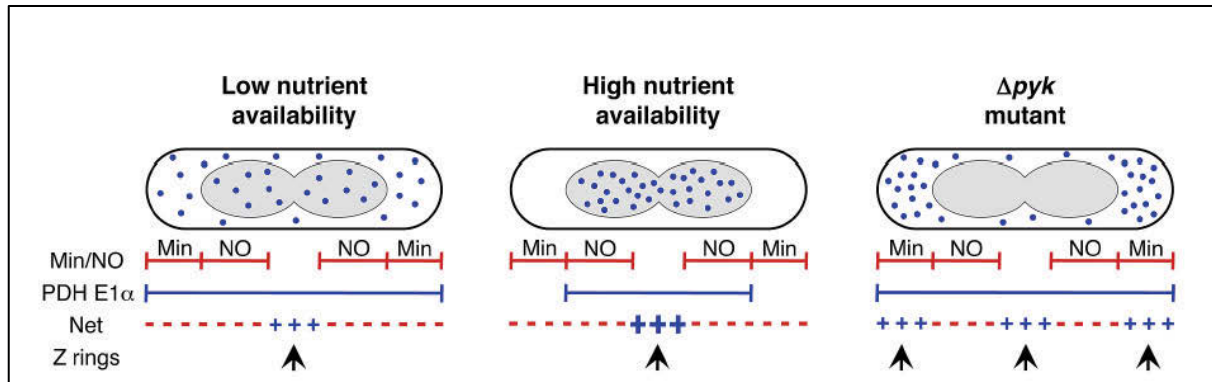


**Figure 1.13. Role of PDHE1 $\alpha$  in Z ring formation.** PDHE1 $\alpha$  (blue circles) localizes over the nucleoid (grey) in a nutrient-dependent manner linked to pyruvate production. Left diagram: under nutrient-poor conditions, PDHE1 $\alpha$  localizes weakly with the nucleoid. Center diagram: under nutrient-rich conditions, PDHE1 $\alpha$  associates strongly over the nucleoid. The action of Min system and the nucleoid occlusion would also help restrict the formation of Z ring to midcell. Right diagram: In *pyk*-mutant cells, when pyruvate synthesis is blocked, PDHE1 $\alpha$  does not co-localize with the nucleoid at all, in fact moves to the cell poles. This polar localization of PDHE1 $\alpha$  could overcome the inhibitory effects of the Min system and can trigger the Z ring formation at these sites [Reproduced from (Monahan et al. 2014a)]

Monahan *et al.* identified the first link between glycolysis and the Z ring placement in *B. subtilis* by making use of a mutant of the enzyme pyruvate kinase (*pyk*). Interestingly, the study by Balasubramanian *et al.* in 2016 deciphered a way by which the production of the enzyme pyruvate kinase and the Z ring forming protein FtsZ are regulated by a single prophage-encoding small RNA, DicF, in *E. coli* (Balasubramanian et al. 2016). The sRNA DicF was

---

discovered in the 1980s to be an inhibitor of the cell division process but after that remained uncharacterised. Using computational and experimental methods, Balasubramanian and colleagues further characterised this sRNA and demonstrated that DicF inhibits cell division by directly base pairing with *ftsZ* mRNA causing repression of the translation process and preventing new synthesis of FtsZ. Furthermore, the other targets of DicF were also identified, wherein the most prominent targets included *pykA* (pyruvate kinase) and *xylR* (xylose regulator). Similar to FtsZ, DicF was also shown to bind to and repress the translation of *pykA* and *xylR* mRNAs. Specifically, the 3' end of DicF was shown to base pair with *ftsZ* as well as *pykA* mRNAs thereby regulating their functions, however the 5' end was required for *xylR* base pairing (Balasubramanian et al. 2016). This identification of a single sRNA controlling the metabolic components (*pykA*, *xylR*) and cell division components (*ftsZ*) in *E. coli* provides another evidence of the connection between metabolism and cell division, and that the simultaneous regulation of these two processes is necessary for a proper coordination between the cell cycle events. Additionally, in *E. coli*, another non-coding RNA Rcd from plasmid ColE1, which is required for maintaining the high-fidelity of the plasmid, has also been shown to stimulate indole production by targeting the enzyme tryptophanase (Gaimster and Summers 2015). Elevated indole levels are then shown to inhibit cell division and plasmid replication simultaneously. This is proposed to allow sufficient time to repair any dimers. This became further prominent from the observation of Rcd being upregulated in the dimer-containing cells, such that plasmid over-replication and hence, further accumulation of dimers can be prevented through elevated indole levels.

Another interesting observation recently published by Jain and Chen in 2018 was the role of central carbon metabolism in ameliorating nickel toxicity in *C. crescentus* via its effect on the cell division process (Jain and Chen 2018). Nickel [Ni(II)] toxicity was observed to induce

---

mislocalization of FtsZ, thereby causing disruption of the cell division process. Metabolomics analysis revealed increased levels of TCA cycle intermediates (citric acid, malic acid) and amino acids (proline, alanine, glutamine, glutamic acid, aminomalonic acid, valie), indicating that these changes in central carbon metabolism and nitrogen metabolism could be linked to the cell division disruption under the conditions of nickel stress. Interestingly, supplementation of some organic acids (citric acid and malic acid) and amino acids (alanine, glutamine and proline) restored the growth of cells undergoing nickel toxicity. This confirmed that these components from central carbon metabolism and nitrogen metabolism indeed show a protective effect on nickel toxicity and that these metabolites play some role in conferring resistance to nickel toxicity in *C. crescentus* via their effect on the cell division process (Jain and Chen 2018).

## 1.8 Thesis aims

For their continued growth and multiplication, bacterial cells must double in mass, replicate their DNA, separate their sister chromosomes and divide at the correct place at the right time to produce two identical daughter cells. Coordination between these events is of utmost importance to ensure that the newborn cells receive a full complement of genetic material and can proceed onto further cycles of division. Not only is it essential to maintain a coordination between these cellular events, but it is also essential to couple all these events with the nutrient availability. Bacterial metabolism, including central carbon metabolism (CCM) and accessory pathways, has emerged as the key player in transmitting nutritional information in the form of metabolic signals to the cell division machinery; however, the precise mechanisms for such coordination is unknown. Hence, the overall objective of the work presented in this thesis is to gain insight into the coordination of CCM and cell division in the soil bacterium *B. subtilis*.

---

Monahan *et al.* (2014) proposed an intimate link between glycolysis (central carbon metabolism) and the Z ring positioning (cell division) in *B. subtilis*, and showed that the loss of pyruvate kinase (*pyk*) disrupts this link leading to the formation of Z rings at acentral positions. Interestingly, the addition of exogenous pyruvate, the product of the pyruvate kinase reaction, to  $\Delta pyk$  cells, restored the link between CCM and Z ring positioning such that the Z rings formed correctly at midcell after pyruvate addition. However, whether pyruvate does this directly or indirectly by first being metabolized into any of its metabolic fates was not explored. Therefore, the primary aim of Chapter 3 is to identify whether pyruvate is directly involved in this CCM-division link or it does this by being metabolized into any of its metabolic fates? This is accomplished by supplementing the growth medium of  $\Delta pyk$  with each of the metabolites derived from pyruvate and testing if any of these metabolites could also rescue the Z ring positioning defect of  $\Delta pyk$  cells, as was shown by pyruvate. As Monahan *et al.* (2014) also reported a slower growth rate of  $\Delta pyk$  cells as compared to wild type cells, the correlation between the Z ring positioning and the growth rate rescue of  $\Delta pyk$  cells as a result of supplementation with different metabolites is also examined in Chapter 3, to determine if the Z ring positioning rescue after metabolite supplementation is growth rate related. Chapter 3 also reports for the first time, the observation of a spread nucleoid morphology in  $\Delta pyk$  cells as compared to the bilobed nucleoid morphology of wild type cells and also examines the correlation between the Z ring positioning rescue and the nucleoid morphology rescue of  $\Delta pyk$  after supplementation with various metabolites.

Considering the polar Z ring positioning phenotype of  $\Delta pyk$  being similar to the Z ring positioning phenotype in  $\Delta min$  cells (that is, formation of acentral Z rings and minicells), chapter 4 examines the involvement of the Min system in the acentral Z ring positioning defect of  $\Delta pyk$  cells. Moreover, following up from the observation of a spread nucleoid morphology

in  $\Delta pyk$ , Chapter 4 also examines the involvement of nucleoid occlusion and DNA replication in the acentral Z ring positioning phenotype of these cells.

Finally, Chapter 5 examines the connection between CCM and cell division at a systems level by using a global transcriptomic approach. This chapter presents the differentially expressed transcriptional profile of  $\Delta pyk$  cells in comparison to the wild type *B. subtilis* cells with an objective of identifying any gene expression change that could potentially contribute to the acentral Z ring positioning defect of these cells. Furthermore, Chapter 5 also investigates whether the differentially expressed profile of  $\Delta pyk$  cells is restored to wild type cells levels after supplementation with any metabolite that rescues the Z ring positioning defect of these cells. This investigation was done to identify the specific role of any differentially expressed genes in  $\Delta pyk$  in their acentral Z ring positioning defect. Lastly, Chapter 6 provides an overview and discusses all the findings presented in Chapter 3-5 of this thesis.



# Chapter 2

---

## Materials and Methods

## 2.1 Chemicals, reagents and solutions

The chemicals and reagents used in this work were typically analytical reagent (AR) grade and were obtained from Amresco, BDH Chemicals or Sigma-Aldrich unless otherwise specified.

Commonly used aqueous buffers and solutions are listed in Table 2.1.

**Table 2.1. Commonly used buffers and solutions**

Buffer/solution	Components *
GTE	50 mM glucose, 20 mM Tris-HCl, 10 mM EDTA, pH 7.5
PBS	137 mM NaCl, 10.1 mM Na <sub>2</sub> HPO <sub>4</sub> , 2.7 mM KCl, 1.8 mM KH <sub>2</sub> PO <sub>4</sub> , pH 7.4
PC buffer (10×)	0.63 mM trisodium citrate (Na <sub>3</sub> C <sub>6</sub> H <sub>5</sub> O <sub>7</sub> ·2H <sub>2</sub> O), 6.1 mM K <sub>2</sub> HPO <sub>4</sub> , 4.4 mM KH <sub>2</sub> PO <sub>4</sub> , pH 7
MSA	8 mM K <sub>2</sub> HPO <sub>4</sub> , 4.4 mM KH <sub>2</sub> PO <sub>4</sub> , 1.5 mM (NH <sub>4</sub> ) <sub>2</sub> SO <sub>4</sub> , 340 mM trisodium citrate dihydrate (Na <sub>3</sub> C <sub>6</sub> H <sub>5</sub> O <sub>7</sub> ·2H <sub>2</sub> O)
TE	10 mM Tris-HCl, 1 mM EDTA, pH 8.0
TES	200 mM Tris-HCl, 100 mM NaCl, 5 mM EDTA, pH 7.5
Trace metals	50 mM CaCl <sub>2</sub> , 5 mM MnCl <sub>2</sub> , 1.6 mg/ml FeCl <sub>3</sub> ·6H <sub>2</sub> O, 430 mg/ml CuCl <sub>2</sub> ·2H <sub>2</sub> O, 170 mg/ml ZnCl <sub>2</sub> , 60 mg/ml CoCl <sub>2</sub> ·6H <sub>2</sub> O, 60 mg/ml Na <sub>2</sub> MoO <sub>4</sub> ·2H <sub>2</sub> O
XS buffer (2×)	pre-heated to 65 °C; 2% (w/v) potassium ethyl xanthogenate, 1600 mM ammonium acetate, 200 mM Tris-HCl, pH 7.4, 36 mM EDTA, 2% SDS
Spore decoating solution	8M Urea, 15mM Tris-HCl (pH=7), 1% SDS, 50mM DTT
STE buffer	10mM Tris-HCl (pH=8), 10mM EDTA, 150mM NaCl

\* All buffers and solutions were made up in Milli-Q<sup>®</sup> purified water (MQW; Millipore) and are listed at the normal working concentration (1×) unless otherwise stated. All percentages are given as weight per volume (w/v) unless otherwise noted

## 2.2 *B. subtilis* strains and growth media

All *B. subtilis* strains used in this work are listed in Table 2.2. For strains produced as part of this work, experimental details regarding strain construction are described in the text when the strains are first used. The *B. subtilis* 168 background strain used in this work was SU5 (*trpC2*). The *trpC2* genotype is an auxotrophic requirement for tryptophan.

**Table 2.2. *B. subtilis* strains**

Strain	Genotype *	Reference/source
SU5	168 <i>trpC2</i>	E. Nester
SU492	168 <i>trpC2 amyE::P<sub>xyI</sub>-ftsZ-yfp-spec</i>	Lab stock
SU657	168 <i>trpC2 Δnoc::tet amyE::P<sub>xyI</sub>-ftsZ-yfp-spec</i>	(Rodrigues and Harry 2012)
SU664	168 <i>trpC2 Δpyk::cat</i>	(Monahan et al. 2014a)
SU679	168 <i>trpC2 Δpyk::cat amyE::P<sub>xyI</sub>-ftsZ-yfp-spec</i>	(Monahan et al. 2014a)
SU682	168 <i>trpC2 ΔminCD::cat amyE::P<sub>xyI</sub>-ftsZ-yfp-spec</i>	Lab stock
SU739	168 <i>trpC2 amyE::P<sub>xyI</sub>-pdhA-yfp</i>	(Monahan et al. 2014a)
SU742	168 <i>trpC2 Δpyk::cat amyE::P<sub>xyI</sub>-pdhA-yfp</i>	(Monahan et al. 2014a)
SU826	168 <i>trpC2 Δald::erm amyE::P<sub>xyI</sub>-pdhA-yfp</i>	This work
SU877	168 <i>trpC2 Δnoc::tet Δpyk::cat amyE::P<sub>xyI</sub>-ftsZ-yfp-spec</i>	This work
SU880	168 <i>trpC2 P<sub>spac</sub>-fabHA amyE::P<sub>xyI</sub>-ftsZ-yfp-spec</i>	(Murray and Koh 2014)
SU883	168 <i>trpC2 ΔminCD::cat Δpyk::tet amyE::P<sub>xyI</sub>-ftsZ-yfp-spec</i>	This work
SU884	168 <i>trpC2 ΔpyrE::kan amyE::P<sub>xyI</sub>-ftsZ-yfp-spec</i>	This work
SU885	168 <i>trpC2 ΔpyrR::kan amyE::P<sub>xyI</sub>-ftsZ-yfp-spec</i>	This work

\* Antibiotic resistance genes are abbreviated as follows: *cat*, chloramphenicol; *erm*, erythromycin; *spec*, spectinomycin; *tet*, tetracycline; *kan*, kanamycin.

Growth media used to cultivate *B. subtilis* cells are listed in Table 2.3. Unless otherwise noted, cells were grown on tryptose blood agar base (TBAB) plates at 37°C. Broth cultures were grown in L-broth, unless otherwise stated. Broth cultures were incubated with vigorous



shaking (>200 rpm) in a gyratory water-bath (G76; New Brunswick and OLS200: Grant Scientific water-baths were used in this study) and growth was monitored by recording the absorbance at 600 nm ( $A_{600}$ ) using a spectrophotometer (UV-120-02; Shimadzu). Antibiotics were used for selection as described in Table 2.4. *B. subtilis* strains were stored as stationary phase cultures suspended in 16% (v/v) glycerol at  $-80^{\circ}\text{C}$ .

**Table 2.3. *Bacillus subtilis* growth media**

Medium	Components *
L-broth	1% tryptone, 0.5% yeast extract, 0.5% NaCl
TBAB	3.3% tryptose blood agar base
MD medium	10% (v/v) 10X PC buffer, 2% glucose, 2.5 $\mu\text{g/ml}$ tryptophan, 0.5% ammonium ferric citrate $[\text{Fe}(\text{NH}_4)_3(\text{C}_6\text{H}_5\text{O}_7)_2]$ , 2.5 $\mu\text{g/ml}$ aspartate, 0.3% $\text{MgSO}_4$

\* All media were made up in reverse osmosis purified water (ROW) and sterilized by either autoclaving or 0.2  $\mu\text{m}$  filtration. Tryptone, sodium chloride, yeast extract, agar and TBAB were obtained from Difco. All percentages are given as w/v unless otherwise stated

**Table 2.4. Antibiotics used for selection in *B. subtilis***

Antibiotic	Working concentration ( $\mu\text{g/ml}$ ) *
Chloramphenicol	5
Erythromycin	0.5
Kanamycin	10
Spectinomycin	80
Tetracycline	10

\* Stock solutions were prepared by dissolving antibiotics either in ethanol or ROW and filter sterilizing (0.2  $\mu\text{m}$  filter). Erythromycin, kanamycin and spectinomycin were stored at  $4^{\circ}\text{C}$ , and chloramphenicol and tetracycline at  $-20^{\circ}\text{C}$

### 2.2.1 Testing for the disruption of the *amyE* locus

Genetic manipulation of *B. subtilis* often involves insertion of gene cassettes into the non-essential *amyE* locus in the chromosome. The *amyE* gene encodes an  $\alpha$ -amylase which breaks down starch into less complex sugars. To test if *amyE* has been disrupted and amylase is no longer produced (indicative of gene cassette insertion), *B. subtilis* cells were patched onto TBAB plates containing 1% (w/v) starch and incubated overnight at 37°C. Plates were then stained by vaporizing 3-5 iodine crystals in the inverted plate lids. The agar remained colorless in the vicinity of cells containing a functional *amyE* gene, while cells which stained purple indicated that the *amyE* gene had been inactivated. This color reaction occurs because of the iodine forming a complex with starch. Since starch is degraded by the enzyme amylase, cells with a functional copy of the *amyE* gene remained colorless.

## 2.3 Preparation and transformation of competent *B. subtilis* cells

### 2.3.1 Preparation of competent *B. subtilis* cells

In culture, *B. subtilis* cells naturally acquire competence for DNA uptake as growth moves into stationary phase (Dubnau 1991). Taking advantage of this fact, competent *B. subtilis* cells were prepared. A single colony of the parent strain to be made competent was freshly cultivated the night before at 37°C in L-broth. Freshly prepared MD medium (10 ml, see Table 2.3) supplemented with 100  $\mu$ l 10% (w/v) casamino acids (CAA, Difco) was inoculated with the overnight culture to an  $A_{600}$  of 0.05 and incubated at 37°C, with shaking until  $A_{600}$  reached a value of 1 - 1.5, indicating entry of cells into the stationary phase of growth. An equal volume (10 ml) of MD medium (minus casamino acids) was added to the culture and incubated for a further one hour at 37°C to fully induce competence. The competent cells prepared were either

used directly for DNA transformation or glycerol was added to the culture to a final concentration of 16% (v/v) and 1 ml aliquots of the competent cell culture were stored at -80°C until required.

### **2.3.2 Transformation of competent *B. subtilis* cells**

Competent cells (500 µl) were aliquoted into 14 ml round-bottom culture tubes and donor chromosomal DNA (5-10 µl; approximately 100 ng) was added, along with a no DNA control. These tubes were shaken at 37°C for 30 minutes. The culture was supplemented with 50 µl 10% (w/v) CAA and incubated for a further 1.5 hours at the same temperature. The entire sample was then pelleted for 2 min at 10, 000 g, supernatant removed and the pellet was resuspended in 200 µL MSA (see Table 2.1). 100 µl of the culture was spread plated onto TBAB plates supplemented with appropriate antibiotic. The plates were incubated at 37 °C overnight for potential transformants to appear.

## **2.4 General DNA methods**

### **2.4.1 *Bacillus subtilis* chromosomal DNA extraction**

Chromosomal DNA was extracted and purified from *Bacillus subtilis* cells as follows. 3ml of overnight culture of the required strain was centrifuged for 2 minutes at 10,000 g. The supernatant was removed and the pellet was resuspended in 500 µl TES. 25 µl of 10 mg/ml lysozyme, made up fresh in TES, was added to the culture and incubated at 37°C for 30 minutes. An equal volume (525 µl) of XS Buffer prewarmed at 65°C (2X; see Table 2.1) was added to the culture and incubated at 65°C for 1-2 hours. Next, the cell culture was vortexed

for 10 seconds, and kept on ice for 30 minutes. The cell suspension was then centrifuged for 10 minutes at 14,000 g to pellet down the debris. The supernatant was aliquoted into fresh 1.5ml microcentrifuge tubes and an equal volume of isopropanol was added to the supernatant. This was then incubated at room temperature for 5 minutes followed by rapid inversions of the tube until the DNA precipitated. The DNA was then pelleted by centrifugation for 2 minutes at 10,000 g, and supernatant was removed. The DNA pellet was resuspended in 500  $\mu$ L ice cold 70% (v/v) ethanol, and then centrifuged for 2 minutes at 10,000 g. The supernatant was removed and the DNA pellet was left to air-dry for 20-30 minutes at room temperature to evaporate any remaining ethanol. The DNA pellet was then resuspended in 200  $\mu$ l TE (1X) supplemented with RNase (100  $\mu$ g/ml). The chromosomal DNA was stored at 4°C.

#### **2.4.2 Measurement of DNA concentration**

DNA concentrations were determined using the spectrophotometry method described by Sambrook *et al.* (Sambrook 1989).

#### **2.4.3 Agarose gel electrophoresis**

Agarose gels were prepared on a horizontal slab gel apparatus (Biorad, 30 ml gel volume). Agarose (type 1: low electroendosmosis; Sigma-Aldrich) was dissolved in TBE electrophoresis buffer at a concentration of 0.8% (w/v) and GelRed<sup>®</sup> (Biotium) was added to a concentration of 60 ng/ml. The gels were then cast with a well-forming comb in place. 6X New England Biolabs DNA loading buffer was added to a final concentration of 1X to DNA samples prior to loading into the pre-cast wells. Bacteriophage  $\lambda$  DNA pre-cut with *Hind*III (New England Biolabs) was used for size standards, enabling the size estimation of DNA fragments greater than 1 kb. For fragments less than 1 kb, 100 bp DNA Ladder (New England Biolabs) was used.

Agarose gels were run submerged under a volume of 1X TBE electrophoresis buffer that lay 2-5 mm above the surface of the gel at 80 V for 1-2 h. The gels were visualised via exposure to short-wavelength UV light (254 nm) using a transilluminator (Ingenius3; Syngene) and recorded as a digital image using a charge-coupled device (CCD) camera (Synoptics CAM-FLXCM; Syngene) linked to GeneSys molecular imaging software, version 1.5.0.0 (Syngene).

#### **2.4.4 Polymerase Chain Reaction (PCR) and oligonucleotides**

PCR was used in this study to validate the deletion of genes from the *Bacillus subtilis* strains created. For all PCR reactions used to check gene deletions, *Taq* polymerase (New England Biolabs) and 1X Thermo Pol buffer (New England Biolabs) was used. Single-stranded oligonucleotide primers for PCR were purchased from IDT and supplied in a lyophilised form. Primers were dissolved in MQW to a final concentration of 100  $\mu$ M and stored at  $-20^{\circ}\text{C}$ . Primers used are listed below in Table 2.5. The PCR reaction mixtures consisted of template DNA (100 ng for chromosomal DNA), 500 nM of each primer (see Table 2.5), 1X amplification buffer, 200  $\mu$ M of dNTP mix (Fermentas) and 1.25 U of DNA polymerase (*Taq* polymerase), made up to 50  $\mu$ l in MQW. PCR mixtures were subjected to the following temperature cycle using a thermo cycler (Mastercycler; Eppendorf): 10 minutes at  $95^{\circ}\text{C}$  (for initial denaturation of the template), 30 cycles consisting of  $95^{\circ}\text{C}$  for 1 minutes, (template denaturation), X  $^{\circ}\text{C}$  for 1 minutes (primer annealing) and  $72^{\circ}\text{C}$  for Y sec (extension), followed by a further 5 minutes at  $72^{\circ}\text{C}$  for final extension (where X = predicted oligonucleotide annealing temperature minus  $\sim 3^{\circ}\text{C}$ , and Y = 1 minutes per kb to be amplified). The PCR reaction products were analysed via agarose gel electrophoresis (See Section 2.4.3).

**Table 2.5. Primers used for PCR reaction, Gibson assembly and Marker frequency analysis**

Sequence 5' to 3'	Description
TTCAAATCAGAAAAACGAAAAATG	Forward primer upstream of <i>ald</i>
AGCTTATTGTGAATTATTCCTCCCGTTAAATAATAG	Reverse primer from <i>erm</i> cassette
CGCCTAATGTTTCATGCTCTTG	Forward primer upstream of <i>pyrE</i>
CCCGATATTTAACATCGCGGAC	Forward primer upstream of <i>pyrR</i>
CCGTATCTTTTACGCAGCGGT	Reverse primer from <i>kan</i> cassette
<b>Primers for Gibson assembly*</b>	
TTCAAATCAGAAAAACGAAAAATG	P1
TATTTTTGTTTCATATCTGTCTCCTCCTGTATATGTG	P2
GGAGGAGACAGATATGAACAAAAATATAAAATATTCTCAAAC	P3
AGCTTATTGTGAATTATTCCTCCCGTTAAATAATAG	P4
CGGGAGGAAATAATTCACAATAAGCTTGCAGAAAG	P5
TATATCCAATCGCATTGG	P6
<b>Primers for Marker frequency analysis</b>	
GAATTCCTTCAGGCCATTGA	<i>OriC</i> forward primer
GATTTCTGGCGAATTGGAAG	<i>OriC</i> reverse primer
TCCATATCCTCGCTCCTACG	<i>ter</i> forward primer
ATTCTGCTGATGTGCAATGG	<i>ter</i> reverse primer

\*Primers P1 to P6 were used for the construction of an *ald* mutant using the Gibson assembly approach, described in Figure 2.1

### 2.4.5 Colony PCR

Colony PCR was performed to screen for the positive clones from the colonies obtained after the transformation step. A volume of 20 µl of sterile milliQ water was added to each PCR tube. A colony was selected from plates and resuspended in the water. Cells were lysed using a thermocycler, for 5 minutes at 95°C. Cell debris were spun down and the samples were then

placed on ice as the following reaction was set up. The following were added to each PCR tube and made to a final reaction volume of 25  $\mu$ l: Thermopol buffer (1 x v/v), dNTPs (200  $\mu$ M), forward and reverse primers (0.2  $\mu$ M), 1 unit of Taq DNA polymerase and 10  $\mu$ l of DNA template (supernatant of lysed cells). PCR reactions were subjected to the following temperature cycling using a thermocycler: 95°C for 30 seconds (initial denaturation of the template), followed by 30 cycles of 95°C for 15 seconds (template denaturation), X°C for 30 seconds (primer annealing), and extension at 68°C for Y seconds (extension), followed by a final extension step was at 68°C for 5 minutes. (where X = predicted oligonucleotide annealing temperature minus  $\sim$ 3 °C, and Y = 1 minutes per kb to be amplified). The PCR reaction products were analysed via agarose gel electrophoresis (See Section 2.4.3).

#### **2.4.6 DNA sequencing**

Specific regions of the *B. subtilis* chromosome were amplified and sequenced during this study to confirm the correct construction of strains and/or the presence of particular mutations (Table 2.2). PCR was employed to amplify the regions of interest, as described in Section 2.4.4, and the PCR product was purified using the GenElute™ PCR Clean-Up Kit (Sigma-Aldrich). The purified PCR products, along with appropriate primers, were then sent to the Australian Genome Research Facility (AGRF; University of Queensland, Australia), where Sanger sequencing was performed. Sequencing data was analyzed using the GenomeCompiler® software.

### **2.5 Gibson assembly**

A mutant of alanine dehydrogenase was constructed by replacing the *ald* gene by an antibiotic (erythromycin) resistance cassette (*erm<sup>R</sup>*), following the Gibson assembly approach (explained

in Figure 2.1). Briefly, *erm<sup>R</sup>* cassette was assembled by PCR amplification of fragments using the primers mentioned in Table 2.5 (primer naming as per the nomenclature in Figure 2.1), following the PCR protocol explained in section 2.4.4. The upstream and downstream fragments (refer to Figure 2.1) were amplified using the SU5 gDNA as template, whereas the *erm<sup>R</sup>* marker was amplified from the pMutin plasmid. All three fragments were then assembled using the Gibson assembly master mix (New England Biolabs) (Gibson et al. 2009) with the reaction set up with 1X Gibson Assembly master mix (v/v) in a final volume of 20  $\mu$ l, as per the manufacturer's instructions. The reaction was incubated in a thermocycler for 15 minutes at 50°C and stored at -20°C until needed for subsequent transformation. 2  $\mu$ l of the Gibson assembly reaction, containing the assembled fragments were transformed into *B. subtilis* SU492 strain (*amyE::Pxyl-ftsZ*) and plated onto erythromycin (0.5  $\mu$ g/ml) supplemented TBAB plates. This resulted in the replacement of *ald* gene in *B. subtilis* chromosome with an *erm<sup>R</sup>* marker by homologous recombination. Finally, the replacement was confirmed by colony PCR (section 2.4.5) using primers targeting the upstream region of the *ald* gene and downstream region of the erythromycin cassette, as well as by DNA sequencing of the *ald* region, which confirmed the presence of *erm<sup>R</sup>*.



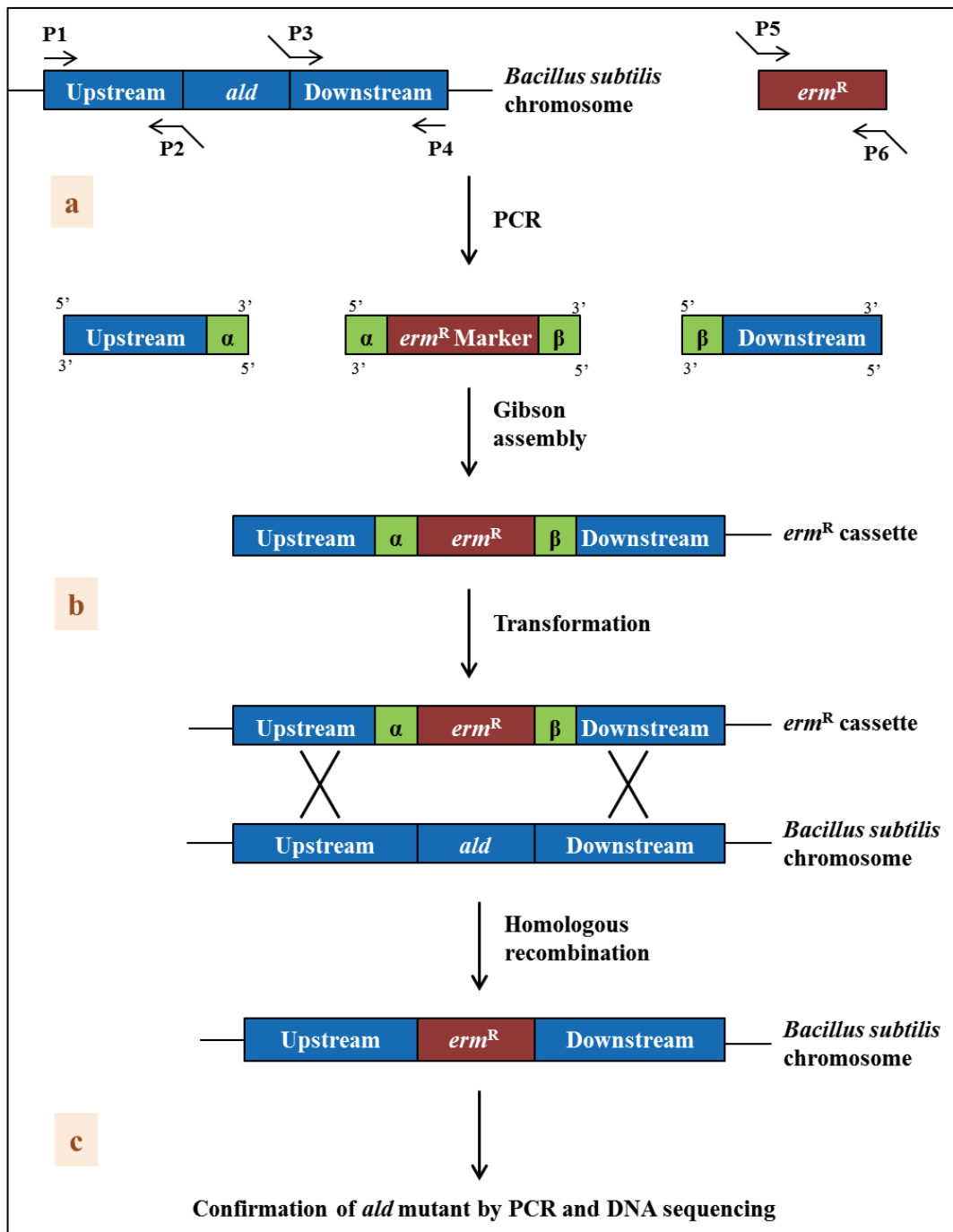


**Figure 2.1.** Schematic diagram of the steps involved in constructing an alanine dehydrogenase (*ald*) mutant. (a) PCR amplification of fragments for assembly into *erm<sup>R</sup>* cassette. Primers P2 and P3, complementary to the upstream and downstream region of *ald* gene, have regions overlapping with the *erm<sup>R</sup>* gene. Primers P5 and P6 encode complementary sequence homology to upstream ( $\alpha$ ) and downstream regions ( $\beta$ ) of the *ald* gene. These overlapping regions facilitate the assembly of fragments. (b) Transformation of the *erm<sup>R</sup>* cassette into *B. subtilis* cells (SU492, *amyE::Pxyl-ftsZ*) results in the

inactivation of *ald* gene by insertion of *erm<sup>R</sup>* cassette at the *ald* locus by homologous recombination.

(c) Colonies obtained were screened by colony PCR and positive clones were further confirmed by DNA sequencing.

## 2.6 Microscopy methods

### 2.6.1 Immunofluorescence microscopy (IFM)

IFM was used for the detection of the FtsZ protein in strains of *B. subtilis* under various conditions as specified in the text. IFM was performed based on a previously described method except that the cells were chemically fixed with ice cold methanol (Harry et al. 1995). Mid-exponential phase vegetative cells (1 ml) were concentrated by centrifugation and resuspension in 500  $\mu$ l PBS. This was then added to 10 ml ice-cold methanol (-20°C), mixed by inversion and fixed at -20°C for 1 h. Fixed cells were washed three times in 0.5 ml PBS, each time recovering the cells by centrifugation in a microfuge (4500 g, 5 min) and the supernatant discarded. Cells were then resuspended in 90  $\mu$ l GTE. Meanwhile, multi-well microscope slides (ICN Biochemicals) were prepared for cell adhesion by incubating the wells with 0.1% solution of poly-L-lysine (Sigma-Aldrich) for 2 min, aspirating the wells dry and rinsing twice with MQW. Slides were allowed to dry completely before applying cell samples.

Cells were permeabilized with the addition of 10 mg/ml lysozyme prepared in GTE (to a final concentration of 1 mg/ml) and immediately added to the wells on the multi-well slide. Cells were incubated for 2-3 min and excess liquid was removed from the slides by aspiration until the wells were dry. Each well was then incubated with blocking solution (2% (w/v) BSA, 0.05% (v/v) Tween 20 in PBS) for 15 min. After this point, wells were kept moist. The wells were washed once with PBS. Antiserum specific to the protein of interest were diluted in PBS

containing 1% BSA. Antibody solution (10  $\mu$ l) was added to each well and the slide was incubated at 4°C overnight in a humidified container.

The following morning, the primary antibody solution was aspirated off and the slide was washed ten times with PBS. The wells were blocked for 30 min with 5% serum (diluted in PBS) specific to the animal the primary antibody was raised in. Blocking solution was aspirated off and wells were washed once with PBS. A secondary antibody with a fluorescence conjugate (for example goat anti-rabbit secondary antibody conjugated to Alexa-488) was diluted in PBS containing 2% BSA and added to the wells and incubated at room temperature for 1 h in the dark. The wells were washed ten times with PBS. The slide was mounted with PBS containing glycerol (50%) and a fluorescent DNA stain 4',6 -diamidino-2-phenylindole (DAPI; 0.4  $\mu$ g/ml), and then covered with a coverslip. The edges of the coverslip were sealed with nail polish. Images were acquired as described in Section 2.6.3 and the slides were stored at -20°C.

## 2.6.2 Preparation of cells for live cell fluorescence microscopy

To examine the *in vivo* localization of various YFP fusion proteins, live cells expressing the fusion of interest were collected and immobilized on agarose coated microscope slides as follows. First, a 1.5  $\times$  1.6 cm rectangular well was created on the surface of the glass slide using a 65  $\mu$ l Gene Frame (ABgene; slides were obtained from Livingstone). Agarose (type 1; Sigma-Aldrich) was dissolved at 2% (w/v) in the same medium used to culture the cells and ~65  $\mu$ l of this solution was applied to the center of the well. A coverslip was immediately placed on top and the agarose was allowed to solidify within the well for ~5 min, producing a flat 'agarose pad'.

To mount cells for fluorescence microscopy, firstly the vegetative cells were pelleted by centrifugation for 2 minutes at 10,000 g using a microcentrifuge. The resultant pellet was

resuspended in 200  $\mu$ l of PBS and DAPI (0.4  $\mu$ g/ml) was added to visualize the nucleoids in live cells. The coverslip on the agarose pad was gently lifted and 3  $\mu$ l of live cell culture was placed on the surface of the agarose pad. A new coverslip was then applied and the cells were viewed immediately.

### **2.6.3 Phase-contrast and fluorescence microscopy**

Cells were visualized using phase-contrast and fluorescence on a Zeiss Axioplan 2 fluorescence microscope at 100x magnification using a Plan ApoChromat (100 $\times$  NA 1.4; Zeiss) objective lens. The light source was a 100 W high pressure mercury lamp passed through the following filter blocks: for visualising Alexa 488 (Filter set 09, Zeiss; 450 - 490 nm BP excitation filter, 515 nm long pass (LP) barrier filter), DAPI (Filter set 02, Zeiss; 365 nm excitation filter, 420 nm long pass (LP) barrier filter), and YFP (Filter set 41029, Chroma Technology). Exposure times of 50 – 700 ms were used. AxioCam MRm camera was used for image collection. Images were processed and analysed using AxioVision software, version 4.8 (Zeiss).

### **2.6.4 Cell scoring and statistics**

Cell length values were scored directly from digital micrographs using AxioVision software, version 4.8 (Zeiss), with the appropriate scaling. The positioning analysis of fluorescent signals of interest (including the Z ring seen as a band) was determined by measuring the distance from the fluorescence signal to the nearest cell pole and by dividing this value by the cell length, with 0.5 being exactly midcell. Numerical values derived for each cell length and position was exported from the AxioVision software as a text file, and imported into Excel (Microsoft) for data processing and statistical analysis. Excel was used to calculate the mean, standard deviation, standard error of the mean (SEM), the 95% confidence interval for the mean, the

number of cells counted (n) for each data set. Excel was used to generate the graphs presented in this study.

Statistical analysis of the data obtained was carried out using the “Kolmogorov - Smirnov” test via an online calculator ([http://www.physics.csbsju.edu/stats/KS-test.n.plot\\_form.html](http://www.physics.csbsju.edu/stats/KS-test.n.plot_form.html)) The “Kolmogorov - Smirnov” test was used to compare the precision of midcell Z ring between wild-type and mutant strains. This test was performed using a 95% confidence interval, where  $P < 0.05$  was indicative of a statistically significant difference between the data sets compared.

## **2.7 Growth curve**

Strain for which growth curve was to be performed was grown overnight in 10 ml of LB at 37°C. Overnight cultures were diluted in 50 ml of LB to an  $OD_{600} = 0.05$ . Cultures were grown over a period of 8 hours. Growth was monitored and recorded using a spectrophotometer every hour. Time point and OD values were exported into excel and plotted onto a semi-logarithmic graph. This method was used to measure growth rate of different strains in this study. Growth curves were performed in biological triplicates and statistical analysis (one-way Anova with a confidence level of >95%) was used to compare the growth rates between different experimental conditions (different strains or the effect of any metabolite on the growth rate).

## **2.8 Measurement of pyruvate in *Bacillus subtilis* cells**

Pyruvate concentration in different strains of *B. subtilis* was measured using the Pyruvate Assay kit (Sigma-Aldrich). Briefly, an overnight culture of bacteria was diluted to a final  $OD_{600}$  of 0.05 in fresh LB medium, and cultivation was continued at 37°C with shaking. Appropriate

volumes of samples were withdrawn at mid-exponential phase normalizing the absorbance values of all cultures to the same, chilled on ice and spun down. Supernatant was discarded and the pellet was resuspended in 200  $\mu$ l of the Pyruvate Assay Buffer. Bacterial lysis was performed by sonication. Cell debris was spun down and the supernatant obtained was passed through 10 kDa MWCO spin filter. Appropriate dilution of the resultant filtrate was made in Pyruvate Assay buffer. Fluorometric quantification of pyruvate concentration was completed as per the manufacturer's protocols.

In the pyruvate measurement experiment, pyruvate levels were measured as per the manufacturer's protocol with an addition of deproteinization step. As pyruvate is a substrate for many enzymes, such as lactate dehydrogenase; the cell lysates were deproteinized by passing through 10 kDa MWCO spin filters immediately after the cell lysis step, to minimize the conversion of pyruvate to other products, such as lactate.

## **2.9 Metabolite-FtsZ interaction using Triple Ligand Detect method**

The triple-ligand detect (TLD) experiment was conducted by Dr Lorna White at the Sydney FBDD Facility within the Sydney Analytical Core Facility, University of Sydney; using the wild type *B. subtilis* FtsZ<sup>12-315</sup> protein purified by Kenardy Kusuma at UTS. The TLD experiment consists of three independent 1D nuclear magnetic resonance (NMR) experiments termed Water-Ligand Observed via Gradient Spectroscopy (Water-LOGSY); Carr, Purcell, Meiboom and Gill (CPMG) NMR and Saturated Transfer Difference (STD) NMR. In these experiments the protein samples were diluted to a final concentration of 10  $\mu$ M in 50 mM Phosphate, 100 mM NaCl (pH 7.4) in 100% D<sub>2</sub>O and DSS. All the experiments were carried out at 290 K with a gas flow at 670 l/h. The data obtained was analysed using the mNova software.

## 2.10 Marker Frequency Analysis

Marker frequency analysis was performed to measure the ratio of origin to terminus in some of the *B. subtilis* strains, following the methodology of Murray and Koh (2014). Briefly, overnight cultures were diluted in fresh L-broth to an  $A_{600}$  of 0.05. Cells were grown to the mid-exponential phase ( $A_{600}$  of 0.3-0.5) and sodium azide was added to the cultures to a final concentration of 0.5% to prevent further cellular metabolism. Cells were harvested by centrifugation at 4500 rpm for 10 min and chromosomal DNA was extracted following the procedure outlined in section 2.4.1. Quantitative PCR (qPCR) was set up using the isolated chromosomal DNA targeting the amplification of *OriC* (representing the origin of DNA replication) and *ter* (representing the terminus of DNA replication) in separate reactions, following the reaction set up explained in section 2.12.2.  $C_T$  values were obtained for *OriC* as well as *ter*, which were then used to perform relative quantification ( $\Delta\Delta C_T$ ) to determine the origin: terminus (*ori:ter*) ratio of samples, following the methodology explained in section 2.12.4. All the values were normalized to the *ori:ter* ratio of a DNA sample obtained from *B. subtilis* spores, which contain only one chromosome and hence have an *ori:ter* ratio of 1.

### 2.10.1 Isolation of spore DNA

DNA from *B. subtilis* spores was extracted following the methodology obtained from the laboratory of Heath Murray, Centre for Bacterial Cell Biology, Newcastle University, UK. 2X 5 ml spores of wild type *B. subtilis* cells were harvested by centrifugation at 3750g/4°C for 30 minutes. The pellet was then washed with a 1 ml solution of 1M KCl and 0.5M NaCl. In the subsequent step, all the vegetative cells were removed by adding 1 ml of 50 mM Tris-HCl (pH=7) and 10  $\mu$ l of 10 mg/ml lysozyme to the cell pellet and incubating the mix at 37°C for 60 minutes. Spores, so obtained, were washed 8 times one by one in different solutions: 1M

NaCl, deionized water, 0.05% SDS, TE containing one complete mini-protease inhibitor (Roche), deionized water, deionized water, deionized water and finally in PBS. Spores were pelleted down and the spore coat proteins were removed by adding 1 ml of freshly prepared decoating solution (see Table 2.1) and incubating at 60°C for 90 minutes, followed by a centrifugation at 10,000g for 1 min at 4°C. The pellet was then washed 3 times in STE (see Table 2.1) and once in a solution of 50 mM NaCl and 100 mM EDTA. Centrifugation was performed at 10,000 g for 1 min and the pellet was used for DNA isolation following the protocol explained in section 2.4.1.

## **2.11 RNA-Sequencing**

The RNA samples for RNA-sequencing were prepared by Dr. Amy Bottomley. Then, the sequencing and initial data analysis was performed by Dr. Gurjeet Singh Kohli at the Singapore Centre for Environmental Life Sciences Engineering (SCELSSE).

### **2.11.1 RNA extraction**

Overnight cultures of SU5 (wt) and SU664 (*Δpyk*) were grown in LB medium, diluted to a final OD<sub>600</sub> of 0.05 in fresh LB only, or in the presence of 1% pyruvate or L-alanine. This was performed in three biological replicates. All the cultures were grown at 37°C/ 200rpm to the mid-exponential phase (~ 5×10<sup>8</sup> cells) and samples were taken for the RNA extraction process. 1 ml of RNA protect reagent (QIAGEN Cat No. 76506) was added to each of the cell pellet, vortexed for 15s and kept at room temperature for 5 min. Cells were spun down by centrifugation at 5000 × g for 10 min. Supernatant was discarded and the tubes were centrifuged at 5000 × g for 2 min. Then 300μl of lysozyme, prepared as 20mg/ml stock in TE



buffer, was added to each of the pellets. The pellet was gently mixed with lysozyme and then mixed by vortexing at slow speeds (1-2) at room temperature for 10 min.

Total bacterial RNA was extracted from all the samples using miRNeasy Mini Kit (Qiagen Cat No. 217004). The first quality check for the extracted RNA samples was performed by measuring A260/280 and A260/230 using a Nanodrop. Next, the RNA samples underwent DNase treatment using the TURBO DNA-free kit (ThermoFischer Cat No. AM1907), followed by a magnetic bead treatment using Agencourt RNAClean XP (Beckman Coulter Cat No. A63987). Afterwards, the second round of RNA quality check was performed using the Nanodrop, the Agilent 2200 TapeStation System, the RNA BR assay kit and dsDNA HS assay kit to measure yield and purity.

### **2.11.2 Sequencing and read mapping**

Prior to the library preparation, RNA samples were quantified using Invitrogen's Ribogreen assay. Library preparation was performed according to Illumina's TruSeq Stranded mRNA protocol with the following modifications. The oligo-dT mRNA purification step was omitted and instead, for all samples 200 ng of total RNA was directly added to the Elution2-Frag-Prime step. The PCR amplification step, which selectively enriches for library fragments that have adapters ligated on both ends, was performed according to the manufacturer's recommendation but the number of amplification cycles was reduced to 12. Each library was uniquely tagged with one of Illumina's TruSeq LT RNA barcodes to enable library pooling for sequencing.

The finished libraries were quantified using Invitrogen's Picogreen assay and the average library size was determined on a Bioanalyzer 2100, using a DNA 7500 chip (Agilent). Library concentrations were then normalized to 4nM and validated by qPCR on a ViiA-7 real-time thermocycler (Applied Biosystems), using qPCR primers recommended in Illumina's

qPCR protocol, and Illumina's PhiX control library as standard. The libraries were then pooled at equimolar concentrations and sequenced in one lane on an Illumina HiSeq2500 sequencer in rapid mode at a read-length of 100bp paired-end.

The sequence reads were mapped to the genome sequence of *Bacillus subtilis* subsp. *subtilis* str. 168 (NCBI Reference Sequence: NC\_000964.3) and the systemic changes between different experimental conditions were obtained using the DESeq2 package. Genes with a fold change equal to or greater than 2 and p-value <0.05 were retained for further analysis.

## **2.12 Validation of RNA-Sequencing results**

### **2.12.1 cDNA preparation**

In order to perform qPCR for the validation of RNA-seq results, total RNA samples extracted for RNA-seq were converted to cDNA (complementary DNA) using the the SuperScript III First-Strand Synthesis System for RT-PCR (Invitrogen Catalog No. 18080-051). Briefly, 50ng of total RNA was mixed with 50ng/μl of random primers, incubated at 65°C for 5 min, and immediately placed on ice. cDNA synthesis mix was prepared and 10μl of the mix was added to RNA-primer mixture, mixed gently, collected by brief centrifugation and incubated at 25°C for 10 min, followed by 50 min at 50°C. The reaction was terminated by chilling on ice and 1μl of RNaseH was added to each of the tube, followed by incubation at 37°C for 20 min. The synthesized cDNA was stored at -20°C until further used for PCR.

### 2.12.2 qPCR reaction set up

qPCR reactions were set up using iTaq Universal Sybr Green Supermix (Sigma-Aldrich Catalog no. 1725121), following the manufacturer's instructions. Very briefly, reactions of 10 $\mu$ l total volume were set up by mixing 5 $\mu$ l of the Sybr Green Supermix, 1 $\mu$ l of forward (5 $\mu$ M) and reverse (5 $\mu$ M) primers each, 1 $\mu$ l of cDNA template (10ng/ $\mu$ l) and 2 $\mu$ l of ultrapure water. The reactions were set up in three technical replicates for all samples, including a no template control in 96 well PCR plate. The plate was then loaded into an Applied BioSystems QuantStudio™ 6 Flex System and experiment was run using the comparative  $\Delta\Delta C_T$  method. The run method included a hold cycle at 50°C for 2 min followed by 10 min at 95°C, and 40 PCR cycles of 15 sec at 95°C and 1 min at 60°C. Melting curve analysis was performed at 95°C for 15 sec, followed by 1 min at 60°C and 15 sec at 95°C.  $C_T$  value was determined for each of the sample, which was used to calculate the log<sub>2</sub> fold change of differential gene expression while comparing different experimental conditions.

### 2.12.3 qPCR efficiency evaluation

PCR efficiency of each primer set was determined using the protocol described by Brzoska and Hassan, 2014 (Brzoska and Hassan 2014). Briefly, qPCR reaction was set up as described in section 2.12.2, however cDNA was replaced by 10-fold serial dilutions of wild type *B. subtilis* (SU5) gDNA isolated from an overnight culture following the protocol described in section 2.4.1. An XY scatter plot was constructed for each primer pair with  $C_T$  values on the Y-axis and log<sub>10</sub> of the gDNA dilution factor on X-axis. Linear analysis was performed and PCR efficiency was determined from the slope of the linear regression line using the formula:

$$Efficiency = 10^{(-1/slope)} - 1 \times 100$$

### 2.12.4 Quantification of mRNA expression using the Comparative C<sub>T</sub> method

The comparative C<sub>T</sub> ( $\Delta\Delta C_T$ ) method quantifies the abundance of an mRNA in a test sample relative to the abundance of the same mRNA in a control sample. C<sub>T</sub> values obtained for target cDNA as well as the endogenous reference cDNA from qPCR reactions set up for test sample as well as the control sample were used to calculate  $\Delta C_T$  by employing the formulae:

$$\Delta C_{T (test\ sample)} = C_{T (target\ cDNA)} - C_{T (endogenous\ reference\ cDNA)}$$

$$\Delta C_{T (control\ sample)} = C_{T (target\ cDNA)} - C_{T (endogenous\ reference\ cDNA)}$$

$\Delta\Delta C_T$  values for the test sample was then calculated using the formula:

$$\Delta\Delta C_T = \Delta C_{T (test\ sample)} - \Delta C_{T (control\ sample)}$$

Relative abundance of the target cDNA in the test sample normalized to the endogenous reference was calculated by applying the formula:

$$Relative\ abundance = 2^{-\Delta\Delta C_T}$$

Next, log<sub>2</sub> of the relative abundance value was calculated to determine the log<sub>2</sub> fold change of target mRNA expression in the test sample as compared to the control sample.



# Chapter 3

---

**Identification of a key metabolite in the  
coordination of central carbon  
metabolism and Z ring positioning in *B.*  
*subtilis***

## 3.1 Introduction

### 3.1.1 The link between central carbon metabolism and cell division in *B. subtilis*

Cell division must be coordinated with other cellular processes such as DNA replication and metabolism to ensure the viability of newborn cells. One such coordination is the control of cell division by metabolic pathways. This becomes increasingly important under conditions of nutritional fluctuation, wherein a bacterial cell needs to regulate its division process as per the concomitant changes in cellular growth rate (Wang and Levin 2009). Recently a number of metabolic enzymes belonging to accessory metabolic pathways such as the glucolipid, phospholipid and glutamate synthesis pathways, have been identified as having a role in regulating the bacterial division process in a number of different bacterial species (Weart et al. 2007; Hill et al. 2013; Shi et al. 2014; Beaufay et al. 2015). These identified links clearly demonstrate that the coordination between metabolism and division is an important regulatory link. However, the study by Monahan *et al.* in 2014 was the first to identify a link between glycolysis, a central carbon metabolic pathway, and cell division in *B. subtilis*.

Initial experiments performed by Monahan *et al.* showed that inactivation of the pyruvate kinase (*pyk*) enzyme that catalyzes the last step of glycolysis, suppressed the inhibition of division phenotype of the temperature-sensitive *ftsZ* mutant (*ts1*) of *B. subtilis* (Monahan et al. 2014a). Subsequently, *pyk* deletion in wild type cells shifted the Z ring positioning away from midcell and towards the cell pole in one third of the cell population, suggesting a role for pyruvate kinase in the correct Z ring positioning of *B. subtilis* cells. Addition of the product of pyruvate kinase, pyruvate, to the growth medium relieved the Z ring positioning defect of  $\Delta$ *pyk* cells (Monahan et al. 2014a). These results demonstrated that pyruvate kinase itself or its activity is not connected to the Z ring positioning. Rather, its product, pyruvate, is important in coordinating cellular metabolic levels with the division

machinery in *B. subtilis* (Monahan et al. 2014a). But, pyruvate, being the end product of glycolysis and being at the intersection of several important metabolic pathways, has a number of fates within a bacterial cell; which raises the possibility that any one of these potential fates being important for the correct *Z* ring positioning in *B. subtilis*.

### **3.1.2 Potential fates of pyruvate in a bacterial cell**

Pyruvate is a key metabolite in the bacterial cell and is found at the intersection of several metabolic pathways. It can be metabolized in a variety of ways into various metabolites, as shown in Figure 3.1. It can be converted to acetyl-CoA by the enzyme pyruvate dehydrogenase, which then gets metabolized into the TCA cycle. Acetyl-CoA is also used for the biosynthesis of fatty acids and acetate. L-alanine is directly produced from pyruvate via the enzyme alanine dehydrogenase, which then gets converted to D-alanine by alanine transaminase. Valine and leucine are the other amino acids that are produced directly from pyruvate. In addition, pyruvate can be fermentatively reduced to lactate and acetoin. Considering the potential metabolism of pyruvate into many metabolic fates, any of these metabolites derived from pyruvate could be actually responsible for the correct *Z* ring positioning in *B. subtilis*.

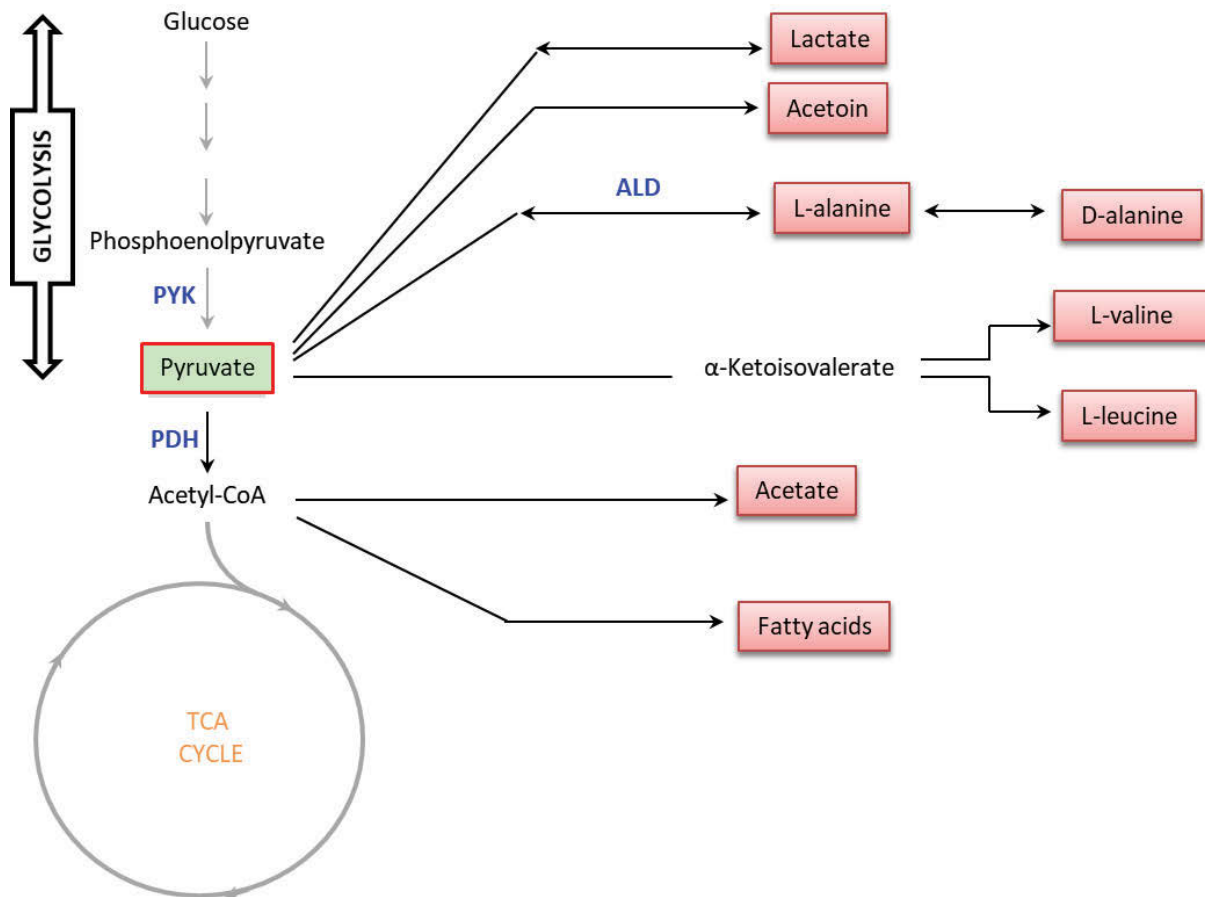


**Figure 3.1. Potential fates of pyruvate in *B. subtilis*.** Pyruvate, produced through glycolysis, can be converted to acetyl-CoA by the enzyme pyruvate dehydrogenase (PDH). Acetyl-CoA can be used for the biosynthesis of fatty acids or acetate or can enter the TCA cycle. Lactate and acetoin are produced fermentatively from pyruvate. Pyruvate can directly produce amino acids like alanine, valine and leucine. Initially, L-alanine is produced from pyruvate, which can then get converted to D-alanine.

### 3.2 Chapter aims

The study by Monahan *et al.* demonstrated the possible role of pyruvate in the Z ring positioning in *B. subtilis*. But as discussed in section 3.1.2, pyruvate has multiple metabolic fates within a bacterial cell. This raises the question of whether pyruvate itself is directly involved in regulating the position of Z ring, or whether it influences division site positioning by being metabolized into any of its downstream metabolites. To answer this question and to



identify the nature of the link between Z ring positioning and central carbon metabolism in *B. subtilis*, the primary objective of this chapter was to test each of the pyruvate fates for their effect on the Z ring positioning in *B. subtilis* cells.

### 3.3 Results

#### 3.3.1 Confirming the results published by Monahan *et al.*

Before testing the pyruvate-derived metabolites, initial experiments were performed to confirm previous data published in the Monahan *et al.* (2014) study and to validate the experimental conditions used. Consistent with the previous work, about 30% of the  $\Delta pyk$  cells formed misplaced Z rings while the wild type control strain formed Z rings almost exclusively at midcell (Figure 3.2). The loss of pyruvate kinase had no effect on the actual frequency of Z rings in  $\Delta pyk$  cells (87% of cells contained a Z ring) as compared to wild type cells (85%); just the position of Z ring was affected. However, similar to the study by Monahan *et al.*,  $\Delta pyk$  cells were much shorter than the wild type cells, as indicated by the measurement values presented in Table 3.1 and further confirmed by statistical analysis (P-value of <0.001). In agreement with the results of Monahan *et al.*, the addition of pyruvate to a final concentration of 1% to the growth medium (L-broth) rescued the Z ring positioning defect of  $\Delta pyk$  cells (P-value<0.001), with pyruvate addition having no effect on the Z ring positioning of wild type cells (P-value = 0.739, Figure 3.2).

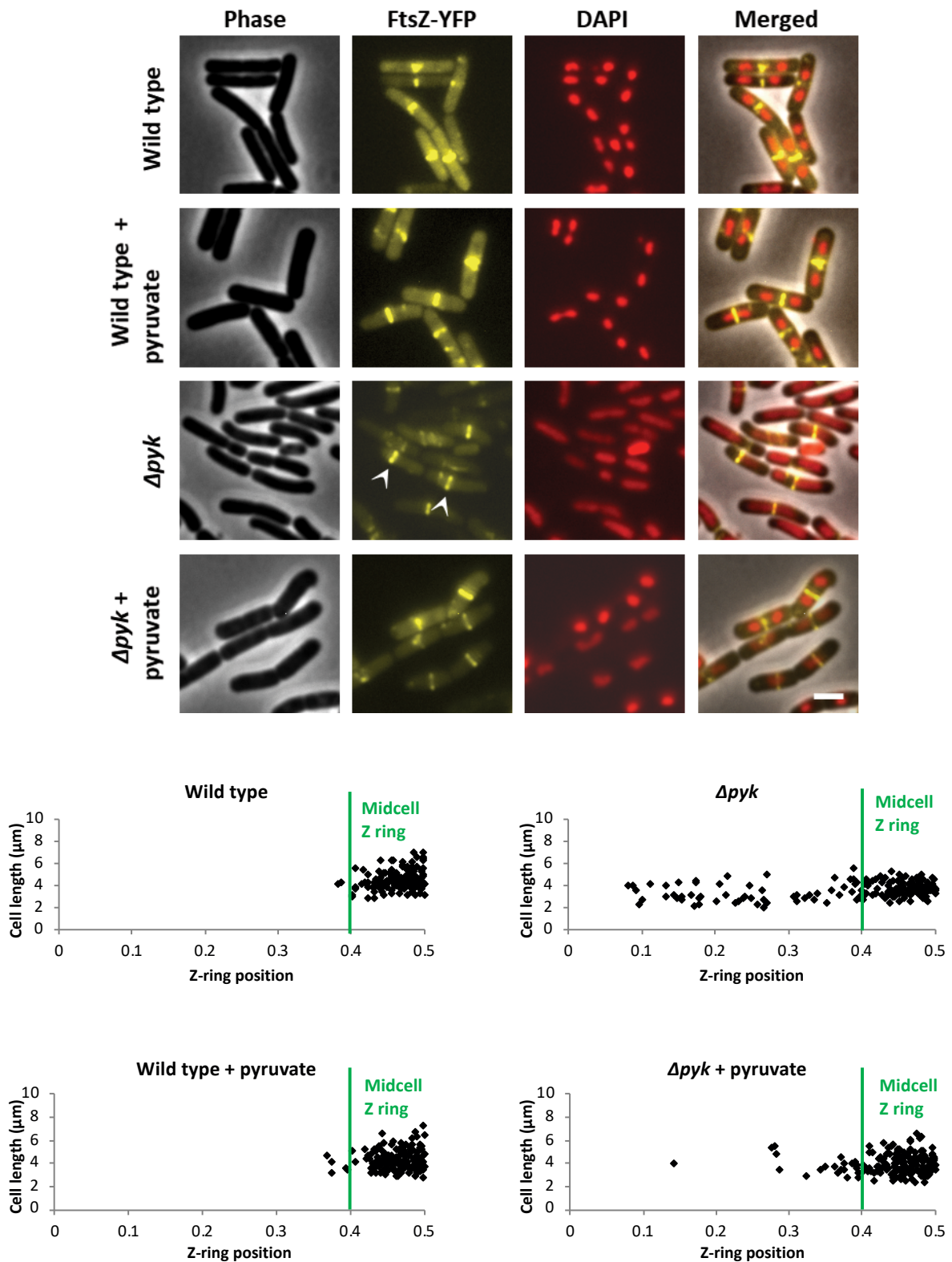


**Figure 3.2.** The effect of pyruvate on the Z ring positioning of  $\Delta pyk$  cells. Cells were grown to mid-exponential phase in the presence of 0.01% xylose in L-broth at 37°C with or without the addition of 1% pyruvate and visualized by phase-contrast and fluorescence microscopy (n=3). Scale bar, 2 $\mu\text{m}$ .

White arrows in the FtsZ-YFP panel point towards the acentral Z rings. Lower panel shows the scatter plots wherein cell length has been plotted as a function of Z ring positioning under different experimental conditions. Here, the Z ring position of 0 and 0.5 on the x-axis signify the cell pole and cell centre, respectively.  $n > 150$ . [Wild type = SU492 (*amyE::Pxyl-ftsZ-yfp*),  $\Delta pyk$  = SU679 (*\Delta pyk amyE::Pxyl-ftsZ-yfp*)]

**Table 3.1. The effect of different metabolites on the doubling time and the Z ring positioning in  $\Delta pyk$  cells**

Strain $\pm$ metabolite	Frequency of acentral Z rings (%)	P value for Z ring positioning in comparison to $\Delta pyk^*$	Cell length ( $\mu\text{m}$ ) (average cell length $\pm$ SEM)	Doubling time (min)**	P value for doubling time in comparison to $\Delta pyk^*$
Wild type	1.9	<0.001***	4.2 $\pm$ 0.06	31 $\pm$ 0.71	0.005***
$\Delta pyk$	30.9	-	3.6 $\pm$ 0.05	54 $\pm$ 1.39	-
$\Delta pyk$ + pyruvate	11.8	<0.001***	4.0 $\pm$ 0.06	48 $\pm$ 4.51	0.264
$\Delta pyk$ + acetate	29.5	0.165	3.6 $\pm$ 0.05	78 $\pm$ 6.39	0.001***
$\Delta pyk$ + acetoin	30.4	0.453	3.7 $\pm$ 0.05	63 $\pm$ 0.47	0.216
$\Delta pyk$ + L-lactate	21.4	0.540	4.3 $\pm$ 0.08	46 $\pm$ 5.09	0.530
$\Delta pyk$ + L-alanine	5.0	0.008**	4.0 $\pm$ 0.06	53 $\pm$ 4.13	0.798
$\Delta pyk$ + D-alanine	30.3	0.290	3.4 $\pm$ 0.08	50 $\pm$ 0.29	0.405
$\Delta pyk$ + L-valine	30.1	0.685	3.4 $\pm$ 0.05	54 $\pm$ 4.69	0.803
$\Delta pyk$ + L-leucine	31.7	0.520	3.6 $\pm$ 0.06	42 $\pm$ 3.83	0.042***

\*P-values were calculated using one-way Anova along with Tukey Pairwise comparison on three biological replicates (Wild type- SU492,  $\Delta pyk$ - SU679)

\*\*Doubling time was calculated by taking an average of the doubling times ( $\pm$  SEM) of three biological replicates obtained, except for wild type and  $\Delta pyk$  (no metabolite added), where the values represent an average of respective growth curves performed during the experiments for all metabolites. Wild type and  $\Delta pyk$  cells were grown in Luria broth in the presence and absence of a particular metabolite (1 %),  $A_{600}$  was recorded every hour for 8 hours, growth curve was plotted and the doubling time was calculated from the exponential phase

\*\*\* denotes that the samples under investigation are significantly different from  $\Delta pyk$  based on one-way Anova

Using DAPI staining to visualize DNA, it was observed that the nucleoids of  $\Delta pyk$  cells were very different from the wild type cells, as shown by the images in Figure 3.2. The nucleoids appeared very dispersed in the  $pyk$  mutant cells with no clear separation of nucleoids in the central region of the cells. This is contrary to the wild type cells where two nucleoid ‘lobes’ per cell are clearly visible. This observation of a change in nucleoid morphology of  $\Delta pyk$  was not reported by Monahan *et al.*, and considering that this change in nucleoid morphology could potentially contribute to the Z ring positioning defect of  $\Delta pyk$  cells, it was investigated further and the correlation of this change in nucleoid morphology with the Z ring positioning defect in  $\Delta pyk$  cells will be discussed in detail in section 3.3.4.

### **3.3.2 L-alanine, a product of pyruvate metabolism, rescues the Z ring positioning defect of $\Delta pyk$ cells in a growth-rate independent manner**

Considering the observation that pyruvate rescued the Z ring positioning defect of  $\Delta pyk$  cells, and the fact that pyruvate can be metabolized into various products; it became crucial to test whether pyruvate availability influences the Z ring positioning in  $\Delta pyk$  cells directly or via conversion into any of its downstream products. In order to investigate this, eight metabolites (L-valine, L-leucine, L-lactate, acetoin, acetate, L-alanine, D-alanine, fatty acids) produced directly from pyruvate were added one by one at a concentration of 1% to the growth medium (L broth) of  $\Delta pyk$  cells to examine whether any of these metabolites rescues the Z ring positioning defect. Each of these metabolites were tested for their effect on the Z ring positioning, as well as the growth rate, in  $\Delta pyk$  cells. Growth rate was monitored to test whether the Z ring positioning rescue, if observed with any of the metabolites, is growth-rate dependent.

This is essential to investigate as the the *pyk* deletion itself causes a significant reduction in growth rate compared to wild type cells (Table 3.1).

Amongst all the metabolites tested, only L-alanine rescued the Z ring positioning defect of  $\Delta pyk$ , as shown in the microscopy images and the scatter plots in Figure 3.3 (also see Table 3.1). The addition of L-alanine to the growth medium was found to have a significant effect on the Z ring positioning in  $\Delta pyk$  cells, while L-alanine addition in wild-type cells had no discernible effect. Other metabolites that were tested and observed not to rescue the Z ring positioning defect of  $\Delta pyk$  cells include L-valine, L-leucine, D-alanine, acetate, acetoin and L-lactate (see Table 3.1). For representative figures of all these metabolites, see Appendix I of this thesis. Fatty acids were not tested by this method as addition to growth media was observed to be inhibitory to the growth of *B. subtilis* cells, therefore, they were tested by the construction of a genetic mutant (results explained in section 3.3.3).

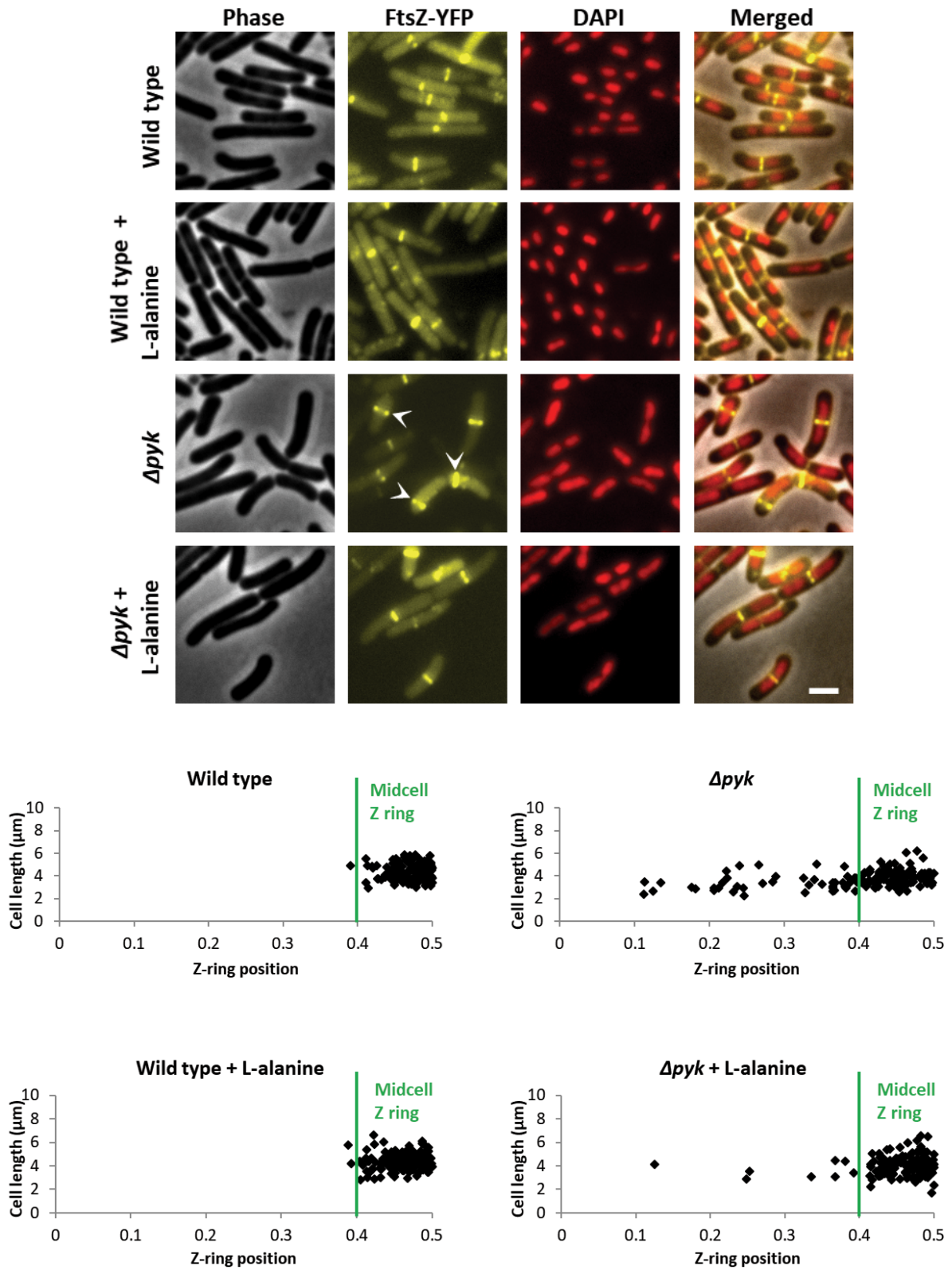


**Figure 3.3.** The effect of L-alanine on the Z ring positioning of  $\Delta pyk$  cells. Cells were grown to mid-exponential phase in the presence of 0.01% xylose in L broth at 37°C with or without the addition of 1% L-alanine and visualized by phase-contrast and fluorescence microscopy (n=3). Scale bar, 2 $\mu\text{m}$ .

White arrows in the FtsZ-YFP panel point towards the acentral Z rings. Lower panel shows the scatter plots wherein cell length has been plotted as a function of the Z ring positioning under different experimental conditions. Here, the Z ring position of 0 and 0.5 on the x-axis signify the cell pole and cell centre, respectively.  $n > 150$ . (Wild type = SU492 (*amyE::Pxyl-ftsZ-yfp*),  $\Delta pyk$  = SU679 (*\Delta pyk amyE::Pxyl-ftsZ-yfp*))

To explore any potential relationship between the cellular growth rate and the Z ring positioning rescue, in addition to looking at the Z ring positioning, the growth pattern of wild type and  $\Delta pyk$  cells in the presence as well as the absence of each of the metabolites was also monitored. The average doubling times of three biological replicates and P-values obtained from the One-way Anova test are shown in Table 3.1. None of the other metabolites had any significant effect on the growth rate of wild type cells (Appendix I Table 1). Both pyruvate and L-alanine, which rescued the Z ring positioning defect of  $\Delta pyk$  cells, had no significant effect on the doubling time of  $\Delta pyk$  cells, suggesting that the Z ring positioning is growth-rate independent. Additionally, L-leucine significantly decreased the doubling time of  $\Delta pyk$  cells (42 min) such that the doubling time became closer to the wild type cells (P-value of 0.042 for  $\Delta pyk + \text{leucine}$  vs.  $\Delta pyk$ ). Yet, L-leucine had no effect on the Z ring positioning of  $\Delta pyk$  cells, confirming that changes in growth rate is not enough to rescue the Z ring positioning in  $\Delta pyk$  cells. None of the other metabolites had any effect on the doubling time of  $\Delta pyk$  cells, except acetate, which increased the doubling time of  $\Delta pyk$  significantly to 78 min, likely due to toxicity.

### 3.3.3 Testing fatty acids for their role in Z ring positioning via the construction of a fatty acid synthesis mutant

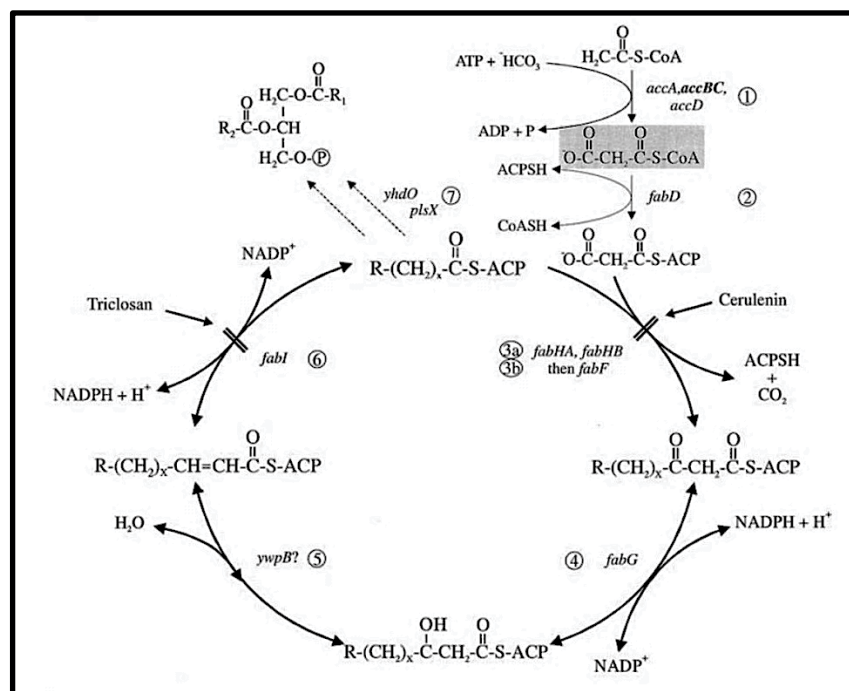
Initially, the role of fatty acids in the ability to rescue the Z ring positioning was investigated using similar methods as described in Section 3.3.2. However, it was found that the oleic acid, a long-chain fatty acid, added to growth medium severely inhibited the growth of *B. subtilis* at all concentrations tested (0.001, 0.1 and 1%) such that the effect of oleic acid on the Z ring positioning of  $\Delta pyk$  could not be tested (data not shown). It has been previously reported that fatty acids are inhibitory to *B. subtilis* growth, however it has been shown that short-chain fatty acids are less toxic as compared to long chain fatty acids (Sheu and Freese 1972). Therefore, the ability of isobutyric acid, a short-chain fatty acid, to rescue the Z ring positioning of  $\Delta pyk$  was investigated. Whilst not inhibitory to wild-type *B. subtilis* growth, the *pyk* mutant could not grow in the presence of isobutyric acid at the lowest concentration tested (0.001%; data not shown), suggesting that  $\Delta pyk$  cells are not able to metabolize even the very low concentrations of fatty acid added to the media. Therefore, the possibility of pyruvate metabolism to fatty acids being responsible for the Z ring positioning rescue of  $\Delta pyk$  cells was investigated by constructing a genetic mutant of the fatty acid synthesis pathway.

Fatty acids are synthesized from pyruvate via the Fab (fatty acid biosynthetic) pathway, which is shown in Figure 3.4A (Schujman et al. 2003). The initial step of fatty acid elongation is carried out by the enzyme FabHA, therefore, a deletion of *fabHA* will not allow the accumulation of intermediate products. Since the Fab pathway, including FabHA, is essential for *B. subtilis* growth, *fabHA* was placed under the control of an inducible promoter (SU880-*Pspac-fabHA amyE::Pxyl-ftsZ-yfp*, Murray and Koh, 2014) to allow for titratable and conditional expression of this gene. As shown in Figure 3.4B, the *fabHA* mutant under uninduced conditions did not show any defect in the Z ring positioning compared to wild-type ( $P = 0.554$ ). This suggests that the production of fatty acids from pyruvate is not essential for



the correct *Z* ring positioning in *B. subtilis*. However, the mutant under uninduced conditions showed decreased cell length as compared to wild type cells (P-value 0.027;  $\Delta fabHA$ - 3.72  $\mu\text{m}$ , wild type – 4.66  $\mu\text{m}$ ), indicating that the deletion of *fabHA* does reduce the cell length in *B. subtilis*. An inhibition of fatty acid synthesis has been shown to cause a decreased cell size in *B. subtilis* (Vadia et al. 2017), indicating that the *fabHA* mutant strain is indeed defective in fatty acid synthesis under the conditions used in this study.

(A)



(B)

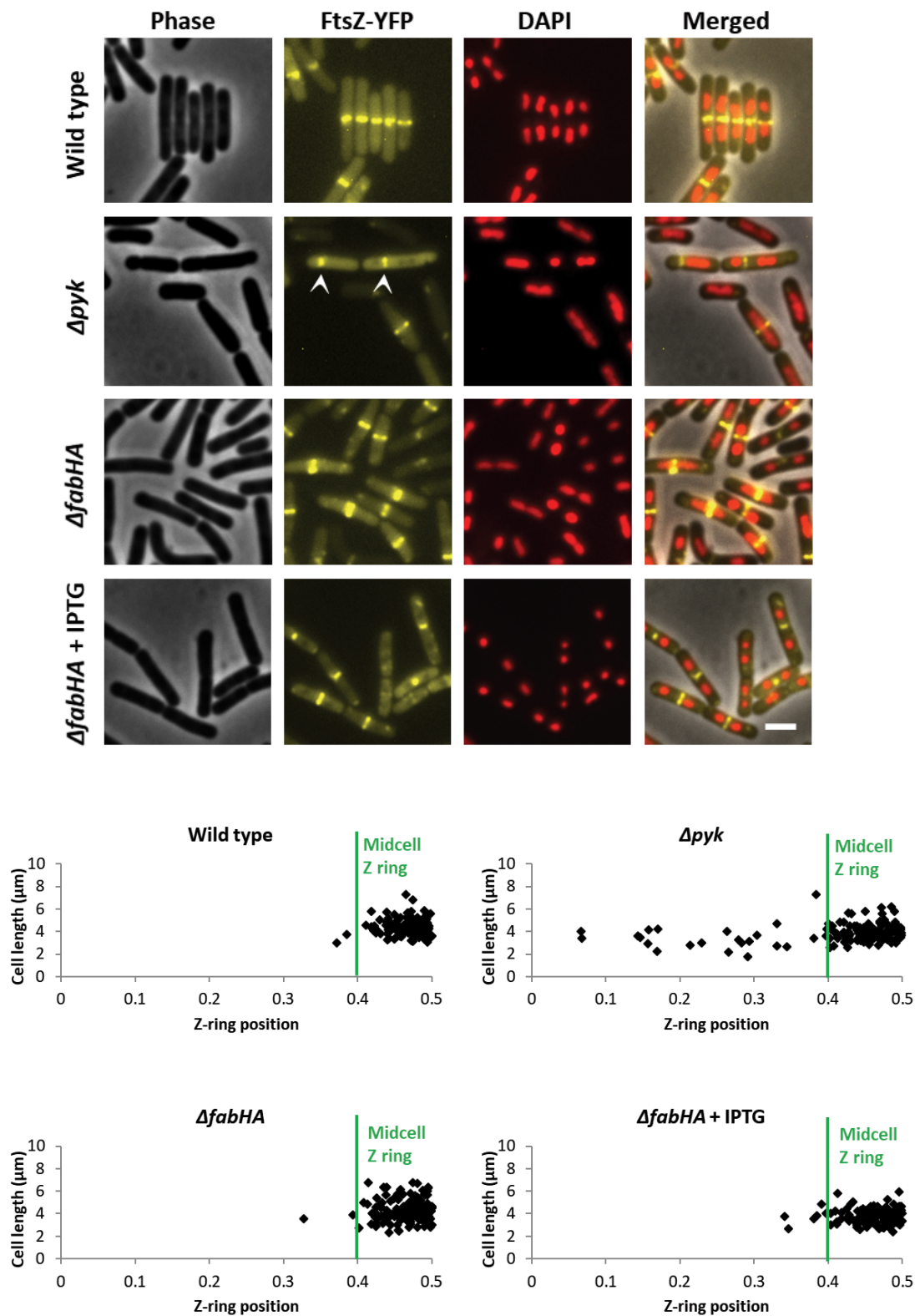


**Figure 3.4.** Role of fatty acids in the Z ring positioning and cell length in *B. subtilis* (A) Fatty acid synthesis pathway in *B. subtilis* (Schujman et al. 2003). The enzyme Acc converts Acetyl-CoA to

malonyl-CoA, which is then transferred to ACP by the enzyme FabD. Subsequently, the enzymes FabHA and FabHB initiate the elongation reactions for the synthesis of short and long-chain fatty acids.




(B) Wild type (SU492) and  $\Delta pyk$  (SU679) were grown to mid-exponential phase in the presence of 0.01% xylose at 37°C, whereas SU880 (*Pspac-fabHA amyE::Pxyl-ftsZ-yfp*) was grown in the presence of 0.01% xylose at 37°C in the absence (uninduced) and presence of 1mM IPTG (induced) to the mid-exponential phase. All the samples were visualized by phase-contrast and fluorescence microscopy (n=2). White arrows in the FtsZ-YFP panel point towards the acentral Z rings. Lower panel shows the scatter plots wherein cell length has been plotted as a function of the Z ring positioning under different experimental conditions. Here, the Z ring position of 0 and 0.5 on the x-axis signify the cell pole and cell centre, respectively. n > 150.

### **3.3.4 Investigating the correlation between nucleoid morphology and Z ring positioning in $\Delta pyk$ cells**

As discussed in section 3.3.1, the nucleoid appeared to occupy more space in  $\Delta pyk$  cells instead of appearing as bilobed nucleoids, as seen in wild type cells. The bilobed nucleoid morphology has been previously reported to be related to an increased frequency of midcell Z rings in *B. subtilis* (Moriya et al. 2010). In our analysis, 96% of the wild type cells displayed the bilobed nucleoid morphology, which correlated with their 98.1% midcell Z ring positioning. Previous studies have also reported that when a specific step of the DNA replication process is blocked, it causes a change in nucleoid morphology. A block in the initiation step of the replication by using a temperature sensitive *dnaB* mutant (*dna-1*) resulted in the formation of 79% single lobed nucleoids (Moriya et al. 2010) and cells arrested for the elongation step of DNA replication displayed a non-compact nucleoid morphology that filled most of the cellular cytoplasm (Goranov et al. 2005). Furthermore, this change in the nucleoid morphology of *dna-1* mutant was shown to result in their acentral Z ring positioning (92%) (Moriya et al. 2010).

As the *pyk* mutant also showed a different nucleoid morphology compared to the wild type cells, in order to ascertain whether there is any correlation between this different nucleoid morphology and the Z ring positioning, a quantification of different nucleoid morphologies was carried out for different experimental conditions. Nucleoid morphologies were categorized into single lobes, bilobes and spread. ‘Single-lobed’ nucleoids had one region of intense staining, ‘bilobed’ nucleoids consisted of two regions of staining, while the ‘spread’ nucleoid consisted of staining distributed throughout the cell. Representative images for each of these nucleoid morphologies along with their percentages in different experimental conditions described so far are given in Table 3.2.

**Table 3.2. Types of nucleoid morphologies observed under different experimental conditions and their correlation with the Z ring positioning**

Strain ± metabolite	Percentage of each nucleoid morphology*			Predominant nucleoid morphology	Z ring positioning
	Single lobes	Bilobes	Spread		
					
Wild type	1.6	96	2.4	Bilobes	Midcell
$\Delta pyk$	0.7	10.3	89	Spread	Acentral
$\Delta pyk$ + pyruvate	1.9	49.2	48.8	Bilobes	Midcell
$\Delta pyk$ + acetate	0	12.2	87.8	Spread	Acentral
$\Delta pyk$ + acetoin	0.3	5.8	93.9	Spread	Acentral
$\Delta pyk$ + L-lactate	1.9	9.9	88.2	Spread	Acentral
$\Delta pyk$ + L-alanine	1.2	6.7	92.1	Spread	Midcell
$\Delta pyk$ + D-alanine	2.7	33.4	63.8	Spread	Acentral
$\Delta pyk$ + L-valine	1.3	12.8	85.9	Spread	Acentral
$\Delta pyk$ + L-leucine	2	12.4	85.6	Spread	Acentral
$\Delta fabHA$	0.4	98.4	1.2	Bilobes	Midcell

\*Percentages represent an average of three biological replicate, except for wild type and  $\Delta pyk$ , where the values represent an average of all the experiments performed for all the metabolites

The primary observation from the nucleoid morphology analysis is the increase in frequency of spread nucleoids in  $\Delta pyk$  cells (89%) as compared to only 2% observed in wild type cells, and a decrease in bilobed nucleoids to only 10% in  $\Delta pyk$  cells from 96% in wild type cells. Furthermore, whether this different nucleoid morphology defect contributes to their Z ring positioning defect, was examined by quantifying different nucleoid morphologies when pyruvate and its various metabolic fates are added to  $\Delta pyk$  cells. Interestingly, pyruvate addition did reverse the nucleoid morphology from spread to bilobes with 49% cells showing bilobed nucleoid morphology, however the rescue was not to the level of wild type cells (96% bilobed nucleoids). However, this did not correlate with the frequency of midcell Z rings after pyruvate addition to  $\Delta pyk$  (refer to Table 3.1). Also, the degree of nucleoid morphology rescue observed after pyruvate addition varied over different experimental replicates, hinting that while the rescue from a mainly spread nucleoid morphology to a bilobed one could be one of the contributing factors that allows the Z ring positioning rescue after pyruvate addition. However, it is not the sole reason for the Z ring positioning rescue of  $\Delta pyk$  cells.

Apart from pyruvate, the addition of D-alanine to  $\Delta pyk$  cells also partially rescued the nucleoid morphology of  $\Delta pyk$  to 33% bilobed nucleoids. However, D-alanine did not rescue their Z ring positioning defect (30% acentral Z rings, Table 3.1). Furthermore, L-alanine addition, which rescued the Z ring positioning defect of  $\Delta pyk$  cells (95% midcell Z rings, Table 3.1) did not change nucleoid morphology back to wild-type levels; there were only 7% bilobed nucleoids (Table 3.2). These results highlight that there is no clear correlation between the nucleoid morphology and the Z ring positioning in  $\Delta pyk$  cells.

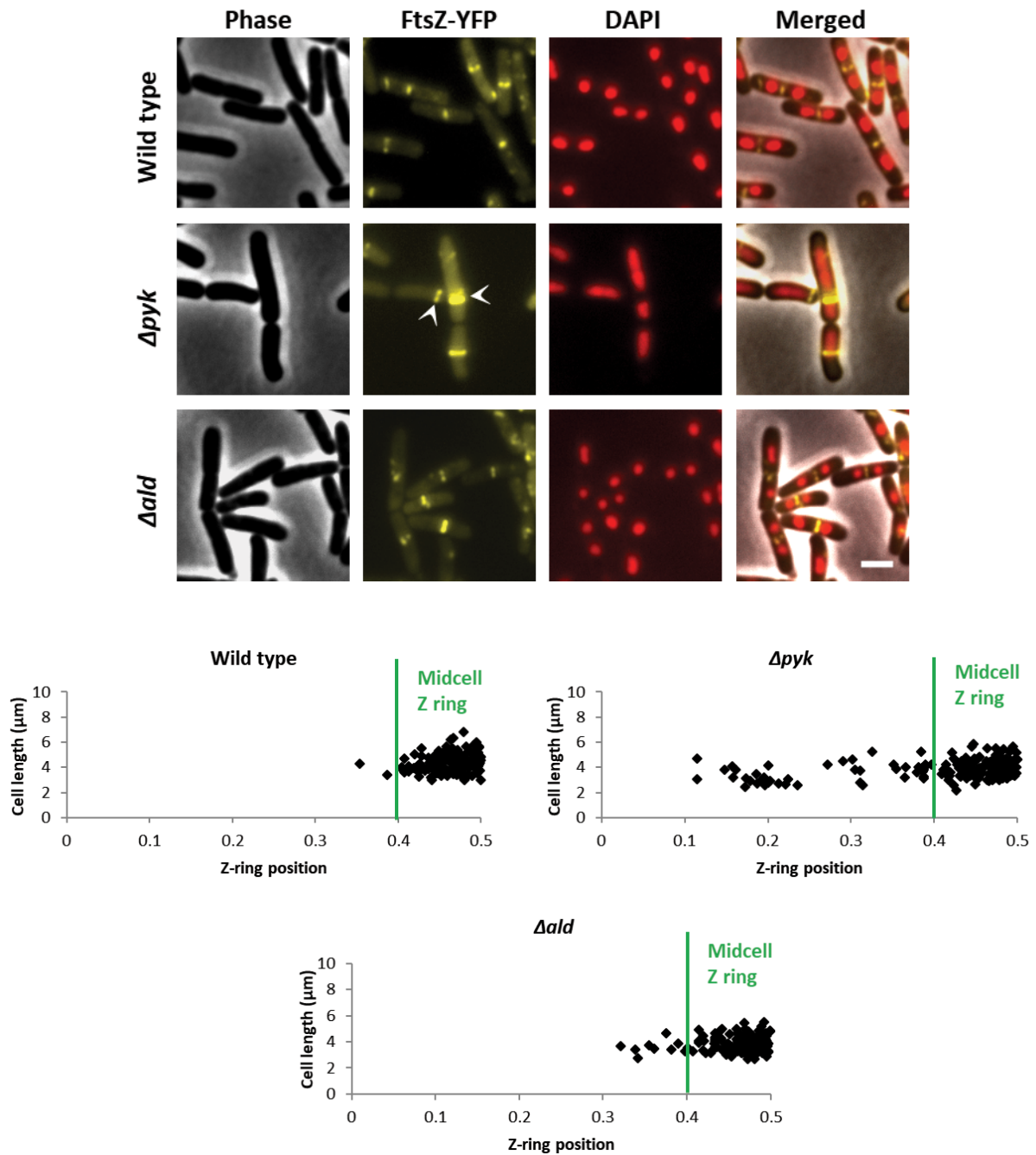
### 3.3.5 L-alanine conversion to pyruvate causes the Z ring positioning rescue

Since pyruvate and a potential fate of pyruvate, L-alanine, rescued the Z ring positioning defect and PDHE1 $\alpha$  localization of  $\Delta pyk$  cells, the metabolic process of pyruvate to L-alanine conversion was further investigated. L-alanine can interconvert with pyruvate by the action of alanine dehydrogenase (Ald) (Ling Ling et al. 2011). Since pyruvate and L-alanine both rescued the Z ring positioning defect of  $\Delta pyk$  cells and they are interconvertible via Ald, either or both of these metabolites could be responsible for the observed rescue. In order to test which of these metabolites is actually responsible for the Z ring positioning rescue of  $\Delta pyk$ , an alanine dehydrogenase deletion mutant, SU826 ( $\Delta ald amyE::Pxyl-ftsZ$ ), was constructed by replacing the *ald* gene by an antibiotic (erythromycin) resistance cassette (ErmR), following the Gibson assembly approach explained in section 2.5. The *ald* mutant would be expected to synthesize pyruvate normally but would not be able to produce L-alanine due to the absence of the Ald enzyme (refer to Figure 3.1). The Z ring phenotype of this mutant strain will provide useful information on isolating the roles of each of these metabolites in the Z ring positioning in *B. subtilis*.

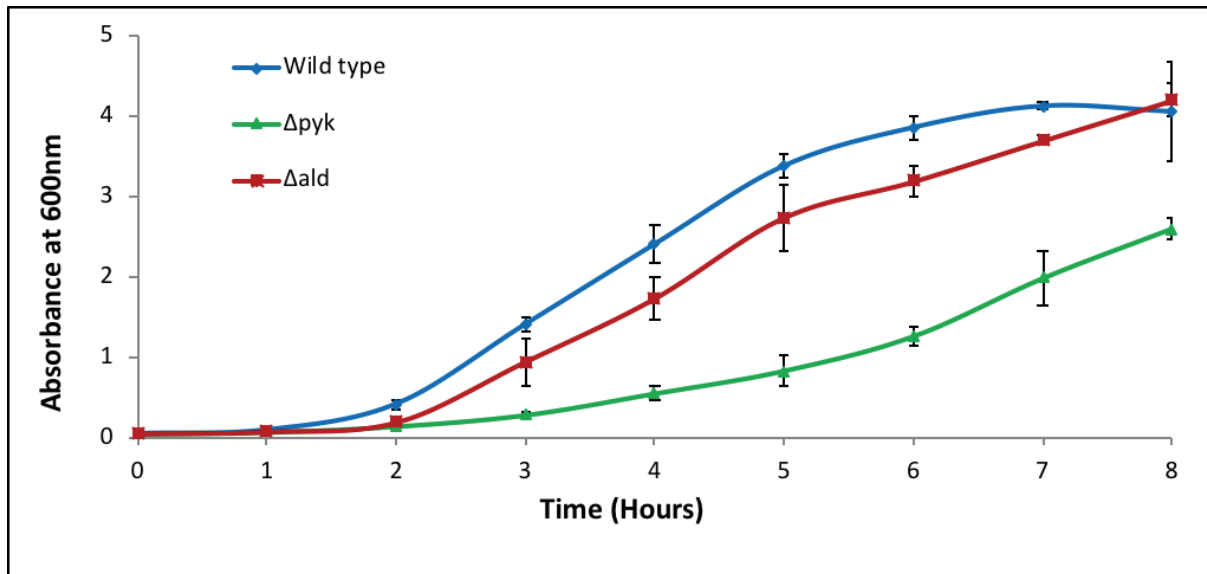
There are two possibilities for the Z ring placement in the *ald* mutant. The first is that the mutant will have a defect in the Z ring positioning (increase in acentral rings compared to wild type), indicating that L-alanine is connected to the Z ring positioning. In this scenario, addition of L-alanine to  $\Delta ald$  cells should rescue the Z ring positioning – so that they return to the midcell site. The second possibility is that the  $\Delta ald$  cells will have all the Z rings positioned at midcell, which would infer that pyruvate and not L-alanine is required for the correct Z ring positioning at the cell centre. As shown in Figure 3.5A,  $\Delta ald$  did not show any defect in the Z ring positioning. That is, 94% of the Z rings formed at midcell, with a P-value of 0.394 compared to the Z ring positioning in wild-type (SU492). This suggested that it is pyruvate and

not L-alanine, which can rescue the Z ring positioning defect of  $\Delta pyk$  cells when L-alanine is added, and that this occurs via the L-alanine to pyruvate conversion, catalysed by Ald.

(A)



(B)



(C)

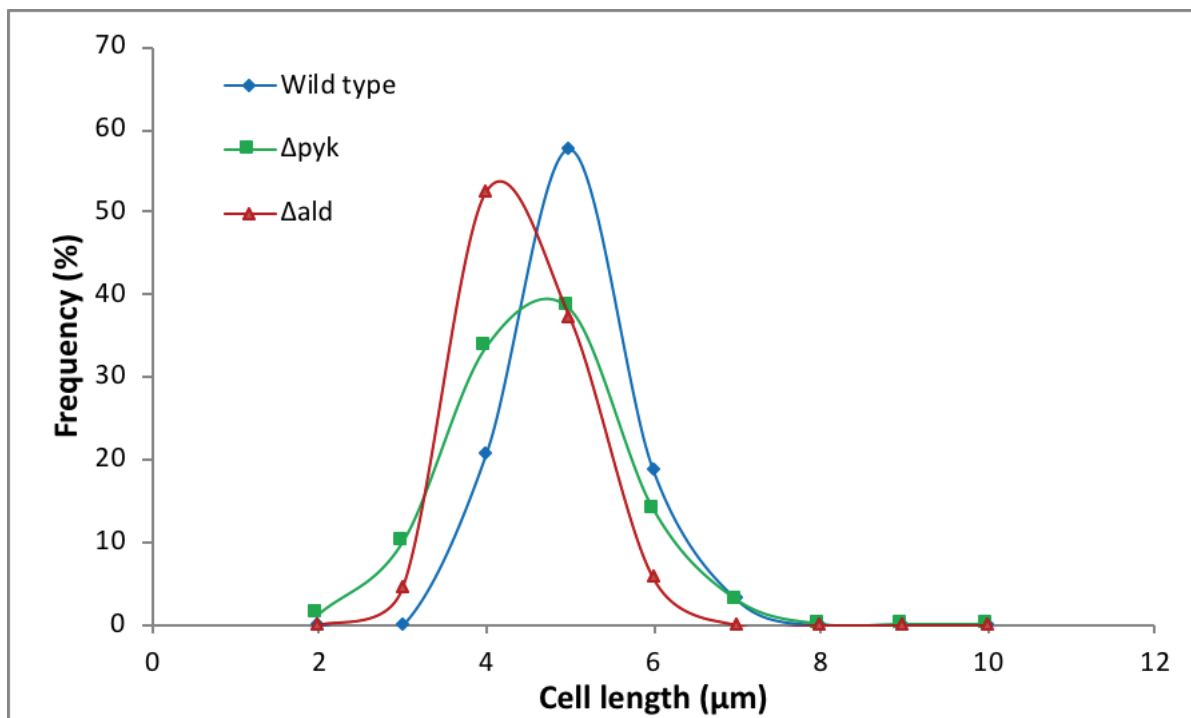


**Figure 3.5. Z ring positioning, growth rate and cell length of the alanine dehydrogenase mutant**

(A) Cells were grown to mid-exponential phase in the presence of 0.01% xylose at 37°C and visualized by phase-contrast and fluorescence microscopy (n=3). Scale bar, 2 $\mu m$ . White arrow points to the acentral Z rings. Lower panel shows the scatter plots wherein cell length has been plotted as a function



of Z ring positioning under different experimental conditions.  $n > 150$ . **(B)** Growth curves of wild type (SU492),  $\Delta pyk$  (SU679) and  $\Delta ald$  (SU826) cells. Overnight cultures were back-diluted in fresh LB to an absorbance of 0.05 and grown for 8 hours in conical baffled flasks at 37°C/ 200 rpm. Absorbance readings were taken every hour and plotted against time. Growth curves were performed in triplicate and the graph represents average values of the three biological replicates, with error bars depicting the standard deviation. **(C)** Line graph depicting the cell length distribution of wild type (SU492),  $\Delta pyk$  (SU679) and  $\Delta ald$  (SU826) cells ( $n > 150$ ).

Although the deletion of *ald* did not show an effect on the Z ring positioning, its deletion did reduce the growth rate, compared to wild type cells (Figure 3.5B, P-value  $< 0.001$ ). A mutation in *ald* has been shown to reduce the rate of alanine utilization (Siranosian et al. 1993), which could explain the observed decrease in growth rate. Also, the *ald* mutant showed a decreased cell length (Figure 3.5C) as compared to wild type cells (P-value  $< 0.001$ ). In fact, the cells were as short as  $\Delta pyk$  cells (P-value 0.054). This decrease in cell length is probably a result of growth rate defect of these cells. Furthermore, the nucleoid morphology of the *ald* mutant was also analysed considering the previous observation of more bilobed nucleoid morphology correlating with an increased frequency of midcell Z rings (section 3.3.4). The nucleoid morphology analysis revealed that 96% of the  $\Delta ald$  cells displayed a bilobed nucleoid pattern, correlating with their midcell Z ring frequency of 94%.

From the Z ring positioning analysis of the *ald* mutant, the conversion of L-alanine to pyruvate appears to be the sole reason for the Z ring positioning rescue observed with L-alanine addition. In other words, the added L-alanine to  $\Delta pyk$  cells gets converted to pyruvate via Ald, increasing the levels of pyruvate in  $\Delta pyk$  cells, rescuing the Z ring positioning. To support this suggestion, pyruvate levels were measured in  $\Delta pyk$  cells supplemented with L-alanine using the Pyruvate Assay kit (Sigma-Aldrich) following the procedure explained in Section 2.8. If

the above hypothesis holds true, the concentration of pyruvate should increase in  $\Delta pyk$  cells when supplemented with L-alanine. Additionally, the level of pyruvate in  $\Delta pyk$  cells supplemented with L-alanine should be approximately equal to the level of pyruvate when pyruvate itself is added to  $\Delta pyk$  cells. Furthermore, to test whether the deletion of alanine dehydrogenase has any effect on pyruvate levels, pyruvate levels were also measured in  $\Delta ald$  cells, which formed Z rings at midcell similarly to wild type cells. The results obtained are shown in Figure 3.6.

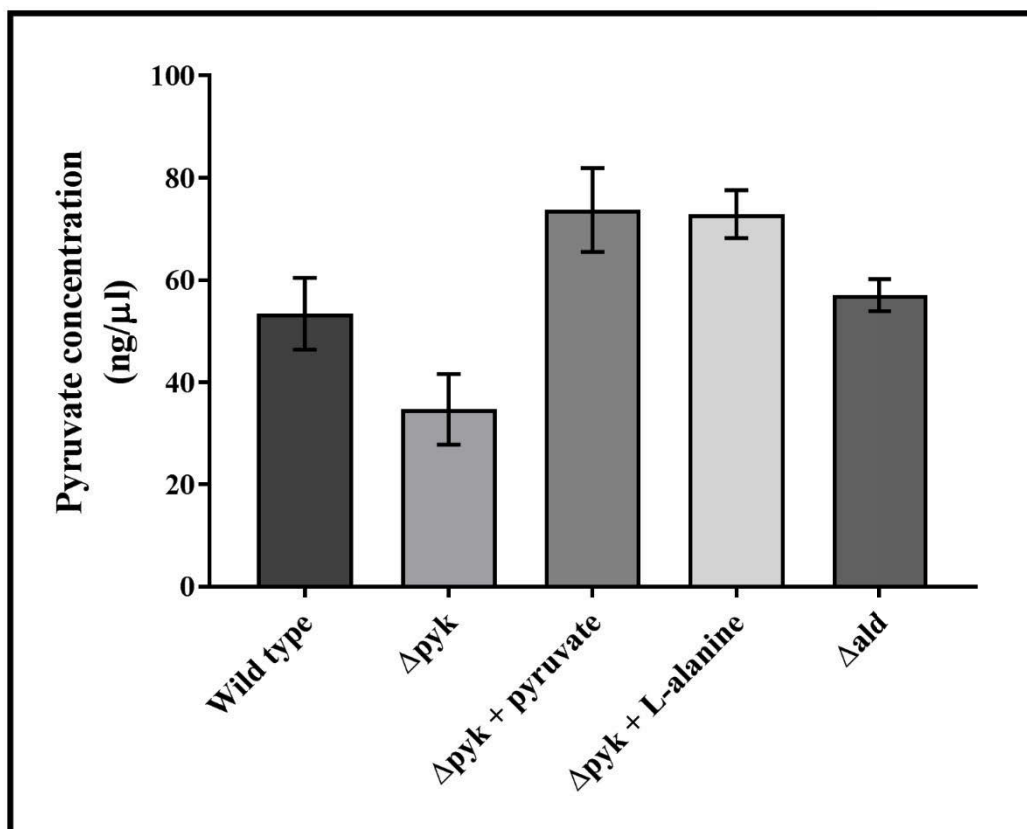


**Figure 3.6.** Measurement of pyruvate levels in wild type (SU5),  $\Delta pyk$  (SU6664),  $\Delta pyk$  +1% pyruvate,  $\Delta pyk$  +1% L-alanine and  $\Delta ald$  (SU826) *B. subtilis* cells. Concentration was measured using the pyruvate assay kit (Sigma-Aldrich), following the manufacturer's instructions leading to the

fluorometric detection of pyruvate. The values represent the pyruvate concentration in cellular extracts prepared from an equal bacterial mass. Error bars represent the SEM of three independent experiments.

Pyruvate concentration in  $\Delta pyk$  cells was 35.45 ng/ $\mu$ l compared to 48.02 ng/ $\mu$ l in wild type cells (Figure 3.6). Hence,  $\Delta pyk$  cells showed 26% lower pyruvate levels than wild type cells. As expected, the addition of 1% pyruvate to  $\Delta pyk$  cells raised cellular pyruvate levels to 71.41 ng/ $\mu$ l. Interestingly,  $\Delta pyk$  cells supplemented with 1% L-alanine yielded the same concentration of pyruvate (68.83 ng/ $\mu$ l) as measured in  $\Delta pyk$  cells supplemented with 1% pyruvate (71.41 ng/ $\mu$ l), further suggesting that L-alanine added to  $\Delta pyk$  cells actually gets converted to pyruvate, causing the Z ring positioning rescue. Also, the concentration of pyruvate in *ald*-deleted cells was 54.93 ng/ $\mu$ l, which is similar to wild type cell levels (48.02 ng/ $\mu$ l), indicating that the *ald* deletion had no significant effect on the pyruvate levels of wild type cells, as expected. Taken together, these results strongly imply that the Z ring positioning rescue observed after L-alanine addition to  $\Delta pyk$  cells is indeed due to its conversion to pyruvate, hence highlighting the importance of pyruvate in the correct Z ring positioning in *B. subtilis*. Furthermore, these results also confirmed that *pyk*-deletion does lead to lowered levels of pyruvate as compared to wild type cells, however pyruvate levels were not zero, likely because experiments were performed using rich media.

### 3.3.6 Pyruvate does not interact directly with FtsZ

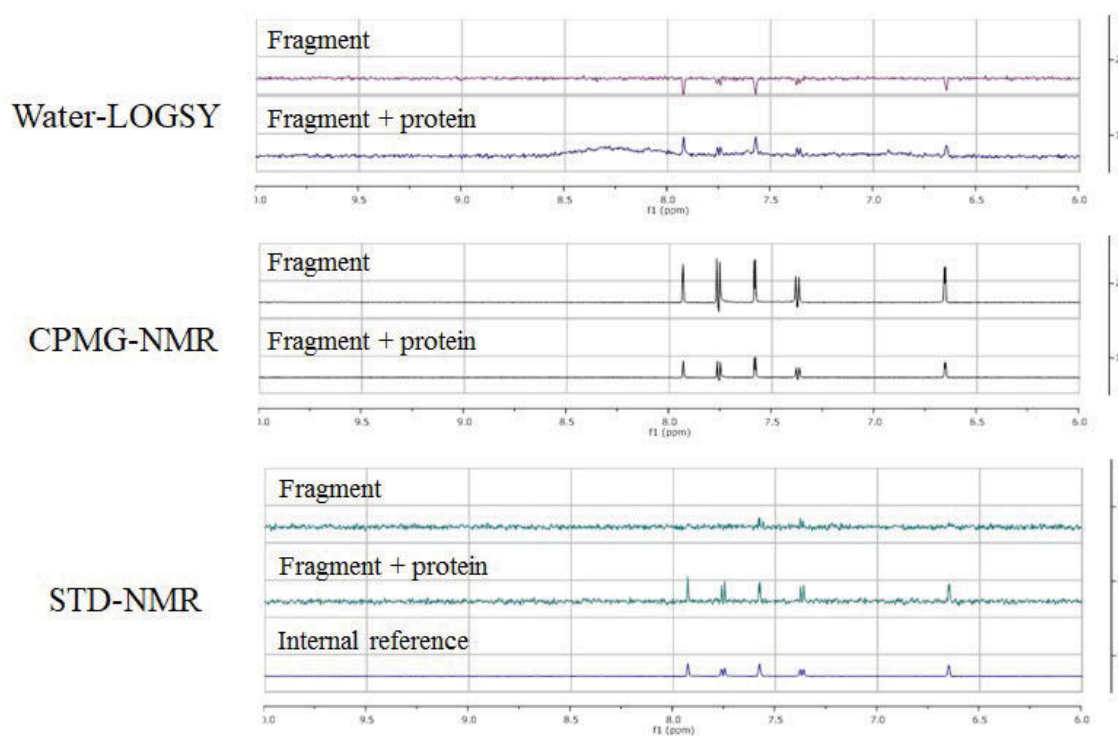
Some recent studies highlight that the metabolites when interacting with a protein may have a direct influence on their function (Link et al. 2013; Matsuda et al. 2014). One interesting example is of the UDP-glucose mediated control of nutrient-dependent cell size control, wherein FtsZ regulation by this metabolite has been shown to be via direct interaction (Chien

et al. 2012b). Since pyruvate appears to play an important role in correct Z ring positioning in *B. subtilis*, one of the ways pyruvate could do this is by interacting directly with FtsZ. To test this possibility, triple ligand detect (TLD) experiments were performed following the procedure explained in section 2.9. It has been previously seen that purified wild-type FtsZ readily forms polymers, even in the absence of GTP (unpublished data), hence the TLD method was chosen, as it allows for the detection of binding through the signals produced by the fragment and not through the protein. The TLD experiment was performed by Dr Lorna White at the University of Sydney using the wild type *B. subtilis* FtsZ<sup>12-315</sup> protein purified by Kenardy Kusuma (PhD student in Prof Liz Harry's laboratory at UTS) and sodium pyruvate.

TLD consists of three independent 1D nuclear magnetic resonance (NMR) experiments termed Water-Ligand Observed via Gradient Spectroscopy (Water-LOGSY); Carr, Purcell, Meiboom and Gill (CPMG) and Saturated Transfer Difference (STD) NMR (Abell and Dagostin 2015). All these methods utilise different unique properties of a sample for recording their fragment spectra and have their own signal change properties for identification of positive interactions (Figure 3.7A). WaterLOGSY detects binding by the transfer of magnetisation from water molecules to the fragment bound to the protein, wherein fragment only gives a negative signal, which changes to a positive signal when the fragment is bound to the protein (Dalvit et al. 2000; Abell and Dagostin 2015)(Figure 3.7A). A change to flat-signal is also considered a positive interaction, however a change to positive signal will signify a stronger binding. STD-NMR works by saturating the signals obtained from methyl groups in the protein and transferring the disturbance in magnetisation to the bound fragment, resulting in a spectrum only when the fragment is bound to the protein (Begley et al. 2013; Abell and Dagostin 2015). Hence, in this NMR, an increase in the size (usually  $\geq 5\%$ ) of fragment only peak in positive direction is considered a positive interaction (Figure 3.7A). Finally, CPMG-NMR is a relaxation-time-edited NMR experiment that makes use of the differences in transverse

relaxation times of proteins and fragments (Meiboom and Gill 1958; Abell and Dagostin 2015). Proteins (and bound ligands) have a small relaxation time, while free ligands have a large relaxation time. Hence, a decrease in the signal (usually  $\geq 30\%$ ) in the fragment peak size when bound to the protein is considered a positive interaction.

(A)



(B)

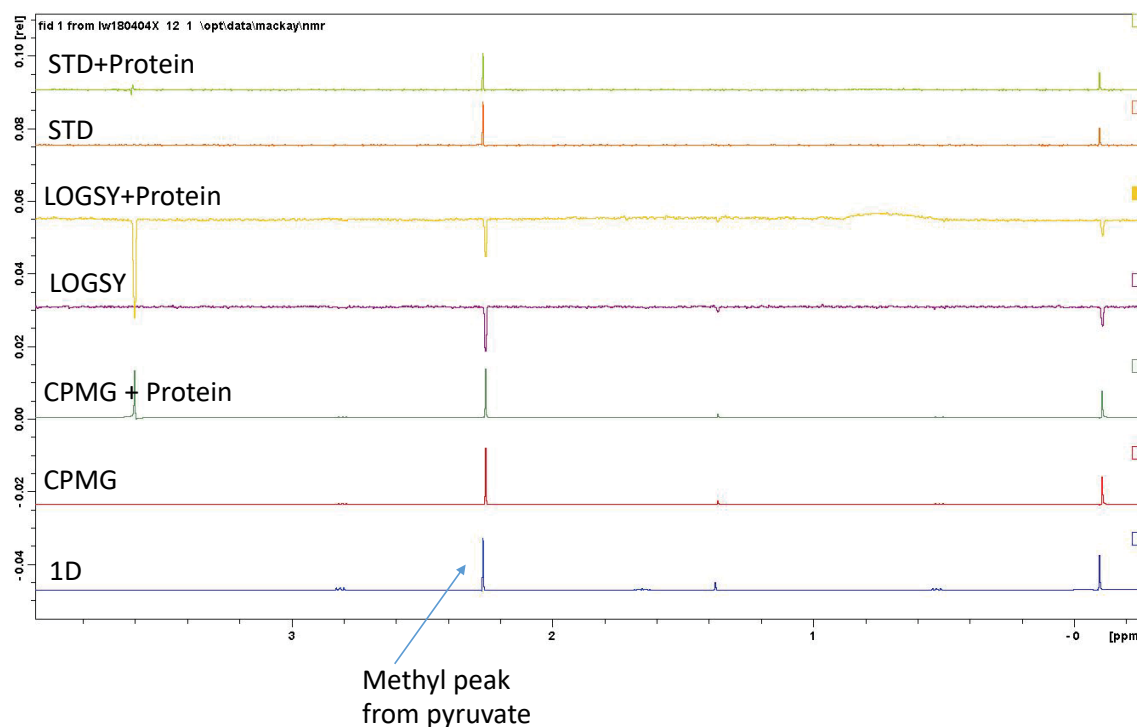


**Figure 3.7. Investigation of the interaction between pyruvate and FtsZ using triple-ligand detect (TLD) NMR. (A) Representative signal change properties for each of the independent TLD-NMR for identification of positive interactions.** In Water-LOGSY NMR experiments, the binding of the fragment (ligand) to protein is signified by the change of the negative signal to a positive signal. In CPMG-NMR binding of the fragment to protein is signified as a signal decrease by at least 30% while in STD-NMR a signal increase of  $\geq 5\%$  is needed to be considered as “binding”. In STD-NMR another spectrum termed internal reference is included to show the expected fragment signal when binding is observed, which serves the role of a positive control. **(B) Interaction spectra of pyruvate and wild type *B. subtilis* FtsZ using Triple Ligand Detect (TLD),** showing no interaction between pyruvate and FtsZ, as there was no change in the peaks of any of the 3 independent TLD experiments.

In the TLD experiment, an interaction is considered to be positive if the fragment shows a signal in at least two of the three TLD independent experiments. In the pyruvate-FtsZ TLD experiment, pyruvate by itself, because of its structure, is expected to give a peak at 2.2 ppm,

as shown in 1D region in Figure 3.7B. For all the TLD independent experiments, no signal was observed for pyruvate interacting with FtsZ (Figure 3.7B). In Water-LOGSY experiment, there was no change in the signal from negative to positive direction after protein addition. Similarly, there was no decrease in the peak size after protein addition in the CPMG-NMR. In the STD-NMR experiment, no peak was observed for pyruvate-FtsZ interaction, except the peak observed for pyruvate only. Hence, the 3 independent TLD experiments collectively indicated that there is no direct interaction between pyruvate and FtsZ, at least under the conditions tested.

### 3.4 Discussion

Understanding the interconnection between central carbon metabolism and the cell division process in bacteria is important in answering a basic biological question of how different processes ‘talk’ amongst themselves inside a bacterial cell and helps us understand the adaptation strategies of a bacterial cell under different nutritional conditions. In this chapter, the connection between central carbon metabolism and Z ring positioning in *B. subtilis* was further investigated. As previously indicated by Monahan *et al.*, pyruvate rescued the Z ring positioning defect of the pyruvate kinase mutant ( $\Delta pyk$ ) (Monahan et al. 2014a). However, pyruvate in a bacterial cell can be metabolized into various potential fates, suggesting that any of the metabolites produced from pyruvate could be the actual cause of the Z ring positioning rescue of  $\Delta pyk$  cells. Therefore, the primary aim of this chapter was to test if any of these potential fates of pyruvate is the actual reason for the Z ring positioning rescue of  $\Delta pyk$ . Although it is possible that the efficiency at which these metabolites are taken up by the cell could be different as well as there could be redundancy in their transport systems, such as that shown for D-alanine and L-alanine (Clark and Young 1974), still the knowledge on their uptake

systems is scarce. For example, in *B. subtilis*, only one pyruvate-specific transporter has so far been identified (Charbonnier et al. 2017). Considering this lack of knowledge, all the metabolites were added at an equal final concentration of 1% to the culture medium.

Metabolites produced immediately from pyruvate were tested for their effect on the Z ring positioning in  $\Delta pyk$  cells. The amino acids L-valine and L-leucine are produced directly from pyruvate via a series of enzymatic reactions (Brinsmade and Sonenshein 2011). Acetate, acetoin and L-lactate are some of the products of fermentative metabolism in *B. subtilis* (Ramos et al. 2000). Therefore, these metabolites were tested to investigate the involvement of the fermentation of pyruvate in the Z ring positioning. Amongst all the fates of pyruvate tested, only L-alanine rescued the Z ring positioning defect of  $\Delta pyk$  cells to midcell site. This rescue was found to be uncoupled to the growth rate rescue of  $\Delta pyk$  cells, as L-alanine did not affect the growth rate of  $\Delta pyk$  cells whilst another metabolite, L-leucine, rescued the growth rate but had no effect on the Z ring positioning of  $\Delta pyk$  cells. These observations ruled out the possibility of a growth rate-dependent Z ring positioning rescue caused by L-alanine. In *B. subtilis*, L-alanine is metabolized to D-alanine by alanine racemase (Kanda-Nambu et al. 2000), however D-alanine did not rescue the Z ring positioning defect of  $\Delta pyk$  cells. This discrepancy in results for alanine isomers could be due to their different rates of transport into the cells, however this is unlikely, as the two systems involved in alanine transport show equal affinity for L- and D-alanine (Clark and Young 1974). Alternatively, this discrepancy might link to the synthesis pathways or different fates of alanine within *B. subtilis* cells. There are three main enzymes involved in alanine metabolism in *B. subtilis*: alanine dehydrogenase (Ald), alanine transaminase (AlaT) and alanine racemase (Alr). In our results, since L-alanine and not D-alanine rescued the Z ring positioning defect of  $\Delta pyk$  cells, the involvement of *ald* in this process is highly likely because Ald in *B. subtilis* is known to be more specific for L-alanine



(Freese and Oosterwyk 1963; Freese et al. 1964; Berberich et al. 1968), which likely explains the disparity we observed in the Z ring positioning rescue by two isomers of alanine.

Fatty acids were initially tested by adding to the growth medium of  $\Delta pyk$  cells, however they were observed to be inhibitory to growth at all concentrations tested (0.001, 0.1 and 1%). Therefore, they were instead tested by constructing a genetic mutant of the enzyme FabHA which is involved in producing fatty acids from pyruvate via the Fab pathway. The *fabHA* mutant did not show any defect in the Z ring positioning, suggesting that the synthesis of fatty acids from pyruvate is not essential for correct Z ring positioning. However, fatty acids can also be synthesized using other alternative pathways (Brinsmade and Sonenshein 2011), thereby raising the possibility that there is no scarcity of fatty acids in  $\Delta fabHA$  and therefore, no Z ring positioning defect would be observed. However, we did observe decreased cell length in these cells (P-value 0.027) and the recent study by Vadia *et al.*, 2017 showed that the inhibition of fatty acid synthesis does cause a decreased cell size in *E. coli* and *B. subtilis* (Vadia et al. 2017). This suggests that  $\Delta fabHA$  cells do indeed experience fatty acid scarcity, although the levels might not be completely abolished, as fatty acids are essential for *B. subtilis* growth. Interestingly, the decreased cell length of  $\Delta fabHA$  correlates with the short cell length phenotype of  $\Delta pyk$  cells. Considering this observation and the recent study published by Vadia *et al.*, the decreased cell length of  $\Delta pyk$  cells could be due to an imbalance in any of the fates of pyruvate, including fatty acids, whose interrupted synthesis has been shown to result in a decreased cell length.

The nucleoid morphology quantification revealed that about 89% of the  $\Delta pyk$  cell population display a spread nucleoid morphology as compared to the wild type cells where 96% of the nucleoids are bilobed. However, there was no clear correlation observed between the Z ring positioning and the nucleoid morphology rescue of these cells. Firstly, pyruvate

addition, which rescued the Z ring positioning defect of  $\Delta pyk$  to ~90% of the Z rings forming at midcell, only rescued the nucleoid morphology from spread to bilobes in 49% of the cell population. Nonetheless, this rescue of nucleoid morphology after pyruvate addition varied over the experimental replicates, indicating that the nucleoid morphology rescue is not the sole reason for the Z ring positioning rescue of  $\Delta pyk$  cells. Additionally, L-alanine addition, which rescued the Z ring positioning defect of  $\Delta pyk$  cells, did not change the nucleoid morphology of  $\Delta pyk$  cells, further signalling towards the presence of other unknown contributing factors to the Z ring positioning of  $\Delta pyk$  cells.

Taken together, the results obtained from the metabolite-supplementation experiments to  $\Delta pyk$  cells, indicated that the metabolism of pyruvate to L-alanine could be the actual reason for the Z ring positioning rescue of  $\Delta pyk$  cells observed after pyruvate addition. However, the construction of an *ald* mutant and measurement of pyruvate levels when either pyruvate or L-alanine is added to  $\Delta pyk$  cells, enabled the conclusion that indeed, pyruvate is the actual key metabolite in CCM linked to Z ring positioning in *B. subtilis*.

Fry *et al.*, 2000 have shown that a *pyk* deletion significantly affects the levels of pyruvate in *B. subtilis* when the cells are grown in minimal medium (Fry *et al.* 2000). In our experiment, surprisingly, pyruvate concentration in  $\Delta pyk$  cells was measured to be only 26% lower than the native levels of pyruvate in wild type *B. subtilis* cells. This indicates that  $\Delta pyk$  cells do experience pyruvate limitation. However, the pyruvate concentration measured in our experiment is higher than those shown by Fry *et al.* in  $\Delta pyk$  cells (0  $\mu\text{g/ml}$ ). This could be due to the rich medium (L broth) used for growing bacterial cells in our experiment, which contains a lot of metabolic nutrients such as amino acids, carbohydrates, minerals and vitamins that can get converted to pyruvate, thereby aiding the bacterial growth; whereas Fry *et al.* performed their experiments in glucose minimal medium with least amount of nutrients supplied to the

cells. Furthermore, the relatively small difference in pyruvate levels in  $\Delta pyk$  and wild type cells could be due to the synthesis of pyruvate through alternative pathways such as the phosphotransferase system (Postma et al. 1993). However, in future, it will be better to include a washing step in the pyruvate measurement experiment, so that the possibility of a carry-over of residual pyruvate from the medium can be avoided and a more precise measurement of intracellular pyruvate levels can be done. Furthermore, it will also be interesting to see if lowering the level of pyruvate in  $\Delta pyk$  cells by growing them in minimal media can exacerbate the Z ring positioning phenotype of these cells.

Continuing from the primary conclusion from this chapter, that pyruvate is the key metabolite regulating the Z ring positioning in *B. subtilis*; it will be important to examine the actual mechanism of this regulation. As explained for other known links between metabolism and cell division, such as UDP-glucose mediated control of nutrient-dependent cell size control, wherein FtsZ regulation by metabolites has been shown to be via direct interaction (Chien et al. 2012b); one possibility is that pyruvate interacts with FtsZ directly thereby controlling the Z ring positioning. While the results of the pyruvate-FtsZ interaction experiments here suggest that this is unlikely, the possibility of pyruvate being able to interact with the polymerized form of FtsZ remains unanswered. This is important to investigate, as one of the ways by which pyruvate can affect the Z ring positioning is by affecting the rate of FtsZ polymerization by influencing the lateral interactions of FtsZ protofilaments, which will disturb the FtsZ assembly dynamics causing the Z rings to form at incorrect positions.

Following up from the work presented in this chapter, a big question that remains unanswered is, how are the pyruvate levels connected to the Z ring positioning? That is, what is the mechanism of this link? Firstly, a noteworthy observation is that the polar Z ring phenotype of  $\Delta pyk$  cells correlates with the polar Z ring phenotype of  $\Delta minCD$  cells (Levin et al. 1998; Gregory et al. 2008; Rodrigues and Harry 2012; Rowlett and Margolin 2013, 2015a);

suggesting that the polar Z rings of  $\Delta pyk$  could be due to an inactivation of the Min system in these cells. Secondly, as discussed in section 3.3.4, the nucleoid morphology of  $\Delta pyk$  cells is more dispersed than the wild type cells, indicating towards the role of nucleoid occlusion in the pyruvate-Z ring positioning link. These are some aspects of the CCM-division link in  $\Delta pyk$  cells, which need further investigation and will be addressed in the following chapter of this thesis.



# Chapter 4

---

**Investigating the possible role for  
known Z ring regulatory mechanisms  
and DNA replication in acentral Z ring  
positioning in  $\Delta pyk$  cells**

## 4.1 Introduction

The results presented in Chapter 3 suggest that pyruvate is a key metabolite linking central carbon metabolism with the Z ring positioning in *B. subtilis*. When this link is disrupted by obstructing pyruvate synthesis in  $\Delta pyk$  cells, it manifests itself as a phenotype in which a significant proportion of cells form Z rings near the cell poles rather than at midcell. The mechanism(s) behind this defect in Z ring positioning in  $\Delta pyk$  cells is not known and understanding this mechanism is the focus of the remainder of this thesis. There are several known Z ring regulatory mechanisms and the inactivation of these systems can result in misplaced Z rings, similar to the phenotype observed in  $\Delta pyk$  cells. The most well-studied Z ring regulatory mechanisms include the Min system and the nucleoid occlusion system. Both these systems provide spatial and temporal regulation of Z ring formation in *B. subtilis* and *E. coli*, such that their combined action prevents the Z ring forming anywhere within a cell except the midcell site (Monahan et al. 2014b).

Nucleoid occlusion prevents the Z ring assembly over the nucleoid, whereas the Min system blocks unwanted potential division sites at the cell poles (Bernhardt and De Boer, 2005). However, Z rings form precisely at midcell site even in the absence of both of these systems (Rodrigues and Harry 2012), suggesting that the division site is positioned at midcell independently of the Min and the nucleoid occlusion system, signifying the occurrence of other yet unknown mechanisms controlling the Z ring positioning. Still, the Min and the nucleoid occlusion system remain the most well-characterized systems regulating the Z ring positioning. Hence, in the *pyk* mutant, there is the possibility that acentral Z rings may be forming as a result of any change in the proper functioning of the Min or the nucleoid occlusion system.

In *B. subtilis*, four proteins named MinC, MinD, MinJ and DivIVA form the Min system, out of which MinC is the actual inhibitor of Z ring assembly that interacts and

destabilizes FtsZ polymers. MinCD inhibitory complex is piloted to the cell poles via the action of DivIVA and MinJ, where it inhibits the formation of the Z ring (Karoui and Errington 2001; Errington et al. 2003; Harry et al. 2006; Monahan et al. 2014b). It has been previously shown that a deletion of *minCD* did not rescue the FtsZ defect of the *tsI* mutant, unlike *pyk* deletion, which rescued their cell division defect (Monahan et al. 2009), suggesting that *pyk* mutation affects the Z ring assembly via a mechanism independent of the MinCD activity (Monahan et al. 2014a). However, these conclusions arose from observations made in the *tsI* mutant, which carries a mutant FtsZ protein and is unable to support lateral interactions between FtsZ polymer strands (Nukushina and Ikeda 1969). Since the situation could be completely different when only *pyk* is deleted in wild type *B. subtilis* cells, the possibility of an effect on the functioning of the Min system being the reason behind the acentral Z ring positioning of  $\Delta pyk$  still remains. Furthermore, as the function of the Min system is to prevent the Z ring formation at the cell poles, mutants of this system form Z rings at the cell poles (Levin et al. 1998), a similar phenotype to the acentral Z ring phenotype of  $\Delta pyk$  cells; raising the possibility that the *pyk* deletion could have influenced the functioning of the Min system thereby making it inactive, resulting in the formation of Z rings at acentral positions. Hence, it becomes important to answer whether the Min system is active in  $\Delta pyk$  cells or not.

Nucleoid occlusion is mediated by a protein called Noc, which binds to specific DNA sequences around the chromosome and inhibits the Z ring assembly over the nucleoid (Wu et al. 2009). In relation to the function of nucleoid occlusion, the binding sequences of Noc are absent in the terminus region of chromosome, which occupies the midcell region when chromosome replication is near completion (Wu et al. 2009). This has been proposed to result in a decrease of Noc levels at these midcell site, subsequently relieving nucleoid occlusion at midcell allowing the Z ring formation at this site toward completion of chromosome segregation (Wu and Errington 2004). This proposed mechanism of action of Noc allows the

spatial and temporal regulation of the Z ring placement in relation to the timing of DNA replication and chromosome segregation and avoids DNA guillotining. Since the nucleoids of  $\Delta pyk$  cells appeared spread as compared to the wild type cells (section 3.3.4), there arises the possibility that this spread morphology of the nucleoid could potentially contribute to the incorrect Z ring positioning of  $\Delta pyk$  cells by nucleoid occlusion being active over a widespread region inside the cell. Hence, one of the crucial aspects that remains to be examined is whether the nucleoid occlusion is active in  $\Delta pyk$  cells; and if so, does it contribute to the acentral Z ring positioning in these cells?

In *B. subtilis*, mutants of DNA replication initiation have been shown to display a distorted chromosome organization that causes the Noc-binding sites to remain in midcell region, which prevents the correct positioning of Z ring at midcell site (Wang et al. 2014). Since the *pyk* deletion did result in a spread nucleoid morphology, which is different from wild type cells (section 3.3.4); pointing towards the possibility of a DNA replication defect in these cells; it is also crucial to test if the  $\Delta pyk$  cells have any DNA replication defect, and if so, is this defect contributing to their acentral Z ring positioning defect? This is important to investigate, as inhibiting the initiation stage of DNA replication has been shown to result in most of the Z rings forming at acentral sites in *B. subtilis* (Harry et al. 1999).

## 4.2 Chapter aims

Central carbon metabolism (CCM) affects the process of cell division by influencing the position of Z ring in *B. subtilis* cells. However, whether this is accomplished by a direct effect of CCM on FtsZ or indirectly through the well-known negative regulators of the Z ring placement, Min system and nucleoid occlusion, is unclear. Therefore, the first aim of this chapter is to determine whether the Min system and/or the nucleoid occlusion are still active in



$\Delta pyk$  cells. In other words, does the deletion of *pyk* affect the functioning of either of these two systems, thereby having a consequential effect on the Z ring positioning? This will be done by disrupting these known systems separately in  $\Delta pyk$  cells and observing possible changes to the Z ring positioning phenotype in these cells.

As reported in section 3.3.4, the *pyk* mutant was observed to display a spread nucleoid morphology, which was different from the bilobed nucleoid morphology of wild type cells. This indicated that the  $\Delta pyk$  cells might be somehow defective in the DNA replication process. Interestingly, the *pyk* mutant has been previously shown to display a defect in the frequency of DNA replication initiation (Murray and Koh 2014). Considering this previous observation, the second aim of this chapter is to investigate if the *pyk* mutant, also displays a defect in the frequency of DNA replication initiation under conditions used in this study. And, if so, does this defect contribute to the acentral Z ring positioning defect of  $\Delta pyk$  cells?, as blocking the initiation stage of DNA replication has been shown to result in the Z rings positioned at acentral sites in *B. subtilis* (Harry et al. 1999).

## 4.3 Results

### 4.3.1 Acentral Z rings of the *pyk* mutant are not due to inactivation of the Min system

The Min system is known to prevent the Z ring formation at the cell poles and its deletion results in the formation of polar Z rings in *B. subtilis* (Levin et al. 1998). Relating this observation to the acentral Z ring positioning phenotype of  $\Delta pyk$  cells, it could be that the Z rings are forming at acentral positions in  $\Delta pyk$  as a direct result of inactivation of the Min

system. In order to test if this is the case, a double mutant of *pyk* and *minCD* was constructed (SU883) by introducing a *pyk::tet* cassette into a strain carrying a *minCD::cat* cassette (Migocki et al. 2002). It was hypothesized that if this double mutant has an increased frequency of acentral Z rings compared to the *pyk* mutant, it would indicate that the Min system is originally active in  $\Delta pyk$  and that the acentral Z rings forming in the *pyk* mutant are not solely forming as a result of complete inactivation of the Min system. However, if the deletion of *minCD* in  $\Delta pyk$  does not increase the frequency of acentral Z rings, it would mean that the acentral Z rings in  $\Delta pyk$  are indeed a direct result of an inactivation of the Min system and that the Min system is inactive in  $\Delta pyk$  cells. Z ring positioning was examined in the *minCD-pyk* double mutant, and the results obtained are shown in Figure 4.1.

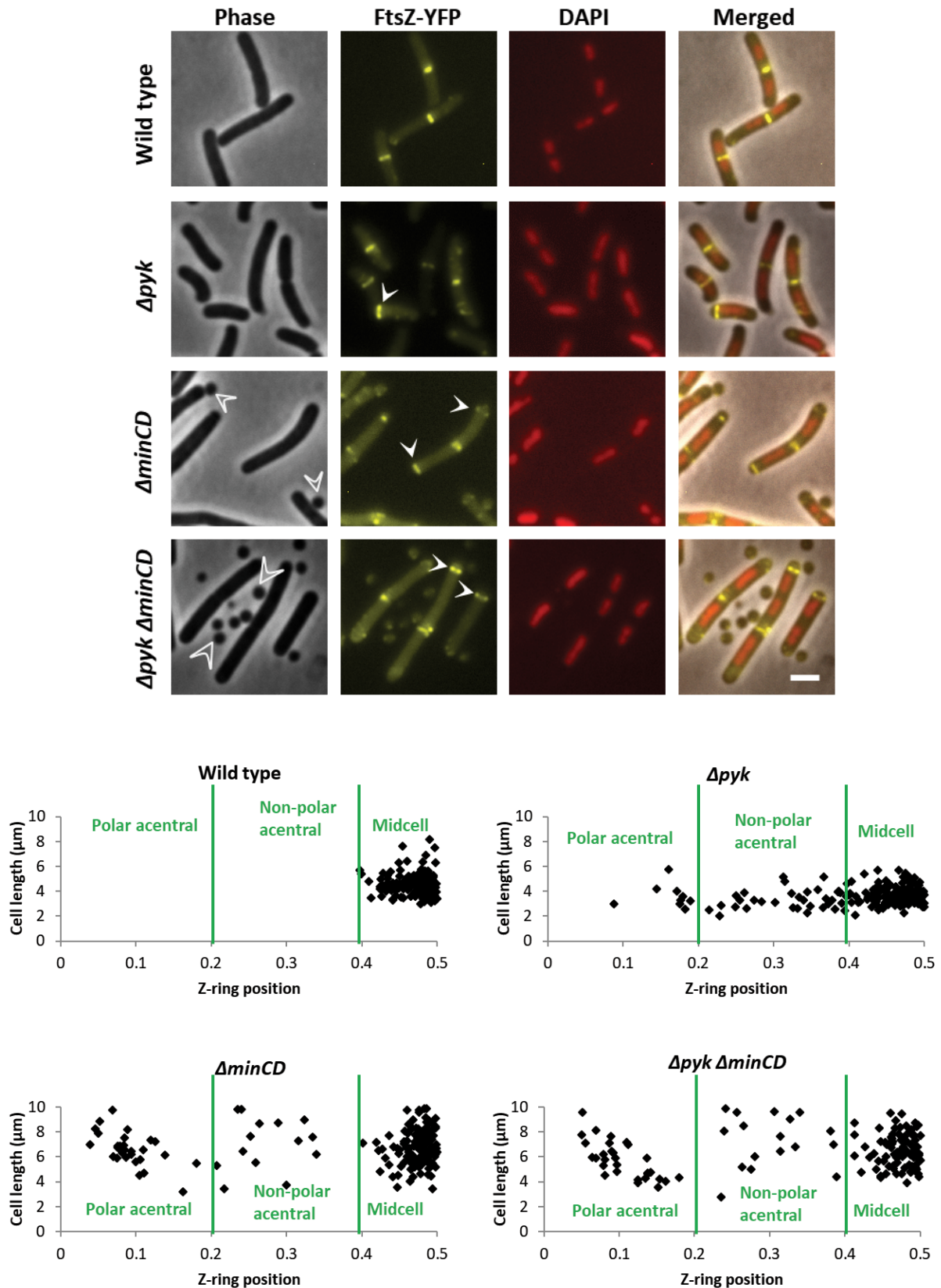


**Figure 4.1.** The effect of *minCD* deletion on the Z ring positioning of  $\Delta pyk$  cells. Cells were grown to mid-exponential phase in the presence of 0.01% xylose in L broth at 37°C and visualized by phase-

contrast and fluorescence microscopy (n=3), Scale bar, 2 $\mu$ m. Filled white arrows show examples of the polar Z ring and open white arrows represent minicells observed in different strains. Lower panel shows the scatter plots wherein cell length has been plotted as a function of the Z ring positioning under different experimental conditions. Here, the Z ring position of 0 and 0.5 on the x-axis signify the cell pole and cell centre, respectively. n > 150. [Wild type = SU492,  $\Delta$ pyk = SU679,  $\Delta$ minCD = SU682 ( $\Delta$ minCD amyE::Pxyl-ftsZ-yfp) and  $\Delta$ minCD  $\Delta$ pyk = SU883 ( $\Delta$ minCD  $\Delta$ pyk amyE::Pxyl-ftsZ-yfp). n > 150.

In *B. subtilis*, the deletion of *minCD* has been reported to increase the cell length by 30-40% compared to wild type cells (Rodrigues and Harry 2012). In our analysis, *minCD*-deletion was also observed to increase the cell length to the same extent as reported previously. However, the increased cell length did not affect the relative Z ring positioning measurements in our analysis, as the Z ring position was calculated by dividing the Z ring measurement from the closest pole to the full cell length for all the strains. This aspect of increased cell length after *minCD* deletion is discussed later in this section.

As can be seen in the cell population scatter plots in Figure 4.1, about 22% of the Z rings in the *pyk* mutant and 23% in the *minCD* mutant formed at acentral positions (0-0.4). This frequency of acentral Z rings falls within the range that has been previously reported (Levin et al. 1998; Migocki et al. 2002; Bramkamp and Baarle 2009; Monahan et al. 2014a). Notably, the frequency of acentral Z rings in the *minCD pyk* double mutant increased to 34%, pointing that the deletion of *minCD* in the *pyk* mutant does allow more Z rings to form at acentral sites. This demonstrates that the Min system is originally active, at least partially, in the *pyk* mutant and the acentral Z rings of the  $\Delta$ pyk are not solely due to an inactivation of the Min system.

An interesting observation made from the scatter plots (Figure 4.1) of the *minCD* and the *pyk* mutant was that the *minCD* mutant had more Z rings that were positioned very close to the pole, within the Z ring position of 0-0.2. This was compared to the *pyk* mutant, which had most of the acentral Z rings positioned outside this range, between positions 0.2-0.4. The frequencies obtained for these ranges of Z ring positioning in all samples were scored and are presented in Table 4.1. These values highlight the difference in the acentral Z ring phenotype of the *pyk* and the *minCD* mutant. The *pyk* mutant has more non-polar acentral Z rings (0.2-0.4) whereas the *minCD* mutant displays more polar acentral Z ring positioning phenotype (0-0.2). So, although both  $\Delta pyk$  and  $\Delta minCD$  single-deletion cells display an acentral Z ring positioning phenotype, there remains a difference in the exact Z ring positioning with respect to how close the pole they are positioned; the acentral Z rings in  $\Delta minCD$  cells are more polar Z rings than the acentral Z rings in  $\Delta pyk$  cells. This further supports the notion that the Min system is not involved in the acentral Z ring positioning phenotype of  $\Delta pyk$  cells, as the actual position of the acentral Z rings in single mutants of *minCD* and *pyk* are different. Nonetheless, the higher frequency of polar Z rings in *minCD-pyk* double mutant (21.1%) than the *minCD* and *pyk* single-gene deletions (Table 4.1), further supported this notion that the Min system is active, at least partially, in  $\Delta pyk$  cells and their acentral Z ring positioning is not due to the complete inactivation of the Min system.

**Table 4.1. Frequencies of polar and non-polar acentral Z rings in different strains.**

Strain	Z ring position frequency (%) <sup>*</sup>			
	Polar acentral (0-0.2)	Non-polar acentral (0.2-0.4)	Midcell (0.4-0.5)	Predominant type of acentral Z ring position
Wild type	0.0	1.2	98.8	Non-polar
$\Delta pyk$	4.3	17.3	78.4	Non-polar
$\Delta minCD$	15.8	7.4	76.8	Polar
$\Delta minCD \Delta pyk$	21.1	12.7	66.2	Polar

<sup>\*</sup>Z ring position frequencies were calculated by measuring the Z ring position from the closest cell pole in at least 150 cells for all the samples and categorizing the Z ring position measurements into three measurement categories (0-0.2, 0.2-0.4, 0.4-0.5), with 0 depicting the cell pole and 0.5 the midcell site

Similar to the production of minicells in  $\Delta pyk$  (Monahan et al. 2014a), the deletion of  $minCD$  is also known to result in the production of minicells, indicating that the polar Z rings can actually undergo the division process (Levin et al. 1998). As the  $minCD$ -deletion resulted in more polar Z rings as compared to  $pyk$ -deletion, it is expected that  $\Delta minCD$  cell population will consist of more minicells than the  $\Delta pyk$  cell population. Furthermore, similar to an increased frequency of acentral Z rings in the  $minCD pyk$  double mutant, the deletion of  $minCD$  in  $\Delta pyk$  cells is also expected to increase the frequency of minicells, if the Min system is originally active in these cells. Hence, the frequency of minicells in  $\Delta pyk$ ,  $\Delta minCD$ , and  $\Delta pyk \Delta minCD$  was also investigated. Firstly, the frequency of minicells observed in  $\Delta pyk$  was 6.1%, which is similar to the ~5% minicells observed by Monahan *et al.* (Monahan et al. 2014a). Secondly, the frequency of minicells in the  $minCD$  mutant was observed to be 21.6%, which is comparable to the ~17% minicells observed by Levin *et al.* (Levin et al. 1998). These frequencies of minicells in the  $pyk$  and the  $minCD$  mutants relate to their polar Z ring frequencies of 4.3% and 15.8% (Table 4.1), suggesting that the polar Z rings forming in both of these mutants are capable of undergoing the division process. Interestingly, 26.8% of the

cell population in *minCD pyk* double mutant was observed to be minicells, which is higher than the *minCD* and the *pyk* mutant by themselves. Since the deletion of *minCD* in the *pyk* mutant background also increased the percentage of minicells, it supports the conclusion made from previous analysis that Min system is originally active, at least partially, in the *pyk* mutant.

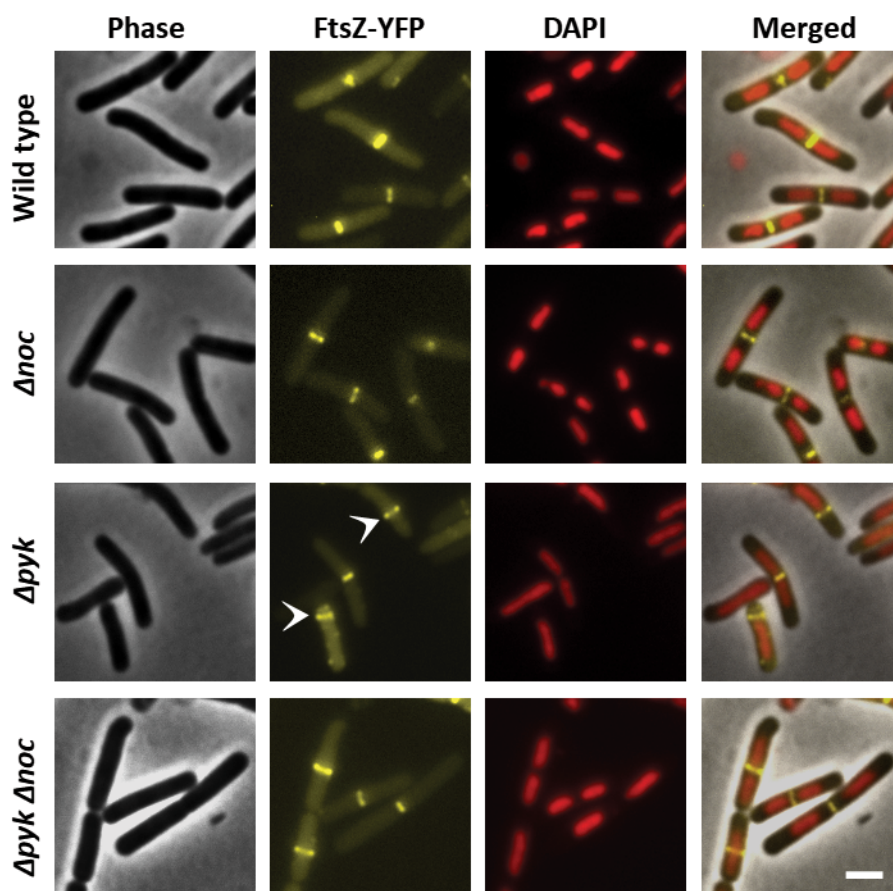
*minCD*-deletion is known to increase the cell length in *B. subtilis* by 30-40% (Rodrigues and Harry 2012). In our analysis, *minCD*-deleted cells were also observed to display an average cell length of 6.8  $\mu\text{m}$  compared to 4.6  $\mu\text{m}$  for wild type cells. This phenotype of increased cell length after *minCD* deletion was also observed in the *minCD pyk* double mutant (Figure 4.1, average cell length - 6.5 $\mu\text{m}$ ). In contrast to the *minCD* deletion that resulted in an increase in cell length, the deletion of *pyk* decreased the cell length to 3.6 $\mu\text{m}$ , again suggesting that the phenotypes produced by *minCD* deletion and *pyk* deletion, whether it be the difference in polar Z ring frequencies or the cell length, are different.

Overall, the Z ring positioning, minicell frequency and cell length data from the  $\Delta\textit{minCD}\Delta\textit{pyk}$  experiment together indicated that the Min system is active, at least partially, in  $\Delta\textit{pyk}$  cells and that the acentral Z ring positioning phenotype in these cells is not solely due to an inactivation of the Min system.

### **4.3.2 Nucleoid occlusion is involved in the acentral Z ring positioning in $\Delta\textit{pyk}$ cells**

Nucleoid occlusion, mediated by the protein Noc in *B. subtilis*, prevents the Z rings forming over the nucleoid during the early stages of DNA replication when the chromosomes have not segregated completely (Moriya et al. 2010). This prevents the guillotining of bacterial DNA and ensures that the daughter cells receive the correct genetic complement. Since, the *pyk* mutant forms the Z rings at acentral positions and it also displays a spread nucleoid morphology (as discussed in section 3.3.4), there is a possibility that these acentral Z rings could be forming

due to the nucleoid occlusion activity at midcell site, causing the Z rings to form at sites where there is decreased inhibition due to the nucleoid occlusion. If this is the case, rendering nucleoid occlusion inactive by deleting *noc* from  $\Delta pyk$  cells would allow more Z rings to form at midcell and there would be a decrease in the proportion of acentral Z rings. In order to examine this possibility, a *noc pyk* double mutant was constructed (SU877) by introducing a *pyk::cat* cassette into a strain carrying a *noc::tet* cassette. The Z ring position was examined in this mutant and the results obtained are shown in Figure 4.2.





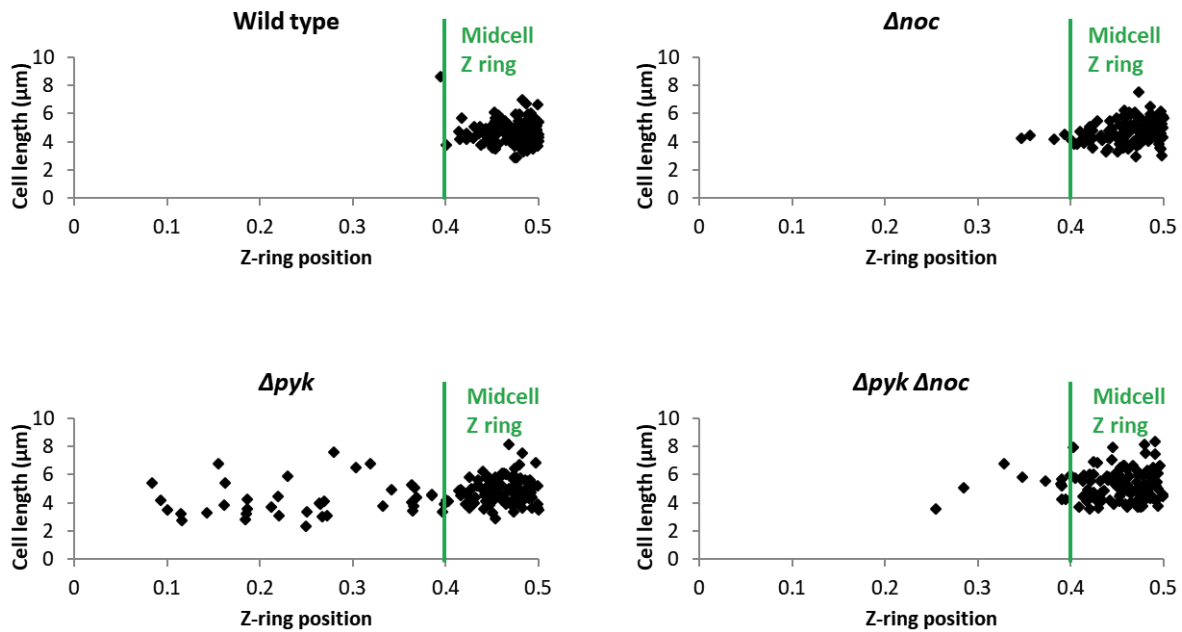


**Figure 4.2.** The effect of *noc* deletion on the Z ring positioning of  $\Delta pyk$  cells. Cells were grown to mid-exponential phase in the presence of 0.01% xylose in L broth at 37°C and visualized by phase-contrast and fluorescence microscopy (n=3), Scale bar, 2 $\mu$ m. Filled white arrows show examples of acentral Z rings. Lower panel shows the scatter plots wherein cell length has been plotted as a function of the Z ring positioning under different experimental conditions. Here, the Z ring position of 0 and 0.5 on the x-axis signifies the cell pole and cell centre, respectively. n > 150. (Wild type = SU492,  $\Delta pyk$  = SU679,  $\Delta noc$  = SU657 (*Δnoc amyE::Pxyl-ftsZ-yfp*) and  $\Delta pyk \Delta noc$  = SU877 (*ΔpykΔnoc amyE::Pxyl-ftsZ-yfp*)).

The *noc* mutant by itself did not show any defect in the Z ring positioning with ~97% Z rings forming at midcell site. This result is in agreement with previously published work (Rodrigues and Harry 2012). Interestingly, the *noc pyk* double mutant had ~92% of the Z rings at midcell site in comparison to ~71% of the Z rings forming at midcell site in the *pyk* mutant. Hence, the deletion of *noc* in the *pyk* mutant rescued the Z ring positioning defect of these cells to almost the midcell Z ring frequency of wild type cells. In addition, the *noc pyk* double mutant

showed a decreased frequency of minicells; 0.6% as compared to 3.7% in  $\Delta pyk$ . Together these results suggest that acentral Z ring assembly and septum formation in  $\Delta pyk$  is mediated by active nucleoid occlusion at the midcell site, making the Z rings form at acentral sites where there is reduced inhibition due to the decreased nucleoid occlusion activity.

### 4.3.3 Quantification of the spread nucleoid morphology of $\Delta pyk$ cells

In wild type *B. subtilis* cells, nucleoid occlusion prevents the Z rings forming over the nucleoid during the early stages of DNA replication when the chromosomes have not replicated completely (Moriya et al. 2010). At the later stages of cell cycle, when the chromosomes have replicated, the midcell site is relieved of the nucleoid occlusion activity, allowing the Z ring formation. The mechanism by which this occurs is via the binding of Noc to the origin-proximal sites on the chromosomes, which are absent in the midcell region when the chromosomes have completely replicated (Wang et al. 2014). In DNA replication initiation mutants, wherein the chromosomes do not replicate at the rate of wild type cells, there is a change in chromosome organization that causes the origin-proximal Noc binding sites to remain in the midcell region even during the later stages of cell cycle, preventing the Z rings to form at midcell site (Wang et al. 2014). As we observed the nucleoid morphology of  $\Delta pyk$  cells to be very spread as compared to wild type cells (section 3.3.4), and that *noc* deletion rescued the Z ring positioning defect of  $\Delta pyk$  cells, there arises the possibility that the Z ring positioning defect of these cells occurs through changes in nucleoid occlusion activity that are in turn mediated by changes in the gross conformation of the nucleoid itself. Hence, to examine this interconnection between the nucleoid morphology and the Z ring positioning in  $\Delta pyk$  cells further in detail, a quantification of the nucleoid morphology of  $\Delta pyk$  cells was performed using the ‘fluorescence

signal profile' tool of the image analysis software 'Oufiti' (Paintdakhi et al. 2016). The results obtained along with the representative microscopy images are shown in Figure 4.3.

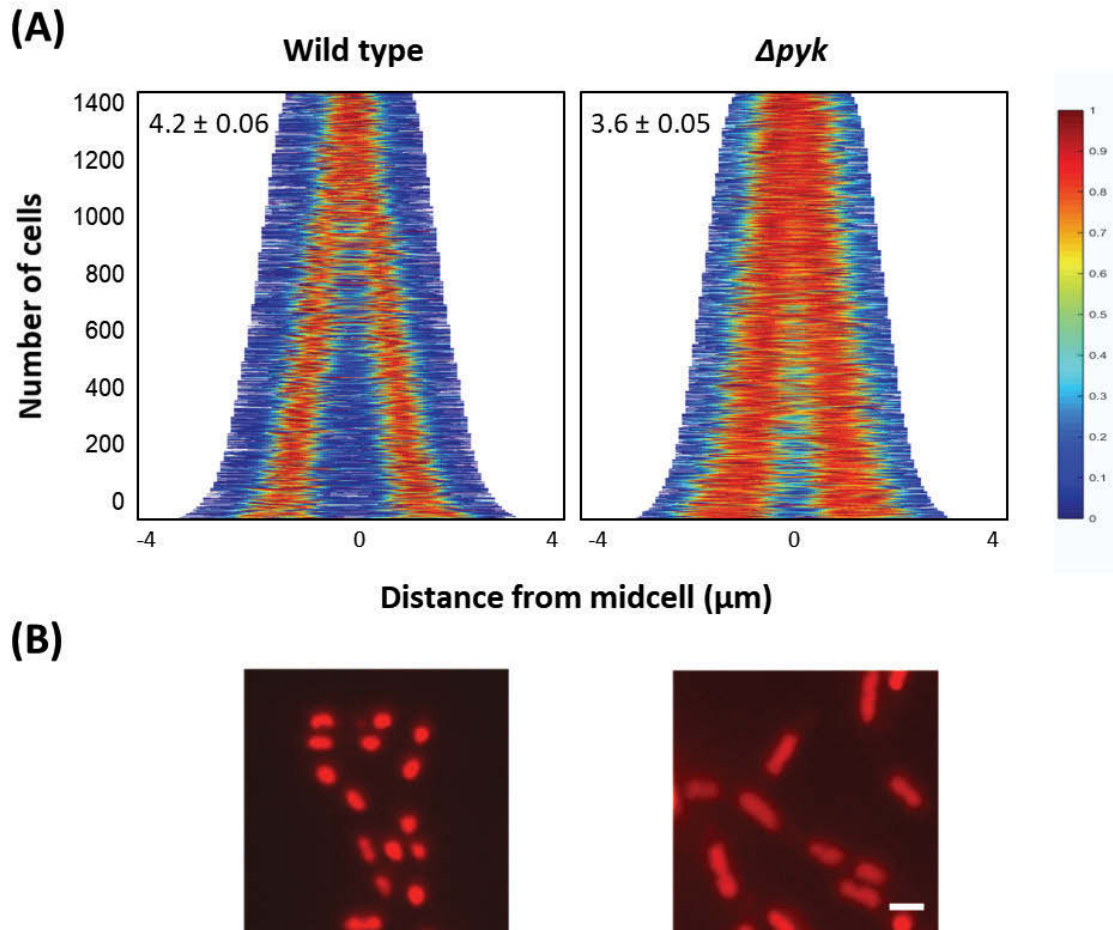


**Figure 4.3. Quantitative analysis of the nucleoid morphology of wild-type (SU492) and  $\Delta pyk$  (SU679).** Cells were grown in L broth media to the mid-exponential phase and DAPI was added at the time of collection ( $0.4 \mu\text{g/ml}$ ). (A) Population demographics illustrating the localisation of nucleoid in different strains, with cells stacked in order of increasing length from top to bottom. Image analysis was performed using the image analysis tool 'Oufiti' (Paintdakhi et al. 2016). Fluorescence intensity is shown on a colour spectrum as illustrated on the right, such that the areas of bright DAPI staining are shown in orange and those with no detectable signal are shown in blue. Values shown are the average cell length  $\pm$  SEM. (B) Representative images of the aforementioned strains stained with DAPI. Scale bars represent  $2\mu\text{m}$ .

As can be seen in the population demographs in Figure 4.3A, the nucleoid, represented by orange colour, occupies more space in  $\Delta pyk$  cells than it does in wild type cells. Two lobes of the nucleoid can be clearly seen in wild type cells demograph, with the middle region of the demograph being completely blue, indicating no fluorescence in this region. In contrast, in the demograph of  $\Delta pyk$  cells, the nucleoid occupies more space in the cell and the two nucleoid lobes are not as distinct as they are in wild type cells. Approximately 50% of the cells (0-700 in the demograph) did show some separation of nucleoids but the remaining ~50% of the cells (700-1400 in the demograph) did not. These results clearly illustrate that the nucleoid morphology of  $\Delta pyk$  cells is different from wild type cells, such that the nucleoids are more spread in  $\Delta pyk$  cells. This spread nucleoid morphology could potentially be a contributing factor to the acentral Z ring position defect of these cells by rendering nucleoid occlusion active over a widespread region within the cells compared to wild type cells. Although, the results presented in section 3.3.4 suggest that there is no correlation between the Z ring positioning rescue and nucleoid morphology rescue of  $\Delta pyk$  cells, still the substantial difference in the nucleoid morphologies of  $\Delta pyk$  and wild type cells, along with the observation of Z ring positioning rescue in  $\Delta pyk$  cells after *noc* deletion does indicate the role of this spread nucleoid morphology in the acentral Z ring positioning of  $\Delta pyk$  cells.

#### **4.3.4 $\Delta pyk$ cells have a DNA replication defect, which is rescued after pyruvate addition**

In *B. subtilis*, mutants of DNA replication initiation have been shown to display a distorted chromosome organization that causes the Noc-binding sites to remain in midcell region, preventing the correct positioning of the Z ring at midcell site (Wang et al. 2014). Since the deletion of *noc* in  $\Delta pyk$  cells rescued their Z ring positioning defect and these cells also showed

a nucleoid morphology different from wild type cells, this indicated towards the possibility of a DNA replication defect in these cells. Additionally, *pyk* mutant in *B. subtilis* has previously been shown to display a DNA replication initiation defect (Murray and Koh 2014), suggesting that this defect could be the reason for the significant proportion of acentral Z rings observed in these cells. Murray *et al.* used a *B. subtilis* strain carrying the *pyk* gene under the control of an IPTG inducible promoter, however our strain is a null mutant of *pyk*. Hence, it was first investigated whether the *pyk* mutant in this study shows the same DNA replication defect as was shown by Murray *et al.* This was done by measuring the origin to terminus ratio following the marker frequency analysis approach described in section 2.10. Secondly, for examining the role of DNA replication in the CCM-division connection in  $\Delta pyk$  cells, the effect of pyruvate addition on the frequency of DNA replication initiation of  $\Delta pyk$  cells was investigated, as pyruvate addition rescued the Z ring positioning defect of these cells. The results obtained for this experiment are presented in Figure 4.4.

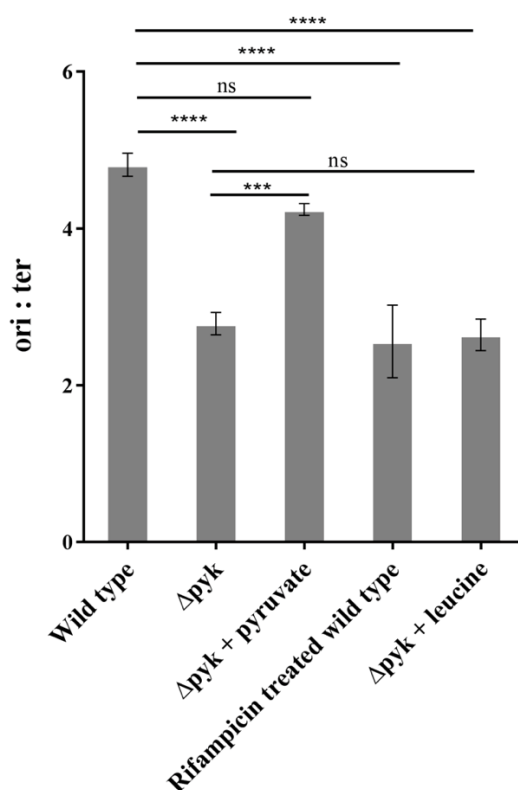


**Figure 4.4. Analysis of the frequency of DNA replication initiation in wild-type (SU492), *Δpyk* (SU679) and *Δpyk* + 1% pyruvate using marker frequency analysis.** Cells were grown in LB medium at 37°C/ 200 rpm with respective treatments to the mid-exponential phase. Sodium azide was added to prevent further growth and DNA replication and genomic DNA was isolated from the harvested cells. The *oriC*-to-terminus (*ori:ter*) ratio of each strain was determined using quantitative PCR (qPCR) using primers specific to the relevant chromosomal regions. The results are shown as the average values of three biological replicates and the error bars indicate standard error of mean of those replicates, obtained using one-way Anova statistical analysis. ‘\*’ represent that the samples under investigation are statistically different, whereas ‘ns’ represents that they are not different.

In marker frequency analysis experiments, rifampicin treated wild type cells was included as a control, as rifampicin treatment is known to reduce the *ori:ter* ratio in *B. subtilis* cells (Von Freiesleben et al. 2000). Rifampicin treatment at the concentration of 50 µg/ml did reduce the *ori:ter* ratio of wild type *B. subtilis* cells, confirming that the conditions under which

our experiment is being conducted are appropriate.  $\Delta pyk$  cells displayed an *ori:ter* ratio that was 42% lower than wild type cells (Figure 4.4), which correlates with the study published by Murray and Koh wherein about 41% reduction in the *ori:ter* ratio was observed for the *pyk* mutant (Murray and Koh 2014). This suggests that  $\Delta pyk$  cells do have an under-initiation DNA replication defect. Interestingly, the addition of pyruvate rescued the *ori:ter* ratio of  $\Delta pyk$  cells to the level of wild type cells, indicating that pyruvate has some effect on the DNA replication process that influences the frequency of initiation step in  $\Delta pyk$  cells. Together, these results point towards the role of pyruvate in maintaining the frequency of DNA replication initiation, hence influencing the Z ring positioning of  $\Delta pyk$  cells.

Furthermore,  $\Delta pyk$  cells supplemented with 1% leucine was also included in the experiment, as leucine was one of the potential metabolic fates of pyruvate that rescued the growth rate of  $\Delta pyk$  cells without affecting their Z ring positioning (section 3.3.2). Leucine addition did not rescue the *ori:ter* ratio of  $\Delta pyk$  cells, suggesting that mere growth rate rescue is not enough to result in the rescue of *ori:ter* ratio of  $\Delta pyk$  cells. As one can expect that an increase in growth rate does require an increased rate of DNA replication, the altered *ori:ter* ratio after leucine addition is intriguing.

#### **4.3.5 The interplay between Noc and DNA replication initiation frequency in $\Delta pyk$ cells**

The nucleoid occlusion factor Noc has been shown to be an inhibitor of DNA replication in *Staphylococcus aureus*, wherein *noc*-deleted cells show an over-initiation of DNA replication phenotype (Pang et al. 2017). However,  $\Delta noc$  cells in *B. subtilis* displayed an *ori:ter* ratio similar to wild type cells (Pang et al. 2017). Still, considering the role of Noc in the DNA replication process of *S. aureus*, there is a possibility of Noc playing some role in the regulation

of the initiation phase of DNA replication in *B. subtilis* but only under certain specific conditions; such as under the conditions of DNA replication defect, nutrient scarcity or metabolic stress. Because the  $\Delta pyk$  is defective in the initiation stage of DNA replication, that could be the stimulation to Noc acting as a regulator of DNA replication in these cells. If Noc is acting as an inhibitor of DNA replication in  $\Delta pyk$  cells, then the Z ring rescue observed after *noc*-deletion in  $\Delta pyk$  cells could be due to the relief of inhibitory action of Noc on DNA replication. This would result in the rescue of the under-initiation DNA replication defect of  $\Delta pyk$  cells, allowing the cells to proceed with DNA replication properly, restoring the nucleoid morphology and causing a rescue of Z ring positioning similar to the results obtained with pyruvate. On the other hand, if the Z ring rescue after *noc*-deletion in  $\Delta pyk$  cells is simply due to the nucleoid occlusion activity of Noc, the *ori:ter* ratio of *noc pyk* double mutant will be no different from  $\Delta pyk$  cells. Marker frequency analysis was performed in  $\Delta noc$  and  $\Delta noc \Delta pyk$  cells and the results obtained are shown in Figure 4.5.



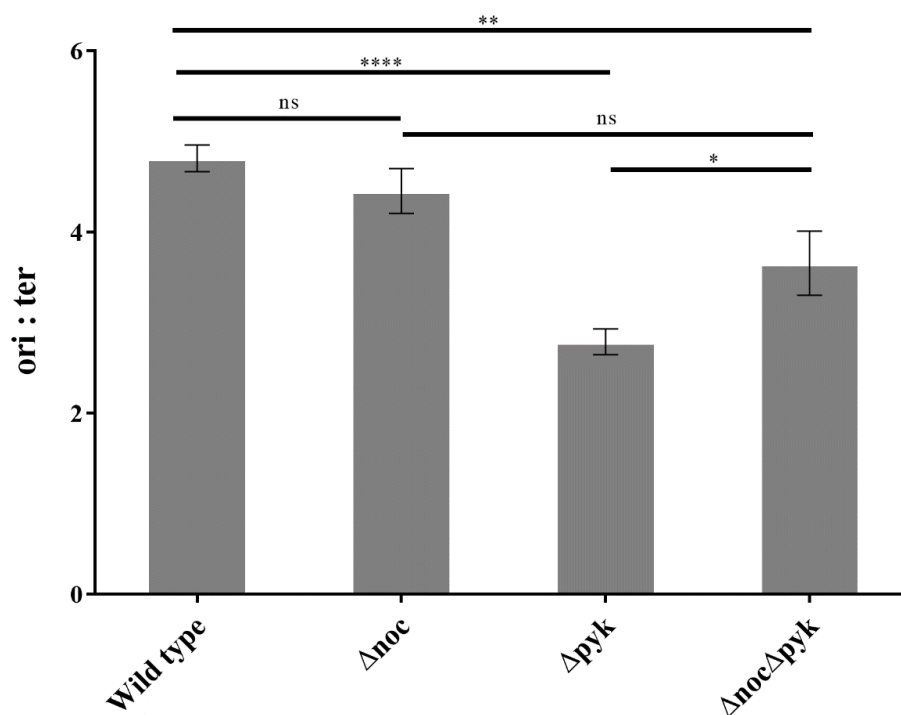


**Figure 4.5. Analysis of the frequency of DNA replication initiation in wild-type (SU492),  $\Delta noc$  (SU657) and  $\Delta noc \Delta pyk$  (SU877) using marker frequency analysis.** Cells were grown in LB medium at 37°C/ 200 rpm to the mid-exponential phase. Sodium azide was added to prevent further growth and genomic DNA was isolated from the harvested cells. The *oriC*-to-terminus (*ori:ter*) ratio of each strain was determined using quantitative PCR (qPCR) using primers specific to the relevant chromosomal regions. The results are shown as the average values of three biological replicates and the error bars indicate standard error of mean of those replicates, obtained using one-way Anova statistical analysis. ‘\*’ represent that the samples under investigation are statistically different, whereas ‘ns’ represents that they are not different.

Similar to the study of Pang et al. (2017), *noc* deletion had no significant effect on the *ori:ter* ratio of wild type cells, suggesting that Noc has no major effects on the frequency of DNA replication initiation, at least in otherwise wild type cells grown under standard laboratory conditions. The *noc pyk* double mutant displayed an *ori:ter* ratio significantly

different from wild type cells as well as different from  $\Delta pyk$  (Figure 4.5). Statistical analysis revealed that the *ori:ter* ratio of  $\Delta noc \Delta pyk$  is different from wild type cells (P value-0.0025) as well as different from  $\Delta pyk$  cells (P value- 0.0291), suggesting that *noc*-deletion did rescue the DNA *ori:ter* ratio of  $\Delta pyk$  cells but did not make it to the wild type cells level. The reason for this slight increase in the *ori:ter* ratio after *noc* deletion in  $\Delta pyk$  cells is unclear. However, the rescue of *ori:ter* in *noc*-deleted  $\Delta pyk$  cells is not to the wild type levels. This suggests that the Z ring positioning rescue in *noc*-deleted  $\Delta pyk$  cells is not due to Noc rescuing the DNA replication defect of  $\Delta pyk$  cells. Instead, these results uphold the idea that Noc is causing the acentral Z rings in *pyk*-deleted cells as a result of its nucleoid occlusion activity and not due to an effect on the DNA replication initiation.

#### 4.4 Discussion

The primary question that this chapter aimed at answering was whether the effect on Z ring positioning in  $\Delta pyk$  cells is due to an indirect effect through the known inhibitors of Z ring formation in *B. subtilis*: the Min and the nucleoid occlusion system? Since the combined action of these systems ensures that the Z ring forms only at the midcell site and not anywhere else in the cell (Rodrigues and Harry 2012), any effect on the functioning of these systems would have an influence on the Z ring positioning. Hence, the possibility of any effect on the functioning of either of these systems causing the Z rings to form at acentral sites in  $\Delta pyk$  was investigated.

Firstly, the possibility of an inactivation of the Min system being the reason for the acentral Z ring positioning phenotype of  $\Delta pyk$  cells was examined by looking at the Z ring positioning phenotype of a *minCD pyk* double mutant. An increased frequency of the acentral Z rings in this mutant compared to the single mutants of *minCD* and the *pyk* indicated that the Min system is active, at least partially, in  $\Delta pyk$  cells and the mechanism of acentral Z ring

positioning in  $\Delta pyk$  cells is not mediated solely via an inactivation of the Min system. Further analysis revealed that the cell length and the Z ring positioning phenotypes in the single mutants of *pyk* and *minCD* are completely different. The deletion of *minCD* increased the cell length in contrast to *pyk* deletion that decreased the cell length. The categorization of acentral Z rings into polar and non-polar acentral Z rings revealed that the *minCD* mutant had more of polar Z rings, whereas the *pyk* mutant had more of non-polar acentral Z rings. Nonetheless, the deletion of *minCD* in the *pyk* mutant increased the frequency of polar Z rings. All these results together showed that although both the *minCD* and the *pyk* mutant, form Z rings at acentral sites, there are certain differences in their acentral Z ring positioning phenotypes; suggesting that the mechanism by which  $\Delta pyk$  cells form the Z rings at acentral site is not via an effect on the Min system and the Min system is active, at least partially, in these cells. However, whether the Min system is completely active, or its activity is altered to some extent cannot be accounted for under the experimental conditions used.

Next, it was investigated whether the nucleoid occlusion is active in  $\Delta pyk$  cells and if so, what is its involvement in the acentral Z ring positioning of these cells? Interestingly, the deletion of *noc* rescued the acentral Z ring positioning defect of  $\Delta pyk$  cells to midcell site, indicating that the nucleoid occlusion is originally active in  $\Delta pyk$  cells and this active nucleoid occlusion does prevent the formation of Z ring at midcell site. Notably, *noc* deletion has no effect on the Z ring positioning in otherwise wild type cells, where the chromosomes replicate properly, are organized in two lobes per cell and the midcell site is relieved of the nucleoid occlusion activity (Rodrigues and Harry 2012). Since the *noc* deletion did rescue the acentral Z ring positioning defect of  $\Delta pyk$  cells, this suggested that the chromosome organization of  $\Delta pyk$  cells is somehow distorted, which prevents the Z rings forming at midcell site. Hence, the quantification of the nucleoid morphology of  $\Delta pyk$  cells was performed, which did confirm that these cells have a spread nucleoid morphology, a morphology different from the bilobed

nucleoid morphology of wild type cells. This raised the possibility that the nucleoid morphology of  $\Delta pyk$  cells could be a contributing factor to their acentral Z ring positioning defect by allowing the nucleoid occlusion to be active over a widespread region within the cell and only allowing the Z rings to form at acentral sites where there is decreased inhibition of the nucleoid occlusion. However, because  $\sim 70\%$  of the Z rings in  $\Delta pyk$  do form at midcell, this indicates that there are some molecular intricacies to the spread nucleoid morphology of  $\Delta pyk$  cells, which allow the sufficient separation of nucleoids at the midcell, allowing the formation of Z rings. This is evident from the nucleoid morphology demographs (Figure 4.3), where  $\sim 50\%$  of the cells (0-700) did show some separation of nucleoids. Considering this, a clear correlation between the Z ring positioning and the spread nucleoid morphology phenotype of  $\Delta pyk$  cells needs to be ascertained, which can be done by visualizing the movement of fluorescently labelled-FtsZ and the origin of DNA replication concurrently in the  $pyk$  mutant. This will provide further evidence on the role of the spread nucleoid morphology, and hence the nucleoid occlusion, in acentral Z ring positioning in  $\Delta pyk$  cells. It would be ideal to perform these experiments in the germinated spores of  $\Delta pyk$ , so that the timing of these events can be monitored from the very first cell cycle event.

As the mutants of DNA replication initiation in *B. subtilis* have been shown to display a distorted chromosome organization (Wang et al. 2014), the spread nucleoid morphology of the  $pyk$  mutant pointed to the possibility of DNA replication being altered in these cells. Nonetheless,  $\Delta pyk$  has previously been shown to display a DNA replication defect with decreased ratio of origin to terminus as compared to wild type cells (Murray and Koh 2014). Consistent with Murray *et al.*, a decreased ratio of *ori: ter* was observed for the  $pyk$  mutant in our experiments as well, confirming that the deletion of  $pyk$  does result in a DNA replication under-initiation phenotype in *B. subtilis* cells. Recently, the study published by Nouri *et al.*

(2018) identified that the enzyme pyruvate kinase is crucial specifically for the formation of an active DnaA/*OriC* complex, and that *pyk* is genetically linked to *dnaC*, *dnaG* and *dnaE*.

As the processes of DNA replication and chromosome segregation occur concomitantly such that the origins of replication move to the future division sites as soon as they are replicated (Berkmen and Grossman 2007), any defect in the initiation step of DNA replication is likely to have a consequential effect on the chromosome segregation process, influencing the chromosome organization (Niki et al. 1991). Hence, the spread nucleoid morphology of  $\Delta pyk$  cells could be attributed to their DNA replication initiation defect. A change in chromosome organization in DNA replication initiation mutants has been previously reported in *B. subtilis*, such that the origins of replication, which move away from the midcell region during the late stages of cell cycle in wild type cells where the rate of chromosome replication is normal; remains in the midcell region in DNA replication initiation mutants (Wang et al. 2014). This also relates to our previous observation of *noc*-deletion rescuing the acentral Z ring positioning defect of  $\Delta pyk$  cells. The Noc-binding sites are present near the origin of replication, which remains at the midcell site when DNA replication initiation is inhibited (Wang et al. 2014). It could be hypothesized that the DNA replication initiation defect of  $\Delta pyk$  cells could be leading to their spread nucleoid morphology such that the Noc-binding sites remain in the midcell region, preventing the formation of Z rings.

Interestingly, the addition of pyruvate rescued the DNA replication initiation defect of  $\Delta pyk$  cells, indicating that wild type pyruvate levels are required to maintain the frequency of DNA replication initiation in these cells. There is evidence in the literature that demonstrate a connection between DNA replication and central carbon metabolism in *B. subtilis* as well as in *E. coli* (Janni re et al. 2007; Maciag et al. 2012; Maciag-Dorszy nska et al. 2012). A connection between glycolysis and DNA synthesis in *B. subtilis* was discovered by Janni re *et al.*, wherein

the viability of the thermosensitive DNA replication elongation mutant of *dnaE* was fully restored by some metabolic alterations belonging to the glycolysis pathway, one of them being the *pyk* deletion (Janni re et al. 2007). Similar results were obtained in *E. coli* by Maciag *et al.* in 2012 with an extension of the role of central carbon metabolism in DNA replication fidelity (Maciag et al. 2012). Another study revealed that the deletions of genes belonging to CCM not only suppress the *E. coli* DNA replication mutants but also rescues their nucleoid position and cell division defects (Maciag-Dorszy nska et al. 2012), indicating a connection between CCM, nucleoid position and cell division. In light of these previous studies that established the involvement of central carbon metabolism in regulating the process of DNA replication, it appears that pyruvate is one of the factors from the CCM that is required for the initiation step of DNA replication in *B. subtilis*.

Overall, the results presented in this chapter indicate towards a model as per which 1/3<sup>rd</sup> of the Z rings are blocked from forming at midcell site in the *pyk* mutant due to the nucleoid occlusion being still active in the midcell region at the time of Z ring formation. This does not occur in wild type cells, as the midcell site is relieved of the nucleoid occlusion activity as a result of completely replicated chromosomes moving away from the midcell site at the later stages of cell cycle. However, the phenotype of acentral Z rings is observed in  $\Delta pyk$  cells, as they have a DNA replication initiation defect due to decreased levels of pyruvate, which results in a change in their chromosome organization such that the Noc-binding sites are not located in the right way around the cell in a spatial sense, blocking midcell Z ring formation in some cells. Following from this model, it would be interesting to investigate the mechanism of how central carbon metabolism affects the process of DNA replication in  $\Delta pyk$  cells. In this perspective, as there are many ways by which the DNA replication could have been affected, a global unbiased approach that gives an overview of all the changes happening in  $\Delta pyk$  cells, such as RNA-seq technology to look at changes in global gene expression, will assist in

deciphering the way by which CCM affects the DNA replication process. This will be the focus of the next chapter in this thesis.



# Chapter 5

---

**Investigating the link between central  
carbon metabolism and cell division  
using a global transcriptomic approach**



## 5.1 Introduction and chapter aims

From the results presented in Chapter 3 of this thesis, pyruvate scarcity does play a role in the acentral Z ring positioning defect of the *pyk* mutant. And, from the results presented in Chapter 4, this link between pyruvate scarcity and acentral Z ring positioning might occur by lowering the frequency of DNA replication initiation, thereby changing the morphology of the nucleoid (Chapter 4) and creating downstream effects on the Z ring positioning. However, the precise mechanism connecting these links is unclear. In order to understand this mechanism of how the decrease in pyruvate levels leads to all these phenotypic changes, an ‘omics’ experiment was performed. ‘Omics’ technologies are aimed at the universal detection of molecules such as the genes (genomics), mRNA (transcriptomics), proteins (proteomics) and metabolites (metabolomics), in a non-biased manner (Horgan and Kenny 2011); and can provide data on a systems scale, allowing the understanding of how the different cellular processes are interconnected in  $\Delta pyk$  cells?

As the type and levels of RNA molecules represent the gene expression profile of an organism and consequently are used as a proxy to signify the phenotypic characteristics of that organism, identifying and characterising changes in the abundance of different RNA transcripts in  $\Delta pyk$  cells is an important way to understand the mechanism that connects pyruvate levels to the Z ring positioning in *B. subtilis*. Hence, amongst all other available ‘omics’ technologies, RNA-Seq was performed on  $\Delta pyk$  cells to identify any gene(s) differentially expressed in these cells that could potentially contribute to the cell division phenotype of these cells, either via an effect on DNA replication or independently.

The RNA-Seq experiment was performed in collaboration with the Singapore Centre for Environmental Life Sciences Engineering (SCELSE). The culture samples for RNA extraction as well as the RNA extraction itself was performed by Dr. Amy Bottomley (UTS),

while initial data analysis was done by Dr. Gurjeet Singh Kohli (SCELSE) to generate the list of differentially expressed (DE) genes. Further, I analyzed this list of DE genes by mapping them onto biological pathways to explore the biological relevance of DE genes.

RNA-Seq, being an unbiased and non-targeted quantitative holistic transcriptome approach, was performed with the objective of measuring some cellular responses that could help understand the mechanism of the cell division defect of  $\Delta pyk$  cells. These cellular responses could include an effect on the expression profile of any cell division protein or a pathway that is known to have an effect on the Z ring positioning. In addition, since the RNA-Seq is an unbiased approach that gives a snapshot of the complete gene expression profile, the data analysis might reveal the differential expression of a new pathway that has no links to any currently known Z ring regulatory mechanisms. In this scenario, the possibility of any such pathway being involved in the Z ring positioning was further investigated by performing some follow up biological experiments.

In addition to investigating the differentially expressed profile of  $\Delta pyk$  cells compared to wild type cells, the expression profile of  $\Delta pyk$  cells after the addition of metabolites – pyruvate and L-alanine, was also investigated in order to look at the effect of these metabolites on the differential expression profile of  $\Delta pyk$  cells. As pyruvate and L-alanine rescued the Z ring positioning of  $\Delta pyk$  cells, the analysis of the expression profile of  $\Delta pyk$  cells after the addition of these two metabolites assisted in further validating the involvement of genes hypothesized to play a role in the Z ring positioning from  $\Delta pyk$  data analysis in the central carbon metabolism (CCM)-division link.

## 5.2 Results

### 5.2.1 Assessing the sample-to-sample variation using PCA and heat map analysis

RNA-Seq data was generated from the *pyk* mutant in the presence and absence of pyruvate and L-alanine to investigate the molecular mechanism underpinning the CCM-division link. As a control, the RNA-Seq data was also generated for wild type cells with and without supplementation with these metabolites, to identify any non-specific differential expression of genes that could result from the addition of these metabolites. Having generated the RNA-seq data for the *pyk* mutant and wild type control under various conditions, it was important to assess the overall sample-to-sample variation within different experimental groups. PCA analysis is a useful tool to represent the sample-to-sample variance in a data set, hence PCA analysis was performed by Dr. Gurjeet in order to visualize the similarity or differences between different experimental samples. The results obtained are shown in Figure 5.1.

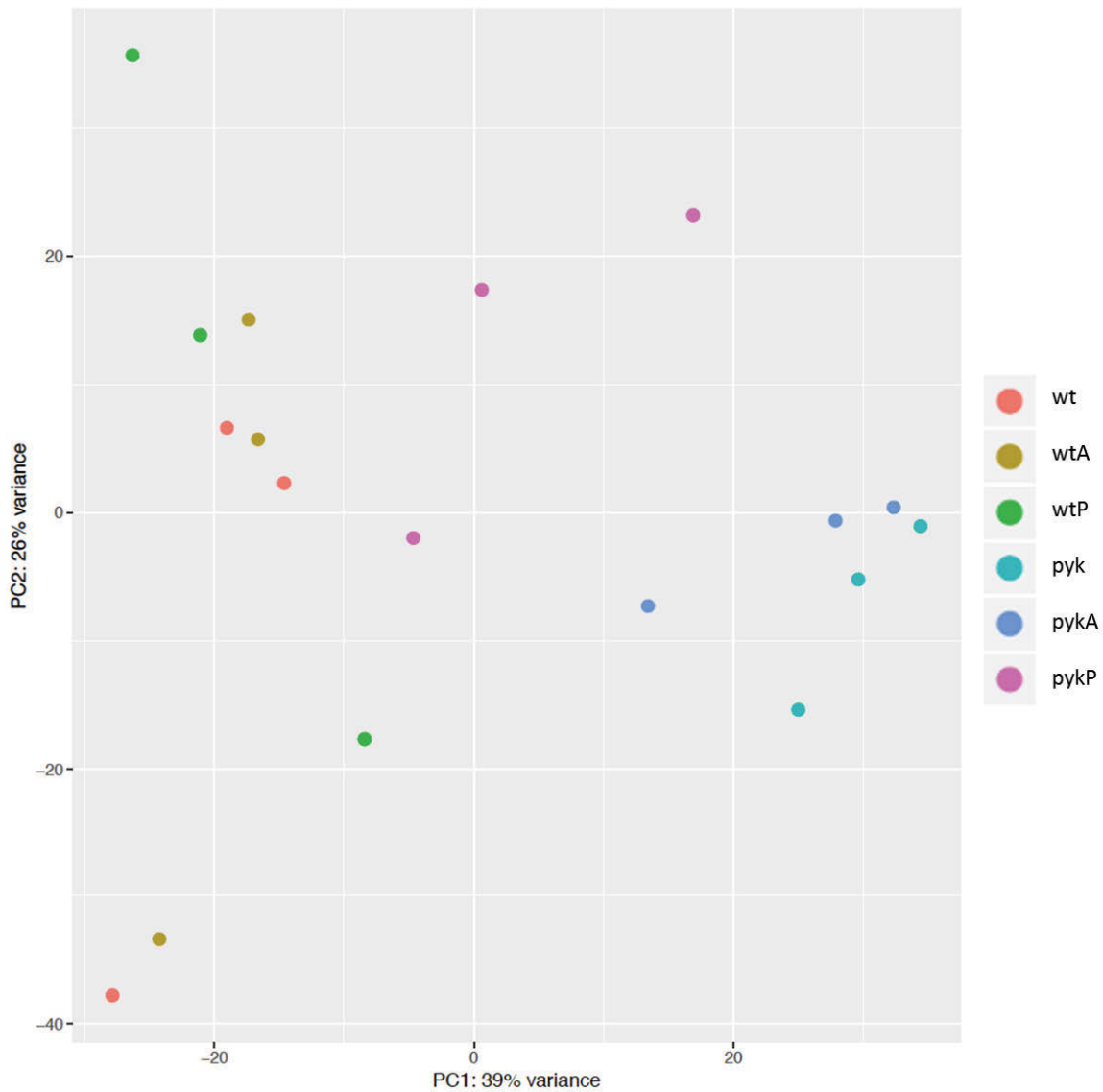


**Figure 5.1. PCA analysis of different experimental groups.** The analysis was performed by Dr. Gurjeet using the DESeq2 package. The axes in this graph depict the two principal components, called PC1 and PC2, which depict the variability present within samples during the analysis process. Different experimental samples are denoted by different colors, as indicated in the chart. In this analysis, PC1 showed a variance of 39% and PC2 a variance of 26%, as depicted on the plot axes (wt- wild type, wtA- wild type + L-alanine, wtP- wild type + pyruvate, pyk-  $\Delta pyk$ , pykA-  $\Delta pyk$  + L-alanine, pykP-  $\Delta pyk$  + pyruvate).

The presence of all the biological replicates of each experimental sample (denoted by different colours) close to each other in the PCA chart, indicated that there was minimal intergroup variation between the biological replicates of each sample. Nevertheless, one of the replicates for each of the wt, wtA and wtP samples were in different quadrants compared to other replicates, indicating some level of variability; however they did not show much variation on the x-axis, which denoted the higher level of variance (39%) than the y-axis (26%). Hence, overall, PCA analysis showed that there was minimal intergroup variation in the samples.

As expected, wild type and  $\Delta pyk$  gene expression profiles were very distantly placed in the chart, indicating they have very distinct gene expression profiles (Figure 5.1). Furthermore, the addition of L-alanine to wild type as well as to  $\Delta pyk$  cells had no significant effect on their gene expression profiles, while the addition of pyruvate did; as demonstrated by the shifts observed after pyruvate addition (wtP and pykP) in the PCA analysis chart (Figure 5.1). Pyruvate addition to  $\Delta pyk$  cells had some effect on the gene expression profile of these cells such that the expression profile of these cells more closely resembled that of wild type cells. This is interesting given that pyruvate addition also shifted Z ring positioning of  $\Delta pyk$  cells towards wild type.

Along with the PCA analysis, a heatmap was also generated to compare the transcriptional profile of different samples, which is shown in Figure 5.2. Heat maps show the entire data matrix with each entry colour-coded with a specific colour according to its value within the entire data set. Hierarchical clustering dendrograms (top of Figure 5.2) are usually represented along with a heat map as it allows the partitioning of samples by reordering the columns, representing the expression measures of different samples, based on their hierarchical clustering results with similar observation columns placed close to each other.

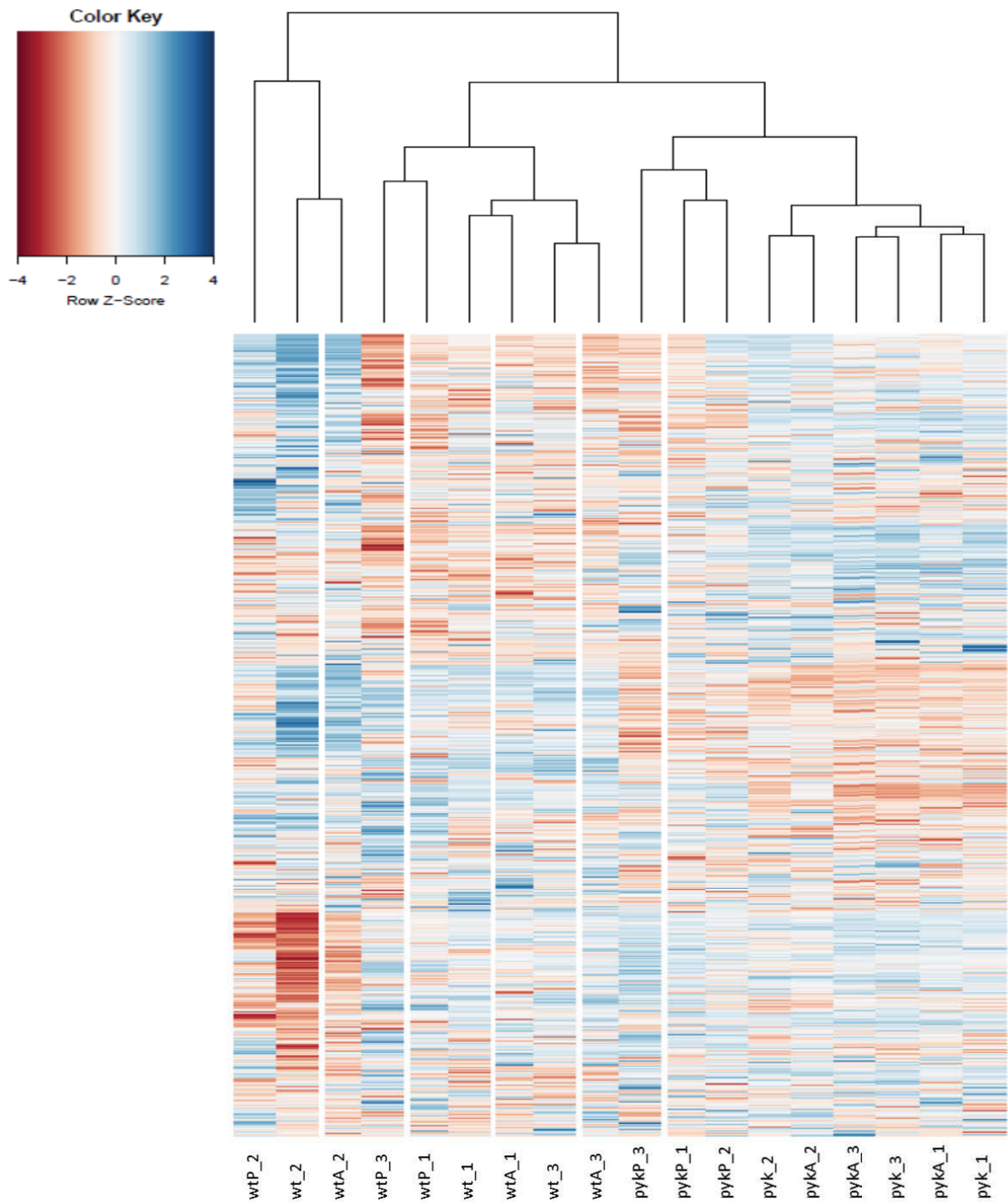


**Figure 5.2. Heat maps combined with hierarchical clustering using a dendrogram.** Heat map and dendrogram were prepared by Dr. Gurjeet using the raw sequencing reads and the DeSeq2 package. Genes are plotted in rows and experimental groups in columns. Numbers in the sample names represent each biological replicate (wt- wild type, wtA- wild type + L-alanine, wtP- wild type + pyruvate, *pyk*- $\Delta$ *pyk*, *pykA*- $\Delta$ *pyk* + L-alanine, *pykP*- $\Delta$ *pyk* + pyruvate). The clustered heatmap shows the Row Z-score,

which is the amount by which counts for a gene deviates in a specific sample from that gene's average across all samples.

In the heat map (Figure 5.2), wild type and  $\Delta pyk$  clustered separately, as was also shown by the PCA analysis; demonstrating that wild type and  $\Delta pyk$  cells have very distinct gene expression profiles. Similar to the observation in PCA chart, where the addition of pyruvate shifted the position of  $\Delta pyk$  samples towards wild type cells, the clustered heat map also showed that addition of pyruvate to  $\Delta pyk$  cells does indeed result in an RNAseq profile similar to wild type cells, as the pykP clustered with the wild type cells. This indicated that the pyruvate addition does shift the gene expression profile of  $\Delta pyk$  cells closer to the wild type cells.

### **5.2.2 Comparison of the quantity of differentially expressed genes under different experimental conditions**

The total number of differentially expressed (DE) genes under different experimental conditions were enumerated after applying the cutoff values of fold change  $\geq 2.0$  and p-value  $< 0.05$ . The numbers of DE genes under different experimental conditions are specified in Table 5.1.

**Table 5.1. The number of differentially expressed genes under each experimental condition**

Datasets compared*	Number of DE genes (up-regulated genes, down-regulated genes, at p-value <0.05 and Fold Change ≥ 2.0)		
	Total	Up-regulated	Down-regulated
pyk vs wt	323	69	254
pykP vs wt	186	43	143
pykP vs pyk	144	85	59
pykA vs pyk	1	1	0
wtP vs wt	83	20	63
wtA vs wt	3	2	1

\*For each dataset, the number of DE genes are upregulated or downregulated in the left dataset in comparison to the right dataset. For example, for pyk vs wt, 323 genes were differentially expressed in the pyk mutant as compared to the wild type cells. Out of these 323 genes, 69 genes were upregulated and 254 genes were downregulated in  $\Delta pyk$  as compared to wild type cells.

In the RNA-Seq, wtP vs wt and wtA vs wt were included as controls to remove any non-specific differential expression that could result after the addition of these metabolites. A total of 83 and 3 genes were differentially expressed in the wtP vs wt and wtA vs wt comparison, respectively, which will be discussed further in section 5.2.4 where the functional annotation of the DE genes will be described.

Out of a total number of 323 DE genes in the  $\Delta pyk$  vs. wt comparison, 254 were downregulated and 69 were upregulated (Table 5.1), indicating that the deletion of the pyruvate kinase gene causes the downregulation of a large number of genes. After the addition of pyruvate to  $\Delta pyk$  cells, only 186 genes were observed to be differentially expressed in comparison to the wild type cells (significantly less than the  $\Delta pyk$  vs. wt comparison in the absence of pyruvate), suggesting that pyruvate addition does make the gene expression profile of  $\Delta pyk$  cells more similar to wild type cells.



Interestingly, comparison of  $\Delta pyk$  cells in the presence and absence of L-alanine showed the differential expression of only one gene, which was upregulated. The functional annotation of this gene revealed it to be *ald*, the gene encoding for alanine dehydrogenase, which was upregulated by a  $\log_2$  fold change of 3.66 in *pykA* vs *pyk*. This result further confirmed the conclusion made in section 3.3.5 that L-alanine causes the Z ring positioning rescue of  $\Delta pyk$  cells by getting converted to pyruvate via the enzyme Ald. Furthermore, this data also provided an ideal internal control for our entire RNA-Seq experiment data.

### **5.2.3 Functional annotation of differentially expressed genes in the pyruvate kinase mutant**

For biological analysis of the DE genes in the *pyk* mutant compared to the wild type cells, the entire set of DE genes was mapped onto functional pathways using the BioCyc Omics Dashboard. The proportion of differentially expressed genes belonging to each functional category was determined to examine the functional profile of the data set, and the percentage share of each biological process differentially expressed in the *pyk* mutant, calculated from the numbers of DE genes in each of these processes, is represented in the pie chart shown in Figure 5.3.

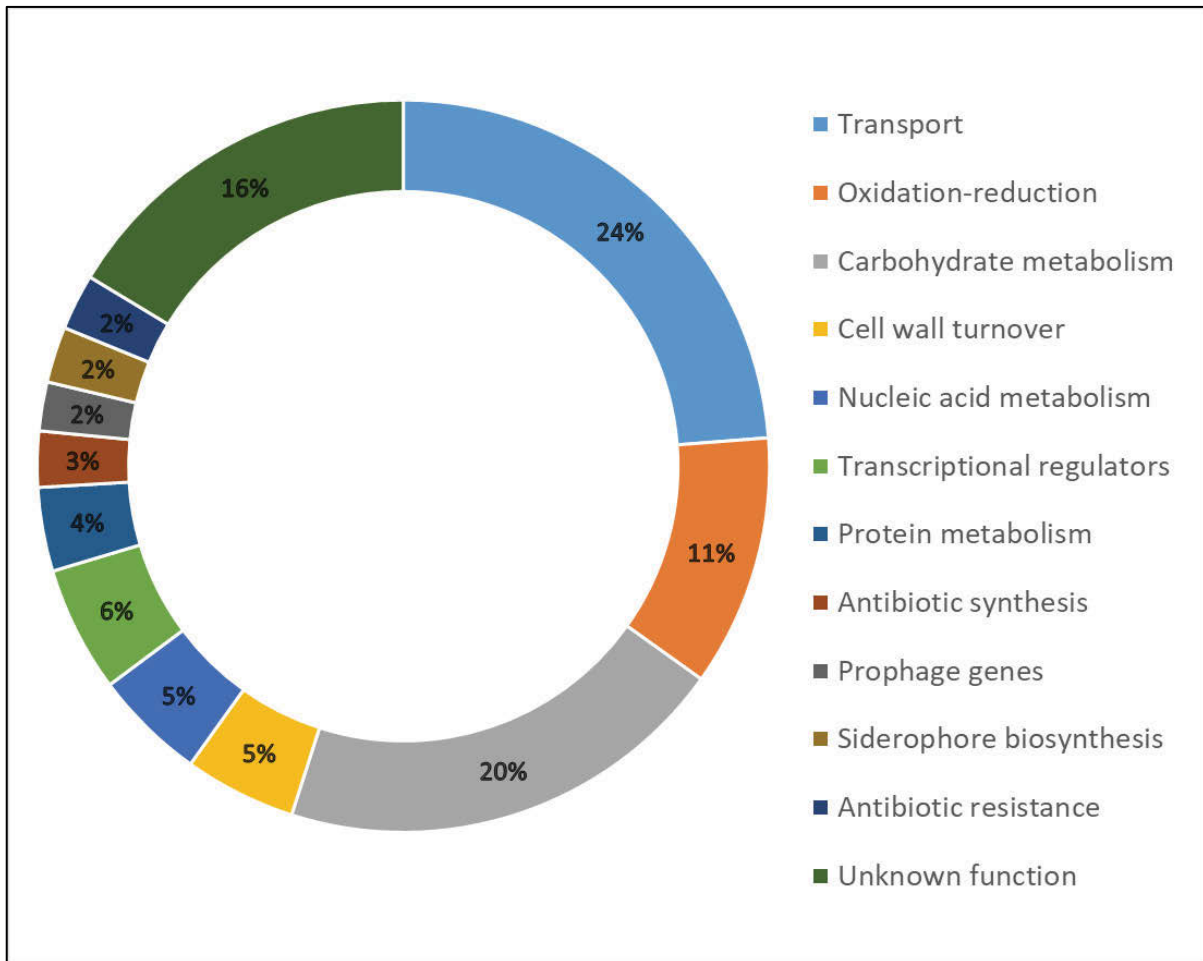


**Figure 5.3.** Pie chart demonstrating the percentage share of different biological processes differentially expressed in  $\Delta pyk$  cells. DE genes in the *pyk* mutant were mapped to the biological process using the BioCyc Omics dashboard tool and numbers of genes belonging to each of these biological processes were enumerated. The percentage representation of each biological process was calculated considering the total numbers of DE genes in the *pyk* mutant, using the formula = (number of genes DE in the specific biological process/ total number of DE genes in  $\Delta pyk$ )  $\times$  100

Functional annotation revealed that most of the DE genes in the  $\Delta pyk$  vs wt comparison were associated with transport systems (24%), followed by carbohydrate metabolism (20%), unknown genes (16%), oxidation-reduction (11%), transcriptional regulators (6%), nucleic acid metabolism (5%), cell wall turnover (5%), protein metabolism (4%), antibiotic synthesis

(3%), prophage genes (2%), siderophore synthesis (2%) and genes conferring antibiotic resistance (2%) (Figure 5.3). The DE genes mapping to each of the biological processes shown in Figure 5.3, were then annotated to a specific molecular function within that biological process. The results obtained along with the fold change of all DE genes are presented in Table 5.2. Interestingly, the gene encoding for the enzyme pyruvate kinase (*pyk*) also came up in the list of downregulated genes in  $\Delta pyk$  compared to wild type cells. This is unlikely to be an expression error in the *pyk* mutant, instead it could be due to the background noise in the RNA-seq data.

Table 5.2. Functional groups differentially expressed in the *pyk* mutant in comparison to the wild type cells

Functional group	Gene*	Annotated product	Response in <i>Δpyk</i>	Fold change
<b>Transport</b>				
Glycine betaine transport	<i>opuAB</i>	Glycine betaine transport system permease protein	Upregulated	3.38
	<i>opuAC</i>	Glycine betaine-binding protein	Upregulated	3.01
	<i>opuCD</i>	Glycine betaine/carnitine/choline transport system permease protein	Upregulated	13.22
	<i>opuCA</i>	Glycine betaine/carnitine/choline transport ATP-binding protein	Upregulated	13.53
	<i>opuAA</i>	Glycine betaine transport ATP-binding protein	Upregulated	3.33
	<i>opuCB</i>	Glycine betaine/carnitine/choline transport system permease protein	Upregulated	15.38
	<i>opuCC</i>	Glycine betaine/carnitine/choline-binding protein	Upregulated	11.40
Arginine/ornithine	<i>rocC</i>	Arginine/ornithine permease	Upregulated	5.99
	<i>rocA</i>	1-pyrroline-5-carboxylate dehydrogenase	Upregulated	9.02
	<i>rocE</i>	Arginine/ornithine permease	Upregulated	5.42
Manganese transporters	<i>mntC</i>	Manganese transport system membrane protein	Downregulated	31.23
	<i>mntH</i>	Divalent metal cation transporter	Downregulated	8.10
	<i>mntB</i>	Manganese transport system ATP-binding protein	Downregulated	20.23
	<i>mntD</i>	Manganese transport system membrane protein	Downregulated	44.47
	<i>mntA</i>	Manganese-binding lipoprotein	Downregulated	17.28
Ribose transporters	<i>rbsA</i>	Ribose import ATP-binding protein RbsA	Downregulated	306.18
	<i>rbsB</i>	Ribose import binding protein	Downregulated	445.90
	<i>rbsC</i>	Ribose import permease protein	Downregulated	2131.77
Phosphotransferase system	<i>malP</i>	PTS system maltose-specific EIICB component	Downregulated	17.72
	<i>treP</i>	PTS system trehalose-specific EIIBC component	Downregulated	9.53
	<i>sacP</i>	PTS system sucrose-specific EIIBC component	Downregulated	12.14

	<i>fruA</i>	PTS system fructose-specific EIIABC component	Downregulated	11.32
	<i>gmuC</i>	Oligo-beta-mannoside permease IIC component	Downregulated	50.84
	<i>nagP</i>	PTS system N-acetylglucosamine-specific EIICB component	Downregulated	4.06
	<i>licC</i>	Lichenan permease IIC component	Downregulated	65.10
	<i>licB</i>	Lichenan-specific phosphotransferase enzyme IIB component	Downregulated	27.01
	<i>licA</i>	Lichenan-specific phosphotransferase enzyme IIA component	Downregulated	262.45
	<i>mtlF</i>	Mannitol-specific phosphotransferase enzyme IIA component	Downregulated	9.00
	<i>levD</i>	Fructose-specific phosphotransferase enzyme IIA component	Downregulated	40.70
Lactate transporters	<i>lctP</i>	L-lactate permease	Downregulated	13.31
	<i>yvfH</i>	L-lactate permease	Downregulated	8.32
Iron transporters	<i>yfmC</i>	Fe(3+)-citrate-binding protein	Downregulated	3.76
	<i>fhuB</i>	Iron(3+)-hydroxamate import system permease protein	Downregulated	3.80
	<i>fhuC</i>	Iron(3+)-hydroxamate import ATP-binding protein	Downregulated	4.00
	<i>fhuD</i>	Iron(3+)-hydroxamate-binding protein	Downregulated	3.01
	<i>fhuG</i>	Iron(3+)-hydroxamate import system permease protein	Downregulated	3.01
	<i>efeU</i>	Ferrous iron permease	Downregulated	2.94
	<i>efeM</i>	Probable iron uptake system component	Downregulated	3.10
	<i>yxeB</i>	Iron(3+)-hydroxamate-binding protein	Downregulated	16.02
Other transporters	<i>lrgB</i>	Pyruvate transporter	Downregulated	257.68
	<i>lrgA</i>	Pyruvate transporter	Downregulated	578.63
	<i>yknX</i>	Putative efflux system component	Downregulated	2.96
	<i>ydaO</i>	Uncharacterized amino acid permease	Downregulated	2.38
	<i>cydC</i>	ATP-binding/permease protein	Downregulated	12.24
	<i>ythP</i>	Uncharacterized ABC transporter ATP-binding protein	Downregulated	3.75
	<i>yknY</i>	Uncharacterized ABC transporter ATP-binding protein	Downregulated	3.60
	<i>sunT</i>	SPBc2 prophage-derived sublancin-168-processing and transport ATP-binding	Downregulated	11.79

---

<i>dctP</i>	C4-dicarboxylate transport protein	Downregulated	22.69
<i>yhfQ</i>	Putative ABC transporter substrate-binding lipoprotein	Downregulated	4.40
<i>msmX</i>	Maltodextrin import ATP-binding protein	Downregulated	8.68
<i>yknZ</i>	Uncharacterized ABC transporter permease	Downregulated	3.23
<i>glpF</i>	Glycerol uptake facilitator protein	Downregulated	10.46
<i>gntP</i>	Gluconate permease	Downregulated	2.27
<i>yhcA</i>	Uncharacterized MFS-type transporter	Upregulated	6.45
<i>cydD</i>	ATP-binding/permease protein	Downregulated	10.23
<i>iolF</i>	Minor myo-inositol transporter	Downregulated	21.92
<i>maeN</i>	Na(+)-malate symporter	Downregulated	5.66
<i>cycB</i>	Cyclodextrin-binding protein	Downregulated	5.63
<i>sufC</i>	Sulfur mobilizing protein	Downregulated	3.11
<i>efeN</i>	Probable deferrochelataase/peroxidase	Downregulated	3.36
<i>glpT</i>	Glycerol-3-phosphate transporter	Downregulated	22.25
<i>yfiQ</i>	Putative metal ion transporter	Upregulated	2.31
<i>ycnB</i>	Uncharacterized MFS-type transporter	Upregulated	3.18
<i>yfiY</i>	Probable siderophore-binding lipoprotein	Downregulated	2.46
<i>nupC</i>	Nucleoside permease	Downregulated	3.25
<i>yhdP</i>	Potential magnesium efflux pump	Upregulated	2.50
<i>frlO</i>	aminosugar ABC transporter- fructose amino acid-binding lipoprotein	Upregulated	22.09
<i>lysP</i>	lysine permease	Upregulated	8.15
<i>yhbJ</i>	putative integral inner membrane protein; putative exporter subunit	Upregulated	7.64
<i>yceF</i>	putative stress adaptation transporter	Downregulated	2.57
<i>yknW</i>	putative permease	Downregulated	2.60
<i>dtpT</i>	di-tripeptide-proton ABC symporter	Downregulated	2.63
<i>xkdM</i>	ABC transporter (permease)	Downregulated	3.91

---

<i>ythQ</i>	putative ABC transporter (permease)	Downregulated	4.30
<i>copB</i>	copper(I)-transporting ATPase	Downregulated	5.09
<i>ytcQ</i>	putative ABC transporter (binding lipoprotein)	Downregulated	5.61
<i>yoaG</i>	putative permease	Downregulated	6.59
<i>cstA</i>	putative peptide transporter, carbon starvation-induced protein	Downregulated	16.01
<b><i>Oxidation-reduction</i></b>			
<i>ytkK</i>	Putative oxidoreductase	Downregulated	2.32
<i>ycaA</i>	Probable tartrate dehydrogenase/decarboxylase	Downregulated	3.15
<i>catE</i>	Catechol-2,3-dioxygenase	Downregulated	5.67
<i>fadhH</i>	Probable 2,4-dienoyl-CoA reductase	Upregulated	6.89
<i>cydB</i>	Cytochrome bd ubiquinol oxidase subunit 2	Downregulated	11.38
<i>hmoA</i>	Heme-degrading monooxygenase	Downregulated	4.30
<i>cccA</i>	Cytochrome c-550	Downregulated	6.20
<i>yrkA</i>	Putative membrane associated protein	Downregulated	2.33
<i>qcrB</i>	Menaquinol-cytochrome c reductase cytochrome b	Downregulated	3.63
<i>cydA</i>	Cytochrome bd ubiquinol oxidase subunit 1	Downregulated	6.85
<i>cypB</i>	Bifunctional cytochrome P450/NADPH--P450 reductase 2	Downregulated	3.15
<i>yrbE</i>	Uncharacterized oxidoreductase	Downregulated	16.74
<i>katA</i>	Vegetative catalase	Downregulated	17.80
<i>yvgN</i>	Glyoxal reductase	Downregulated	3.51
<i>yffR</i>	Uncharacterized oxidoreductase	Downregulated	4.00
<i>ahpC</i>	Alkyl hydroperoxide reductase subunit C	Downregulated	5.03
<i>des</i>	Fatty acid desaturase	Downregulated	4.66
<i>mmsA</i>	Methylmalonate semialdehyde dehydrogenase	Downregulated	50.16
<i>ydbP</i>	Thioredoxin-like protein	Downregulated	2.28
<i>bdbB</i>	SPBc2 prophage-derived disulfide bond formation protein B	Downregulated	7.45

<i>ycgT</i>	Ferredoxin--NADP reductase 1	Downregulated	4.37
<i>lutB</i>	Lactate oxidase	Upregulated	2.98
<i>yfhC</i>	Putative NAD(P)H nitroreductase	Downregulated	2.58
<i>ywbO</i>	Uncharacterized protein	Downregulated	2.11
<i>dhbA</i>	2,3-dihydro-2,3-dihydroxybenzoate dehydrogenase	Downregulated	35.21
<i>qcrC</i>	Menaquinol-cytochrome c reductase cytochrome b/c subunit	Downregulated	3.88
<i>tdh</i>	L-threonine 3-dehydrogenase	Downregulated	7.86
<i>yfmJ</i>	Putative NADP-dependent oxidoreductase	Downregulated	3.44
<i>yhcB</i>	Uncharacterized protein	Upregulated	5.04
<i>ahpF</i>	NADH dehydrogenase	Downregulated	5.52
<i>ykuN</i>	Probable flavodoxin-1	Downregulated	27.49
<i>ykuP</i>	Probable flavodoxin-2	Downregulated	15.74
<i>bdbA</i>	SPBc2 prophage-derived disulfide bond formation protein A	Downregulated	26.10
<i>sufU</i>	Zinc-dependent sulfur transferase	Downregulated	2.90
<i>ohrA</i>	Organic hydroperoxide resistance protein	Downregulated	4.02
<b><i>Carbohydrate metabolism</i></b>			
<i>gmuG</i>	Mannan endo-1,4-beta-mannosidase	Downregulated	9.56
<i>araA</i>	L-arabinose isomerase	Downregulated	6.36
<i>pel</i>	Pectate lyase	Downregulated	8.90
<i>iolJ</i>	6-phospho-5-dehydro-2-deoxy-D-gluconate aldolase	Downregulated	9.02
<i>iolE</i>	Inosose dehydratase	Downregulated	54.02
<i>iolC</i>	5-dehydro-2-deoxygluconokinase	Downregulated	46.83
<i>iolD</i>	3D-(3,5/4)-trihydroxycyclohexane-1,2-dione hydrolase	Downregulated	110.26
<i>iolB</i>	5-deoxy-glucuronate isomerase	Downregulated	21.25
<i>iolI</i>	inosose isomerase	Downregulated	14.96
<i>iolG</i>	Inositol 2-dehydrogenase/D-chiro-inositol 3-dehydrogenase	Downregulated	67.88



<i>iolH</i>	putative sugar-phosphate epimerase/isomerase	Downregulated	56.38
<i>pyk</i>	Pyruvate kinase	Downregulated	824.12
<i>xylA</i>	Xylose isomerase	Downregulated	78.41
<i>xylB</i>	Xylose kinase	Downregulated	32.00
<i>gapA</i>	Glyceraldehyde-3-phosphate dehydrogenase 1	Downregulated	3.19
<i>galT</i>	Galactose-1-phosphate uridylyltransferase	Downregulated	3.59
<i>rocB</i>	putative N-deacylase involved in arginine and ornithine utilization	Upregulated	6.91
<i>rocD</i>	ornithine transaminase	Upregulated	4.52
<i>manA</i>	Mannose-6-phosphate isomerase	Downregulated	66.87
<i>glpK</i>	Glycerol kinase	Downregulated	6.08
<i>hxlB</i>	3-hexulose-6-phosphate isomerase	Downregulated	3.82
<i>rbsK</i>	Ribokinase	Downregulated	68.39
<i>rbsD</i>	D-ribose pyranase	Downregulated	570.94
<i>fbpA</i>	Probable fructose-bisphosphate aldolase	Downregulated	40.99
<i>pckA</i>	Phosphoenolpyruvate carboxykinase [ATP]	Downregulated	4.47
<i>bglC</i>	Aryl-phospho-beta-D-glucosidase	Upregulated	17.06
<i>sacA</i>	Sucrose-6-phosphate hydrolase	Downregulated	9.52
<i>maeA</i>	Probable NAD-dependent malic enzyme 2	Upregulated	3.20
<i>ald</i>	Alanine dehydrogenase	Downregulated	13.42
<i>kbl</i>	8-amino-7-oxononanoate synthase 1	Downregulated	14.07
<i>deoC</i>	Deoxyribose-phosphate aldolase	Downregulated	2.84
<i>bglS</i>	Beta-glucanase	Downregulated	6.76
<i>hxlA</i>	3-hexulose-6-phosphate synthase	Downregulated	6.17
<i>mtlD</i>	Mannitol-1-phosphate 5-dehydrogenase	Downregulated	10.91
<i>treA</i>	Trehalose-6-phosphate hydrolase	Downregulated	19.32
<i>gmuF</i>	Probable mannose-6-phosphate isomerase	Downregulated	22.28

---

<i>frlB</i>	Fructosamine deglycase	Upregulated	7.04
<i>uxaC</i>	Uronate isomerase	Downregulated	27.40
<i>gapB</i>	Glyceraldehyde-3-phosphate dehydrogenase 2	Downregulated	11.87
<i>fruK</i>	1-phosphofructokinase	Downregulated	9.25
<i>ldh</i>	L-lactate dehydrogenase	Downregulated	6.80
<i>licH</i>	Probable 6-phospho-beta-glucosidase	Downregulated	464.63
<i>acuB</i>	Acetoin utilization protein	Downregulated	4.74
<i>yyaH</i>	lactoylglutathione lyase	Upregulated	11.44
<i>ywpJ</i>	Putative phosphatase	Upregulated	8.96
<i>proJ</i>	glutamate 5-kinase	Upregulated	5.92
<i>maa</i>	maltose O-acetyltransferase	Upregulated	5.55
<i>argI</i>	arginase	Upregulated	4.66
<i>lutA</i>	lactate oxidase	Upregulated	3.48
<i>lysC</i>	aspartokinase II (alpha and beta subunits)	Upregulated	2.95
<i>lutC</i>	lactate catabolic enzyme	Upregulated	2.73
<i>prs</i>	phosphoribosylpyrophosphate synthetase	Upregulated	2.61
<i>menH</i>	menaquinone biosynthesis methyltransferase	Upregulated	2.02
<i>yvdD</i>	putative lysine decarboxylase	Downregulated	2.33
<i>bkdAA</i>	branched-chain alpha-keto acid dehydrogenase E1 subunit	Downregulated	2.41
<i>sufS</i>	cysteine desulfurase	Downregulated	2.97
<i>ppnKB</i>	inorganic polyphosphate/ATP-NAD kinase	Downregulated	3.23
<i>lpdV</i>	branched-chain alpha-keto acid dehydrogenase E3 subunit (dihydrolipoamide)	Downregulated	3.49
<i>buk</i>	butyrate kinase	Downregulated	3.77
<i>bcd</i>	branched-chain amino acid dehydrogenase	Downregulated	4.26
<i>fabHB</i>	beta-ketoacyl-acyl carrier protein synthase III 2	Downregulated	5.01
<i>acsA</i>	acetyl-CoA synthetase	Downregulated	5.23

---

<i>glpQA</i>	glycerophosphoryl diester phosphodiesterase	Downregulated	15.64
<i>fbpB</i>	regulator of iron homeostasis	Downregulated	22.37
<i>racX</i>	Probable amino-acid racemase	Downregulated	3.53

**Cell wall turnover**

<i>murQ</i>	N-acetylmuramic acid 6-phosphate etherase	Downregulated	3.74
<i>pdaC</i>	Peptidoglycan-N-acetylmuramic acid deacetylase	Downregulated	5.37
<i>lytE</i>	Probable peptidoglycan endopeptidase	Upregulated	4.41
<i>wprA</i>	Cell wall-associated protease	Downregulated	4.54
<i>gcaD</i>	bifunctional N-acetylglucosamine-1-phosphate uridyltransferase/glucosamine-1-	Upregulated	2.94
<i>yocH</i>	peptidoglycan hydrolase	Upregulated	5.95
<i>cwlO</i>	D,L-endopeptidase-type autolysin	Upregulated	5.56
<i>ydjM</i>	member of the WalR regulon, may be involved in cell wall metabolism	Upregulated	4.46
<i>yabE</i>	putative cell wall shaping enzyme	Upregulated	3.16
<i>bcrC</i>	undecaprenyl pyrophosphate phosphatase	Downregulated	2.22
<i>pbpH</i>	penicillin-binding enzyme for formation of rod-shaped peptidoglycan cell wall	Downregulated	2.54
<i>ybfG</i>	putative peptidoglycan binding protein	Downregulated	2.88
<i>tasA</i>	Spore coat-associated protein N	Downregulated	4.30
<i>pbpE</i>	Penicillin-binding protein 4	Downregulated	4.62
<i>spo0M</i>	Sporulation-control protein	Downregulated	5.55
<i>iseA</i>	inhibitor of cell-separation enzymes	Downregulated	6.52

**Nucleic acid metabolism**

<i>dnaB</i>	Replication initiation and membrane attachment protein	Upregulated	2.26
<i>nrdEB</i>	Ribonucleoside-diphosphate reductase NrdEB subunit alpha	Upregulated	8.15
<i>nucA</i>	DNA-entry nuclease	Downregulated	2.05
<i>deaD</i>	ATP-dependent RNA helicase	Downregulated	3.16
<i>sigW</i>	ECF RNA polymerase sigma factor	Downregulated	2.55

<i>pucF</i>	allantoate amidohydrolase	Upregulated	23.06
<i>yerA</i>	putative adenine deaminase YerA	Downregulated	5.72
<i>pyrG</i>	CTP synthase	Downregulated	2.57
<i>pyrE</i>	Orotate phosphoribosyltransferase	Downregulated	61.62
<i>pyrF</i>	Orotidine 5'-phosphate decarboxylase	Downregulated	48.31
<i>pyrK</i>	Dihydroorotate dehydrogenase B [NAD(+)], electron transfer subunit	Downregulated	25.00
<i>pyrD</i>	Dihydroorotate dehydrogenase B [NAD(+)], catalytic subunit	Downregulated	32.02
<i>Ndk</i>	Nucleoside diphosphate kinase	Downregulated	4.27
<i>cmk</i>	cytidylate kinase	Upregulated	2.04
<i>pdp</i>	pyrimidine nucleoside phosphorylase	Downregulated	4.40
<i>recQ</i>	Probable ATP-dependent DNA helicase	Upregulated	2.01
<b><i>Transcriptional regulators</i></b>			
<i>hutP</i>	Hut operon positive regulatory protein	Downregulated	7.98
<i>yhbI</i>	Uncharacterized HTH-type transcriptional regulator	Upregulated	11.08
<i>rsiW</i>	Anti-sigma-W factor	Downregulated	2.83
<i>fruR</i>	Uncharacterized HTH-type transcriptional regulator	Downregulated	6.95
<i>treR</i>	Trehalose operon transcriptional repressor	Downregulated	4.54
<i>ykoM</i>	Uncharacterized HTH-type transcriptional regulator	Downregulated	8.31
<i>ansR</i>	HTH-type transcriptional regulator	Upregulated	2.94
<i>cueR</i>	HTH-type transcriptional regulator	Upregulated	2.72
<i>glcR</i>	HTH-type transcriptional repressor	Upregulated	15.71
<i>acoR</i>	Acetoin dehydrogenase operon transcriptional activator	Downregulated	16.87
<i>Fur</i>	Ferric uptake regulation protein	Downregulated	2.58
<i>yvdT</i>	Uncharacterized HTH-type transcriptional regulator	Downregulated	4.45
<i>Abh</i>	Putative transition state regulator	Downregulated	2.45
<i>yvbF</i>	HTH-type transcriptional repressor	Upregulated	7.33

<i>Btr</i>	HTH-type transcriptional activator	Downregulated	6.13
<i>rbsR</i>	Ribose operon repressor	Downregulated	55.89
<i>salA</i>	MRP family regulator	Downregulated	2.42
<i>ccpC</i>	transcriptional repressor of <i>citB</i> and <i>citZ</i>	Downregulated	4.46
<b><i>Protein metabolism</i></b>			
<i>sunS</i>	SPBc2 prophage-derived glycosyltransferase	Downregulated	6.71
<i>rapH</i>	Response regulator aspartate phosphatase H	Upregulated	5.25
<i>glmS</i>	Glutamine--fructose-6-phosphate aminotransferase	Downregulated	3.06
<i>yraA</i>	Putative cysteine protease	Downregulated	3.59
<i>htpX</i>	Protease HtpX homolog	Downregulated	3.12
<i>rapC</i>	Response regulator aspartate phosphatase	Downregulated	2.17
<i>pepF</i>	Oligoendopeptidase F homolog	Downregulated	2.17
<i>clpP</i>	ATP-dependent Clp protease proteolytic subunit	Downregulated	2.29
<i>sppA</i>	Putative signal peptide peptidase	Downregulated	2.97
<i>yxdK</i>	Sensor histidine kinase	Upregulated	2.31
<i>groEL</i>	chaperonin large subunit	Downregulated	4.61
<i>groES</i>	chaperonin small subunit	Downregulated	5.51
<b><i>Antibiotic synthesis</i></b>			
<i>ppsE</i>	Plipastatin synthase subunit E	Upregulated	4.50
<i>ppsD</i>	Plipastatin synthase subunit D	Upregulated	3.61
<i>srfAD</i>	Surfactin synthase thioesterase subunit	Downregulated	9.50
<i>pksL</i>	Polyketide synthase	Upregulated	2.06
<i>srfAC</i>	Surfactin synthase subunit 3	Downregulated	11.03
<i>srfAB</i>	Surfactin synthase subunit 2	Downregulated	12.45
<i>srfAA</i>	Surfactin synthase subunit 1	Downregulated	12.40
<i>sunA</i>	sublancin 168 lantibiotic antimicrobial precursor peptide	Downregulated	5.47

***Prophage genes***

<i>xtmA</i>	PBSX phage terminase small subunit	Downregulated	5.09
<i>xtmB</i>	PBSX phage terminase large subunit	Downregulated	3.76
<i>yomE</i>	putative glycosyl hydrolase; phage SPbeta	Upregulated	19.43
<i>pspA</i>	phage shock protein A homolog	Downregulated	3.72
<i>xkdF</i>	conserved hypothetical protein; putative PBSX prophage protein	Downregulated	3.97
<i>yxiF</i>	putative phage reverse transcriptase or polymerase	Downregulated	4.37
<i>yxiK</i>	putative phage head maturation protein	Downregulated	4.83

***Siderophore biosynthesis***

<i>dhbE</i>	2,3-dihydroxybenzoate-AMP ligase	Downregulated	35.69
<i>dhbA</i>	2,3-dihydro-2,3-dihydroxybenzoate dehydrogenase	Downregulated	35.21
<i>dhbB</i>	isochorismatase	Downregulated	26.61
<i>dhbF</i>	Siderophore 2,3-dihydroxybenzoate-glycine-threonine trimeric ester bacillibactin	Downregulated	28.23
<i>dhbC</i>	isochorismate synthase	Downregulated	30.53
<i>sufB</i>	FeS cluster formation protein	Downregulated	2.72
<i>sufD</i>	FeS assembly protein	Downregulated	3.11
<i>besA</i>	trilactone hydrolase	Downregulated	7.68

***Antibiotic resistance***

<i>yqfA</i>	conserved hypothetical protein	Downregulated	2.10
<i>yqfB</i>	resistance protein	Downregulated	2.30
<i>yqeZ</i>	putative membrane bound hydrolase	Downregulated	2.11
<i>bcrC</i>	undecaprenyl pyrophosphate phosphatase	Downregulated	2.22
<i>ydbT</i>	conserved hypothetical protein	Downregulated	3.23
<i>ohrA</i>	Organic peroxide resistance	Downregulated	4.02
<i>fosB</i>	fosfomicin resistance protein	Downregulated	4.84
<i>yxel</i>	penicillin acylase	Downregulated	17.02

**Unknown function**

<i>ytoA</i>	similar to ferripyochelin binding protein	Upregulated	5.32
<i>yhcC</i>	Hypothetical protein	Upregulated	4.97
<i>yhjN</i>	putative integral inner membrane protein	Upregulated	4.62
<i>yjoB</i>	ATPase possibly involved in protein degradation, similar to FtsH	Downregulated	3.55
<i>yomU</i>	hypothetical protein; phage SPbeta	Upregulated	4.53
<i>yonB</i>	conserved hypothetical protein; phage SPbeta	Upregulated	3.81
<i>bsrI</i>	Unknown	Upregulated	3.55
<i>kswB</i>	Unknown	Upregulated	2.87
<i>yocA</i>	putative transposon-related lytic enzyme	Upregulated	2.55
<i>ytxB</i>	putative integral inner membrane protein	Upregulated	2.49
<i>yvfG</i>	cytidylate kinase	Upregulated	2.03
<i>ypbE</i>	conserved hypothetical protein	Upregulated	2.00
<i>yvlD</i>	putative integral inner membrane protein	Downregulated	2.11
<i>yceG</i>	conserved hypothetical protein	Downregulated	2.25
<i>ysdB</i>	conserved hypothetical protein	Downregulated	3.68
<i>ywsB</i>	conserved hypothetical protein	Downregulated	7.80
<i>yxaL</i>	membrane associated protein kinase with beta-propeller domain	Downregulated	2.64
<i>yceE</i>	putative stress adaptation protein	Downregulated	2.77
<i>yvlB</i>	conserved hypothetical protein	Downregulated	2.88
<i>nfrAA</i>	FMN-containing NADPH-linked nitro/flavin reductase	Downregulated	2.90
<i>yobJ</i>	hypothetical protein	Downregulated	2.93
<i>xkdO</i>	conserved hypothetical protein; PBSX phage protein	Downregulated	2.96
<i>yteJ</i>	putative integral inner membrane protein	Downregulated	2.96
<i>xkdV</i>	conserved hypothetical protein; putative PBSX prophage protein	Downregulated	2.99
<i>yxiH</i>	hypothetical protein	Downregulated	3.08

---

<i>xkdK</i>	conserved hypothetical protein in phage element PBSX	Downregulated	3.17
<i>yceD</i>	putative stress adaptation protein	Downregulated	3.17
<i>nfsB</i>	NAD(P)H-flavin oxidoreductase (nitroreductase)	Downregulated	3.29
<i>ydbS</i>	conserved hypothetical protein	Downregulated	3.32
<i>yoaF</i>	hypothetical protein	Downregulated	3.34
<i>yxxG</i>	hypothetical protein	Downregulated	3.43
<i>yceC</i>	putative stress adaptation protein	Downregulated	3.50
<i>yxzC</i>	putative nucleic acid binding protein	Downregulated	3.52
<i>yxzG</i>	putative nucleic acid binding protein	Downregulated	3.67
<i>yvlA</i>	conserved hypothetical protein	Downregulated	3.73
<i>yxiG</i>	conserved hypothetical protein	Downregulated	3.86
<i>ybfF</i>	conserved hypothetical protein	Downregulated	3.94
<i>yxjI</i>	conserved hypothetical protein	Downregulated	4.34
<i>yxiI</i>	conserved hypothetical protein	Downregulated	4.55
<i>xpaC</i>	putative phosphatase	Downregulated	4.58
<i>yaaN</i>	conserved hypothetical protein	Downregulated	6.14
<i>yxiJ</i>	conserved hypothetical protein	Downregulated	6.47
<i>ywrE</i>	conserved hypothetical protein	Downregulated	6.90
<i>ylbP</i>	putative acetyltransferase	Downregulated	7.36
<i>yeaA</i>	conserved hypothetical protein	Downregulated	7.47
<i>ydjP</i>	putative peroxydase	Downregulated	8.95
<i>yxiM</i>	putative esterase (lipoprotein)	Downregulated	10.45
<i>ykuO</i>	conserved hypothetical protein	Downregulated	16.80
<i>ybdZ</i>	conserved hypothetical protein	Downregulated	23.48
<i>cidA</i>	holin regulator of murein hydrolases	Downregulated	27.37
<i>ytwI</i>	putative integral membrane protein	Downregulated	45.84

---



---

<i>ywbG</i>	holin-like auxiliary protein	Downregulated	61.79
<i>ytzA</i>	putative integral inner membrane protein	Downregulated	169.15

---

\*Highlighted regions represent pathways for which more than one gene were identified to be differentially expressed in the *pyk* mutant, wherein each colour represents a different pathway

The objective of the RNA-Seq analysis was to identify the differential expression of any gene(s) that could potentially contribute to the acentral Z ring positioning defect of  $\Delta pyk$  cells. In addition to identifying the overall biological processes that are differentially expressed in these cells, specific pathways were also identified for which more than one gene was differentially expressed. All these pathways in the *pyk* mutant are highlighted in different colours in Table 5.2. Since the differential expression of a pathway, rather than a single gene belonging to a pathway, would demonstrate a higher probability of playing a role in the Z ring positioning defect of  $\Delta pyk$  cells, these differentially expressed pathways remained the focus of further biological analysis of the RNA-Seq data.

As demonstrated in Figure 5.3, most of the genes differentially expressed in the *pyk* mutant mapped to transport systems. Within the transport systems, many genes belonging to the glycine betaine transport system were upregulated along with two genes of the arginine/ornithine transport system being upregulated as well. On the contrary, multiple genes belonging to the manganese, ribose, lichenan, pyruvate and iron transporters were downregulated. The downregulation of these transporters might represent a limitation of these substrates in the growth medium of  $\Delta pyk$  cells, whereas the upregulation of glycine betaine and arginine transporters is potentially due to the abundance of these molecules in the growth medium. However, on the contrary, the upregulation of glycine betaine and arginine transporters could also be due to the limitation of these nutrients in the growth medium of  $\Delta pyk$  cells.

Carbohydrate metabolism formed a significant proportion (20%) of the genes differentially expressed in  $\Delta pyk$  cells. This is expected, as *pyk* is an important enzyme of the central carbon metabolic pathway of glycolysis, and its deletion will require the cells to do a lot of metabolic adaptations for fulfilling their metabolic and energy needs. Within the many carbohydrate

metabolism changes observed in  $\Delta pyk$ , two pathways from which multiple genes were differentially expressed were the inositol and xylose degradation pathways. Both of these pathways were downregulated in  $\Delta pyk$ , suggesting a limited amount of these carbohydrates may be available to the cells for degradation. In accordance with the upregulation of arginine transporters and downregulation of ribose and lichenan transporter genes, as previously discussed, the genes involved in the metabolism of arginine were observed to be upregulated whereas those for ribose and lichenan utilization were downregulated in  $\Delta pyk$ .

Around 16% of the genes differentially expressed in  $\Delta pyk$  were of unknown function and 11% of the DE genes were related to oxidation-reduction pathways. However, there was no specific oxidation-reduction pathway that was differentially expressed. 6% of the DE genes in  $\Delta pyk$  were transcriptional regulators, some of which were upregulated, and others downregulated. Most of these regulators were identified to control the utilization of various carbohydrates such as fructose and ribose, and hence their differential expression is most probably the metabolic response of cells to the metabolic perturbation after the deletion of *pyk*. About 5% of the DE genes in  $\Delta pyk$  were associated with the cell wall turnover process. Out of a total number of 16 genes that were under the category of cell wall turnover, 10 were downregulated and 6 were upregulated. 5% of the DE genes in  $\Delta pyk$  were mapped to the nucleic acid metabolism, which showed the downregulation of multiple genes belonging to the pyrimidine synthesis pathway. This category also included the most upregulated gene in the *pyk* vs wt comparison, *pucF*, which is involved in the utilization of purines.

Around 4% of the genes differentially expressed in  $\Delta pyk$  were involved in the processes of protein metabolism, but the DE genes were from a range of different pathways with no specific protein processing pathway being differentially expressed. Further, about 3% of the genes in  $\Delta pyk$

were mapped to the antibiotic synthesis process, 2% to the prophage genes, 2% to the antibiotic resistance genes and the remaining 2% to the siderophore biosynthesis machinery. Although siderophore synthesis only comprised a 2% proportion of the total DE genes in  $\Delta pyk$ , the entire operon of *dhb* genes involved in siderophore (bacillibactin) synthesis was observed to be downregulated.

#### **5.2.4 Major pathways whose genes are altered in $\Delta pyk$ cells**

Comparing the transcriptomes of  $\Delta pyk$  cells with wild type cells revealed the differential expression of numerous genes as described above. However, for some of the functional categories, multiple genes belonging to the same pathway were differentially expressed. Any of these pathways could potentially contribute to the acentral Z ring positioning defect of  $\Delta pyk$  cells. This list of pathways with their genes observed to be differentially expressed in  $\Delta pyk$  is shown in Table 5.3.

**Table 5.3. Differential expression of selected pathways in the *pyk* mutant**

Pathway	Differentially expressed genes
Glycine-betaine transporter	<i>opuAB, opuAC, opuCD, opuCA, opuAA, opuCB, opuCC</i>
Arginine/ornithine metabolism	<i>rocA, rocB, rocC, rocD, rocE</i>
Manganese transporter	<i>mntC, mntH, mntB, mntD, mntA</i>
Ribose metabolism	<i>rbsA, rbsB, rbsC, rbsD, rbsK, rbsR</i>
Lichenan metabolism	<i>licC, licB, licA, licH</i>
Iron transporter	<i>fhuB, fhuC, fhuD, fhuG</i>
Pyruvate transporter	<i>lrgA, lrgB</i>
Inositol degradation	<i>iolJ, iolE, iolC, iolD, iolB, iolI, iolG, iolH, iolF</i>
Xylose degradation	<i>xylA, xylB</i>
Cell wall turnover	<i>murQ, pdaC, lytE, wprA, gcaD, yocH, cwI, ydjM, yabE, bcrC, pbpH, ybfG, iseA</i>
Pyrimidine synthesis	<i>pyrG, pyrE, pyrF, pyrK, pyrD</i>
Siderophore synthesis	<i>dhbE, dhbA, dhbB, dhbF, dhbC</i>

Since the addition of pyruvate to  $\Delta pyk$  cells rescued their Z ring positioning to midcell (comparable to wild type Z ring positioning), it was investigated whether pyruvate addition also restores the transcriptional profile of  $\Delta pyk$  to wild type cells. It was hypothesized, if pyruvate restores the expression pattern of any gene(s) differentially expressed in  $\Delta pyk$  to wild type levels, it would support the idea that the differential expression of that gene(s) may contribute to the acentral Z ring positioning of  $\Delta pyk$  cells. On the other hand, genes that remain differentially expressed in the *pyk* mutant even in the presence of pyruvate (i.e. under conditions that rescue midcell Z ring formation) are unlikely to be involved in the acentral Z ring phenotype of  $\Delta pyk$  cells. For this analysis, initially a Venn diagram was prepared to rule out any pathway(s) that remained differentially expressed in  $\Delta pyk$  even after the addition of pyruvate, as these pathways are unlikely to contribute to the Z ring positioning defect of  $\Delta pyk$  cells (Figure 5.4). For a full list

of DE genes in pykP vs wt comparison, along with the type of response and their fold change, refer to Table 1 in Appendix II.

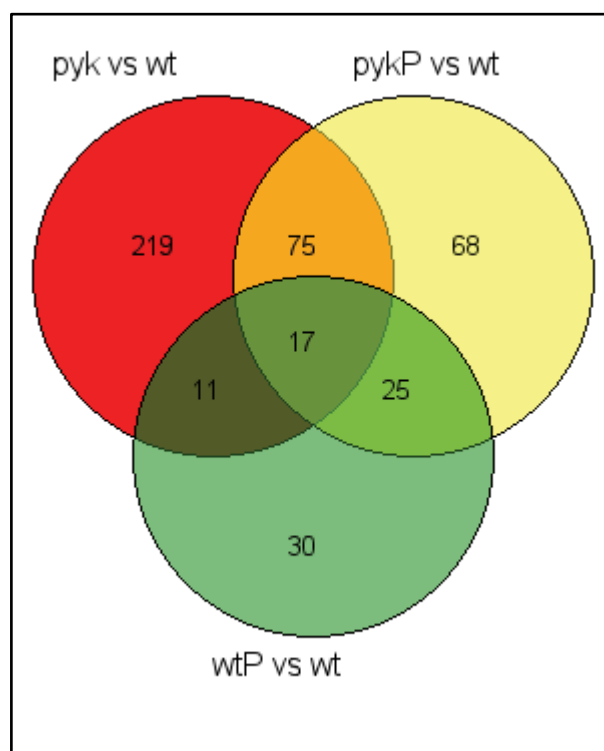


**Figure 5.4. A Venn diagram representing the number of differentially expressed genes overlapping under different experimental conditions.** (pyk-pyruvate kinase mutant, pykP- pyruvate kinase mutant supplemented with pyruvate, wt-wild type, wtP- wild type supplemented with pyruvate)

In the Venn diagram, wtP vs wt was included as a control to remove any non-specific differential expression that could result after pyruvate addition. 42 genes (25+17) were observed to overlap in wtP vs wt and pykP vs wt comparisons, which included the genes mainly belonging to oligopeptide transporters, TCA cycle enzymes and lactate utilization. Hence, these changes

observed in *pykP* vs *wt* comparison were considered to be non-specific changes as a result of pyruvate addition and not contributors to the  $\Delta$ *pyk* Z ring positioning phenotype.

92 (17+75) genes were observed to overlap in *pyk* vs *wt* and *pykP* vs *wt* comparisons. Functional annotation of these genes revealed that they were mainly associated with carbohydrate metabolism. Furthermore, it was analysed whether the pathways shortlisted to potentially play a role in the Z ring positioning defect of  $\Delta$ *pyk* (Table 5.3), were present in this overlap of *pyk* vs *wt* and *pykP* vs *wt*. Genes belonging to glycine-betaine transport, ribose transport, iron transport, cell wall turnover, inositol degradation and xylose degradation were found to be present in this overlap, indicating that these pathways still remained differentially expressed after the addition of pyruvate to  $\Delta$ *pyk* cells. The Glycine-betaine transport system was found to remain upregulated in the *pykP* vs *wt* by a mean  $\log_2$  fold change of 1.82, whereas the ribose metabolism was downregulated by a mean  $\log_2$  fold change of 4.18. The inositol degradation and xylose degradation pathways were downregulated by a mean  $\log_2$  fold change of 3.54 and 6.03 respectively. All four of these pathways displayed the same trend of differential expression in *pykP* vs *wt* comparison as they showed in the *pyk* vs *wt* comparison (see Table 5.3). Furthermore, some of the genes from the cell wall turnover showed the same trend of differential expression as was shown in  $\Delta$ *pyk* cells. This included the downregulation of *murQ*, *wprA*, *pbpH* and *pbpE*, and the upregulation of *yocH*, *cwlO* and *yabE*. Hence, it was concluded that the differential expression of glycine-betaine transport, ribose transport, cell wall turnover, inositol degradation and xylose degradation pathways in  $\Delta$ *pyk* cells is likely not contributing to the acentral Z ring positioning phenotype of  $\Delta$ *pyk* cells. In contrast to the  $\Delta$ *pyk* vs *wt* comparison, one of the iron transport gene '*fhuG*' was upregulated in *pykP* vs *wt* comparison, suggesting that the differential expression of iron transport could potentially contribute to the Z ring positioning defect of  $\Delta$ *pyk*.

Overall, the analysis performed so far, narrowed down the list of differentially expressed pathways that could be involved in the CCM-division link in  $\Delta pyk$  cells to arginine/ornithine metabolism, manganese metabolism, lichenan metabolism, iron transport, pyruvate transport, pyrimidine synthesis and siderophore synthesis. Next, the 68 genes which were only differentially expressed in the *pyk* vs wt comparison were functionally annotated to pinpoint any hints for the acentral Z ring positioning of  $\Delta pyk$  cells. Particular attention was paid to the shortlisted pathways described above, with an aim of identifying any genes that are somehow related to the functioning of these pathways. This was done to further narrow down this list of pathways by specifically identifying one or more pathways that are more significantly affected than the others within this shortlisted list of pathways. None of the genes related to arginine/ornithine metabolism, manganese metabolism and lichenan metabolism came up in this analysis. However, the iron transport genes *feuB* and *feuC* were upregulated by a mean  $\log_2$  fold change of 2.02. Hence, in contrast to *pyk* vs wt comparison, the iron transporters were upregulated in *pykP* vs wt. As the synthesis of siderophores is related to the iron uptake mechanisms of a bacterial cell, it was inferred that the siderophore synthesis pathway and iron transporters together could potentially contribute to the acentral Z ring positioning defect of  $\Delta pyk$  cells. Since the synthesis of pyrimidines is required for the DNA replication process, it was investigated whether any gene belonging to the DNA replication process is also differentially expressed in the *pyk* mutant. Two genes involved in DNA replication, *dnaC* and *dnaE*, were observed to be upregulated in *pykP* vs wt by a  $\log_2$  mean fold change of 1.31; suggesting that the downregulation of pyrimidine synthesis in  $\Delta pyk$  could also be involved in the CCM-division link in these cells.

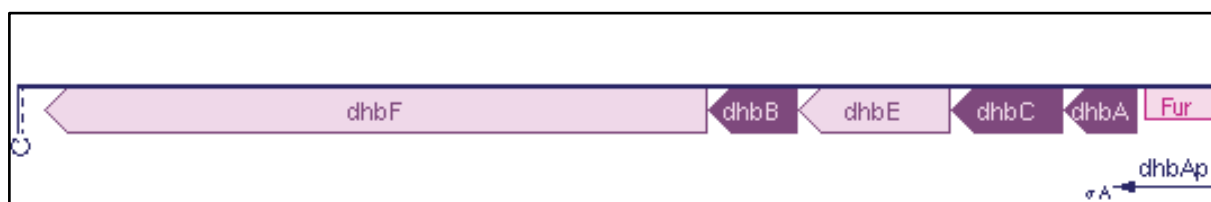
In summary, from a list of 12 pathways (Table 5.3) identified to potentially contribute to the acentral Z ring positioning defect of  $\Delta pyk$ , functional annotation of the genes differentially



expressed in the *pykP* vs *wt* comparison highlighted the most likely candidate pathways as iron metabolism and pyrimidine synthesis.

For the iron uptake mechanisms in  $\Delta$ *pyk* cells, the genes *dhbA*, *dhbB*, *dhbC*, *dhbE* and *dhbF*, belonging to the *dhb* operon (Figure 5.5A) involved in the synthesis of siderophore bacillibactin (2,3-dihydroxybenzoate) were downregulated; whereas for pyrimidine synthesis, the genes *pyrD*, *pyrE*, *pyrF*, *pyrG* and *pyrK* were downregulated. All these genes, except *pyrG*, are part of the same operon, which is shown in Figure 5.5B.

(A)



(B)

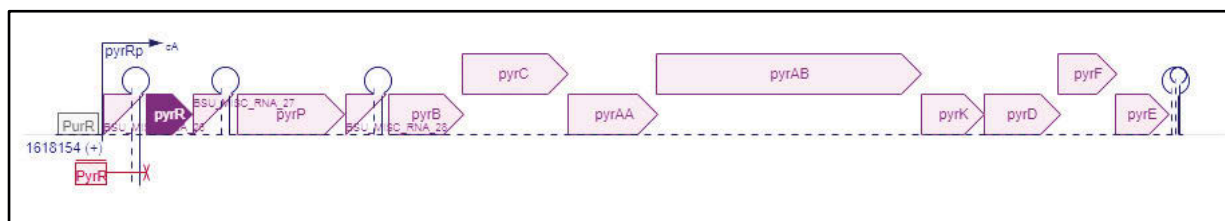


**Figure 5.5. The siderophore and pyrimidine synthesis gene clusters differentially expressed in the *pyk* mutant.** (A) the *dhb* gene cluster, required for the synthesis of the siderophore bacillibactin in *B. subtilis*. (*dhbF*-unknown product, *dhbB*-isochorismatase, *dhbE*-2,3-dihydroxybenzoate-AMP ligase, *dhbC*-isochorismate synthase, *dhbA*-2,3-dihydro-2,3-dihydroxybenzoate dehydrogenase). (B) The *pyr* gene cluster required for the synthesis of pyrimidines in *B. subtilis* (*pyrR*- transcriptional attenuator and uracil phosphoribosyltransferase activity, *pyrP*-uracil permease, *pyrB*-aspartate carbamoyltransferase, *pyrC*-dihydroorotase, *pyrAA*- pyrimidine-specific carbamoyl-phosphate synthetase, *pyrAB*- pyrimidine-specific

carbamoyl-phosphate synthetase, pyrK-dihydroorotate dehydrogenase electron transfer subunit, pyrD-dihydroorotate dehydrogenase catalytic subunit, pyrF- orotidine 5'-phosphate decarboxylase, pyrE-orotate phosphoribosyltransferase).

Amongst the pathways of iron uptake and pyrimidine synthesis, either one of them or both of them could be contributing to the acentral Z ring positioning defect of  $\Delta pyk$  cells. With respect to iron metabolism, very few studies have been published that would suggest a connection to the bacterial cell division process. One such study shows that iron starvation can inhibit the cell division process in *E. coli*, and also reports the molecular mechanism by which this occurs (Santos et al. 2018). The study reports that iron starvation downregulates the expression of late cell division proteins such as FtsN, FtsK, FtsQ, FtsW, which then inhibits the formation of a complete division septum (Santos et al. 2018). Since, none of these genes from the cell division process were differentially expressed in  $\Delta pyk$ , it seems unlikely that iron metabolism is contributing to the acentral Z ring positioning phenotype of these cells, at least via the mechanism described for *E. coli*.

As discussed in section 4.3.4,  $\Delta pyk$  cells were observed to display a DNA replication initiation defect, the mechanism for which remains unknown. This underinitiation of DNA replication phenotype of  $\Delta pyk$  could be explained by the downregulation of the pyrimidine synthesis operon such that a limited level of available pyrimidines, due to the downregulation of the pyrimidine synthesis operon, could be causing the cells to reduce their initiation frequency of the DNA replication process. Moreover, not only did the addition of pyruvate restore the frequency of DNA replication initiation of  $\Delta pyk$  cells to wild type cell levels, but the downregulation of the pyrimidine synthesis operon was not observed in  $\Delta pyk$  cells after pyruvate addition; again

upholding the idea that this downregulation of the pyrimidine synthesis operon could be the reason for the DNA replication defect of  $\Delta pyk$  cells. Hence, considering this hypothesis, the downregulation of the *pyr* genes belonging to the pyrimidine synthesis operon was confirmed in  $\Delta pyk$  cells using qPCR, with an aim of identifying the mechanism underlying the DNA replication initiation defect of  $\Delta pyk$  cells.

### 5.2.5 qPCR validation of the downregulation of *pyr* genes

Validation is an important part of any gene expression study for the confirmation of results obtained from one technique using another. For RNA-seq data validation, a set of genes chosen from the differentially expressed profile of  $\Delta pyk$  cells was validated using qPCR, as described below.

#### 5.2.5.1 Selection of target genes

Genes encoding ribosomal proteins, *rpsE* and *rpsJ*, have been used in the past as reference controls for *B. subtilis* gene expression studies and have shown to exhibit a constant expression pattern (Jordan et al. 2006; Wecke et al. 2011). Hence, the gene *rpsE* was used as a constitutive reference control in our qPCR experiments.

Considering the hypothesis that downregulation of the pyrimidine synthesis operon could lead to the decreased frequency of DNA replication initiation in  $\Delta pyk$  cells, the downregulation of several genes belonging to the pyrimidine synthesis operon – *pyrE*, *pyrF*, *pyrD* and *pyrK* were chosen to be confirmed using qPCR. The downregulation of *pyrG* was not confirmed because of

the lower fold change obtained for *pyrG* (1.36) in RNA-seq results. In addition to the confirmation of results for  $\Delta pyrK$  vs wt, the upregulation of *ald* in *pykA* vs  $\Delta pyrK$  was also confirmed using qPCR.

### 5.2.5.2 PCR efficiency evaluation and confirmation of RNA-seq results

Primers for qPCR were designed using the online tool ‘Primer 3’ following the protocol described by Brzoska and Hassan, 2014 (Brzoska and Hassan 2014)(primer sequences can be found in Table 2.5). Prior to their use in qPCR, the PCR efficiency of each primer set was evaluated, as PCR inefficiencies can cause suboptimal primer-template binding resulting in experimental errors. PCR efficiency of the primer sets for *rpsE*, *pyrE*, *pyrF*, *pyrD*, *pyrK* and *ald* was calculated to be 99.06, 90.54, 90.98, 90.10, 94.44 and 93.06%; all of which are within the acceptable range (80-100%) for qPCR (Brzoska and Hassan 2014).

The relative abundances of the mRNAs of *pyrE*, *pyrF*, *pyrD* and *pyrK* in  $\Delta pyrK$  as compared to the wild type cells were calculated as described in section 2.12.4, with test sample being  $\Delta pyrK$  and control sample being wild type cells extracted RNA. Relative abundance was calculated by normalizing the  $C_T$  value of the test gene (*pyrX*) to the  $C_T$  value of endogenous control (*rpsE*).  $C_T$  (cycle threshold) value is defined as the number of cycles required for the fluorescence signal to cross the threshold, i.e. the background fluorescence.  $C_T$  values are inversely proportional to the amount of target nucleic acid present in the sample, i.e. lower the  $C_T$ , greater the amount of target nucleic acid and vice versa. qPCRs were set up for all three biological replicates and the results obtained are summarized in Table 5.4. Similar to the pattern seen in RNA-seq, all the genes involved in pyrimidine synthesis were downregulated in  $\Delta pyrK$  compared to wild type cells, as

shown by the  $\log_2$  fold change values obtained using qPCR that were very similar to those observed in the RNA-seq results.

**Table 5.4. Relative abundance of pyrimidine synthesis gene transcripts in  $\Delta pyk$  as compared to wild type *B. subtilis* cells**

Gene symbol	Log <sub>2</sub> fold change from qPCR				Log <sub>2</sub> fold change from RNA-seq
	Biological replicate 1	Biological replicate 2	Biological replicate 3	Average of all biological replicates	
<i>pyrE</i>	-5.12	-7.82	-4.14	-5.69	-5.94
<i>pyrF</i>	-4.64	-7.30	-4.29	-5.41	-5.59
<i>pyrD</i>	-4.43	-7.00	-4.50	-5.31	-5.00
<i>pyrK</i>	-3.86	-6.54	-4.79	-5.06	-4.64

Furthermore, the upregulation of *ald* gene in *pykA* as compared to  $\Delta pyk$  cells was also confirmed using qPCR, wherein the  $\log_2$  fold change for the relative abundance of *ald* in *pykA* compared to  $\Delta pyk$  was calculated to be 4.28 with values for each biological replicate being 4.20, 4.10 and 4.53. Hence, these results confirmed the upregulation of *ald* in *pykA* as compared to  $\Delta pyk$ , as was presented by the  $\log_2$  fold change of 3.66 in RNA-seq results.

### 5.2.6 Testing the role of pyrimidine synthesis in the Z ring positioning by constructing pyrimidine synthesis mutants

From the RNA-Seq data, it was observed that the downregulation of the pyrimidine synthesis operon could underlie the Z ring positioning defect in  $\Delta pyk$  cells. Hence, a mutant of *pyrE*, the

most downregulated gene amongst all pyrimidine synthesis genes observed in  $\Delta pyk$ , was constructed, to test if this mutant displays any Z ring positioning defect. If this mutant displays a Z ring positioning defect, it will show that the downregulation of the *pyr* operon could be the actual reason for the Z ring positioning defect of  $\Delta pyk$ , possibly via an effect on the DNA replication process. A mutant of *pyrE* (SU884) was constructed by transforming the *pyrE* mutant strain obtained from the addgene *B. subtilis* strain collection (Koo et al. 2017) into wild type strain SU492 (SU5 *amyE::ftsZ-yfp*). The enzyme PyrE encodes for orotate phosphoribosyltransferase involved in UMP (Uridine monophosphate) synthesis that forms an intermediate in the pyrimidine metabolism pathway. Hence, a deletion of *pyrE* will result in a perturbation of pyrimidine synthesis. Z ring positioning was examined in the *pyrE* mutant and the results obtained are shown in Figure 5.6.

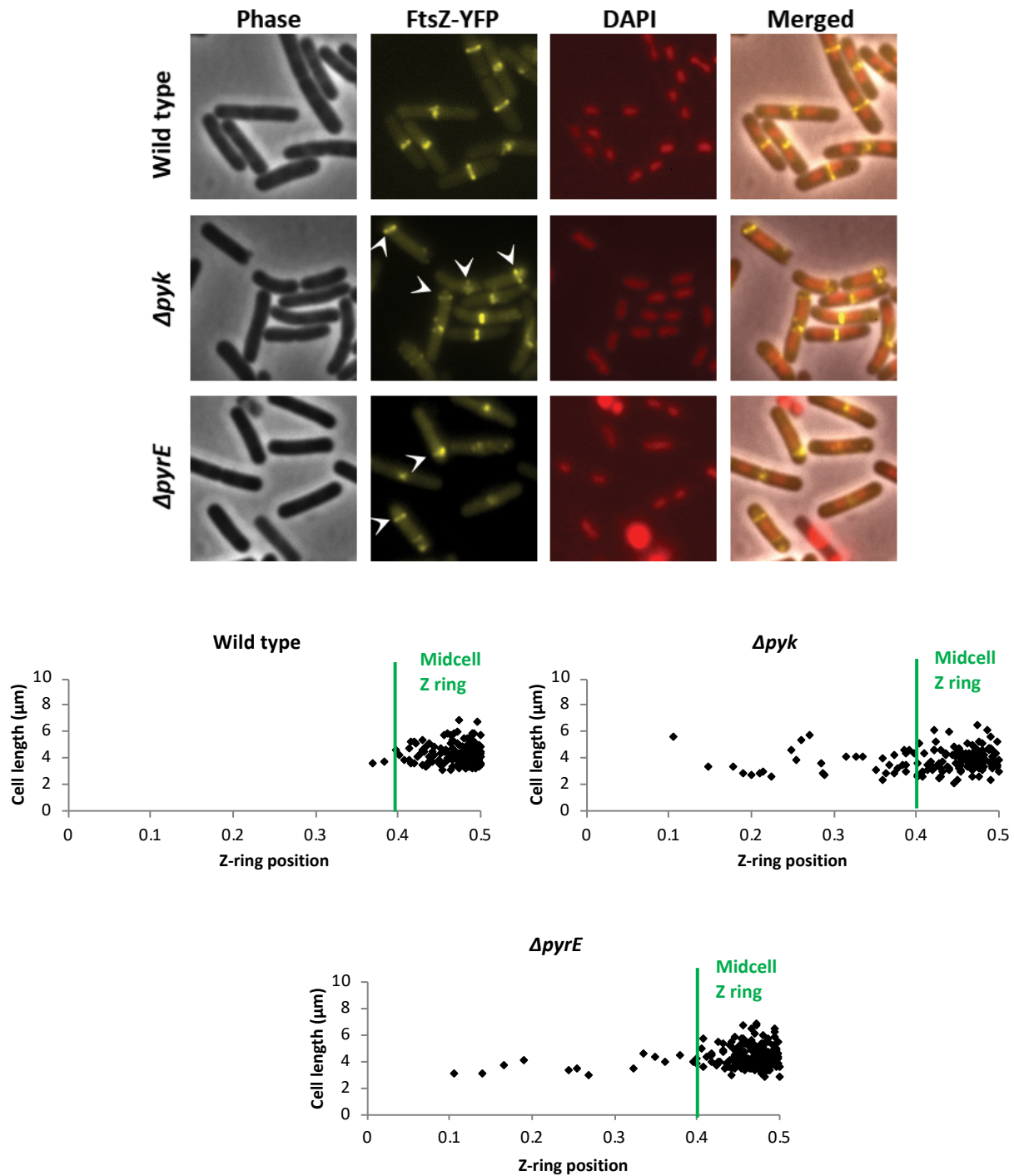


**Figure 5.6.** The effect of *pyrE* deletion on the Z ring positioning. Cells were grown to mid-exponential phase in the presence of 0.01% xylose in L-broth at 37°C and visualized by phase-contrast and fluorescence microscopy (n=3). Scale bar, 2 $\mu\text{m}$ . White arrows in the FtsZ-YFP panel point towards acentral Z rings.

Lower panel shows the scatter plots wherein cell length has been plotted as a function of the Z ring positioning under different experimental conditions. Here, the Z ring position of 0 and 0.5 on the x-axis signify the cell pole and cell centre, respectively.  $n > 150$ . [Wild type = SU492 (*amyE::Pxyl-ftsZ-yfp*),  $\Delta pyk$  = SU679 ( $\Delta pyk amyE::Pxyl-ftsZ-yfp$ ),  $\Delta pyrE$  = SU884 ( $\Delta pyrE amyE::Pxyl-ftsZ-yfp$ )]

As shown in Figure 5.6, about 8% of the Z rings did form at acentral sites in the *pyrE* mutant, pointing that the downregulation of the *pyr* operon does contribute to the Z ring positioning defect of  $\Delta pyk$  cells. However, the frequency of acentral Z rings in the *pyrE* mutant (~8%) was observed to be much lower compared to the *pyk* mutant (~21%). Further, statistical analysis performed using the KS (Kolmogorov–Smirnov) test revealed that the Z ring measurements in  $\Delta pyrE$  cells are not significantly different from wild type cells, as determined from the P-value of 0.309. However, the P-value for the comparison of  $\Delta pyrE$  and  $\Delta pyk$  cells was obtained to be 0.254, suggesting that the Z ring measurements of  $\Delta pyrE$  cells are not statistically different from  $\Delta pyk$  cells. Hence, it was concluded that *pyrE* deletion did result in an acentral Z ring positioning phenotype, although not quite as severe as that of the *pyk* deletion. This result indicated that the downregulation of the *pyr* operon in  $\Delta pyk$  does play an important role in their acentral Z ring positioning defect, however it does not appear to be the sole contributor to this phenotype.

The transcription of the *pyr* operon is controlled by the availability of pyrimidines via an autogenous transcriptional attenuation mechanism. High intracellular levels of pyrimidines cause the formation of the terminator loop, which leads to the termination of the operon by the PyrR protein binding to the *pyr* mRNA (Turner et al. 1994). Considering this mechanism of regulation of the *pyr* operon, it could be that the  $\Delta pyk$  cells could be experiencing an abundance of pyrimidines leading to the downregulation of this operon, and this pyrimidine abundance could be



the reason for their Z ring positioning defect. To test this scenario, a mutant of *pyrR* (SU885) was constructed by transforming the *pyrR* mutant obtained from the addgene *B. subtilis* strain collection (Koo et al. 2017) into wild type strain SU492 (SU5 *amyE::ftsZ-yfp*). As the function of PyrR is to terminate the *pyr* operon (Turner et al. 1994), its deletion will result in the constitutive expression of the *pyr* operon, causing an increase in pyrimidine synthesis. If the increased levels of pyrimidines are causing the Z rings to form at acentral sites in the *pyk* mutant, a deletion of *pyrR* is expected to result in a Z ring positioning defect. Hence, Z ring position was examined in the *pyrR* mutant and the results obtained are presented in Figure 5.7.

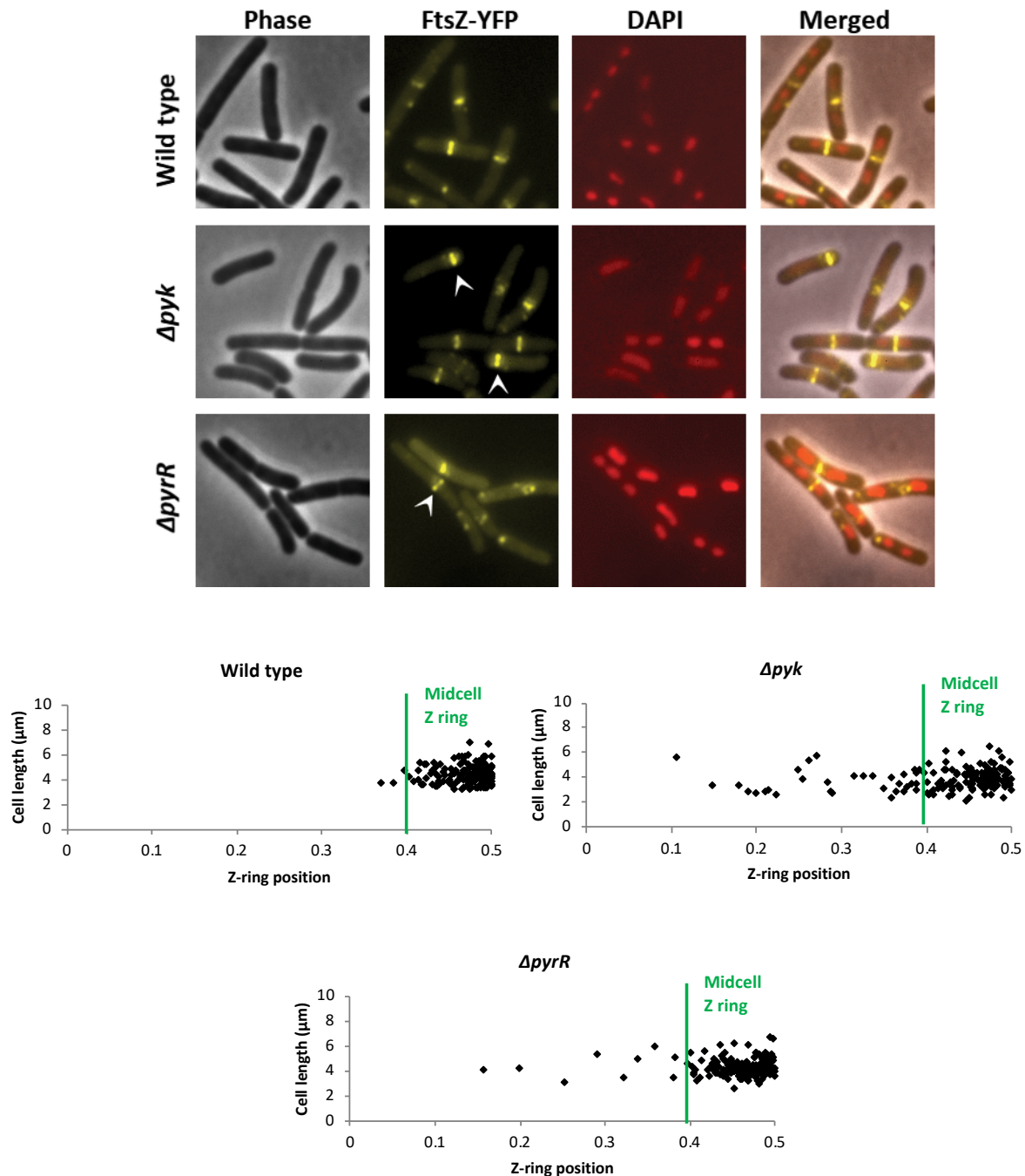


**Figure 5.7.** The effect of *pyrR* deletion on the Z ring positioning. Cells were grown to mid-exponential phase in the presence of 0.01% xylose in L-broth at 37°C and visualized by phase-contrast and fluorescence microscopy (n=2). Scale bar, 2 $\mu\text{m}$ . White arrows in the FtsZ-YFP panel point towards acentral Z rings. Lower panel shows the scatter plots wherein cell length has been plotted as a function of the Z ring

positioning under different experimental conditions. Here, the Z ring position of 0 and 0.5 on the x-axis signify the cell pole and cell centre, respectively.  $n > 150$ . [Wild type = SU492 (*amyE::Pxyl-ftsZ-yfp*),  $\Delta pyk$  = SU679 (*\Delta pyk amyE::Pxyl-ftsZ-yfp*),  $\Delta pyrR$  = SU887 (*\Delta pyrR amyE::Pxyl-ftsZ-yfp*)]

About 6% of the Z rings in  $\Delta pyrR$  cells formed at acentral positions (Figure 5.7). Further, statistical analysis performed using the KS (Kolmogorov–Smirnov) test revealed that the Z ring measurements in  $\Delta pyrR$  cells are significantly different from wild type cells, as determined from the P-value of 0.005. Hence, this confirmed that *pyrR* deletion does cause a statistically significant defect in the Z ring positioning. However, the P-value for  $\Delta pyrR$  and  $\Delta pyk$  cells comparison was also obtained to be 0.005, suggesting that the Z ring measurements of  $\Delta pyrR$  cells are somewhere in between the measurements for wild type and  $\Delta pyk$  cells. Together, the positioning of Z rings at acentral sites in the *pyrR* mutant suggest that the overexpression of the *pyr* operon as a result of *pyrR* deletion, potentially leading to an increased level of pyrimidines, does cause a shift in the Z ring positioning; even though the frequency of acentral Z rings was much lower in  $\Delta pyrR$  (6%) as compared to the  $\Delta pyk$  (21%).

Overall, since the deletion of *pyrE* and *pyrR* individually did cause a shift in the Z ring positioning to acentral sites, this indicates that an imbalance in nucleotide levels in  $\Delta pyk$  cells does contribute to their Z ring positioning defect. However, because the magnitude of this effect is not as high as that of  $\Delta pyk$  cells, it can be concluded that an imbalance in pyrimidine levels by themselves cannot account for the Z ring positioning defect observed in  $\Delta pyk$  cells. Hence, it can be inferred from this data that the downregulation of pyrimidine synthesis operon observed in  $\Delta pyk$  is not the only reason for their Z ring positioning defect, however it can be one of the contributing

factors, amongst others, such as the DNA replication defect described in section 4.3.4, leading to the acentral Z ring positioning in these cells.

### 5.3 Discussion

The main objective of this chapter was to identify any set of DE genes that could underlie the possible mechanism for the Z ring positioning defect in  $\Delta pyk$  cells. In our analysis, no characterised genes involved in the cell division process or the well-characterised Z ring regulatory mechanisms (min and noc), were differentially expressed in  $\Delta pyk$ ; indicating the mechanism by which Z rings form at acentral sites in this mutant is unlikely a direct effect of CCM on cell division genes/proteins. This was not necessarily surprising, as the known mechanisms by which metabolism controls the cell division process is via moonlighting proteins that have no previously identified division function. Hence, the differential expression of other genes that could have a possible role in the Z ring positioning of  $\Delta pyk$  was investigated.

Biological mapping of DE genes in  $\Delta pyk$  highlighted the differential expression of 12 major pathways, which could contribute to their acentral Z ring phenotype. These included genes belonging to glycine-betaine transport, arginine-ornithine metabolism, manganese transport, ribose metabolism, lichenan metabolism, iron transport, pyruvate transport, inositol degradation, xylose degradation, cell wall turnover, pyrimidine synthesis and siderophore synthesis. Next, the specific role of any of these pathways in the CCM-division link in  $\Delta pyk$  was investigated by looking at the differentially expressed profile of  $\Delta pyk$  cells after pyruvate addition compared to wild type cells. This was done because the expression profile of any gene(s) with a specific role in the Z ring positioning of  $\Delta pyk$  cells is expected to be restored to the wild type levels after pyruvate

addition, as pyruvate addition rescued the Z ring positioning defect of  $\Delta pyk$  cells. From this analysis, the list of pathways that could be the best candidates in the CCM-division link was narrowed down to iron metabolism and pyrimidine synthesis.

Iron starvation is known to inhibit the cell division process in *E. coli* by downregulating the expression of late cell division proteins (Santos et al. 2018); however in our RNA-Seq data, none of the cell division genes were differentially expressed in  $\Delta pyk$ . Hence, it was concluded that iron metabolism is probably not contributing to the acentral Z ring positioning phenotype of  $\Delta pyk$  cells. Furthermore, the downregulation of the pyrimidine synthesis operon also related to our previous observation of the underinitiation of DNA replication in  $\Delta pyk$ . Taken together, these results suggested that the downregulation of the pyrimidine synthesis operon could be leading to a limited level of pyrimidines causing the cells to reduce their initiation frequency of the DNA replication process, hence causing the Z rings to form acentrally. Cellular dNTPs levels outside the normal physiological range have been shown to affect the proofreading activity during the process of DNA replication in bacteria (Gon et al. 2011; Pai and Kearsley 2017), pointing to the possibility of the downregulation of the *pyr* operon being the reason for the DNA replication initiation defect of  $\Delta pyk$  cells. Hence, the downregulation of the *pyr* genes belonging to the pyrimidine synthesis operon was confirmed in  $\Delta pyk$  cells using qPCR.

Since the downregulation of *pyr* operon could be the reason for the decreased frequency of DNA replication initiation in  $\Delta pyk$  cells, resulting in the acentral Z ring positioning; the Z ring positioning was examined in a *pyrE* mutant. This mutant displayed ~8% of its Z rings at acentral sites, suggesting that the loss of *pyrE* does have an effect on the Z ring positioning. However, as the acentral Z ring frequency of  $\Delta pyrE$  is lower than the *pyk* mutant; it indicates that the downregulation of *pyr* operon is not the sole reason for the acentral Z ring positioning defect of

$\Delta pyk$  cells. The transcription of *pyr* operon is controlled by the availability of pyrimidines via an autogenous transcriptional attenuation mechanism (Turner et al. 1994). The leader (*pyrR-pyrP*) region of the operon contains three stem loop structures called transcriptional terminators, each preceded by another stem loop structure- the antiterminator. The formation of the terminator would cause the termination of the operon, whereas the formation of the antiterminator loop would allow the expression of the operon. When pyrimidines are in abundance, the PyrR protein binds to the *pyr* mRNA and interrupts the antiterminator, allowing the formation of the terminator loop and causing transcription termination (Turner et al. 1994). Considering the mechanism by which the *pyr* operon is regulated, in  $\Delta pyk$ , the observed downregulation of the *pyr* genes could be due to the presence of abundant pyrimidines within the cell. Hence, the Z ring positioning was examined in a *pyrR* mutant. This mutant displayed ~6% of the Z rings at acentral sites, suggesting that the loss of *pyrR*, potentially causing the overexpression of the *pyr* operon and leading to an increased level of pyrimidines, does have an effect on the Z ring positioning; even though the magnitude of this effect was not as severe as the *pyk* mutant (~21%). Overall, as the deletion of *pyrE* and *pyrR* individually did result in a shift in the Z ring positioning to acentral sites, it can be inferred that an imbalance in nucleotide levels in  $\Delta pyk$  cells does contribute to their Z ring positioning defect. However, because the frequency of acentral Z rings in these mutants was much lower than the *pyk* mutant, this indicates that an imbalance in nucleotide levels by themselves cannot account for the Z ring positioning defect observed in  $\Delta pyk$  cells. Hence, it can be concluded that the downregulation of pyrimidine synthesis operon observed in  $\Delta pyk$  is not the only reason for their Z ring positioning defect, although it can be one of the contributing factors, amongst others, leading to the acentral Z ring positioning in these cells.

A link between DNA replication and nucleotide synthesis has been shown in *B. subtilis* by Goranov *et al.*, wherein the transcriptional response of cells after a block at the initiation or the elongation step of DNA replication was investigated using whole-genome DNA microarray technology (Goranov *et al.* 2005). Both, purine and pyrimidine synthesis operons were observed to be downregulated when either the initiation or the elongation stage of DNA replication was blocked. Furthermore, using the chromatin immunoprecipitation technique, the pyrimidine synthesis, but not the purine synthesis operon, was observed to contain the binding site for DnaA – the DNA replication initiation protein (Goranov *et al.* 2005). Hence, the transcriptional response of the downregulation of pyrimidine synthesis in addition to other transcriptional responses was observed to be DnaA-mediated. Since in our *pyk* vs *wt* analysis, no downregulation of the purine synthesis operon was observed, it suggests that the downregulation of pyrimidine synthesis in  $\Delta pyk$  could also be DnaA-mediated. Putting our results side by side to the study by Goranov *et al.*, it can be interpreted that the downregulation of *pyr* operon seen in our RNA-Seq data is a result of the DNA replication initiation defect of  $\Delta pyk$  cells. However, this possibility needs further investigation as to whether the DNA replication initiation defect is affecting pyrimidine synthesis or vice versa. The second scenario of pyrimidine synthesis affecting the frequency of DNA replication initiation is also possible in the *pyk* mutant, as the deletion of *pyrE* and *pyrR* individually did cause the Z rings to form at acentral positions, even though the effect was not as prominent as seen in  $\Delta pyk$  cells. In future, it will be interesting to perform marker frequency analysis on the pyrimidine synthesis mutants to see if a defect in pyrimidine synthesis can lead to a DNA replication defect or not.

In relation to the various experiments performed with pyruvate, it was observed that pyruvate addition caused a rescue of the Z ring positioning defect as well as the DNA replication

defect of  $\Delta pyk$  cells to wild type levels. It also restored the downregulation of pyrimidine synthesis operon in  $\Delta pyk$  cells to wild type. Furthermore, after the addition of pyruvate to  $\Delta pyk$  cells, an upregulation of two genes encoding for DNA replication proteins, *dnaC* and *dnaE*, was also observed in our RNA-Seq data. Interestingly, a recent study published by Nouri *et al.* (2018) suggested that pyruvate kinase is important for the initiation stage of DNA replication from the formation of the DnaA/OriC complex up to the recruitment of DnaC (helicase), DnaG (primase) and DnaE (polymerase) to form a fully-fledged replisome (Nouri et al. 2018). Pyruvate kinase does this by affecting the activity of DnaC, DnaG and DnaE. However, a previous study by Janni re *et al.* showed that *pyk* is not acting directly on the expression of these genes (Janni re et al. 2007). Since we did see the upregulation of *dnaC* and *dnaE* after pyruvate addition to  $\Delta pyk$  cells in our experiments, it could be speculated that pyruvate kinase could be acting on the expression of these genes via the production of the metabolite – pyruvate.

Chapter 3 and 4 of this thesis gave us insights into specific factors involved in the CCM-division link, including the role of pyruvate itself as the key metabolite in this link and that pyruvate scarcity could be leading to the acentral Z ring positioning by lowering the frequency of DNA replication initiation. Results from this chapter provided us with a global perspective of the *pyk* mutant that allowed us to create a more complete picture of the interconnection between pyruvate and other cellular events. RNA-seq identified the involvement of pyrimidine synthesis in the CCM-division in  $\Delta pyk$  cells. Putting this result along with other experimental data that we had in relation to the *pyk* mutant suggested that both the DNA replication defect and the pyrimidine synthesis, could be important role players in the CCM-division link in  $\Delta pyk$  cells. But, how much importance each of them has in this link and which one leads to the other, that is, whether DNA replication defect causes pyrimidine synthesis defect or vice versa, still remains to be explored.



Another question that remains unanswered is whether the  $\Delta pyk$  cells have high levels of nucleotides or lower levels? This question can be answered by performing targeted metabolomics on  $\Delta pyk$  with the aim of measuring the levels of different nucleotides. Depending on whether the levels of nucleotides in  $\Delta pyk$  is higher or lower, the ratio of *ori:ter* will be determined in  $\Delta pyrR$  or  $\Delta pyrE$  respectively. This will answer if a defect in nucleotide synthesis results in a DNA replication defect or not. If it does, it will suggest the role of a defect in nucleotide synthesis in the DNA replication initiation defect of  $\Delta pyk$  cells.



# Chapter 6

---

## General Discussion

## 6.1 Introduction

For their continued growth and multiplication, bacterial cells must double in mass, replicate their DNA, separate their sister chromosomes and divide at the correct place at the right time to produce two genetically identical daughter cells. Coordination between these events is of utmost importance to ensure that the newborn cells receive a full complement of genetic material and can proceed onto further cycles of division. In addition, for their survival, bacteria must adjust these cell-cycle processes in accordance with changing environmental conditions. How bacteria fine-tune their cell cycle events to compensate for changes in nutrient availability is an unsolved question. Recent breakthrough studies have shown that metabolic pathways can act as the point of contact with external nutrient levels and play a key role in this coordination (Weart et al. 2007; Bernard et al. 2012; Hill et al. 2013; Shi et al. 2014; Beaufay et al. 2016). Monahan *et al.* (2014) proposed an intimate link between glycolysis (central carbon metabolism) and the Z ring positioning (cell division) in *B. subtilis*, and showed that the loss of pyruvate kinase (*pyk*) disrupts this link leading to the formation of the Z rings at acentral positions; however the precise mechanism of this link was unknown. To better understand this link, the overall aim of this thesis was to gain insight into the mechanism connecting central carbon metabolism and cell division in *B. subtilis*, as was originally proposed by Monahan *et al.* (2014).

In the study by Monahan *et al.* (2014), the addition of exogenous pyruvate, the product of the pyruvate kinase reaction, to  $\Delta pyk$  cells, restored the link between CCM and Z ring positioning such that the Z rings formed correctly at midcell after pyruvate addition. However, whether pyruvate does this directly or indirectly by first being metabolized into any of its metabolic fates was not explored. Hence, the first aim of this thesis was to answer this question by supplementing the growth medium of  $\Delta pyk$  cells with each of the potential metabolic fates of pyruvate and

observing their effect on the Z ring positioning (Chapter 3). Secondly, since the polar Z ring positioning phenotype of  $\Delta pyk$  is similar to the Z ring positioning phenotype in  $\Delta min$  cells (that is, formation of acentral Z rings and minicells), the possibility of Min system inactivation causing the acentral Z ring formation in  $\Delta pyk$  cells was investigated in Chapter 4. Furthermore, during this project, the  $pyk$  mutant was shown by others (Murray and Koh 2014) to exhibit a DNA replication initiation defect. The involvement of this DNA replication defect in the cell division phenotype of these cells was also investigated in Chapter 4. Finally, a global transcriptional profile of the  $pyk$  mutant was examined to provide broader insights into the CCM-division mechanism at a systems level in  $\Delta pyk$  cells (Chapter 5).

## 6.2 Pyruvate is the key metabolite in the CCM-division link

Prior to this work, Monahan *et al.* (2014) demonstrated the importance of pyruvate levels in the Z ring assembly of *B. subtilis* cells. However, pyruvate has a number of potential metabolic fates *in vivo* and any of these fates could potentially connect to the cell division process. From the experiments performed in Chapter 3 of this thesis, the possibility of any of the metabolic fates of pyruvate regulating the Z ring positioning was effectively ruled out, indicating that pyruvate levels, and not any of the metabolites derived from pyruvate, coordinate CCM to the division process. These results suggest that cells might be utilizing pyruvate as a signaling molecule to coordinate nutritional availability with cellular growth and other cell cycle processes. This makes sense, as pyruvate being the end product of glycolysis, sits at the intersection of several important metabolic pathways, making it an ideal candidate to act as a marker of nutritional status.

The pyruvate concentration in  $\Delta pyk$  was shown to be 26% lower than that of wild type cells (section 3.3.5), which increases to a concentration 48% higher than wild type cells when pyruvate is supplemented (at 1% w/v) to the growth medium of  $\Delta pyk$  cells. Since this supplementation of pyruvate also rescues the acentral Z ring positioning defect of  $\Delta pyk$  cells, this indicates that a proper maintenance of pyruvate levels is important for the correct Z ring positioning in *B. subtilis* cells, and that pyruvate is the key metabolite required for the CCM link with cell division. However, it remains to be seen as to how much pyruvate is enough to cause the Z ring formation at the midcell site. It will be particularly interesting to know the threshold level of pyruvate that is sufficient for the correct Z ring positioning under normal physiological conditions, and whether this changes under different conditions of growth or stress conditions.

The results presented in Chapter 3 also suggest that the means by which pyruvate affects the Z ring positioning is not by interacting directly with FtsZ, at least in its monomeric form. Although, there still remains a possibility that pyruvate interacts with FtsZ only in its polymerised form to influence the Z ring assembly, thereby having an effect on the Z ring positioning. Apart from this, a crucial aspect that remains unanswered is the effect of pyruvate limitation on cellular energy levels. As pyruvate is a key metabolite at the intersection of multiple metabolic pathways, its lowered availability might significantly decrease cellular energy levels resulting in the perturbation of various cellular processes including the Z ring formation step of cell division. As GTP induces the polymerization of FtsZ required for the formation of the Z ring (Romberg et al. 2001), any effect on GTP levels could also affect the rate of Z ring formation. This aspect needs further investigation.

### 6.3 A role for nucleoid occlusion in the acentral Z ring positioning of *Δpyk* cells

Since the cell division process is essential for the survival of bacteria, a number of regulators of this process have been identified. Amongst all these known negative and positive regulators of the cell division process, the two most well-studied are the Min and the nucleoid occlusion systems that prevent the formation of Z rings at inappropriate sites. In our efforts to understand the link between CCM and cell division, it was important to consider the possibility that pyruvate levels play some role in the proper functioning of either the Min system or the nucleoid occlusion system such that any variation in pyruvate levels could influence the functioning of any of these systems, resulting in the acentral Z ring positioning, as seen in *Δpyk* cells.

From the experimental results presented in Chapter 4, it appears that the Min system is active, at least partially, in *Δpyk* cells and the acentral Z rings of this mutant are not solely due to the Min system being inactivated in these cells. Interestingly, it was also observed that while *Δpyk* cells can clearly form the Z rings at acentral positions, the *ΔminCD* mutant is able to form rings at positions much closer to the extreme cell pole, indicating that the phenotypes of the *minCD* and the *pyk* mutant are very different. Nonetheless, the deletion of *minCD* in the *pyk* mutant increased the frequency of polar Z rings. All these results together showed that although both, the *minCD* and the *pyk* mutant display the formation of acentral Z rings, there are certain differences in the acentral Z ring positioning phenotypes of the *minCD* and the *pyk* mutants; suggesting that the mechanism by which *Δpyk* cells form the Z rings at acentral positions is not via an effect on the Min system, which is at least partially active in these cells. Hence, from the observations from Chapter 4, it can be concluded that the mechanism by which pyruvate levels control the Z ring

positioning is not solely through the Min system, indicating the involvement of other systems in this pyruvate-Z ring positioning link.

The data presented in Chapter 4 of this thesis suggests a role for the nucleoid occlusion system in the acentral Z ring positioning of  $\Delta pyk$  cells, as the deletion of *noc* rescued the acentral Z ring positioning defect of  $\Delta pyk$  cells to the midcell site. This indicated that the nucleoid occlusion is originally active in  $\Delta pyk$  cells and that this active nucleoid occlusion does prevent the formation of Z rings at the midcell site. In wild-type *B. subtilis*, the protein Noc facilitates the correct Z ring positioning by binding to specific DNA sequences on the chromosome that are scarce near the terminus region of the chromosome (Wu et al. 2009). This terminus region of the chromosome occupies the midcell site when chromosome replication is near completion (Wu et al. 2009), thereby relieving the midcell site from the inhibitory effects of nucleoid occlusion on the Z ring formation (Wu and Errington 2004). Thus, Noc helps to mediate the spatial and temporal regulation of the Z ring placement with respect to the timing of DNA replication and chromosome segregation. Inhibition of DNA replication initiation in *B. subtilis*, such as in the *dnaB* mutant, has been shown to result in only a few Z rings placed at the midcell site (Wang et al. 2014). However, relieving nucleoid occlusion by deleting *noc* in these cells, has been shown to increase the frequency of midcell Z rings (Moriya et al. 2010). Since the deletion of *noc* also rescued the acentral Z ring positioning of  $\Delta pyk$  to midcell site, this indicated the possibility of a DNA replication defect in these cells, which is discussed below.

## 6.4 Insights into other factors contributing to the formation of acentral Z rings in $\Delta pyk$ cells

### 6.4.1 Does the DNA replication defect of $\Delta pyk$ cells contribute to their Z ring positioning defect?

The rescue of Z ring positioning after *noc* deletion in  $\Delta pyk$  cells indicated the possibility of a DNA replication defect in  $\Delta pyk$  cells. Indeed, the *pyk* mutant has already been shown to display a DNA replication underinitiation phenotype in *B. subtilis* (Murray and Koh 2014). However, whether this DNA replication defect contributes to their Z ring positioning defect was unknown. To answer this question, we looked at the origin to terminus ratio of  $\Delta pyk$  cells in the presence and absence of pyruvate to investigate if pyruvate has any effect on DNA replication rate. As was reported previously, we also observed the *pyk* to display an underinitiation of DNA replication phenotype. In addition, pyruvate addition was found to rescue the DNA replication rate, and also rescued the Z ring positioning defect of  $\Delta pyk$  cells (Chapter 4), suggesting that the DNA replication defect of these cells does contribute to their Z ring positioning defect.

An interesting observation in relation to the DNA replication defect of  $\Delta pyk$  cells is that leucine addition, which rescued the growth rate defect of  $\Delta pyk$  cells, did not rescue the DNA replication defect. As one can expect that an increase in growth rate does require an increased rate of DNA replication, this discrepancy in leucine results indicates that leucine could be acting on some other cellular process, such as cell wall synthesis and membrane synthesis, that helps restore cellular growth. However, the reason for this result is still unclear.

A link between the early stages of DNA replication and the Z ring positioning was established in *B. subtilis* about two decades ago (Harry et al. 1999). It is likely that such a link is



also present in the *pyk* mutant, as pyruvate addition rescued the DNA replication as well the Z ring positioning defect. However, the exact point of connection between these processes in  $\Delta pyk$  cells remains to be investigated. Pyruvate could be acting as a potential regulator of DNA replication by influencing the expression of any of the DNA replication proteins. DnaA, a DNA replication initiator protein, is one of the most well-characterized proteins of the replisome in *B. subtilis* and holds the potential to connect cell physiology to the DNA synthesis process (Murray and Koh 2014). In *C. crescentus*, carbon starvation has been shown to alter the expression of important cell cycle proteins, one of them being DnaA (Jain and Chen 2018). Considering this observation, it will be relevant to measure the levels of DnaA in  $\Delta pyk$  cells, as the lowered levels of this protein could be the possible reason behind the DNA replication defect of these cells.

A direct link between *pyk* deletion and DNA replication was shown by Janni re *et al.*, where *pyk* deletion rescued a thermosensitive elongation (*dnaE*) mutant of *B. subtilis* (Janni re *et al.* 2007). Furthermore, pyruvate accumulation resulting from alterations in pyruvate dehydrogenase activity has been shown to suppress thermal-sensitive mutants of *dnaA* in *E. coli* (Tymecka-Mulik *et al.* 2017), hence demonstrating a link between pyruvate levels and DNA replication in *E. coli*. Correlating these observations with our finding that pyruvate levels are essential for DNA replication in *B. subtilis*, highlights the importance of pyruvate acting as a linking metabolite between the DNA replication and metabolic pathways in *B. subtilis*, and potentially across many bacteria.

### **6.4.2 Does the dispersed nucleoid morphology of $\Delta pyk$ cells contribute to their Z ring positioning defect?**

The presence of replication-inhibited, unsegregated chromosomes at the midcell site has been shown to block the Z ring formation (Cambridge et al. 2014). Since quantification analysis revealed that the nucleoid of  $\Delta pyk$  cells is more spread than in wild type cells, it was investigated whether there is any correlation between this different nucleoid morphology and the Z ring positioning of  $\Delta pyk$  cells. The addition of pyruvate did reverse the nucleoid morphology from spread to bilobed with 49% cells showing bilobed nucleoid morphology, however the rescue was not to the level of wild type cells. Furthermore, the addition of L-alanine, which rescued the Z ring positioning defect of  $\Delta pyk$ , was observed not to rescue their nucleoid morphology defect; while D-alanine, which did not rescue the Z ring positioning, was able to rescue the nucleoid morphology of  $\Delta pyk$  cells to the bilobed morphology. Collectively, there was no clear correlation observed between the nucleoid morphology rescue and the Z ring positioning rescue of  $\Delta pyk$  cells. This suggests that the change from a mainly spread nucleoid to a bilobed morphology could be one of the contributing factors that allows the Z ring positioning rescue after pyruvate addition. However, it does not appear to be the sole reason for the Z ring positioning rescue of  $\Delta pyk$  cells.

### **6.4.3 Does the downregulation of pyrimidine synthesis in $\Delta pyk$ cells contribute to their Z ring positioning defect?**

As presented in Chapter 5 of this thesis, transcriptomic analysis showed that the pyrimidine synthesis operon is downregulated in  $\Delta pyk$  cells, which could contribute to the acentral Z ring positioning defect of these cells. As the nucleotides are synthesized from substrates present

upstream as well as the downstream of the pyruvate kinase reaction (Lee et al. 1997), a clear prediction about the effect of *pyk* deletion on nucleotide levels cannot be made. However, considering that the *pyr* operon is downregulated in response to high concentrations of pyrimidines (Turner et al. 1994) and that the  $\Delta pyk$  cells showed downregulation of this operon, it is likely that  $\Delta pyk$  cells experience an abundance of pyrimidines. Yet, more work needs to be done to correctly answer whether the  $\Delta pyk$  cells have an increased or decreased level of nucleotides. This can be accomplished by performing a targeted metabolomics experiment on the *pyk* mutant with an aim of measuring the concentrations of different nucleotides. Whether it be an increase or decrease in nucleotide levels, since the deletion of *pyrE* and *pyrR* individually did cause a shift in the Z ring positioning to acentral sites, an imbalance in nucleotide levels in  $\Delta pyk$  cells does contribute to their Z ring positioning defect. However, because the frequency of acentral Z rings in the *pyrE* and *pyrR* single mutants was much lower as compared to the *pyk* mutant, an imbalance in the levels of nucleotides appears to be only one of the many factors that could be contributing to the acentral Z ring positioning phenotype of  $\Delta pyk$ .

Goranov and colleagues have shown the downregulation of purine and pyrimidine (*pyr*) synthesis operons in response to a block in the initiation or elongation stage of chromosome replication (Goranov et al. 2005), suggesting that the under-initiation of DNA replication in  $\Delta pyk$  cells could be the reason for this observed downregulation of the *pyr* operon. However, this possibility needs further investigation because the other scenario, that is, of nucleotide synthesis leading to DNA replication initiation defect is also possible. Indeed, the deletion of *pyrE* or *pyrR* did result in some Z ring positioning defect in  $\Delta pyk$  cells, which could occur by this alternative mechanism. Overall, with the current experimental results, the mechanism for the Z ring positioning defect of  $\Delta pyk$  cells could be via the effect of DNA replication on nucleotide synthesis

or vice versa. This can be tested by performing marker frequency analysis on the *pyrE* or *pyrR* mutants, with an aim of checking if they show any DNA replication defect.

## 6.5 Concluding remarks and future directions

How bacteria adapt their cell cycle processes in different nutritional standings is an intriguing question that demands further exploration. The work presented in this thesis uncovers one of the ways this might occur. This work highlights that pyruvate levels are important in determining the correct division site in *B. subtilis*. However, the threshold level of pyruvate that could result in the correct Z ring positioning remains to be determined. Considering the key role of pyruvate in bacterial metabolism, it is an ideal candidate to mark the nutritional status of a cell. However, it will be interesting in future work to define how well conserved this division function of pyruvate is across different bacterial species.

Furthermore, the results presented in this thesis also help to address the question of how pyruvate levels are coupled with the Z ring positioning in *B. subtilis*. We hypothesize that pyruvate levels are important for the correct rate of chromosome replication as well as nucleotide synthesis in *B. subtilis*, and a perturbation in pyruvate synthesis, as seen in  $\Delta pyk$  cells, has an effect on these systems. Subsequently, an influence on these systems, either independently or together, has an effect on the Z ring positioning. However, it will be intriguing to explore in future whether an effect on one of these systems (chromosome replication or nucleotide synthesis) show a subsequent effect on the other, causing a subsequent shift in the Z ring positioning; or whether the functions of these two systems are affected independently by pyruvate unavailability, with each exerting some influence on the Z ring position. We also observed a role of spread nucleoid morphology in

the acentral Z ring positioning of *Δpyk*. Taken together, we identified three aspects of the *Δpyk* cells that could contribute to their cell division phenotype, which includes their DNA replication initiation defect, the downregulation of pyrimidine synthesis and their spread nucleoid morphology. However, we don't know for sure whether these aspects are connected to one another, and how much they contribute to the Z ring positioning defect of *Δpyk* cells. Furthermore, it is also possible that pyruvate deficiency could be leading to a general metabolic dysregulation in the cells, causing a decrease in general cellular energy levels, replication initiation and pyrimidine levels. These together result in the Z rings to be positioned at acentral sites in *Δpyk* cells. This will be another interesting area of future research.

Lastly, two important aspects that remain untouched in this work are the role of (p)ppGpp, a global prokaryotic alarmone, in the acentral Z ring positioning of *Δpyk* cells and the timing of Z ring formation in *Δpyk* cells. (p)ppGpp is a starvation-induced molecule, known to regulate various cellular processes, including the DNA replication and cell division processes (Wang and Levin 2009). It is also a global regulator of the transcriptional expression of a number of genes, including the *dnaA* expression. Since, in the *pyk* mutant, many factors were observed to potentially contribute to their Z ring positioning defect, a probable role of a global regulator controlling all these processes is highly likely. Since we have shown that active nucleoid occlusion at the midcell site is preventing the correct midcell positioning of the Z rings in *Δpyk* cells, a possibility arises that the Z rings are forming earlier than the segregation of replicated chromosomes in the *pyk* mutant. Hence, in future, time-lapse microscopy of the Z ring formation in the synchronised cells of the *pyk* mutant will be performed to investigate the timing of the Z ring formation and chromosome segregation in these cells.

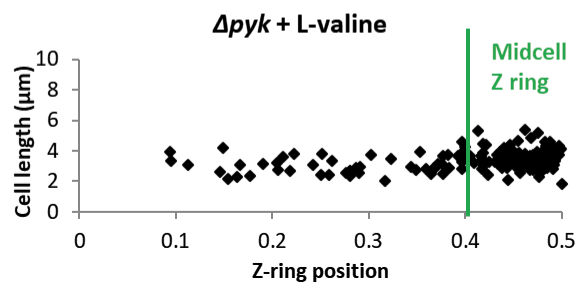
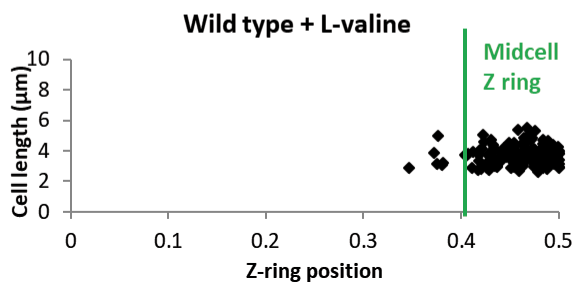
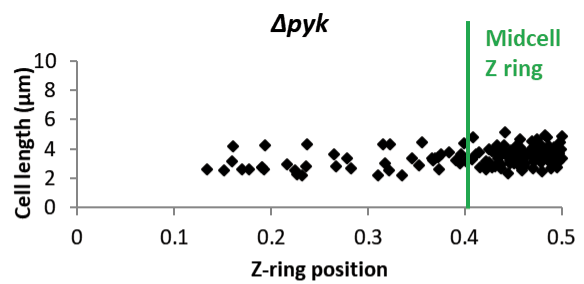
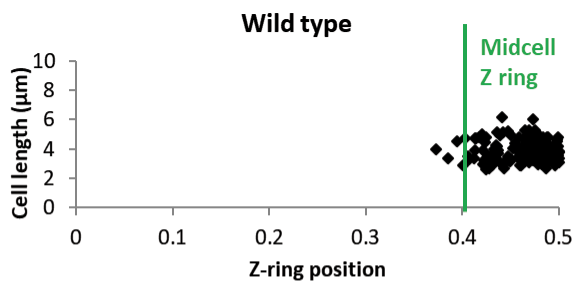
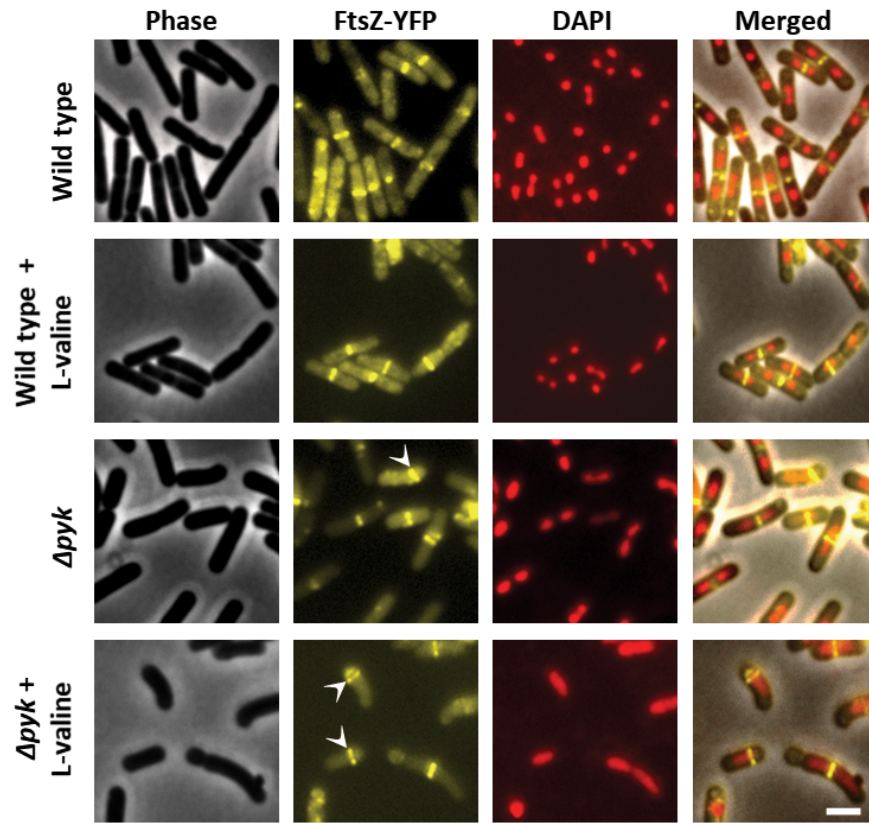




# Appendices

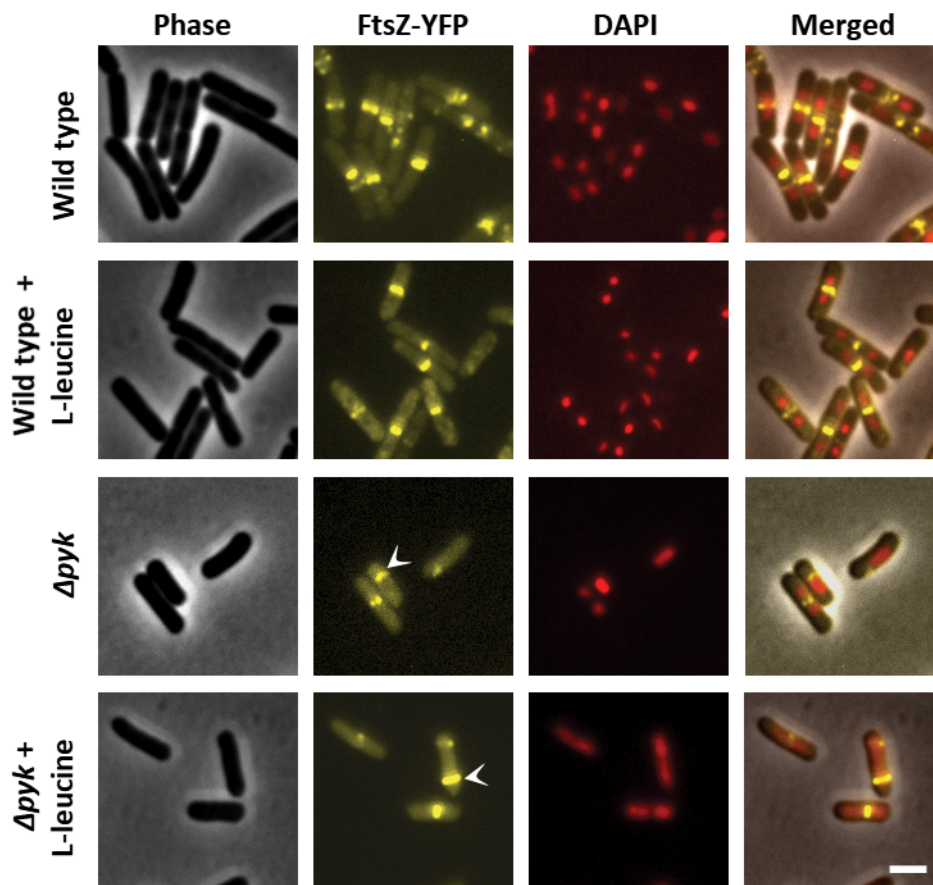
---

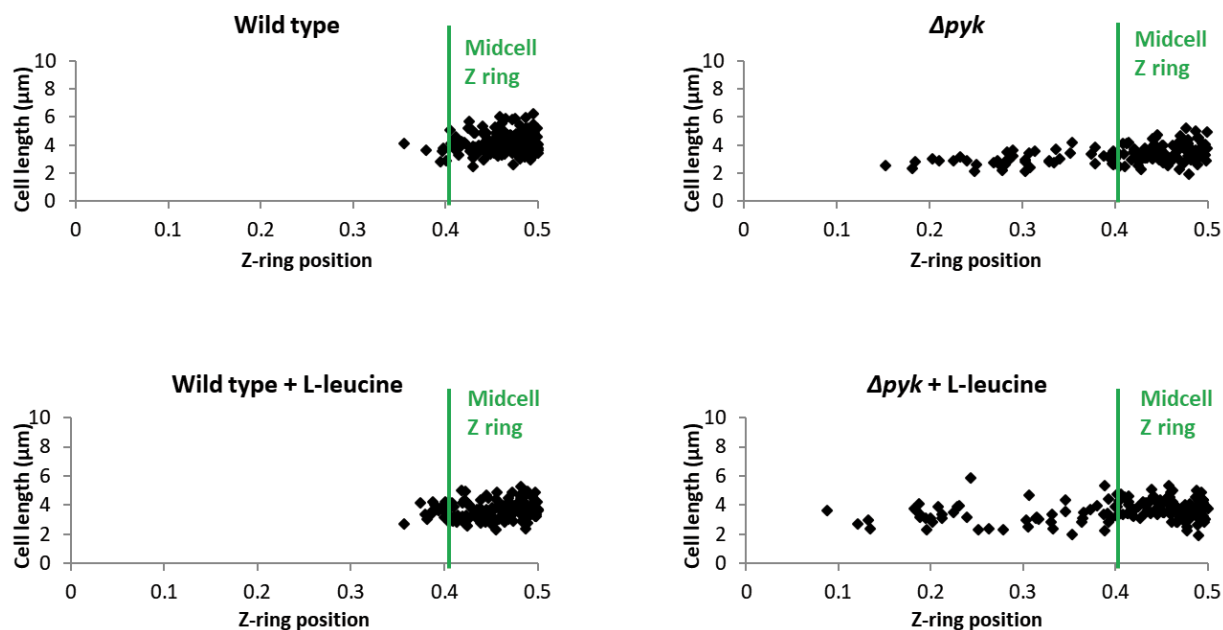
# Appendix I



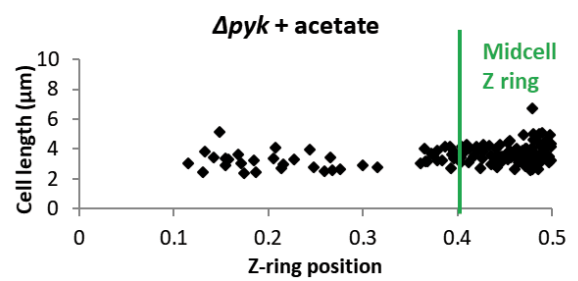
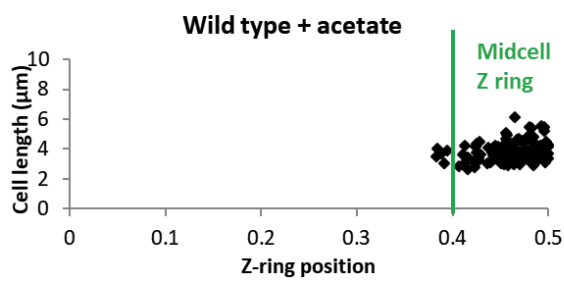
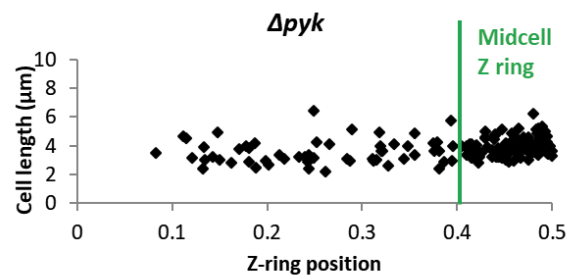
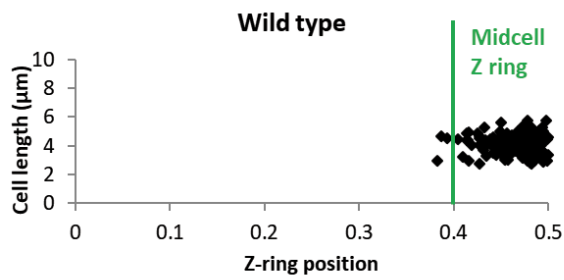
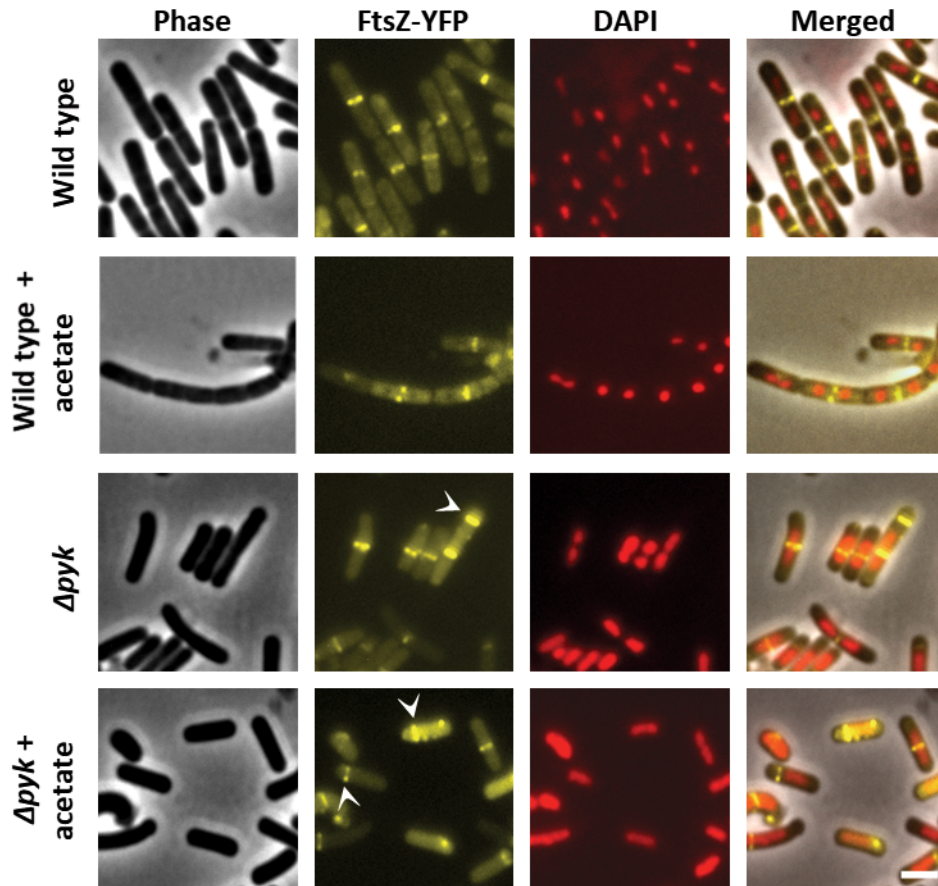


**Figure 1. The effect of L-valine on the Z ring positioning of  $\Delta pyk$  cells.** Cells were grown to mid-exponential phase in the presence of 0.01% xylose in L-broth at 37°C with or without the addition of 1% L-valine and visualized by phase-contrast and fluorescence microscopy (n=3). Scale bar, 2 $\mu$ m. White arrows in the FtsZ-YFP panel point towards acentral Z rings. Lower panel shows the scatter plots wherein cell length has been plotted as a function of the Z ring positioning under different experimental conditions. Here, the Z ring position of 0 and 0.5 on the x-axis signify the cell pole and cell centre, respectively. n > 150. [Wild type = SU492 (*amyE::Pxyl-ftsZ-yfp*),  $\Delta pyk$  = SU679 ( *$\Delta pyk$  amyE::Pxyl-ftsZ-yfp*)]

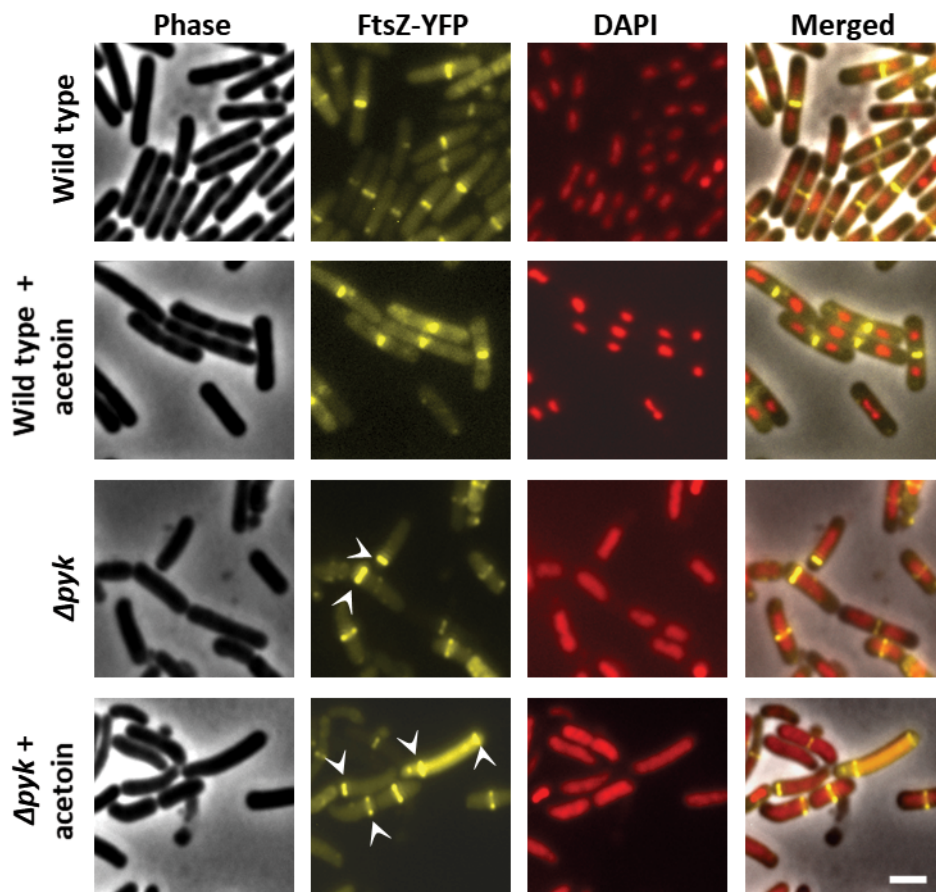


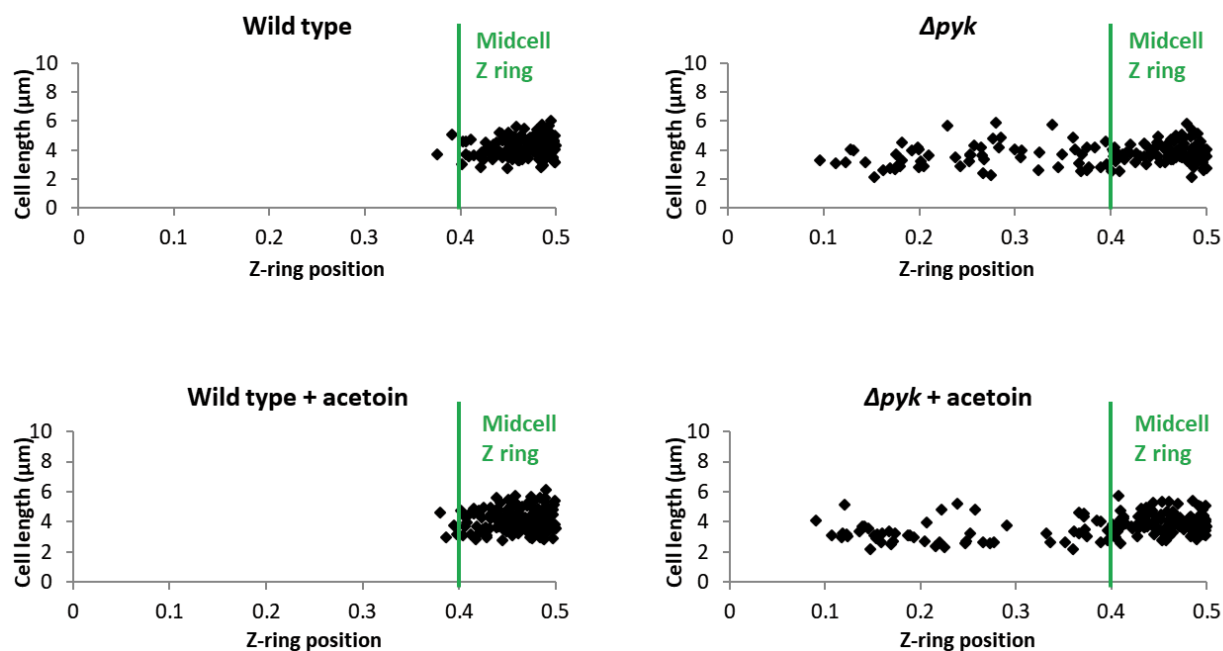


**Figure 2. The effect of L-leucine on the Z ring positioning of  $\Delta pyk$  cells.** Cells were grown to mid-exponential phase in the presence of 0.01% xylose in L-broth at 37°C with or without the addition of 1% L-leucine and visualized by phase-contrast and fluorescence microscopy (n=3). Scale bar, 2μm. White arrows in the FtsZ-YFP panel point towards acentral Z rings. Lower panel shows the scatter plots wherein cell length has been plotted as a function of the Z ring positioning under different experimental conditions. Here, the Z ring position of 0 and 0.5 on the x-axis signify the cell pole and cell centre, respectively. n > 150. [Wild type = SU492 (*amyE::Pxyl-ftsZ-yfp*),  $\Delta pyk$  = SU679 ( $\Delta pyk amyE::Pxyl-ftsZ-yfp$ )]

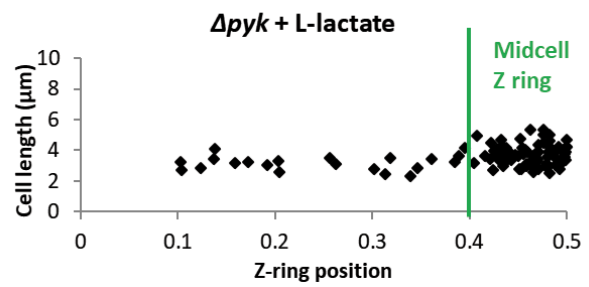
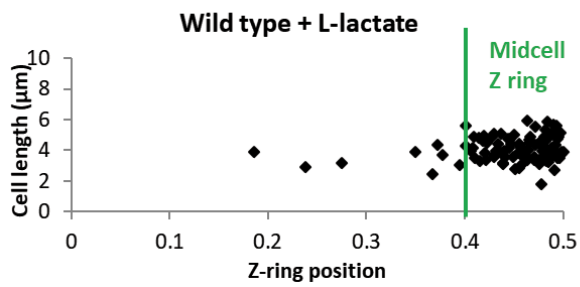
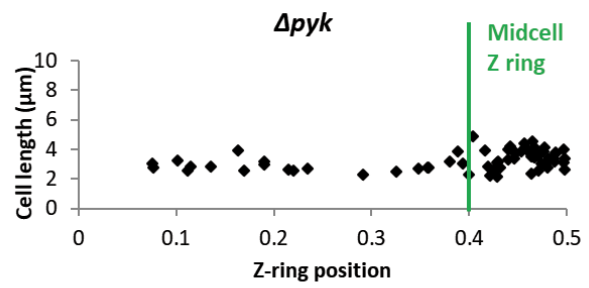
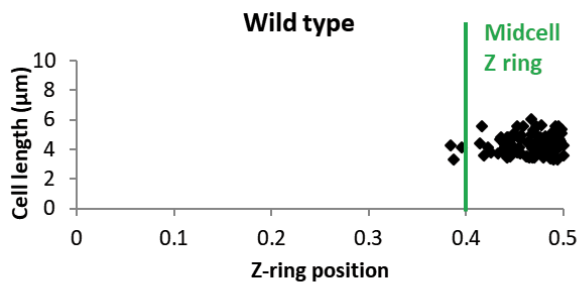
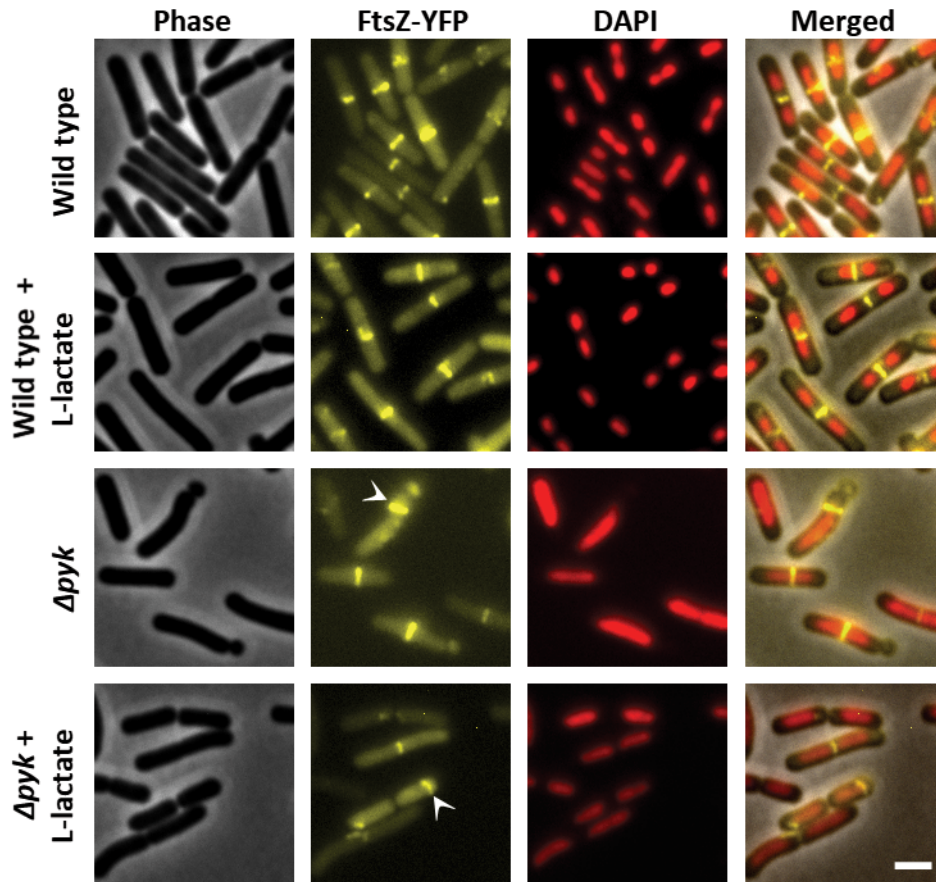


**Figure 3. The effect of acetate on the Z ring positioning of  $\Delta pyk$  cells.** Cells were grown to mid-exponential phase in the presence of 0.01% xylose in L-broth at 37°C with or without the addition of 1% acetate and visualized by phase-contrast and fluorescence microscopy (n=3). Scale bar, 2 $\mu$ m. White arrows in the FtsZ-YFP panel point towards acentral Z rings. Lower panel shows the scatter plots wherein cell length has been plotted as a function of the Z ring positioning under different experimental conditions. Here, the Z ring position of 0 and 0.5 on the x-axis signify the cell pole and cell centre, respectively. n > 150. [Wild type = SU492 (*amyE::Pxyl-ftsZ-yfp*),  $\Delta pyk$  = SU679 ( *$\Delta pyk$  amyE::Pxyl-ftsZ-yfp*)]

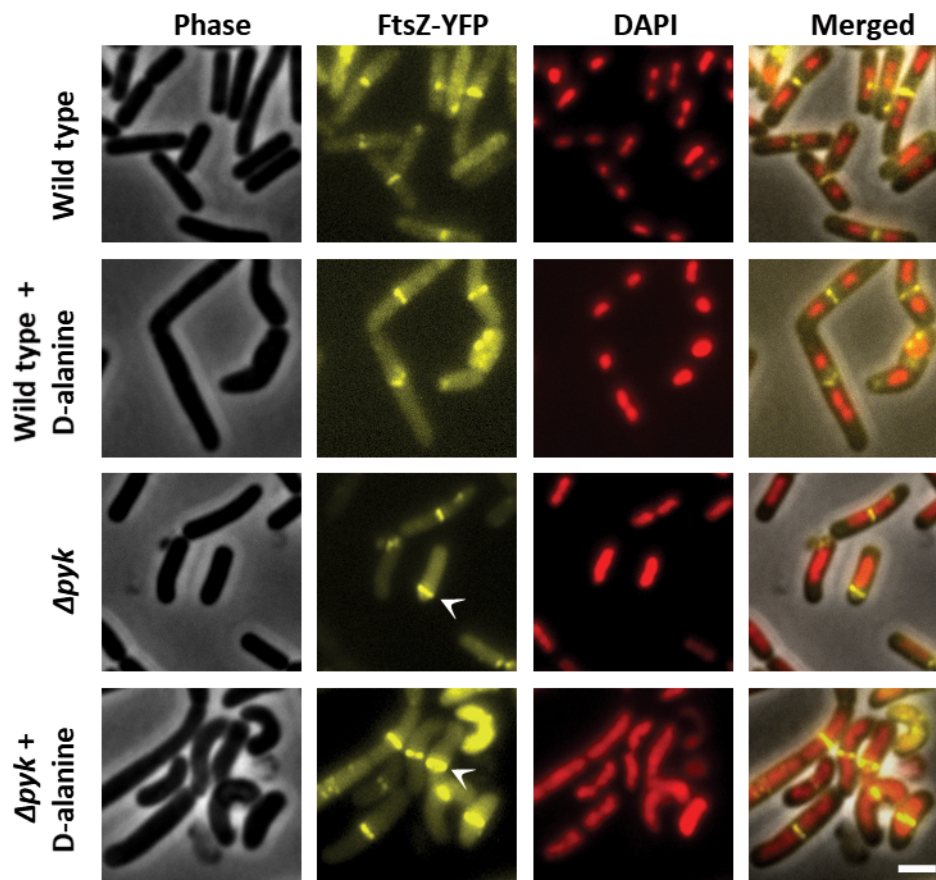




**Figure 4. The effect of acetoin on the Z ring positioning of  $\Delta pyk$  cells.** Cells were grown to mid-exponential phase in the presence of 0.01% xylose in L-broth at 37°C with or without the addition of 1% acetoin and visualized by phase-contrast and fluorescence microscopy (n=3). Scale bar, 2μm. White arrows in the FtsZ-YFP panel point towards acentral Z rings. Lower panel shows the scatter plots wherein cell length has been plotted as a function of the Z ring positioning under different experimental conditions. Here, the Z ring position of 0 and 0.5 on the x-axis signify the cell pole and cell centre, respectively. n > 150. [Wild type = SU492 (*amyE::Pxyl-ftsZ-yfp*),  $\Delta pyk$  = SU679 (*Δpyk amyE::Pxyl-ftsZ-yfp*)]



**Figure 5. The effect of L-lactate on the Z ring positioning of  $\Delta pyk$  cells.** Cells were grown to mid-exponential phase in the presence of 0.01% xylose in L-broth at 37°C with or without the addition of 1% L-lactate and visualized by phase-contrast and fluorescence microscopy (n=3). Scale bar, 2 $\mu$ m. White arrows in the FtsZ-YFP panel point towards acentral Z rings. Lower panel shows the scatter plots wherein cell length has been plotted as a function of the Z ring positioning under different experimental conditions. Here, the Z ring position of 0 and 0.5 on the x-axis signify the cell pole and cell centre, respectively. n > 150. [Wild type = SU492 (*amyE::Pxyl-ftsZ-yfp*),  $\Delta pyk$  = SU679 ( *$\Delta pyk$  amyE::Pxyl-ftsZ-yfp*)]



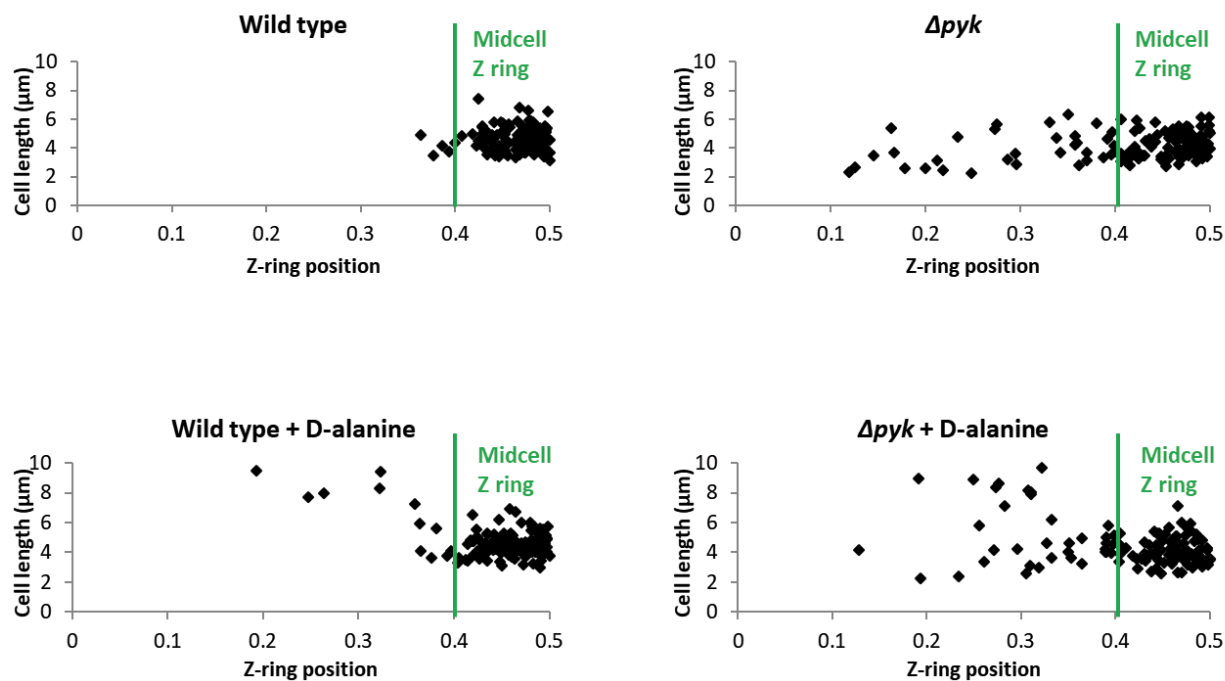


**Figure 6. The effect of D-alanine on the Z ring positioning of  $\Delta pyk$  cells.** Cells were grown to mid-exponential phase in the presence of 0.01% xylose in L-broth at 37°C with or without the addition of 1% L-lactate and visualized by phase-contrast and fluorescence microscopy (n=3). Scale bar, 2μm. White arrows in the FtsZ-YFP panel point towards acentral Z rings. Lower panel shows the scatter plots wherein cell length has been plotted as a function of the Z ring positioning under different experimental conditions. Here, the Z ring position of 0 and 0.5 on the x-axis signify the cell pole and cell centre, respectively. n > 150. [Wild type = SU492 (*amyE::Pxyl-ftsZ-yfp*),  $\Delta pyk$  = SU679 ( $\Delta pyk$  *amyE::Pxyl-ftsZ-yfp*)]



**Table 1. The effect of different metabolites on the doubling time of wild type cells**

<b>Strain ± metabolite</b>	<b>Doubling time (min)*</b>	<b>P value for doubling time in comparison to wild type cells**</b>
Wild type (WT)	31 ± 0.71	-
WT + pyruvate	33 ± 0.98	1.000
WT + acetate	38 ± 0.65	0.281
WT + acetoin	35 ± 0.16	0.984
WT + L-lactate	30 ± 1.46	0.997
WT + L-alanine	33 ± 2.19	0.989
WT + D-alanine	31 ± 0.83	0.857
WT + L-valine	32 ± 1.92	0.667
WT + L-leucine	32 ± 0.34	0.988

\*Doubling time was calculated by taking an average of the doubling times ( $\pm$  SEM) of three biological replicates obtained, except for wild type (no metabolite added), where the values represent an average of respective growth curves performed during the experiments for all metabolites. Wild type cells were grown in Luria broth in the presence and absence of a particular metabolite (1 %),  $A_{600}$  was recorded every hour for 8 hours, growth curve was plotted, and the doubling time was calculated from the exponential phase

\*\*P-values were calculated using one-way Anova along with Tukey Pairwise comparison on three biological replicates (Wild type- SU492)

## Appendix II

**Table 1. Comparing the RNA-Seq transcriptomes of pyruvate kinase mutant with the addition of pyruvate (1%) (pykP) and wild type *B. subtilis* cells.** Table showing the DE genes of pykP vs. wt comparison at p-value <0.05 and Fold Change  $\geq 2.0$ .

Gene	Response in pykP vs wt	log2FoldChange
pyk	Downregulated	-9.2432734
ytzA	Downregulated	-7.2045725
xylA	Downregulated	-6.0314444
yhfH	Downregulated	-5.842031
iolF	Downregulated	-5.35327
ytwI	Downregulated	-5.3054417
epsA	Downregulated	-5.1417276
ganB	Downregulated	-4.8559804
rbsA	Downregulated	-4.6559211
tasA	Downregulated	-4.6062466
ald	Downregulated	-4.4903726
rbsB	Downregulated	-4.4036698
cimH	Downregulated	-4.3967087
iolH	Downregulated	-4.2576152
gmuC	Downregulated	-4.1772768
ylbP	Downregulated	-3.9970851
rbsK	Downregulated	-3.9508799
oxdC	Downregulated	-3.9259672
kbl	Downregulated	-3.8075059
rbsR	Downregulated	-3.7552507
ganP	Downregulated	-3.6718486
iolC	Downregulated	-3.6390051
acsA	Downregulated	-3.525624
dctP	Downregulated	-3.5051165
gapB	Downregulated	-3.4347717
ilvD	Downregulated	-3.3897995
yvfH	Downregulated	-3.3824852
treA	Downregulated	-3.3702705
ysmA	Downregulated	-3.3640527
cstA	Downregulated	-3.2947498
gmuD	Downregulated	-3.2453564
iolD	Downregulated	-3.2176935
yrbE	Downregulated	-3.1179278

ykoM	Downregulated	-3.0988741
leuB	Downregulated	-3.0899291
oppA	Downregulated	-3.0040086
ganA	Downregulated	-2.9743727
gltA	Downregulated	-2.8978511
sunA	Downregulated	-2.8785077
citZ	Downregulated	-2.8662651
mmsA	Downregulated	-2.8336669
sdhB	Downregulated	-2.8119652
tdh	Downregulated	-2.79239
ywsB	Downregulated	-2.7863986
gltB	Downregulated	-2.7262061
sdhC	Downregulated	-2.7215951
gmuG	Downregulated	-2.696316
lutB	Downregulated	-2.6885365
yxiM	Downregulated	-2.6383501
ppnKB	Downregulated	-2.6047008
yrpD	Downregulated	-2.6008193
malR	Downregulated	-2.5927487
leuA	Downregulated	-2.5908817
sdhA	Downregulated	-2.5845627
maeN	Downregulated	-2.5387274
qcrC	Downregulated	-2.5367801
wprA	Downregulated	-2.53466
yukJ	Downregulated	-2.518683
sucC	Downregulated	-2.5001248
ymfJ	Downregulated	-2.4939412
cysJ	Downregulated	-2.4702142
phoP	Downregulated	-2.4678143
lutC	Downregulated	-2.4582708
ilvA	Downregulated	-2.4509853
oppC	Downregulated	-2.4474158
odhB	Downregulated	-2.4410424
ilvC	Downregulated	-2.4389125
oppB	Downregulated	-2.4288012
sucD	Downregulated	-2.4189943
lutA	Downregulated	-2.4061925
etfA	Downregulated	-2.3780611
cysI	Downregulated	-2.2925815
fruA	Downregulated	-2.2208846
odhA	Downregulated	-2.1954682

yxjG	Downregulated	-2.1790872
ndk	Downregulated	-2.1623569
treR	Downregulated	-2.1463774
yxii	Downregulated	-2.1378912
yxij	Downregulated	-2.1190665
acuB	Downregulated	-2.1144123
yflP	Downregulated	-2.1082567
racX	Downregulated	-2.1017484
scuA	Downregulated	-2.0612473
ohrA	Downregulated	-2.0567485
ykvS	Downregulated	-2.0408208
oppF	Downregulated	-2.0159847
pbpE	Downregulated	-2.0143035
yokE	Downregulated	-1.9479337
hxlA	Downregulated	-1.9185161
mcpC	Downregulated	-1.8944262
mtnK	Downregulated	-1.8889045
ytkA	Downregulated	-1.8880232
yxxG	Downregulated	-1.8780046
ycaA	Downregulated	-1.8759048
galT	Downregulated	-1.867051
yxik	Downregulated	-1.8488257
oppD	Downregulated	-1.8469979
murQ	Downregulated	-1.8353717
mtnA	Downregulated	-1.8351305
yxzG	Downregulated	-1.8260125
scoC	Downregulated	-1.8212986
putR	Downregulated	-1.8145668
ylbA	Downregulated	-1.8042977
yuaE	Downregulated	-1.7888174
ybeC	Downregulated	-1.7666634
sipU	Downregulated	-1.751331
yxjH	Downregulated	-1.7317686
citB	Downregulated	-1.7042523
yukE	Downregulated	-1.6775948
qcrA	Downregulated	-1.654656
pckA	Downregulated	-1.6415735
gapA	Downregulated	-1.5869795
gcvPB	Downregulated	-1.5723563
yxih	Downregulated	-1.5344595
spo0M	Downregulated	-1.5228433

yvgN	Downregulated	-1.5008298
nfrAB	Downregulated	-1.4608788
dtpT	Downregulated	-1.4486234
yhjA	Downregulated	-1.4386841
icd	Downregulated	-1.4210219
yokF	Downregulated	-1.4181884
abh	Downregulated	-1.4066551
mdh	Downregulated	-1.3656661
ysdC	Downregulated	-1.3653743
nagP	Downregulated	-1.3317639
abrB	Downregulated	-1.3088813
yteJ	Downregulated	-1.2958261
iolS	Downregulated	-1.2861344
ydaO	Downregulated	-1.2625678
sppA	Downregulated	-1.2539421
salA	Downregulated	-1.2307146
sigL	Downregulated	-1.2298708
pepF	Downregulated	-1.2188604
yvdD	Downregulated	-1.2108704
yjoA	Downregulated	-1.1895871
pbpH	Downregulated	-1.1885989
yutJ	Downregulated	-1.1708578
yhaH	Downregulated	-1.1666214
ylaL	Downregulated	-1.1400956
gudB	Downregulated	-1.1162876
ybzI	Downregulated	-1.0954828
yoxD	Downregulated	-1.073377
gltT	Downregulated	-1.0387118
yfjQ	Upregulated	1.04436217
menH_2	Upregulated	1.11704315
tboG	Upregulated	1.17735358
lysC	Upregulated	1.18979983
dnaE	Upregulated	1.20986683
fbpA	Upregulated	1.2674539
fabZ	Upregulated	1.33691791
yfkC	Upregulated	1.3814244
thiL	Upregulated	1.40138627
dnaC	Upregulated	1.42495191
cwlO	Upregulated	1.42799477
ribH	Upregulated	1.43826164
ycnB	Upregulated	1.4789435

ylbF	Upregulated	1.48456898
yabE	Upregulated	1.59385689
yckB	Upregulated	1.62496836
ylbM	Upregulated	1.62713689
BSU_misc_RNA_52	Upregulated	1.66838291
fhuG	Upregulated	1.71065605
opuAC	Upregulated	1.71261454
opuAA	Upregulated	1.74601876
clsA	Upregulated	1.77734932
yczE	Upregulated	1.79272914
opuCC	Upregulated	1.80486318
opuAB	Upregulated	1.84462035
feuB	Upregulated	1.97150687
yfkA	Upregulated	2.0034479
mrgA	Upregulated	2.0220092
opuCD	Upregulated	2.02809802
ybbA	Upregulated	2.06029641
feuC	Upregulated	2.08749857
yocH	Upregulated	2.13334257
yhcC	Upregulated	2.24221073
yuiF	Upregulated	2.4172253
yhcB	Upregulated	2.50788353
bglC	Upregulated	2.79350724
yhcA	Upregulated	2.9998786
ywpJ	Upregulated	3.0035178
yhbJ	Upregulated	3.0095033
yhbI	Upregulated	3.86828798
glpD	Upregulated	4.10425793
alsS	Upregulated	4.18507065
glcR	Upregulated	4.35581716

---

# References

---

- Aarsman MEG, Piette A, Fraipont C, et al (2005) Maturation of the *Escherichia coli* divisome occurs in two steps. *Mol Microbiol* 55:1631–1645. doi: 10.1111/j.1365-2958.2005.04502.x
- Abell C, Dagostin C (2015) Different Flavours of Fragments. In: *Fragment-Based Drug Discovery*. Royal Society of Chemistry, pp 1–18
- Adams DW, Errington J (2009) Bacterial cell division: assembly, maintenance and disassembly of the Z ring. *Nat Rev Microbiol* 7:642–653. doi: 10.1038/nrmicro2198
- Adams DW, Wu LJ, Errington J (2014) Cell cycle regulation by the bacterial nucleoid. *Curr Opin Microbiol* 22:94–101. doi: 10.1016/j.mib.2014.09.020
- Adams DW, Wu LJ, Errington J (2015) Nucleoid occlusion protein Noc recruits DNA to the bacterial cell membrane. *EMBO J* 34:491–501. doi: 10.15252/embj.201490177
- Arjes HA, Lai B, Emelue E, et al (2015) Mutations in the bacterial cell division protein FtsZ highlight the role of GTP binding and longitudinal subunit interactions in assembly and function. *BMC Microbiol* 15:1–16. doi: 10.1186/s12866-015-0544-z
- Arkus Gardner KAJ, Osawa M, Erickson HP (2017) Whole genome re-sequencing to identify suppressor mutations of mutant and foreign *Escherichia coli* FtsZ. *PLoS One* 12:1–15. doi: 10.1371/journal.pone.0176643
- Baker TA, Sauer RT (2012) ClpXP, an ATP-powered unfolding and protein-degradation machine. *Biochim Biophys Acta* 1823:15–28. doi: 10.1016/j.bbamcr.2011.06.007
- Balasubramanian D, Ragunathan PT, Fei J, Vanderpool CK (2016) A Prophage-Encoded Small RNA Controls metabolism and cell division in *Escherichia coli*. *mSystems* 1:1–18. doi: 10.1128/mSystems.00021-15.Editor
- Beaufay F, Coppine J, Mayard A, et al (2015) A NAD-dependent glutamate dehydrogenase coordinates metabolism with cell division in *Caulobacter crescentus*. *EMBO J* 34:1786–1800. doi: 10.15252/embj.201490730
- Beaufay F, De Bolle X, Hallez R (2016) Metabolic control of cell division in  $\alpha$ -proteobacteria by a NAD-dependent glutamate dehydrogenase. *Commun Integr Biol*

- 9:e1125052. doi: 10.1080/19420889.2015.1125052
- Beech PL, Nheu T, Schultz T, et al (2000) Mitochondrial FtsZ in a chromophyte alga. *Science* (80- ) 287:1276–1279. doi: 10.1126/science.287.5456.1276
- Begley DW, Moen SO, Pierce PG, Zartler ER (2013) Saturation Transfer Difference NMR for Fragment Screening. *Curr Protoc Chem Biol* 5:251–268. doi: 10.1002/9780470559277.ch130118
- Berberich R, Kaback M, Freese E (1968) D-amino acids as inducers of L-alanine dehydrogenase in *Bacillus subtilis*. *J Biol Chem* 243:1006–1011
- Berkmen MB, Grossman AD (2007) Subcellular positioning of the origin region of the *Bacillus subtilis* chromosome is independent of sequences within oriC, the site of replication initiation, and the replication initiator DnaA. *Mol Microbiol* 63:150–165. doi: 10.1111/j.1365-2958.2006.05505.x
- Bernard E, Rolain T, David B, et al (2012) Dual Role for the O-Acetyltransferase OatA in Peptidoglycan Modification and Control of Cell Septation in *Lactobacillus plantarum*. *PLoS One* 7:. doi: 10.1371/journal.pone.0047893
- Bernhardt TG, De Boer PAJ (2005) SlmA, a nucleoid-associated, FtsZ binding protein required for blocking septal ring assembly over chromosomes in *E. coli*. *Mol Cell* 18:555–564. doi: 10.1016/j.molcel.2005.04.012
- Boye E, Nordström K (2003) Coupling the cell cycle to development. *EMBO Rep* 4:757–760. doi: 10.1242/dev.021931
- Bramkamp M, Baarle S van (2009) Division site selection in rod-shaped bacteria. *Curr Opin Microbiol* 12:683–688. doi: 10.1016/j.mib.2009.10.002
- Brinsmade SR, Sonenshein AL (2011) Dissecting complex metabolic Integration provides direct genetic evidence for codY activation by guanine nucleotides. *J Bacteriol* 193:5637–5648. doi: 10.1128/JB.05510-11
- Brzoska AJ, Hassan KA (2014) Quantitative PCR for detection of mRNA and gDNA in environmental isolates. In: *Environmental Microbiology: Methods and Protocols*. pp 25–42
- Buchakjian MR, Kornbluth S (2010) The engine driving the ship: metabolic steering of cell proliferation and death. *Nat Rev Mol Cell Biol* 11:715–27. doi: 10.1038/nrm2972
- Cambridge J, Blinkova A, Magnan D, et al (2014) A Replication-inhibited unsegregated nucleoid at mid-cell blocks Z-ring formation and cell division independently of SOS and



- the SlmA nucleoid occlusion protein in *Escherichia coli*. *J Bacteriol* 196:36–49. doi: 10.1128/JB.01230-12
- Campos M, Surovtsev I V., Kato S, et al (2014) A constant size extension drives bacterial cell size homeostasis. *Cell* 159:1433–1446. doi: 10.1016/j.cell.2014.11.022
- Charbonnier T, Le Coq D, McGovern S, et al (2017) Molecular and Physiological Logics of the Pyruvate-Induced Response of a Novel Transporter in *Bacillus subtilis*. *MBio* 8:1–18. doi: 10.1128/mbio.00976-17
- Chien A-C, Hill NS, Levin PA (2012a) Cell Size Control in Bacteria. *Curr Biol* 22:340–349. doi: 10.1016/j.cub.2012.02.032
- Chien A-C, Zareh SKG, Wang YM, Levin PA (2012b) Changes in the oligomerization potential of the division inhibitor UgtP co-ordinate *Bacillus subtilis* cell size with nutrient availability. *Mol Mi* 86:594–610. doi: 10.1111/mmi.12007
- Clark VL, Young FE (1974) Active transport of D-alanine and related amino acids by whole cells of *Bacillus subtilis*. *J Bacteriol* 120:1085–1092
- Commichau FM, Rothe FM, Herzberg C, et al (2009) Novel Activities of Glycolytic Enzymes in *Bacillus subtilis*. *Mol Cell Proteomics* 8:1350–1360. doi: 10.1074/mcp.M800546-MCP200
- Dalvit C, Pevarello P, Tato M, et al (2000) Identification of compounds with binding affinity to proteins via magnetization transfer from bulk water. *J Biomol NMR* 18:65–68. doi: 10.1023/A:1008354229396
- Daniel RA, Noirot-Gros MF, Noirot P, Errington J (2006) Multiple interactions between the transmembrane division proteins of *Bacillus subtilis* and the role of FtsL instability in divisome assembly. *J Bacteriol* 188:7396–7404. doi: 10.1128/JB.01031-06
- de Boer PAJ (2010) Advances in understanding *E. coli* cell fission. *Curr Opin Microbiol* 13:730–737. doi: 10.1016/j.mib.2010.09.015
- de Boer PAJ, Crossley RE, Rothfield LI (1989) A division inhibitor and a topological specificity factor coded for by the minicell locus determine proper placement of the division septum in *E. coli*. *Cell* 56:641–649. doi: 10.1016/0092-8674(89)90586-2
- Divakaruni A V., Baida C, White CL, Gober JW (2007) The cell shape proteins MreB and MreC control cell morphogenesis by positioning cell wall synthetic complexes. *Mol Microbiol* 66:174–188. doi: 10.1111/j.1365-2958.2007.05910.x
- Dubnau D (1991) Genetic competence in *Bacillus subtilis*. *Microbiol Rev* 55:395–424. doi:

- 10.1111/j.1365-2958.1991.tb01820.x
- Eichenberger P (2012) Genomics and Cellular Biology of Endospore Formation. In: *Bacillus: Cellular and Molecular biology*. Caister Academic Press
- Erickson HP (2007) Evolution of the Cytoskeleton. *Bioessays* 29:668–677. doi: 10.1002/bies.20601.Evolution
- Erickson HP, Anderson DE, Osawa M (2010) FtsZ in Bacterial Cytokinesis : Cytoskeleton and Force Generator All in One †. *Microbiol Mol Biol Rev* 74:504–528. doi: 10.1128/MMBR.00021-10
- Erickson HP, Taylor DW, Taylor KA, Bramhill D (1996) Bacterial cell division protein FtsZ assembles into protofilament sheets and minirings, structural homologs of tubulin polymers. *Proc Natl Acad Sci U S A* 93:519–523. doi: 10.1073/pnas.93.1.519
- Errington J (2003) Regulation of endospore formation in *Bacillus subtilis*. *Nat Rev Microbiol* 1:117–126. doi: 10.1038/nrmicro750
- Errington J, Daniel RA (2002) Cell division during growth and sporulation. In: Sonenshein AL, Hoch JA, Losick R (eds) *Bacillus subtilis and Its Closest Relatives*. American Society of Microbiology
- Errington J, Daniel RA, Scheffers D-J (2003) Cytokinesis in bacteria. *Microbiol Mol Biol Rev* 67:52–65. doi: 10.1128/MMBR.67.1.52-65.2003
- Fantes P, Nurse P (1977) Control of cell size at division in fission yeast by a growth-modulated size control over nuclear division. *Exp Cell Res* 107:377–386. doi: 10.1016/0014-4827(77)90359-7
- Fleurie A, Lesterlin C, Manuse S, et al (2014) MapZ marks the division sites and positions FtsZ rings in *Streptococcus pneumoniae*. *Nature* 516:259–262. doi: 10.1038/nature13966
- Freese BE, Park SW, Cashel M (1964) The developmental significance of alanine dehydrogenase in *Bacillus subtilis*. *PNAS* 51:1164–1172
- Freese E, Oosterwyk J (1963) The Induction of Alanine Dehydrogenase. *Biochemistry* 2:1212–1216. doi: 10.1021/bi00906a006
- Fry B, Zhu T, Domach MM, et al (2000) Characterization of growth and acid formation in a *Bacillus subtilis* pyruvate kinase mutant. *Appl Environ Microbiol* 66:4045–9
- Gaimster H, Summers D (2015) Plasmids in the driving seat: The regulatory RNA Rcd gives plasmid ColE1 control over division and growth of its *E.coli* host. *Plasmid* 78:59–64.

- doi: 10.1016/j.plasmid.2014.11.002
- Gamba P, Veening JW, Saunders NJ, et al (2009) Two-step assembly dynamics of the *Bacillus subtilis* divisome. *J Bacteriol* 191:4186–4194. doi: 10.1128/JB.01758-08
- Gerosa L, Sauer U (2011) Regulation and control of metabolic fluxes in microbes. *Curr Opin Biotechnol* 22:566–575. doi: 10.1016/j.copbio.2011.04.016
- Gibson DG, Young L, Chuang R-Y, et al (2009) Enzymatic assembly of DNA molecules up to several hundred kilobases. *Nat Methods* 6:343–5. doi: 10.1038/nmeth.1318
- Goehring NW, Beckwith J (2005) Diverse paths to midcell: Assembly of the bacterial cell division machinery. *Curr Biol* 15:514–526. doi: 10.1016/j.cub.2005.06.038
- Goehring NW, Gonzalez MD, Beckwith J (2006) Premature targeting of cell division proteins to midcell reveals hierarchies of protein interactions involved in divisome assembly. *Mol Microbiol* 61:33–45. doi: 10.1111/j.1365-2958.2006.05206.x
- Gon S, Napolitano R, Rocha W, et al (2011) Increase in dNTP pool size during the DNA damage response plays a key role in spontaneous and induced-mutagenesis in *Escherichia coli*. *Proc Natl Acad Sci* 108:19311–19316. doi: 10.1073/pnas.1113664108
- Goranov AI, Katz L, Breier AM, et al (2005) A transcriptional response to replication status mediated by the conserved bacterial replication protein DnaA. *Proc Natl Acad Sci* 102:12932–12937. doi: 10.1073/pnas.0506174102
- Grangeasse C, Lesterlin C (2015) Mapping mid-cell: MapZ shows the way. *Cell Cycle* 14:937–938. doi: 10.1080/15384101.2015.1010978
- Gregory JA, Becker EC, Pogliano K (2008) *Bacillus subtilis* MinC destabilizes FtsZ-rings at new cell poles and contributes to the timing of cell division. *Genes Dev* 22:3475–3488. doi: 10.1101/gad.1732408
- Haeusser DP, Levin PA (2008) The great divide: coordinating cell cycle events during bacterial growth and division. *Curr Opin Microbiol* 11:94–99. doi: 10.1016/j.mib.2008.02.008
- Haeusser DP, Margolin W (2016) Splitsville: structural and functional insights into the dynamic bacterial Z ring. *Nat Rev Microbiol* 14:305–319. doi: 10.1038/nrmicro.2016.26
- Hajduk I V, Rodrigues CDA, Harry EJ (2016) Connecting the dots of the bacterial cell cycle: Coordinating chromosome replication and segregation with cell division. *Semin Cell Dev Biol* 53:2–9
- Harry E, Monahan L, Thompson L (2006) *Bacterial Cell Division: The Mechanism and Its*

- Precision. *Int Rev Cytol* 253:27–94. doi: 10.1016/S0074-7696(06)53002-5
- Harry EJ (2001) Bacterial cell division: Regulating Z-ring formation. *Mol Microbiol* 40:795–803. doi: 10.1046/j.1365-2958.2001.02370.x
- Harry EJ, Pogliano K, Losick R (1995) Use of Immunofluorescence to Visualize Cell-Specific Gene-Expression During Sporulation in *Bacillus-Subtilis*. *J Bacteriol* 177:3386–3393
- Harry EJ, Rodwell J, Wake RG (1999) Co-ordinating DNA replication with cell division in bacteria: A link between the early stages of a round of replication and mid-cell Z ring assembly. *Mol Microbiol* 33:33–40. doi: 10.1046/j.1365-2958.1999.01439.x
- Heinemann M, Sauer U (2010) Systems biology of microbial metabolism. *Curr Opin Microbiol* 13:337–343. doi: 10.1016/j.mib.2010.02.005
- Higgins D, Dworkin J (2012) Recent progress in *Bacillus subtilis* sporulation. *FEMS Microbiol Rev* 36:131–148. doi: 10.1111/j.1574-6976.2011.00310.x
- Hill NS, Buske PJ, Shi Y, Levin PA (2013) A Moonlighting Enzyme Links *Escherichia coli* Cell Size with Central Metabolism. *PLoS Genet* 9:1–14. doi: 10.1371/journal.pgen.1003663
- Hill NS, Zuke JD, Buske PJ, et al (2018) A nutrient-dependent division antagonist is regulated post-translationally by the Clp proteases in *Bacillus subtilis*. *BMC Microbiol* 18:1–14. doi: 10.1186/s12866-018-1155-2
- Holečková N, Doubravová L, Massidda O, et al (2015) LocZ Is a New Cell Division Protein Involved in Proper Septum Placement in *Streptococcus pneumoniae*. *MBio* 6:1–13. doi: 10.1128/mBio.01700-14.Invited
- Horgan RP, Kenny LC (2011) ‘Omic’ technologies : genomics, transcriptomics, proteomics and metabolomics. *Obstet Gynaecol* 13:189–195. doi: 10.1576/toag.13.3.189.27672
- Jain A, Chen WN (2018) Involvement of organic acids and amino acids in ameliorating Ni(II) toxicity induced cell cycle dysregulation in *Caulobacter crescentus*: a metabolomics analysis. *Appl Microbiol Biotechnol* 102:4563–4575. doi: 10.1007/s00253-018-8938-0
- Jannièrè L, Canceill D, Suski C, et al (2007) Genetic evidence for a link between glycolysis and DNA replication. *PLoS One* 2:. doi: 10.1371/journal.pone.0000447
- Jeffery CJ (2009) Moonlighting proteins—an update. *Mol Biosyst* 5:345–350. doi: 10.1039/b900658n

- Jonas K (2014) To divide or not to divide: Control of the bacterial cell cycle by environmental cues. *Curr Opin Microbiol* 18:54–60. doi: 10.1016/j.mib.2014.02.006
- Jordan S, Junker A, Helmann JD, Mascher T (2006) Regulation of LiaRS-dependent gene expression in *Bacillus subtilis*: Identification of inhibitor proteins, regulator binding sites, and target genes of a conserved cell envelope stress-sensing two-component system. *J Bacteriol* 188:5153–5166. doi: 10.1128/JB.00310-06
- Kanda-Nambu K, Yasuda Y, Tochikubo K (2000) Isozymic nature of spore coat-associated alanine racemase of *Bacillus subtilis*. *Amino Acids* 18:375–387. doi: 10.1007/s007260070076
- Karoui M El, Errington J (2001) Isolation and characterization of topological specificity mutants of minD in *Bacillus subtilis*. *Mol Microbiol* 42:1211–1221. doi: 10.1046/j.1365-2958.2001.02710.x
- Koo BM, Kritikos G, Farelli JD, et al (2017) Construction and Analysis of Two Genome-Scale Deletion Libraries for *Bacillus subtilis*. *Cell Syst* 4:291-305.e7. doi: 10.1016/j.cels.2016.12.013
- Leggett MJ, McDonnell G, Denyer SP, et al (2012) Bacterial spore structures and their protective role in biocide resistance. *J Appl Microbiol* 113:485–498. doi: 10.1111/j.1365-2672.2012.05336.x
- Levin PA, Shim JJ, Grossman AD (1998) Effect of minCD on FtsZ ring position and polar septation in *Bacillus subtilis*. *J Bacteriol* 180:6048–6051
- Ling Ling T, Ahmad M, Yook Heng L (2011) An amperometric biosensor based on alanine dehydrogenase for the determination of low level of ammonium ion in water. *J Sensors* 2011:1–10. doi: 10.1155/2011/980709
- Link H, Kochanowski K, Sauer U (2013) Systematic identification of allosteric protein-metabolite interactions that control enzyme activity in vivo. *Nat Biotechnol* 31:357–361. doi: 10.1038/nbt.2489
- Lock RL, Harry EJ (2008) Cell-division inhibitors: new insights for future antibiotics. *Nat Rev Drug Discov* 7:324–338. doi: 10.1038/nrd2510
- Lok C (2015) Mining the microbial dark matter. *Nature* 522:270–273. doi: 10.1038/522270a
- Löwe J, Amos L a (1998) Crystal structure of the bacterial cell-division protein FtsZ. *Nature* 391:203–206. doi: 10.1038/34472
- Löwe J, Amos LA (1999) Tubulin-like protofilaments in Ca<sup>2+</sup>-induced FtsZ sheets. *EMBO J*

- 18:2364–2371
- Lu C, Reedy M, Erickson HP (2000) Straight and Curved Conformations of FtsZ Are Regulated by GTP Hydrolysis. *J Bacteriol* 182:164–170
- Lu C, Stricker J, Erickson HP (1998) FtsZ from *Escherichia coli*, *Azotobacter vinelandii*, and *Thermotoga maritima*--quantitation, GTP hydrolysis, and assembly. *Cell Motil Cytoskeleton* 40:71–86. doi: 10.1002/(SICI)1097-0169(1998)40:1<71::AID-CM7>3.0.CO;2-I
- Ma X, Ehrhardt DW, Margolin W (1996) Colocalization of cell division proteins FtsZ and FtsA to cytoskeletal structures in living *Escherichia coli* cells by using green fluorescent protein. *Proc Natl Acad Sci U S A* 93:12998–3003. doi: 10.1073/pnas.93.23.12998
- Maciag-Dorszyńska M, Ignatowska M, Jannièrè L, et al (2012) Mutations in central carbon metabolism genes suppress defects in nucleoid position and cell division of replication mutants in *Escherichia coli*. *Gene* 503:31–35. doi: 10.1016/j.gene.2012.04.066
- Maciag M, Nowicki D, Szalewska-Pałasz A, Wegrzyn G (2012) Central carbon metabolism influences fidelity of DNA replication in *Escherichia coli*. *Mutat Res* 731:99–106. doi: 10.1016/j.mrfmmm.2011.12.005
- Margolin W (2005) FtsZ and the division of prokaryotic cells and organelles. *Nat Rev Mol Cell Biol* 6:862–871. doi: 10.1038/nrm1745
- Matsuda R, Bi C, Anguizola J, et al (2014) Studies of metabolite – protein interactions : A review. *J Chromatogr* 966:48–58
- Meiboom S, Gill D (1958) Modified Spin-Echo Method for Measuring Nuclear Relaxation Times. *Rev Sci Instrum* 29:688–691. doi: 10.1063/1.1716296
- Migocki MD, Freeman MK, Wake RG, Harry EJ (2002) The Min system is not required for precise placement of the midcell Z ring in *Bacillus subtilis*. *EMBO Rep* 3:1163–1167. doi: 10.1093/embo-reports/kvf233
- Monahan LG, Hajduk I V, Blaber SP, et al (2014a) Coordinating Bacterial Cell Division with Nutrient Availability : a Role for Glycolysis. *MBio* 5:1–13. doi: 10.1128/mBio.00935-14.Editor
- Monahan LG, Harry EJ (2016) You Are What You Eat : Metabolic Control of Bacterial Division. *Trends Microbiol* 24:181–189. doi: 10.1016/j.tim.2015.11.007
- Monahan LG, Liew ATF, Bottomley AL, Harry EJ (2014b) Division site positioning in bacteria : one size does not fit all. *Front Microbiol* 5:1–7. doi:

- 10.3389/fmicb.2014.00019
- Monahan LG, Robinson A, Harry EJ (2009) Lateral FtsZ association and the assembly of the cytokinetic Z ring in bacteria. *Mol Microbiol* 74:1004–1017. doi: 10.1111/j.1365-2958.2009.06914.x
- Moriya S, Rashid RA, Rodrigues CDA, Harry EJ (2010) Influence of the nucleoid and the early stages of DNA replication on positioning the division site in *Bacillus subtilis*. *Mol Microbiol* 76:634–647. doi: 10.1111/j.1365-2958.2010.07102.x
- Mukherjee A, Lutkenhaus J (1994) Guanine nucleotide-dependent assembly of FtsZ into filaments. *J Bacteriol* 176:2754–2758
- Murray H, Koh A (2014) Multiple Regulatory Systems Coordinate DNA Replication with Cell Growth in *Bacillus subtilis*. *PLoS Genet* 10:1–15. doi: 10.1371/journal.pgen.1004731
- Niki H, Jaffe A, Imamura R, et al (1991) The new gene mukB codes for a 177 kd protein with coiled-coil domains involved in chromosome partitioning of *E. coli*. *EMBO J* 10:183–193
- Noirot-Gros M-F, Dervyn E, Wu LJ, et al (2002) An expanded view of bacterial DNA replication. *PNAS* 99:8342–8347. doi: 10.1073/pnas.122040799
- Nouri H, Monnier A-F, Fossum-Raunehaug S, et al (2018) Multiple links connect central carbon metabolism to DNA replication initiation and elongation in *Bacillus subtilis*. *DNA Res* 0:1–13. doi: 10.1093/dnares/dsy031
- Nukushina J, Ikeda Y (1969) Genetic analysis of the developmental processes during germination and outgrowth of *Bacillus subtilis* spores with temperature-sensitive mutants. *Genetics* 63:63–74
- Pai CC, Kearsy SE (2017) A critical balance: DNTPs and the maintenance of genome stability. *Genes (Basel)* 8:1–14. doi: 10.3390/genes8020057
- Paintdakhi A, Parry B, Campos M, et al (2016) Oufiti: An integrated software package for high-accuracy, high-throughput quantitative microscopy analysis. *Mol Microbiol* 99:767–777. doi: 10.1111/mmi.13264
- Pang T, Wang X, Lim HC, et al (2017) The nucleoid occlusion factor Noc controls DNA replication initiation in *Staphylococcus aureus*. *PLoS Genet* 13:1–26. doi: 10.1371/journal.pgen.1006908
- Pichoff S, Lutkenhaus J (2001) *Escherichia coli* division inhibitor mincd blocks septation by

- preventing Z-ring formation. *J Bacteriol* 183:6630–6635. doi: 10.1128/JB.183.22.6630-6635.2001
- Pinho MG, Kjos M, Veening J-W (2013) How to get (a)round: mechanisms controlling growth and division of coccoid bacteria. *Nat Rev Microbiol* 11:601–14. doi: 10.1038/nrmicro3088
- Postma PW, Lengeler JW, Jacobson GR (1993) Phosphoenolpyruvate:carbohydrate phosphotransferase systems of bacteria. *Microbiol Rev* 57:543–94
- Pulschen AA, Sastre DE, Machinandiarena F, et al (2017) The stringent response plays a key role in *Bacillus subtilis* survival of fatty acid starvation. *Mol Microbiol* 103:698–712. doi: 10.1111/mmi.13582
- Radhakrishnan SK, Pritchard S, Viollier PH (2010) Coupling Prokaryotic Cell Fate and Division Control with a Bifunctional and Oscillating Oxidoreductase Homolog. *Dev Cell* 18:90–101. doi: 10.1016/j.devcel.2009.10.024
- Ramos HC, Hoffmann T, Marino M, et al (2000) Fermentative Metabolism of *Bacillus subtilis* : Physiology and Regulation of Gene Expression. *J Bacteriol* 182:3072–3080. doi: 10.1128/JB.182.11.3072-3080.2000.Updated
- Reeve JN, Mendelson NH, Coyne SI, et al (1973) Minicells of *Bacillus subtilis*. *J Bacteriol* 114:860–873
- Reichmann NT, Piçarra Cassona C, Monteiro JM, et al (2014) Differential localization of LTA synthesis proteins and their interaction with the cell division machinery in *Staphylococcus aureus*. *Mol Microbiol* 92:273–286. doi: 10.1111/mmi.12551
- Robichon C, King GF, Goehring NW, Beckwith J (2008) Artificial septal targeting of *Bacillus subtilis* cell division proteins in *Escherichia coli*: An interspecies approach to the study of protein-protein interactions in multiprotein complexes. *J Bacteriol* 190:6048–6059. doi: 10.1128/JB.00462-08
- Rodrigues C (2011) Establishing how Bacterial Cells Position the Division Site
- Rodrigues CDA, Harry EJ (2012) The Min System and Nucleoid Occlusion Are Not Required for Identifying the Division Site in *Bacillus subtilis* but Ensure Its Efficient Utilization. *PLoS Genet* 8:1–20. doi: 10.1371/journal.pgen.1002561
- Romberg L, Simon M, Erickson HP (2001) Polymerization of FtsZ, a bacterial homolog of tubulin. Is assembly cooperative? *J Biol Chem* 276:11743–11753. doi: 10.1074/jbc.M009033200



- Rowlett VW, Margolin W (2015a) The Min system and other nucleoid-independent regulators of Z ring positioning. *Front Microbiol* 6:478. doi: 10.3389/fmicb.2015.00478
- Rowlett VW, Margolin W (2015b) The bacterial divisome : ready for its close-up. *Philos Trans R Soc B Biol Sci* 370:20150028. doi: 10.1098/rstb.2015.0028
- Rowlett VW, Margolin W (2013) The bacterial min system. *Curr Biol* 23:R553–R556. doi: 10.1016/j.cub.2013.05.024
- Ryan KR, Shapiro L (2003) Temporal and Spatial regulation in prokaryotic cell cycle progression and development. *Annu Rev Biochem* 72:367–394. doi: 10.1146/annurev.biochem.72.121801.161824
- Sambrook J (1989) *Molecular cloning : a laboratory manual*, 2nd edn. Cold Spring Harbor, N.Y. : Cold Spring Harbor Laboratory Press
- Santos TMA, Lammers MG, Zhou M, et al (2018) Small Molecule Chelators Reveal That Iron Starvation Inhibits Late Stages of Bacterial Cytokinesis. *ACS Chem Biol* 13:235–246. doi: 10.1021/acscchembio.7b00560
- Schaechter M, Maaløe O, Kjeldgaard NO (1958) Dependency on Medium and Temperature of Cell Size and Chemical Composition during Balanced Growth of *Salmonella typhimurium*. *J Gen Microbiol* 19:592–606. doi: 10.1099/00221287-19-3-592
- Schreiber G, Ron EZ, Glaser G (1995) ppGpp-mediated regulation of DNA replication and cell division in *Escherichia coli*. *Curr Microbiol* 30:27–32. doi: 10.1007/BF00294520
- Schujman GE, Paoletti L, Grossman AD, de Mendoza D (2003) FapR, a bacterial transcription factor involved in global regulation of membrane lipid biosynthesis. *Dev Cell* 4:663–672. doi: 10.1016/S1534-5807(03)00123-0
- Sheu CW, Freese E (1972) Effects of Fatty Acids on Growth and Envelope Proteins of *Bacillus subtilis*. *J Bacteriol* 111:516–524
- Shi Z, Xuan C, Han H, et al (2014) Gluconate 5-dehydrogenase (Ga5DH) participates in *Streptococcus suis* cell division. *Protein Cell* 5:761–769. doi: 10.1007/s13238-014-0074-8
- Siranosian KJ, Ireton K, Grossman AD (1993) Alanine dehydrogenase (ald) is required for normal sporulation in *Bacillus subtilis*. *J Bacteriol* 175:6789–6796. doi: 10.1128/jb.175.21.6789-6796.1993
- Smith TJ, Foster SJ (1995) Characterization of the Involvement of two Compensatory Autolysins in Mother Cell-Lysis During Sporulation of *Bacillus-Subtilis* 168. *J Bacteriol*

- 177:3855–3862
- Söderstrom B, Mirzadeh K, Toddo S, et al (2016) Coordinated disassembly of the divisome complex in *Escherichia coli*. *Mol Microbiol* 101:425–438. doi: 10.1111/mmi.13400
- Song HK, Song W, Kim M, et al (2017) Bacterial strategies along nutrient and time gradients, revealed by metagenomic analysis of laboratory microcosms. *FEMS Microbiol Ecol* 93:. doi: 10.1093/femsec/fix114
- Sperber AM, Herman JK (2017) Metabolism shapes the cell. *J Bacteriol* 199:1–14. doi: 10.1128/JB.00039-17
- Taheri-Araghi S, Bradde S, Sauls JT, et al (2014) Cell-Size Control and Homeostasis in Bacteria. *Curr Biol* 25:1–7. doi: 10.1016/j.cub.2014.12.009
- Teather RM, Collins JF, Donachie WD (1974) Quantal behavior of a diffusible factor which initiates septum formation at potential division sites in *Escherichia coli*. *J Bacteriol* 118:407–413
- Tehranchi AK, Blankschien MD, Zhang Y, et al (2010) The Transcription Factor DksA Prevents Conflicts between DNA Replication and Transcription Machinery. *Cell* 141:595–605. doi: 10.1016/j.cell.2010.03.036
- Thanbichler M, Shapiro L (2006) MipZ, a Spatial Regulator Coordinating Chromosome Segregation with Cell Division in *Caulobacter*. *Cell* 126:147–162. doi: 10.1016/j.cell.2006.05.038
- Thompson LS, Beech PL, Real G, et al (2006) Requirement for the cell division protein DivIB in polar cell division and engulfment during sporulation in *Bacillus subtilis*. *J Bacteriol* 188:7677–7685. doi: 10.1128/JB.01072-06
- Traag BA, van Wezel GP (2008) The SsgA-like proteins in actinomycetes: Small proteins up to a big task. *Antonie Van Leeuwenhoek* 94:85–97. doi: 10.1007/s10482-008-9225-3
- Treuner-Lange A, Aguiluz K, van der Does C, et al (2013) PomZ, a ParA-like protein, regulates Z-ring formation and cell division in *Myxococcus xanthus*. *Mol Microbiol* 87:235–253. doi: 10.1111/mmi.12094
- Turner RJ, Lu Y, Switzer RL (1994) Regulation of the *Bacillus subtilis* pyrimidine biosynthetic (pyr) gene cluster by an autogenous transcriptional attenuation mechanism. *J Bacteriol* 176:3708–3722. doi: 10.1128/jb.176.12.3708-3722.1994
- Tymecka-Mulik J, Boss L, Maciąg-Dorszyńska M, et al (2017) Suppression of the *Escherichia coli* dnaA46 mutation by changes in the activities of the pyruvate-acetate

- node links DNA replication regulation to central carbon metabolism. *PLoS One* 12:1–24. doi: 10.1371/journal.pone.0176050
- Vadia S, Tse JL, Lucena R, et al (2017) Fatty Acid Availability Sets Cell Envelope Capacity and Dictates Microbial Cell Size. *Curr Biol* 27:1757–1767. doi: 10.1016/j.cub.2017.05.076
- Vaughan S, Wickstead B, Gull K, Addinall SG (2004) Molecular Evolution of FtsZ Protein Sequences Encoded Within the Genomes of Archaea , Bacteria , and Eukaryota. *J Mol Evol* 58:19–39. doi: 10.1007/s00239-003-2523-5
- Vendeville A, Lariviere D, Fourmentin E (2011) An inventory of the bacterial macromolecular components and their spatial organization. *FEMS Microbiol Rev* 35:395–414. doi: 10.1111/j.1574-6976.2010.00254.x
- Vitha S, McAndrew RS, Osteryoung KW (2001) FtsZ ring formation at the chloroplast division site in plants. *J Cell Biol* 153:111–119. doi: 10.1083/jcb.153.1.111
- Von Freiesleben U, Rasmussen K V., Atlung T, Hansen FG (2000) Rifampicin-resistant initiation of chromosome replication from oriC in ihf mutants. *Mol Microbiol* 37:1087–1093. doi: 10.1046/j.1365-2958.2000.02060.x
- Wang JD, Levin PA (2009) Metabolism, cell growth and the bacterial cell cycle. *Nat Rev Microbiol* 7:822–827. doi: 10.1038/nrmicro2202
- Wang X, Montero Llopis P, Rudner DZ (2014) *Bacillus subtilis* chromosome organization oscillates between two distinct patterns. *Proc Natl Acad Sci* 111:12877–12882. doi: 10.1073/pnas.1407461111
- Weart RB, Lee AH, Chien A-C, et al (2007) A Metabolic Sensor Governing Cell Size in Bacteria. *Cell* 130:335–347. doi: 10.1016/j.cell.2007.05.043
- Weart RB, Levin PA (2003) Growth rate-dependent regulation of medial FtsZ ring formation. *J Bacteriol* 185:2826–2834. doi: 10.1128/JB.185.9.2826
- Wecke T, Bauer T, Harth H, et al (2011) The rhamnolipid stress response of *Bacillus subtilis*. *FEMS Microbiol Lett* 323:113–123. doi: 10.1111/j.1574-6968.2011.02367.x
- Weiss DS (2004) Bacterial cell division and the septal ring. *Mol Microbiol* 54:588–597. doi: 10.1111/j.1365-2958.2004.04283.x
- Westfall CS, Levin PA (2018) Comprehensive analysis of central carbon metabolism illuminates connections between nutrient availability, growth rate, and cell morphology in *Escherichia coli*. *PLoS Genet* 14:1–25. doi: 10.1371/journal.pgen.1007205

- 
- Westfall CS, Levin PA (2017) Bacterial cell size: Multifactorial and Multifaceted. *Annu Rev Microbiol* 71:499–517
- Wiener N (1961) *Cybernetics; or, Control and communication in the animal and the machine.* M.I.T. Press
- Willemse J, Borst JW, Waal E De, et al (2011) Positive control of cell division : FtsZ is recruited by SsgB during sporulation of *Streptomyces*. *Genes Dev* 25:89–99. doi: 10.1101/gad.600211
- Wu LJ, Errington J (2004) Coordination of cell division and chromosome segregation by a nucleoid occlusion protein in *Bacillus subtilis*. *Cell* 117:915–925. doi: 10.1016/j.cell.2004.06.002
- Wu LJ, Ishikawa S, Kawai Y, et al (2009) Noc protein binds to specific DNA sequences to coordinate cell division with chromosome segregation. *EMBO J* 28:1940–1952. doi: 10.1038/emboj.2009.144
- Xiao J, Goley ED (2016) Redefining the roles of the FtsZ-ring in bacterial cytokinesis. *Curr Opin Microbiol* 34:90–96. doi: 10.1016/j.mib.2016.08.008
- Yamamoto K, Nagura R, Tanabe H, et al (2000) Negative regulation of the *bolA1p* of *Escherichia coli* K-12 by the transcription factor OmpR for osmolarity response genes. *FEMS Microbiol Lett* 186:257–262. doi: 10.1016/S0378-1097(00)00143-9
- Yao Z, Davis RM, Kishony R, et al (2012) Regulation of cell size in response to nutrient availability by fatty acid biosynthesis in *Escherichia coli*. *Proc Natl Acad Sci* 109:E2561–E2568. doi: 10.1073/pnas.1209742109